Cranfield Institute of Technology

Department of Materials

DOCTOR OF PHILOSOPHY THESIS

FAROUK SHEHATA

THE WARM FORMING OF ALUMINIUM / MAGNESIUM ALLOY SHEET

Supervisor, R. PEARCE

August. 1979.

BEST COPY
AVAILABLE
Variable print
quality

CONTENTS

		Page
Abstract		I
Acknowledgements		II
List of Figures		III
Introduction		1
Chapter I	Forming at elevated temperature	3
1.1.	General	3
1.1.1.	Effect of temperature and flow properties	4
1.1.2.	Effect of strain rate and flow properties	5
1.1.3.	Mechanics of stable deformation at elevated temperatures	8
1.1.4.	Ductility at elevated temperature	10
1.2.	Metallurgy of warm forming	12
1.2.1.	Dynamic recovery and recrystallisation	14
1.2.2.	Cavitation	16
1.2.3.	Fracture at elevated temperature	19
1.3.	Biaxial forming	20
1.3.1.	Deep draining	20
1.3.1.1.	Deep drawing at elevated temperature	21
1.3.2.	Biaxial bulge and stretch forming	23
1.3.2.1.	Bulging at elevated temperature	25
1.3.2.2.	Stretching at elevated temperature	28
Chapter II	Materials and experimental techniques	41
2.1.	Materials	41
2.2.	Experimental techniques	41
2.2.1.	Uniaxial tests	41
2.2.2.	Hot pressing tests	42
2.2.3.	Hot bulging tests	42
2.2.4.	Microstructure examinations	43
ChapterIII	Experimental results	48
3.1.	Commercial purity aluminium	48
3.1.2.	Al - 2.2% Mg alloys	48
3.1.3.	Al - 3% Mg alloys	49
3.1.4.	Al - 4.4% Mg alloys	49
3.1.5.	Al - 6.6% Mg alloys	50
3.1.6.	Results from all tests	52
3.2.	Experimental results in biaxial stretch forming	53
3.2.1.	Results of Al/2 Mg alloy	53
3.2.2.	Results of Al/6.6% Mg alloy	54
3.2.3.	A comparison between 2 Mg and 6 Mg hot pressings	55

3.2.4.	Results of hot bulging tests	55
3.3.	Discussion	57
3.3.1.	Uniaxial tensile test	57
3.3.2.	Biaxial press-stretching at elevated temperatuures	58
3.4.	Metallography of Al/6 Mg alloys	62
3.4.1.	Optical microscopy	62
3.4.2.	Scanning electron microscopy	64
3.4.3.	Transmission electron microscopy	64
3.5.	Discussion	66
3.5.1.	Optical metallography	66
3.5.2.	Transmission electron microscopy	69
3.6.	Determination of activation energy	72
3.6.1.	Activation energy for tensile deformation	72
3.6.2.	Activation energy for dynamic recovery	73
3.7.	Discussion	76
Chapter IV	General discussions, conclusions and recommendations	77
4.1.	General discussion and conclusions	77
4.2.	Recommendations for future work	81
	Tables	82
	References	85
	Figures and results.	

ABSTRACT

The desire to reduce the overall motor vehicle weight, and so use less fuel, means that aluminium alloys are now being considered for car bodies. Unfortunately, increase in strength generally leads to a decrease in ductility, because of the alloying additions. Warm forming however, of the Al/Mg series of alloys restores and enhances ductility to a remarkable degree.

The work for this thesis investigated the whole range of commercial aluminium/magnesium alloy (0-6.6% Mg) over a range of temperatures from 20 to 300°C and strain rates from $8.3 \times 10^{-3} - 1.67 \times 10^{-4}$ sec^{-1}. Tests were carried out in both uniaxial and biaxial tension and elongations of more than 200% and $\underline{m}$ values of ~0.32 were obtained. A close correlation between $\underline{m}$ value and elongation was found.

The effect of prior cold working and annealing on ductility was also studied, it was found that greater the prior cold work the higher the ductility at elevated temperatures.

The biaxial tests carried out indicated a higher cup or bulge height resulted from higher magnesium contents and/or higher temperatures up to 300°C. The biaxial tests were less sensitive to strain rate than the uniaxial tests. Tensile data was correlated with the biaxial forming characteristics.

The microstructure of warm-formed materials was studied. Microstructures showed distorted grains and the second phase (β) precipitated mainly in the grain boundaries. A subgrain structure and the formation of regular-mesh dislocation networks were observed by means of transmission electron microscopy.

On the basis of these investigations dynamic recovery is concluded to be the main softening mechanism. The small equiaxed grains which appeared in the grain boundaries of worked grains are believed to be formed after deformation.

Cavitation developed as a result of warm forming and was pronounced in both the gauge length and in the vicinity of the fracture. Cavitation showed a distinct preferance for grain boundaries particularly at triple points. The cavity size increased with increasing temperature and decreasing strain rate. Cavitation seemed to be more severe in annealed metals than in the cold-worked alloys.

The activation energy for dynamic recovery was obtained and it corresponded to that for cross-slip of screw dislocations, which leads to the formation of stable dislocation networks and subgrain structures.

ACKNOWLEDGEMENTS

I am greatly indebted to my supervisor R. Pearce for his interest, patient guidance, active advice and encouragement throughout the course of this work.

I am grateful to Dr. M. Painter, for his helpful discussions and invaluable assistance.

I gratefully acknowledge the courtesy of the Department of Industrual Metallurgy, University of Birmingham for the use of their hot pressing facility.

Finally I am grateful for financial support received from the Cranfield Institute of Technology and Alcan Laboratories Ltd, Banbury, Oxon. Also thanks to Alusuisse Ltd., Zurich and Birmetals Ltd, Birmingham, for the provision of material.

LIST OF FIGURES

Fig.		Page
1.	Stress-strain curves for aluminium (Ref.4)	29
2.	The temperature change test	29
3.	Effect of strain rate on the tensile strength (Ref.6)	30
4.	The strain rate cycling test	30
5.	Rate of decrease of area against cross sectional area for different values of m (Ref.19)	31
6.	Effect of m and n on elongation (Ref.29)	31
7.	Ductility of o.14c, 0.56si, o.65mn, 10.3Ni 18cr steel deformed in tension at two strain rates (Ref.27)	32
8.	Schmatic relationship between strain rate and stress (Ref.28)	32
9.	Microstructure of various regions in a superplastic alloy (Ref.28)	33
10.	Non-newtonian viscous and diffuse cavity growth (Ref.51)	34
11.	Schematic illustration of fracture of a solid cylinder and a cable specimen (Ref.53)	33
12.	Deep drawing process	35
13	Punch-stretching process	35
14.	Forming limit diagram for different materials (Ref.61).	36
15.	A schematic diagram for bulge profile	36
16.	The calculated relationship between mean tangational strain and pressure componsated time. Points were obtained experimentally (Ref.84)	36
17.	FLD's of Aluminium alloy as a function of punch rate and temperature (Ref.88)	37
18.	Oil pans formed at various temperatures showing critical regions 1, 2 and 3 (Ref.89)	38
19.	Strains in critical regions 1-3 of an oil pan successufllly formed at 180°C	38

20. Typical hot hydraulic bulge test, carried out at 200°C (Ref.90) 39

21. The total elongation of longitudinal and transverse tension test on annealed AL 6 Mg (Ref.100) 40

22. A machine for stretch forming and deep drawing sheet materials at elevated temperature (Ref.91) 45

23. Sectional plan of hot plate showing the radial arrangement of cartridge heaters 46

24. Schematic representation of hot bulge forming rig. 47

25. Variation in total elongation with testing

26. Effect of strain rate on m value for 0Mg(25) over a range of temperatures and strain rates

27. Effect of initial sheet temper on total elongation for 2 Mg alloy at initial strain rate of 8.3×10^{-3} sec^{-1}, and various temperatures

28. Effect of initial sheet temper on total elongation for 2 Mg alloy at initial strain rate of $1/67 \times 10^{-3}$ sec^{-1} at various temperatures

29. Effect of initial sheet temper on total elongation for 2 Mg alloy at initial strain rate of 4.17×10^{-4} sec^{-1} at various temperatures

30. Effect of initial sheet temper on toal elongation for 2 Mg alloy at initial strain rate of 1.67×10^{-4} sec^{-1} and various temperatures

31. Effect of temperature on m value for various temper conditions at initial strain rate of 1.67×10^{-3} sec^{-1}

33. Variation temperature on 3 Mg(62) at various strain rates

34. Effect of strain rate on m value for 3 Mg(62) over a range of temperature and strain rates

35. Effect of initial sheet hardness on elongation for 4 Mg alloy at various temperatures and strain rate of 8.3 x 10^{-3} sec^{-1}

36. Effect of initial sheet hardness on elongation for 4 Mg alloy at various temperatures at an initial strain rate of 1.67 x 10^{-3} sec^{-1}

37. Effect of initial sheet hardness on elongation at various temperatures and an initial strain rate of 4.17 x 10^{-4} sec^{-1}

38. Effect of initial sheet hardness on elongation at various temperatures at an initial strain rate of 1.67 x 10^{-4} sec^{-1}

39. Typical deformed specimens of 4 Mg(134) deformed at 300°C and various strain rates

40. Typical deformed specimens of 4 Mg(64) deformed at an initial strain rate of 4.17 x 10^{-4} sec^{-1} and various temperatures

41. Total elongation on 4 Mg alloy at various temperatures and strain rate versus $\underline{m}$ value

42. Effect of initial strain rate on total elongation for 4 Mg(64) at various temperatures

43. Effect of initial strain rate on total elongation for 4 Mg(84) at various temperatures

44. Effect of initial strain rate on total elongation for 4 Mg(134) at various temperatures

45. Effect of initial sheet thickness on total elongation at various temperatures at an initial strain rate of 8.3 x 10^{-3} sec^{-1}

46. Effect of initial sheet hardness on total elongation at various temperatures at an initial strain rate of 1.67 x 10^{-3} sec^{-1}

47. Effect of initial sheet hardness on total elongation at various temperatures and $\dot{\varepsilon}$ = 4.17 x 10^{-4} sec^{-1} for 6 Mg alloy

48. Effect of initial sheet hardness on total elongation at various temperatures and an initial strain rate of 1.67 x 10^{-4} sec^{-1}

49. Typical deformed specimens of 6 Mg(105) at 250°C and various strain rates

50. Typical deformed specimens of 6 Mg(84) at initial strain rate of 4.17×10^{-4} sec^{-1} and various temperatures.

51. Influence of water quenched and annealing on total elongation at various temperatures for 6 Mg alloys

52. Effect of temperature on $\underline{m}$ value for 6 Mg(153) at various strain rates

53. Relationship between $\underline{m}$ and elongation for 6 Mg alloys at various strain rates

54. Variation of hardness after uniaxial deformation at 300°C for cold-rolled and annealed 6 Mg

55. The influence of prior cold work on the total elongation during tension testing at elevated temperatures

56. Effect of magnesium content on elongation at various temperatures

57. Effect of initial strain rate on total elongation for various magnesium content

58. Influence of initial sheet hardness on total elongation for 4 Mg and 6 Mg alloys at various temperatures

59. Relationship between $\underline{m}$ and elongation for all alloys tested

60. Effect of magnesium content on the maximum flow strength at 250°C and strain rate 4.17×10^{-3} sec^{-1}

61. Flow strength versus temperature for 6 Mg alloy together with result of Matsuki

62. The change in punch height at fracture h^* with test temperature

63. The effect of temperature on the limiting bulge height h^* for hemispherical punch stretching on 2 Mg, at different temperatures and punch speeds

78. Typical fractured cups as punch speeds of 5mm/min and various temperatures

79. Typical fractured cups at 250°C and various punch speeds

80. A comparison between the strain distribution across the pole of fractured cups of 2 Mg(56) and 6 Mg(84)

81. A comparison between the strain gradient across the pole of fractured cups on 2 Mg(56) and 6 Mg(84)

82. A comparison of the stretch forming behaviour of 2 Mg(64) and 6 Mg(84) for different punch speeds

83. The relationship between the cup height at fracture h* and tensile parameters, elongations and m values

84. The relationship between the cup height h* and tensile test parameters

85. A combination of figures 83 and 84

86. Thickness distribution across the pole of the bulge for 0 Mg(25) alloy at constant pressure 1.03 x 10^6 Pa at 300°C

87. Thickness distribution across the pole of the bulge for 2 Mg(56) alloy at constant gas pressure 1.03 x 10^6 Pa at 300°C

88. Thickness distribution across the pole of the bulge for 6 Mg(86) alloy at constant gas pressure 1.03 x 10^6 Pa at 300°C

88. Thickness distribution across the pole of the bulge for 6 Mg(86) alloy at constant gas pressure 1.03 x 10^6 Pa at 300°C

89. Variation in true thickness strain with the current distance from the pole for three different alloys at constant pressure and 300°C

90. Variation in the true thickness strain with the current distance from the pole for 6 Mg(84) at various temperatures at a constant presssure.

91. Typical complete bulge 6 Mg(84) tested at 350°C and Pa = 1.03 x 10^6 Pa

92. Typical bulges after sectioning deformed at 300°C and 1 MP_a.
(a) 6 Mg(84) (b) 6 Mg(56) and (c) 0 Mg(25).

93. Microstructure of (a) 6 Mg(84), furnace cooled from 350°C and (b) 6 Mg(153), 40% cold rolled. (x 200).

94. The undeformed grip ends structure where deformation time is 160 minutes at 300°C.
(a) 6 Mg(84) (b) 6 Mg(153). (x 200).

95. Microstructure after 50% elongation at 300°C and $\dot{\varepsilon} = 1.67 \times 10^{-4}$ sec^{-1}.
(a) 6 Mg(84) (b) 6 Mg(153). (x 200).

96. Microstructure after 100% elongation at 300°C and $\dot{\varepsilon} = 1.67 \times 10^{-4}$ sec^{-1}.
(a) 6 Mg(84) (b) 6 Mg(153). (x 200).

97. Microstructure after 200% elongation at 300°C and $\dot{\varepsilon} = 1.67 \times 10^{-4}$ sec^{-1}.
(a) 6 Mg(84) (b) 6 Mg(153). (x 200).

98. Microstructure after 250% elongation at 300°C and $\dot{\varepsilon} = 1.67 \times 10^{-4}$ sec^{-1}.
(a) 6 Mg(84) (b) 6 Mg(153). (x 200).

99. Unetched specimen showing the cavitation after deformation at 250°C and $\dot{\varepsilon} = 1.67 \times 10^{-4}$ sec^{-1}.
(a) 6 Mg(153), E_l = 200% (b) 6 Mg(153) at fracture (c) 6 Mg(84), E_l = 200%, and (d) 6 Mg(84) at fracture. (x 75).

100. Same as Fig. 99 , at deformation temperature of 300°C.

101. Unetcned specimens near fracture deformed at 250°C and $\dot{\varepsilon} = 1.67 \times 10^{-3}$ sec^{-1}.
(a) 6 Mg(153) (b) 6 Mg(84). (x 75).

102. Microstructure of 6 Mg(84) deformed at 300°C and $\dot{\varepsilon} = 1 \times 10^{-3}$ sec^{-1}.
(a) 200% elongation (b) 100% elongation and(c) grip end. (x 200).

103. Microstructure of 6 Mg(84) deformed at 400°C and $\dot{\varepsilon} = 1 \times 10^{-3}$ sec^{-1}.
(a) grip end (b) 100% elongation and (c) 200% elongation. (x 200).

104. Microstructure of 6 Mg(84) deformed at 450°C and $\dot{\varepsilon} = 1 \times 10^{-3}$ sec^{-1}.
(a) grip end (b) 100% elongation (c) 200% elongation. (x 200).

105. Microstructure of 6 Mg(84) deformed at 500°C and $\dot{\varepsilon} = 1 \times 10^{-3}$ sec^{-1}.
(a) grip end (b) 200% elongation and (c) 100% elongation. (x 200).

106. Microstructure of 6 Mg(84) deformed to 200% elongation and $\dot{\varepsilon} = 1 \times 10^{-3}$ sec^{-1}.
(a) 300°C, (b) 400°C, (c) 450°C and (d) 500°C. (x 800).

107. Unetched specimens deformed at 500°C and $\dot{\varepsilon} = 1 \times 10^{-3}$ sec^{-1}.
(a) grip end (b) 100% elongation (c) 200% elongation. (x 200).

108. Scanning fractographs for specimens deformed at $\dot{\varepsilon} = 1.67 \times 10^{-4}$ sec^{-1}.
(a) 6 Mg(153) at 300°C, (b) 6 Mg(84) at 300°C, (c) 6 Mg(153) at 250°C and (d) 6 Mg(84) at 250°C

109. Thin foil from grip end of 6 Mg(84) specimen deformed at strain rate of 1.67×10^{-4} sec^{-1}.
(a) 250°C and (b) 300°C. (x 25 K).

110. Thin foil from grip end of 6 Mg(153) specimen deformed at strain rate of 1.67×10^{-4} sec^{-1}.
(a) 250 and (b) 300°C. (x 25 K).

111. Thin foil taken from deformed gauge length (200% elongation) of 6 Mg(84) at 250°C and $= 1.67 \times 10^{-4}$ sec^{-1}. (x 25 K).

112. Thin foil taken from deformed gauge length (200% elongation) of 6 Mg(153) at 250°C and $= 1.67 \times 10^{-4}$ sec^{-1}. (x 25 K).

113. Thin foil taken from deformed gauge length (200% elongation) of 6 Mg(84) at 300°C and $\dot{\varepsilon} = 1.67 \times 10^{-4}$. (x 25 K).

114. Thin foil taken from deformed gauge length (200%) of 6 Mg(153) at 300°C and $\dot{\varepsilon} = 1.67 \times 10^{-4}$
(x 25 K).

115. Similar to Fig. 113 but at $\dot{\varepsilon} = 1.67 \times 10^{-3}$ sec^{-1}
(x 100 K).

116. Similar to Fig. 114 but at $\dot{\varepsilon} = 1.67 \times 10^{-3}$ sec^{-1}
(x 100 K).

117. The aluminium end of the Al-Mg equilibrium diagram.

118. True stress versus strain rate for 6Mg(153) at various temperatures.

119. True stress versus reiprocal temperature for 6 Mg(153) at various strain rates.

120. Variation of activation energy for deformation of 6 Mg(153) with temperature at various strain rates.

121. Schematic stress-strain curves at true temperatures T_l and T_h ($T_h > T_l$)

122. Elastic modulus (E) versus temperature (Ref.125).

123. Variation of relative function of dynamic recovery with temperature for 6 Mg(153) at various strain rates

124. Variation of rate of dynamic recovery with reciprocal temperature at strain of 0.1 and relative fraction of dynamic recovery 0.5 in 6 Mg(153).

Chapter 1

Forming at elevated temperature.

INTRODUCTION

Recently, the increase in the cost of oil and the risks of petroleum scarcity have accentuated the use of aluminium in the motor industry. It seems very likely that certain medium strength aluminium alloy sheets will soon be used for the mass-production of motor car body parts, as, from an energy conservation stand-point, lighter cars use less fuel.

A comparison of the tensile properties of aluminium alloys and of extra deep drawing quality steels shows that at equal strength levels, the aluminium alloys have little more than 50% of the elongation of steel and so thoughts have turned to forming at elevated temperatures as, in general, metals become more ductile as the temperature is increased. Hot forming of sheets immediately suggests superplasticity, where generally, under rather special conditions of alloy composition, temperatures and strain rate, large elongations (800 - 2500%) can be achieved.

It would be desirable, however, if some more modest increase in ductility could be produced, in conventional alloys, at lower temperatures under uncritical operating conditions, and it is from this springboard that work on the warm forming of aluminium alloys was begun.

In 1946 Dorn& Co-workers (Ref.1.) demonstrated that deep drawing of cylindrical cups and box type parts could be enhanced by a quite modest (200°C) increase in temperature.

In the 1950's an aluminium alloy containing 3 - 4% magnesium was generally used for press forming panels for the more expensive range of cars. This was a non-heat treatable, strain-hardening alloy, but inevitably of reduced ductility, because of alloying additions.

More recently, Taylor et al (Ref.2.) and Ayres (Ref.3.) have shown that the tensile elongations of annealed Al - 4% Mg alloys (5182 - 0), considered for use as autobody sheet, could be increased by deforming at elevated temperatures if the strain rates were low.

The present work is in three main parts, first, an investigation of the tensile properties of a series of commercial Al/Mg alloys, 0 - 6.6% Mg, at temperatures up to 300°C, and over a wide range of strain rates.

Secondly, an investigation in the laboratory of hot pressing and bulging to study the biaxial stretching behaviour of Al - 2 Mg and Al - 6 Mg.

Thirdly, metallography was done in an attempt to explain the metallurgical reasons for this enhanced plasticity.

Chapter 1.

Forming at elevated temperature

1.1. General

During manufacturing processes, the deformation temperature and the strain rate are often controlled to develop the optimum structure and properties in the products.

The best way to compare the mechanical properties of different materials at various temperatures is that of Homologous temperature, T_H; this is defined as:-

$$T_H \approx \frac{\text{Testing temperature in degrees Kelvin}}{\text{Melting point in degrees Kelvin}}$$

At $T_H < 0.3$, metals become harder during the working process and the flow curve rises with increasing deformation, movement and interlocking of dislocations. The greater the degree of deformation the larger the number of dislocations produced, and because of their mutual interaction and obstruction, larger stresses are required to force their movement and hence cause further plastic flow, very simply, this explains strain-hardening.

Forming at $T_H > 0.4$ (so called warm forming) but below the recrystallisation temperature, metals may be worked and large strains can be achieved with essentially limited amount of strin hardening.

Warm forming is a relatively new technique and seems to offer the possibility of producing in sheet a range of rather complex shapes without the risk of cracking.

At $T_H > 0.5$, usually the recrystallisation temperature, T_r, hot working is conducted. At this temperature, a balance has been established between the tendency to strain harden and the tendency to soften concurrently. The softening processes are recovery, recrystallisation and grain growth, and they are all thermally activated ones.

1.1.1. Effect of temperature on flow properties

The stress-strain curve and the flow, and fracture properties are strongly dependant on the temperature, T_H, at which the test is conducted. In general, strength decreases and ductility increases as the test temperature is increased. However, structural changes such as precipitation, strain ageing, or recrystallisation may occur in certain temperature ranges to alter this general behaviour.

The change with temperature of the engineering stress-strain curve in superpure aluminium is shown in figure (1), (Ref.4.).

In F.C.C. metals, the flow stress is not strongly dependant on temperature, but strain hardening decreases with increasing temperature. This results in the stress-strain curve flattening out with increasing temperature and the tensile strength being more temperature dependant than the yield strength.

The tensile strength at elevated temperature is complicated by the formation of more than one neck (Ref.5.) in the specimen.

The temperature dependance of the flow stress at a constant strain rate can generally be expressed by:-

$$\sigma = K \quad e^{Q/RT}\Big|_{\varepsilon,\dot{\varepsilon}} \qquad (2)$$

where Q = an activation energy for plastic flow (cal/g mole)
R = universal gas constant 1.98 cal/deg mole
T = testing temperature (°K)

If this expression is obeyed, a plot of ln σ versus 1/T will give a straight line with slope Q/R.

The value of flow stress depends on the dislocation structures existing at the time the flow stress is measured. The dislocation structure will change with temperature, strain rate, and strain. One way to separate these effects is to evaluate Q by a temperature change test as in figure (2); the stress-strain curve is obtained on a constant strain rate machine and at the desired value of plastic strain, the temperature is changed from T_2 to T_1.

After the temperature is changed activation energy is given by:-

$$Q = R \ln \left(\frac{\sigma_1}{\sigma_2}\right) \left(\frac{T_1 \ T2}{T_2 - T_1}\right) \qquad (3)$$

1.1.2. Effect of strain rate on flow properties

The rate at which the strain is applied to a specimen can have an important influence on the flow stress; true strain rate is defined as $\dot{\varepsilon} = d\varepsilon/dt$.

Figure (3) shows that the increasing strain rate increases the tensile strength. Moreover, the strain rate dependance of strength and flow stress at lower plastic strains are more dependant on strain rate than tensile strength.

The strain rate expressed in terms of conventional linear strain (e) can be written as follows:-

$$\dot{e} = \frac{de}{dt} = \frac{d(l-l_0)/l_0}{dt} = \frac{1}{l_0}\frac{dl}{dt} = \frac{V}{l_0} \qquad (4)$$

Where V is the cross head velocity; $V = \frac{dl}{dt}$

The true strain rate $\dot{\varepsilon}$ is given by:-

$$\dot{\varepsilon} = \frac{d\varepsilon}{dt} = \frac{d[\ln(l/l_0)]}{dt} = \frac{1}{l}\frac{dl}{dt} = \frac{v}{l} \qquad (5)$$

This equation (5) indicates that for a constant cross head velocity, the true strain rate will decrease as the specimen elongates. To maintain a constant true strain rate, the cross head velocity must increase in proportion to the increase in length of the specimen.

The true strain rate is related to the conventional strain rate by the following equation:-

$$\dot{\varepsilon} = \frac{V}{l} = \frac{l_0}{l} \times \frac{de}{dt} = \frac{1}{1+e} \times \frac{de}{dt} = \frac{\dot{e}}{1+e} \qquad (6)$$

The most common relationship between flow stress and strain rate, at constant temperature and strain is

$$\sigma = K \dot{\varepsilon}^{m} \Big|_{\varepsilon,T} \qquad (7)$$

Where K is a material constant, that depends upon test temperature and defect structure of the specimen, while m is the strain rate sensitivity index.

Conventionally, m is determined by changing the cross head speed during tensile testing or alternatively, m may be measured from a stress relaxation experiment (Ref.6.)

For the changing of the cross head speed approach, which is more convenient than stress relaxation, the specimen is deformed to a specific strain, and before significant necking occurs, the cross head velocity is rapidly increased or decreased by a factor of 2 - 2.5 and deformation is continued. Figure (4) shows schematically the type of stress/strain behaviour generally obtained.

There are five methods of analysing the data which depend on taking different points from figure (4); however, one of the first two methods is preferred, because these provide more consistency (± 0.02) between incremental and decremental strain-rate changes.

Method I (Ref.7.)

In this case the parameter m is given by:-

$$m = \frac{\log (P_A/P_B)}{\log (V_2/V_1)} \qquad (8)$$

Where A is the maximum load at cross head velocity V_2, and B is the extrapolation of the curve for V_1 to the same strain as A. This is the most common method of determining the strain rate sensitivity. However it has the disadvantage of extrapolation errors.

Method II (Ref.8.)

In this case the parameter m is evaluated by:-

$$m = \frac{\log (\sigma_A/\sigma_C)}{\log (\dot{\varepsilon}_A/\dot{\varepsilon}_C)} \qquad (9)$$

Where A and C are the points of maximum load, Figure (4). This method has the advantage that no extrapolation is required so that only small strains need to be accumulated between changes in cross head velocities.

Method III (Ref.9.)

This is a variant of method I, i.e. the parameter m is given by:-

$$m = \frac{\log(P_E/P_D)}{\log(V_2/V_1)} \qquad (10)$$

Where E is the back extrapolation of velocity V_2 to the strain at which the change was made.

Method IV (Ref.10.)

Here the strain-rate sensitivity is measured using the limit F of the linear region of the curve after the velocity change to give:-

$$m = \frac{\log(P_F/P_D)}{\log(V_2/V_1)} \qquad (11)$$

Method V (Ref.11.)

In this method the parameter m is given by:-

$$m = \frac{\log(\sigma_A/\sigma_D)}{\log(\dot{\varepsilon}_A/\dot{\varepsilon}_D)} \qquad (12)$$

Because of a neck developing at higher strains, the effect of strain on m is very important. Unfortunately, only limited data was available on the effect of strain on m values.

Morrison (Ref.12.) found that m decreased with increasing strain in Sn-Pb eutectic alloys, which he attributed to structural changes, probably grain growth accompanying deformation. However more complex behaviour was reported for steels, in which m first increased and then decreased with increasing strain (Ref.13.), again because of structural changes, and m also reported to be independent of strain in case of Al killed and rimmed steel (Ref.14.). In aluminium alloys m was reported to increase with increasing strain (Ref.15.) and is also reported to be independent in the case of pure Al (Ref.16.) and Cu-Al eutectic (Ref.17.)

Returning to the effect of strain rate on flow properties, the relationship:-

$$\sigma = K \varepsilon^{n} \dot{\varepsilon}^{m} \qquad (13)$$

is useful in materials where m changes as a function of strain.

1.1.3. Mechanics of stable deformation at elevated temperatures

A ductile material when stretched by a tensile force, can deform uniformly only while stable flow occurs. The limit of stable flow is marked by the onset of geometrical instability; that is, after a certain uniform extension, deformation concentrates at a given point and ceases elsewhere. Such instability produces the commonly observed regions of localised deformation (necks) which eventually lead to rupture.

At temperatures below 0.3 Tm (where Tm is the melting temperature of the metal or alloy in question in degrees Kelvin) instability occurs when the material has exhausted its capacity for strain-hardening and the true strain ε at this point is shown to be numerically equal to the strain hardening index n, if the material under test obeys the relationship

$$\sigma = K \varepsilon^{n} \qquad (14)$$

It follows therefore, that as the index n has values generally at < 0.3, uniform elongation will not exceed 30% strain. For further stable extension, the material must be unloaded and then softened, thus restoring the ability to strain hardening again on re-applying the load.

If a material does not strain harden there can be no uniform elongation, yet at temperatures above 0.5 Tm, materials often exhibit a certain range of uniform deformation and also quite high elongations can result (super plastic materials).

In these circumstances, therefore some factor other than strain hardening must control the deformation ability in a stable manner. Above 0.5 Tm, where an equilibrium between restoration and hardening exists, the important parameter is strain-rate sensitivity and this replaces the strain hardening index n, which is the controlling factor at low temperatures.

The magnitude of the strain-rate sensitivity index m, is of considerable importance in most cases of deformation. This was demonstrated analytically by Rossards (Ref.18.) and experimentally by Backofen (Ref.19.). Rossard's treatment of mechanical instability, during creep deformation, assumes that a mechanical equation of state exists of the form:-

$$\sigma = K \varepsilon^{n} \dot{\varepsilon}^{m} \tag{13}$$

Assuming n is constant, a more simplified analytical form is often used to demonstrate that high values of m are required for resistance to normal neck formation, reduce equation (13) to

$$\frac{P}{A} = K \dot{\varepsilon}^{m} \tag{15}$$

or

$$\dot{\varepsilon} = \left(\frac{P}{K}\right)^{1/m} \left(\frac{1}{A}\right)^{1/m} \tag{16}$$

From definition of true strain rate

$$\dot{\varepsilon} = \frac{1}{L}\frac{dL}{dt} = -\frac{1}{A}\frac{dA}{dt} \tag{17}$$

Where t is the time, it follows from a combination of equations (16) and (17) that

$$-\frac{dA}{dt} = \left(\frac{P}{K}\right)^{1/m} (A)^{(m-1)/m} \tag{18}$$

When m = 1 the deformation is Newtonian viscous and $\frac{dA}{dt}$ is independent of area (A) and any incipient neck is simply preserved during elongation and does not propagate inward. As m approaches unity, the rate of growth of incipient necks is drastically reduced and large elongations are therefore possible. In superplastic materials

where m is high but less than unity, this effect still exists. In a nonsuperplastic in which m is always < 0.2 a pronounced change in cross section (neck) occurs where the area is a minimum and the stress higher than elswhere. Figure (5) shows how the area decreases varies with m values.

Figure (6a), presented by Ghosh (Ref.20.), shows the influence of a small m - value (0.01 - 0.05) in extending the post-uniform strain at a constant n - value of 0.1, while figure (6b) shows the influence of n on the engineering stress strain curves for m = 0, for n = 0.05, 0.10, 0.20 and 0.04. As n increases, post uniform portions drop more slowly.

Ghosh also suggested a constitutive equation which governs the relationship between n, m and strain:-

$$\sigma = K \left[\varepsilon^{n} + m \ln (\dot{\varepsilon}/\dot{\varepsilon}_0)\right] \qquad (19)$$

Where K is a strength coeficient, and $\dot{\varepsilon}_0$ is a reference strain-rate at which strain rate hardening is negligible.

Figure (6c) again from Ghosh shows plots of post-uniform strain as function of m for n = 0.05, 0.1 and 0.2. The increase in post-uniform strain produced by n alone (for m = 0) is enhanced many times as m increases. On the other hand, the effect of m is complimented by larger values of n. This combined effect of n and m is significantly greater than that of either n or m alone.

1.1.4. Ductility at elevated temperature

The basic problem in ductility is to explain why for a given material, different strains are possible in different working processes before fracture occurs. One proposal (Refs.21.,22.) involves the application of a workability equation:-

$$\text{workability} = f_1(\text{material}) \times f_2(\text{process, friction,...}) \qquad (20)$$

Where f_1 is a function of the basic ductility of the metal, and f_2 that of the external factors which modify the basic ductility.

The two most widely used tests to measure ductility are tension and torsion tests; compression and bend tests have a limited use for assessing the ductility of relatively brittle materials.

The data obtained from hot tensile tests have been used both to determine optimum hot-working conditions and to grade materials for a particular working process. Thus, for example, in figure 7, the ductility passes through a minimum around 1050°C and then rises to a maximum at around 1350°C after which it falls sharply to zero in only 75-100°C. This so called "hot shortness" is associated with localised melting in segregated regions and defines the upper limit of the working range; the lower limit is set by the critical ductility for successful working in a given process.

Variation in strain rate can alter the relative values of measured tensile ductility and thus the critical ductility at a given temperature, though the same general form of ductility/temperature relationship remains. For meaningful results, specimens with a reduced gauge length must be used (Ref.23.), so that deformation is confined to a volume where the temperature can be held constant.

In contrast to tension, where deformation at high strains becomes localised in the necked region, very large torsional strains can be applied with essentially constant specimen geometry up to fracture.

Although, in torsion, the materials undergo larger strains before fracture than in tension, it is hard to place any fundamental significance on the number of twists to fracture when the number is very large. For instance, it is very difficult to differentiate between a specimen that twists 600 times and one that twists 400 times except to say that both are ductile. With less ductile materials, if the number of twists is reproducible within close limits then this number can be used as a quantitative measure of ductility.

1.2. Metallurgy of warm forming at $< 0.6\ T_m$

Most hot forming operations are carried out at high temperatures $> 0.6\ T_m$, where T_m is the melting temperature in degrees Kelvin and at relatively high strain rates (10^{-1} to 10^{3} sec^{-1})

Conventionally, cold working refers to room temperature forming, where strain hardening occurs in most materials. Warm forming, by arbitrary definition, is carried out at temperatures less than 0.6 T_m, but above the ambient temperature and at relatively slow strain rates (10^{-4} - 10^{-2} sec^{-1})

Difficulties associated with hot forming include scaling of material, rapid tool wear and the undesired grain growth that might occur subsequent to recrystallisation, especially if the difficulties of reduced ductility in cold forming can be avoided or minimised by using warm forming techniques.

In some ways, warm forming shows similarities to superplasticity as mentioned before. For example, the shape of warm forming stress strain curves, frequently resembles those obtained from tensile testing of superplastic materials. In both cases, large strains are achieved and grains in a superplastic material and the subgrains in certain warm formed materials remain equiaxed throughout deformation.

On the other hand, it is reasonable to suggest that warm-forming is more closely related to creep conditions because of relatively high stresses and the more common grain size range, and the presence of a dislocation substructure in warm formed metals is similar to that of creep specimens, whereas in superplastic materials a dislocation substructure is absent.

Two mechanisms have been proposed for the hot working process depending on the metal in question. In Al and α Fe, dynamic recovery is the softening mechanism. This occurs through the formation of well-developed subgrain structures by cross-slip and climb, as occurs in creep. The activation energy of hot working in these materials is equal to that for creep and self diffusion, whilst in materials with a lower stacking fault energy as Cu, Ni and austentic stainless steel, the activation energy for softening in hot work is higher than for creep. For these metals the softening process is dynamic recrystallisation.

There is still much discussion (Ref.24.) as to whether recrystallisation does occur continuously and similtaneously during hot working, and of the alternative softening process, which would have to operate. For example, it is contended that in some materials conventional recrystallisation occurs after straining ceases.

1.2.1. Dynamic recovery and recrystallisation

Considerable work in recent years (Refs.25-27.) has led to an increased understanding of the mechanism of hot working. The predominant softening mechanism is dynamic recovery. When dynamic recovery has occurred, the microstructure consists of elongated grains with a fine substructure.

Transmission electron microscopy shows the grains divided by dislocation sub-boundaries into subgrains with diameters in the order of 1 to 10 μm. Becuase this sub-structure resembles that found in cold worked metals which have been annealed to a static recovery structure, the process has been called dynamic recovery.

Dynamic recovery is the main softening mechanism, where climb and cross slip of dislocations are relatively easy. As a result, the misorientation of the subboundaries are maintained at a sufficiently low angle so that they never become capable of migrating as grain boundaries of recrystallisation nuclei.

In superplastity, the relationship between stress and strain rate figure (8) can be interpreted on the basis of dynamic recovery. At high stresses deformation is faster and at low stresses is slower than that given by extrapolating the superplastic range (Ref.28.). This suggests that recovery properties of the matrix are dependant on stress and may be related to the observed changes in metallographic structure in each of these ranges, indicating that the shape of configurations of the second phase are an important factor.

In the superplastic region, the second phase appears round and bulbous (Ref.28.) as in figure (9a), whereas at high stresses it becomes elongated, figure (9b), in the direction of the tensile axis, and in the lightly stressed range remains unaltered from the annealed configuration, i.e. angular and interlocking figure (9c).

In cold worked materials, the dislocation densities are much larger and hence these have a higher stored energy than the annealed materials.

From thermodynamic reasoning, the specimen will tend towards a minimum stored elastic energy under the favourable conditions of an elevated temperature. The dislocations of like sign would tend to stack above each other; a process which requires dislocation climb and substantial diffusion. Vacancies that were created during the cold working operation can contribute to this process by aiding diffusion and by migrating to edge dislocations.

When these cold-worked materials are heated up the dislocations and point defects introduced by deformation either annihilate each other or rearrange themselves into some low-energy configurations. A considerable amount of stored energy is then released, and the crystal softens.

The low-energy stable configuration of dislocations are called low angle boundaries and can be represented by a uniform array of one or more sets of dislocations. These boundaries separate regions of the crystal which differ in orientation by only a few degrees.

When plastically deformed metals are deformed at higher temperature, dislocations can glide completely out of each grain (Ref.29.) so as to allow the formation of completely new grains of very low dislocation density; they have high-angle boundaries with misorientations normally more than 10°. This process is known as dynamic recrystallisation.

It has been suggested that dynamic recrystallisation is an important component of the superplastic deformation of certain alloys (Ref.30,31.). In addition, it has been suggested that recrystallisation occurs in some commercial alloys (Ref.32,33.) during at least the initial stages of superplastic deformation. Nevertheless, recrystallisation does not appear to be important in most superplastic materials.

By prolonged heating the recrystallised grains grow in size by the migration of their boundaries, leading to grain growth. When grain growth takes place, on average at a uniform rate throughout the material, it will result in a more or less uniform grain size. But when the migration is restricted to some boundaries, a nonuniform structure of grains will be produced - this is called abnormal grain growth.

It was found that the alloying elements present in the matrix affect the recrystallisation process to a large extent (Ref.34.). For instance, manganese in solid solution was observed to be more effective in raising the recrystallisation temperature of aluminium, due to interaction between solute atoms and high-angle boundaries caused by the difference in the atomic radii of Mn and Al atoms (Ref.35.). Zirconium, however, is reported to inhibit recrystallisation by precipitation of a second phase, $ZrAl_3$, in the matrix (Ref.36.). The amount of zirconium present is also important.

1.2.2. Cavitation

Metals often fail during forming in the temperature range of 0.3 - 0.9 Tm because of the formation of cavities (or voids) at grain boundaries. The significance of cavities in limiting the ductility of metals was first realized about 25 years ago by Greenwood (Refs. 37-40.). Since this time much work has gone into understanding their nucleation and growth and also the mechanisms by which failure is initiated.

The general features of cavitation failure are an increasing loss of ductility with increasing temperature and decreasing strain rate.

Voids show a distinct preference to form on the grain boundaries approximately perpendicular to the applied stress. The onset of cavitation coincides with the onset of grain boundary sliding but not all boundaries develop cavities (Ref.41.)

The nucleation and subsequent growth mechanisms can be considered separately.

Nucleation of cavities

The original proposal was that lattice vacancies agglomerated under the influence of the applied stress on to grain boundaries perpendicular to that stress. These vacancy groupswould then grow by further vacancy condensation. Further work (Refs.42,43.) concluded that homogeneous void nucleation by vacancy diffusion is impossible due to the high supersaturation of vacancies that is required. Since then, all models have assumed nucleation to be heterogeneous and based on the grain boundaries sliding and the stress applied(Ref.44).

Other workers (Refs.45,46.) associated cavitation with slip lines; and intersecting slip line trace would cause a jog in the grain boundary which could be opened up into a void by grain boundary sliding. It is argued here that grain boundary jogs would be removed by grain boundary migration or recrystallisation. Migration could be prevented by solute atom segregation to a boundary and, in preventing migration, the likelihood of cavitation would be increased. Transmission electron microscopy showed that the majority (75%) of voids nucleated on cusps in grain boundaries resulting from sub-boundary intersection (Refs.47,48.).

In summary, experiments have shown that grain boundary sliding with a net stress across the grain boundary is essential for the nucleation of cavities. Cavities form on grain boundaries which are approximately perpendicular to the tensile axis, begin to form very early in the test and continue to form at a rate which is proportional to the strain.

The sliding of grain boundaries causes stress concentrations to be set up at irregularities in the boundaries. These local stresses cause separation to occur and cavities to initiate.

Grain boundary sliding will cause cavities to develop at irregularities whenever plastic flow or diffusion is not fast enough to prevent it.

Two types of mechanisms have been invoked. First, steps or ledges in grain boundaries have been supposed to result from intersection of slip traces or subgrain boundaries with the grain boundary. Secondly, local breakdown of coherency associated with precipitates or inpurity particles, possibly of low coherence with the matrix, has been suggested and removal of such particles increases ductility, due possibly to grain boundary migration which increases ductility by preventing cavitation.

Cavity Growth

Greenwood (Refs. 37-39) had envisaged both nucleation and growth of cavities to be occurring by vacancy condensation at high temperatures and low strain rates. Growth should also be aided by local stress concentrations at void peripheries.

Experimental support for the vacancy growth model comes from a number of pieces of work and it was also found that void volume was linearly related to strain at a given temperature and stress level.

The shape of voids was studied by Taplin et al (Ref.51.). They found that cavities were very irregular in shape and they did not accept that diffusional processes were responsible. They put forward a number of other mechanisms:-

(a) crack propagation from void apices

(b) tearing

(c) internal necking with enhanced inter-cavity sliding

(d) grain boundary sliding

A further study of void shapes showed different types of cavities mixed together. Crystallographic voids resulting from diffusional growth and irregular orientated cavities due to sliding and, on occasions, both types together.

Recently, Dyson and Taplin (Ref.52) derived a cavity growth mechanism map, figure (10). Here cavity growth is assumed to depend upon temperature and strain rate, whether it is viscous or diffusive growth.

The main feature of the rupture of superplastic alloys via cavitation is the extended stage of cavity linkage. In this case it seems that the ligaments between the cavities are as resistant to internal necking as is the bulk material to external necking. It is clear that at some stage linkage begins and an autocatalytic response arises, giving rapid fracture with little or no external necking. The simple model of Rogers (Ref. 53.) figure (11) applied to a material containing a high volume fraction of cavities provides some insight here. One factor of importance may be grain coarsening. Any microstructure coarsening destroys the superplastic properties of the material by reducing its strain rate sensitivity.

Thus, two processes are occurring:-

(1) The cavities are very slowly merging together and the ligaments thinning, whilst the strain rate sensitivity of the ligaments is decreasing.

(2) At some point, rapid linkage occurs and a chain reaction follows.

1.2.3. Fracture at elevated temperature

The end result of stressing a metal, whether it flows plastically or not, is fracture. The fracture in deformed specimens at elevated temperature, is usually associated with the development of intergranular cracks and cavities.

In earlier studies, fracture was discussed simply in terms of the linking together of cavities to form a crack. The propagation of such cracks was attributed to stress concentrations at the crack tips.

Later on, a theory of propagation (Ref. 54.), in which a crack of a few atoms wide and of the order of 100 - 1000 °A long was shown able to grow as the result of the stress field generated by the piling-up of dislocations. The simplest analysis of interlinkage involves internal necking of the ligaments between the cavities. Rogers (Ref. 53.) presented a simple illustration, figure, (11) of the effect of fracture centre distribution on both overall ductility and macroscopic necking. This is termed the void sheet mechanism. Later on, Taplin (Ref. 56.) attributed the onset of fracture to the case with which voids are able to interlink to form a crack capable of spontaneous propagation. An aspect of crack propagation by cavity linkage is the effect of grain size. In some materials, cavities link until the grain boundary is filled. If the critical Griffith crack lenght is exceeded in the process then failure follows. If not, then an interaction between cavity groups on different boundaries is necessary for crack propagation.

This aspect was studied by Cocks and Taplin (Ref. 57.) who followed this feature of the grain size effect. Small grain sizes do require such an interlinkage between grain edges for failure by plastic tearing. At very small grain sizes a different mechanism is preferred. This is the ductile sheet effect where failure is dominantly related to the reduced specimen cross-section rather than to cavity linkage. However, at these small grain sizes, the microstructure is not completely stable and boundary migration may occur to repel failure.

In coarse grained materials, failure is a question of critical crack-length. In fine grained materials in which such a critical crack cannot be formed on the given grain edges because they are too short, failure occurs by the ductile sheet mode.

Cracking between cavities to lead to failure is not confined to simple systems. Bonisrewski et al (Ref. 58.) showed that a three dimensional crack network between cavities was responsible for failure in CrMoV steel, while Tipler et al (Ref. 59.) working with the same alloy found that the resulting fracture resembled a honeycomb.

1.3. Biaxial forming of sheet metal

This section provides a very brief description of deep drawing, stretch forming and bulging of diaphragms at both elevated and ambient temperatures.

1.3.1 Deep drawing

The simplest deep drawing process is the production of a cylindrical cup from a flat circular blank of isotropic sheet metal. The essential tools are shown diagrammatically in figure (12). The dominant stress system is radial tension combined with circumferential compression in the drawing zone, while that in the base and lower cup wall is biaxial tension. The latter stress is equivalent to a through-thickness compression, plus a hydrostatic tension which does not affect the state of yielding. Drawing failure occurs when the central stretch-forming zone is insufficiently strong to support the load needed to draw the outer part of the blank through the die.

To improve drawability, the potential failure site near the bottom of the cup wall must be strengthened relative to the metal deforming by radial drawing near the cup wall (Ref.60) and some improvement can be obtained by shifting the failure site up the cup wall. Roughening the punch by giving the punch nose a knurled finish, or no lubrication between blank and punch (Ref.61.) may improve the drawability. However, by far the greatest improvement comes by controlling the crystallographic texture in the sheet that is to be drawn. The correct texture gives the proper orientation of slip systems so that the strength in the thickness direction is greater than that in the plane of the sheet.

The resistance to through thickness thinning is measured by the $\underline{r}$-value, the coefficient of normal anisotropy. It is given by:-

$$\underline{r} = \frac{w}{t} = \ln(w_o/w)/\ln(t_0/t)$$

$$= \ln(w_0/w)/\ln(wl/w_0l)$$

Where w_0, l_0, t_0 are the original dimensions of width, length and thickness and w, l and t are the corresponding dimensions after straining, which are derived assuming that no change in volume occurs. If $\underline{r}$ 1 then the material strains in the thickness direction in preference to straining in plane of the sheet, if $\underline{r}$ 1 the reverse is correct, and if $\underline{r}$ = 1, than the material is isotropic.

It was found (Ref.62.) that the r-value correlated very well with the material performance in a simple drawing operation and hence, for a given blank diameter, a deeper cup would result from a high r-value material. The formation of "ears" at the free edges of a drawn cup is caused by planar anisotropy. In drawing of a cylindrical cup, four ears usually form in steel and aluminium and two ears in zinc. Earing can be directly correlated with the planar anisotropy, measured by Δr (Ref.63.).

$$\Delta r = (r_0 + r_{90} - 2r_{45}) / 2$$

Anisotropy can also influence stretch forming, because the distribution of strain is affected by the variation of the flow stress in different stress states as well as by the strain-hardening behaviour, (Ref.64.). So in the case of bulging, if the difference between the flow stress under plane strain i.e., at the periphery of the bulge and that under equi-biaxial tension at the pole is low, then an even distribution of strain is promoted.

It was found by Heyer (Ref.65.) that under punch stretching conditions, with steels ranging in r, from 1 to 2, stretchability was reduced as r increased. As r increased, the failure site moved away from the pole i.e., the strain distribution became worse. In this case, however, this may only be indirectly due to the anisotropy, since coincident with the increase in r is an increase in flow stress and hence in punch load which in turn causes an increase in friction which changes the strain distribution.

1.3.1.1. Deep drawing at elevated temperatures

If the deformation temperature is increased the ductility generally increases and the limit of deformation should also increase; Dorn (Ref.1.) showed that deep drawability of aluminium alloys was improved at 200°C. However deep drawing of superplastic materials at $> 0.5\ T_m$, poses problems because, in order to draw in the flange, the material in contact with the punch must strain harden, as must the material forming the cup walls. At such deformation temperature ($> 0.5\ T_m$) the materials do not strain-harden, and, in the absence of strain-hardening, the blank will not draw and the process will be similar to stretch forming. i.e., the punch will either pierce the blank, or, if the friction between the blank and punch nose is high, the cup walls will stretch and finally fail.

There are however, a number of ways in which the problem of deep drawing at elevated temperature can be overcome. These include:-

(1) The application of pressure to the periphery of the blank - the pressure-augmented, deep-drawing process. Here, the material is pushed into the die throat rather than being pulled by the punch (Ref.66.). It could be argued that this is a hydrostatic extrusion process and not deep drawing.

(2) Simulation of the effects of strain hardening by using a temperature gradient. If the punch is maintained at a temperature below the critical forming temperature, as material contacts the punch, it is cooled and hence its flow strength increases with respect to the material not in contact with the punch (Ref.67.).

(3) The sliding velocities between the blank and various parts of deep-drawing tools are highly variable e.g. the vertical walls of cup slide at a speed equal to the draw velocity whereas the sliding speed gradually diminishes around the die radii and in the undeformed part of the flange. In strain-rate sensitive materials, this variation in velocities will give rise to flow stress variations and the results will be similar to strain hardening of the material. Oshita et al (Ref.68.) studied the effects of strain rate and drawing temperature on deep drawing of superplastic Zn-Al alloys but the results were not so good as those from the pressure-augmented process.

1.3.2. Biaxial bulge test and stretch forming

The biaxial bulge test, in essence, consists in taking a circular sheet of material, clamping it around its edge and bulging it by hydraulic pressure from one side.

Grids of radius and hoop circles, or small circles or squares, are usually scribed or photo-printed on the blanks, to facilitate strain distribution measurements.

Measurements of the hydraulic pressure make it possible to calculate the membrane stress near to the pole (with knowledge of the curvature and the thickness).

Deformation of bulging is noted for giving a longer strain to instability than is possible in conventional uniaxial tensile testing, and many theoretical treatments have attempted to analyse this mode (Refs. 69-71).

The biaxial bulge test is also an example of a pure stretch-forming operation, so that the strain hardening coefficient 'n' may be taken as a measure of stretch formability, i.e. the greater n, the greater is the thinning and hence the stretching when the maximum load is attained.

The stretch forming of a circular blank by a hemispherical punch, figure (13), presents a situation similar to that of the bulge test. This is stretching under biaxial tension, with the flange securely clamped to prevent the material from moving into the die cavity as the punch descends. In this case, deformation is restricted to the area of the material within the die, and it takes place over the punch nose.

The great drawback, however concerns the prevailing frictional conditions, which are related to the interfacial pressure between sheet and punch surface (Ref.72.).

The end of useful straining in a stretch forming operation is difficult to define. Certainly with annealed material a maximum in the fluid pressure in the bulge test may signal the instability condition, but with many materials it must be acknowledged that some further straining is obtained under falling pressure. General instability conditions were first discussed by Swift (Ref.73.) and many others have done so since.

Because sheet-forming is mainly a plane stress operation, wrinkling or compressive instability, local tensile instability and failure in regions of biaxial tensile strain may be associated with specific parts of the yield ellipse.

Interest in the end of useful straining was made more quantitative by the idea of limit strains, related to forming limit diagrams. With the help of a grid of lines or circles, photographed or etched on to the sheet which is to be pressed, a combination can be found for major and minor strains in the plane of the sheet, which at some point is critical. A diagram constructed for a given metal appears as in figure (14). If at a region in a real pressing a pair of strains is known to be imposed, then, if the combination falls below the critical line in the forming limit diagram, a pressing can be achieved with safety. If the point (or strain pair) falls on or above the line, then changes in die geometry, lubrication or material are required for success. (Refs. 74-75).

Keeler and Goodwin considered the failure criteria to be only affected by the ability of the material to distribute the strain uniformly and ignored the effect of material properties.

It has been reported by Pearce (76), that limit strains are expected to vary with material, strain ratio, and the method used to obtain the diagram. Woodthorpe and Pearce (77) showed the effect of n and r on limit strains during biaxial stretching. The higher the n-value the higher the level of the forming limit diagram. This was explained on the basis of increased strain hardening capacity helping in distributing the strain more uniformly. Later, Painter and Pearce (Ref. 78) indicated the effect of inclusion content and pearlite morphology on the level of forming limit diagrams of high-strength, low-alloy steel sheets.

The technique used to produce forming limit diagram has also been found to affect the limit strain. Pearce and Ganguli (Ref. 79) produced forming limit diagrams for a series of Al/Mg alloys by both friction and frictionless forming. In the case of frictionless forming, (hydraulic bulging), the level of the forming limit was 10-20% lower than in the test involving friction. They also found that the level of FLD fell with increasing Mg content in the aluminium/magnesium series of alloys.

The effect of the amount of prestrain was discussed theoretically by Dillamore (Ref. 80) in an attempt to predict FLD's, according to which, the increase in prestrain for a given inhomogeneity (f) was found to produce a considerable decrease in the value of plane strain limit.

1.3.2.1. Bulging at elevated temperature

Material bulged at an elevated temperature has a low strength and a large capacity for stretching. The application of the pressure forming or 'blowing' technique used in the polymer and glass industries was used in forming superplastic metals at elevated temperatures (Refs. 81,82). In many superplastic materials, the strain rate range must be kept within the range appropriate to the particular material. The relationship between pressure, strain and time should therefore be controlled, so that the strain rate is within the chosen range.

Simplifying assumptions are usually used to obtain an approximate analysis of the process and also to determine the shape of bulged sheet and the distribution of sheet thickness.

An analysis of bulging of a circular sheet clamped at its perimeter was first published by Jovane (Ref. 83) who assumed that the sheet thickness remained uniform. Later Holt (Ref. 84) presented an analysis for bulging in which he considered the nonuniformity in sheet thickness, as follows:-

The sheet is bulged to a pole height of H at a constant pressure, P, figure (1.5). An element of the sheet initially at a radius r_0 where the sheet thickness is the initial value t_0, is displaced to a radius r where the sheet thickness is t. The inclination of the sheet surface is θ.

Let σ_h be the circumferential or hoop stress in the bulge and let σ_t be the tangential stress in the plane of figure 15. The corresponding strains are ε_1 and ε_2. Then:-

$$\varepsilon_1 = \ln r/r_0 \quad \text{and} \quad \dot{\varepsilon}_1 = \dot{r}/r \qquad \text{—(1)}$$

For equilibrium under vertical forces:-

$$P.\ r^2.\pi = \sigma_t\ (2\pi\ r\ t \sin\theta)$$

$$\sigma_t = \frac{Pr}{2t \sin\theta} \qquad \text{—(2)}$$

Making the approximation that the stress and strain rate is balanced biaxial, then:-

$$\varepsilon_1 = \varepsilon_2 \quad \text{and} \quad \sigma_1 = \sigma_2 \qquad \text{—(3)}$$

Equation 3 is only exact at the pole, for at the clamped perimeter, plane strain prevails. The strain in the sheet thickness direction is given by:-

$$\varepsilon_3 = -2\,\varepsilon_1 = -2\,\varepsilon_2 \qquad \text{—(4)}$$

The stress state in the sheet (from equation 3) is equivalent to a hydrostatic tension added to compressive stress, $\bar{\sigma}_3$, in the sheet thickness direction, where

$$\bar{\sigma}_3 = -\sigma_1 = -\sigma_2 \qquad \text{—(5)}$$

A hydrostatic stress does not cause flow so that the flow equation ($\bar{\sigma}_3 = K\,\dot{\varepsilon}_3^{\,m}$) can be written as if the sheet were undergoing a through-thickness compression test.

$$\bar{\sigma}_3 = K\,\dot{\varepsilon}_3^{\,m} \qquad \text{—(6)}$$

Combining equation (1) through (6) we get:-

$$\frac{Pr}{2t\,\sin\theta} = K\left(\frac{2\dot{r}}{r}\right)^m \qquad \text{—(7)}$$

From equation (1) and (4):-

$$\frac{t}{t_0} = \left(\frac{r_0}{r}\right)^2 \qquad \text{—(8)}$$

Substituting in equation 7:-

$$\frac{Pr^3}{2t_0\,r_0^2\,\sin\theta} = K\left(\frac{2\dot{r}}{r}\right)^m \qquad \text{—(9)}$$

Which can be written in the form

$$\frac{2r}{D} = \frac{1}{2}\left(\frac{rD}{4\ t_0 K}\right)^{1/m} \left(\frac{2r}{D}\right)^{(3/m)+1} \left(\frac{2r_0}{D}\right) \sin\Theta^{-1/m}$$

This equation was used to follow the development of a bulge under a constant pressure. A numerical, iterative method of solution was adopted. The procedure is very similar to that used by Woo (Ref. 85).

The calculated relationship between the mean tangential strain and pressure compensated time for the condition m = 0.5 is shown in Fig. (16) (Ref. 84). The points on the curve were obtained experimentally with some pb-Sn alloy.

1.3.2.2. Stretching at elevated temperature

In general sheet metal formability increases with increasing temperature. However in some materials, deformation at elevated temperatures can give rise to the operation of strengthening mechanisms such as dynamic strain-ageing, which is often expected to cause a reduction in ductility in uniform stretching. In practical sheet forming however, it might be exploited to give improved strain distribution, greater overall depth of pressing and higher final strength of the component.

Dorn and co workers (Ref. 1) demonstrated, some thirty years ago, that the deep-drawing properties of aluminium alloys improved substantially with increased temperature up to 200°C and more recently, Taylor et al (Ref. 86) and Ayres (Ref. 87) have shown tensile elongation of the Al/Mg alloys could be increased by testing at elevated temperatures and low strain rates.

Further work of Ayres et al (Ref. 88) has produced FLD's of 5182-0 aluminium alloy sheet as a function of punch rate and temperature, figure (17). At higher rates the level of the FLD is similar to room temperature behaviour. At 200°C, the FLD becomes a much stronger function of punch rate. It is also indicated that at 130°C and 200°C, there is a tendency for the biaxial portion of FLD to extend to larger values of minor strain for slower punch rates, but it is not quite clear whether this is because of differing test conditions (i.e. strain path) or material behaviour at such temperatures.

More recently, an attempt by Ayres (Ref. 89) to form an oil pan from 5182-0 aluminium alloy at 180°C and 130°C was made. He examined the strains in critical regions, zones 1, 2 and 3 in figure (18); the minor and the major strains from those regionswere plotted in figure (19).

The strains at regions 1 and 2 were lower than the ambient FLD, while region 3 showed a marked increase of strains. The locus shown of $\varepsilon_3 = 0$ indicates the border between sheet thickening and thinning. At these elevated temperatures the flange was able to thicken to such a degree that quite large strains are achieved.

A report by Willis (Ref. 90) shows a hot hydraulic bulge test, carried out at 200°C. He concludes that higher temperatures reduce the forming pressure and improves the depth of draw, figure (20).

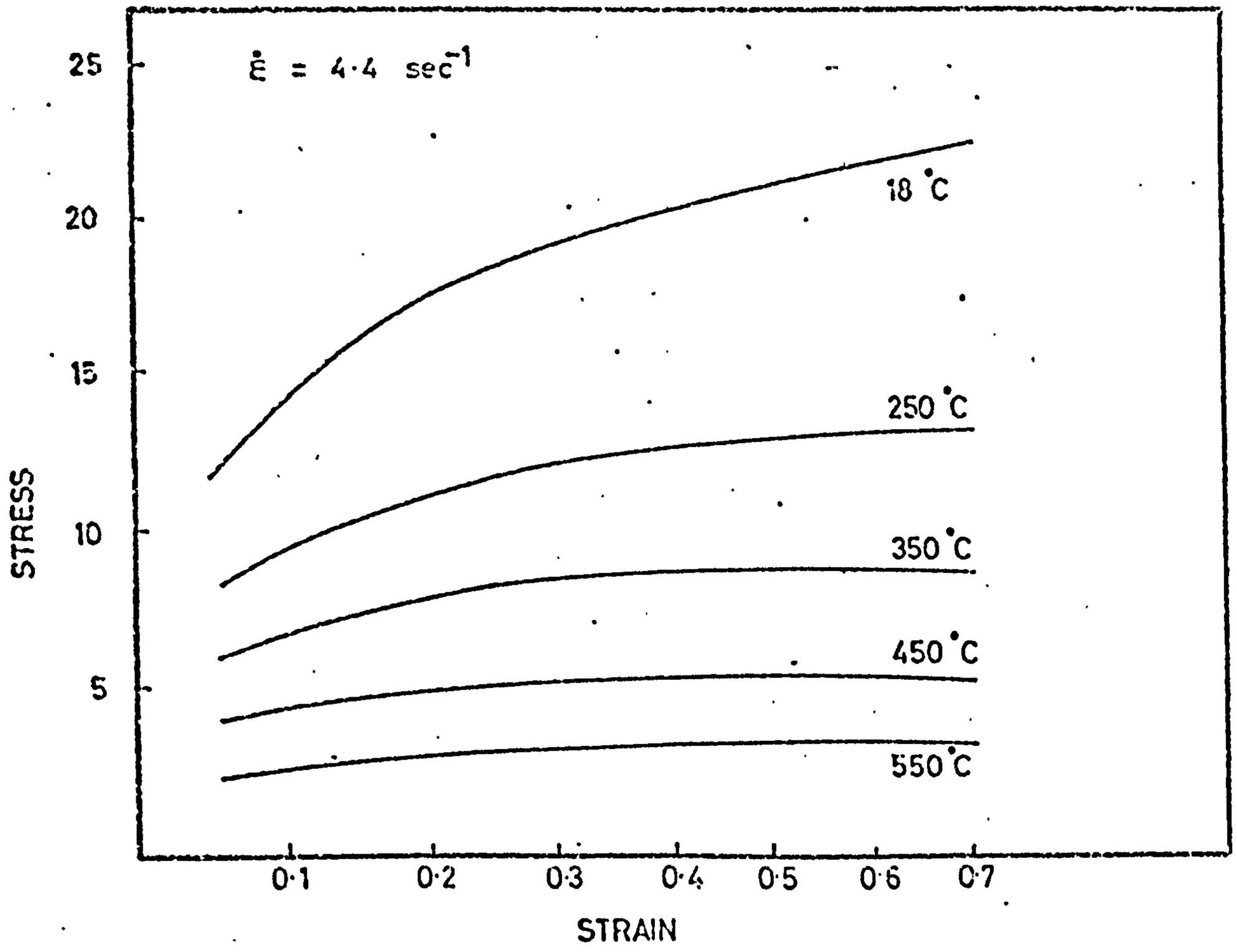


FIG.1. STRESS - STRAIN CURVES FOR ALUMINIUM (REF 4)

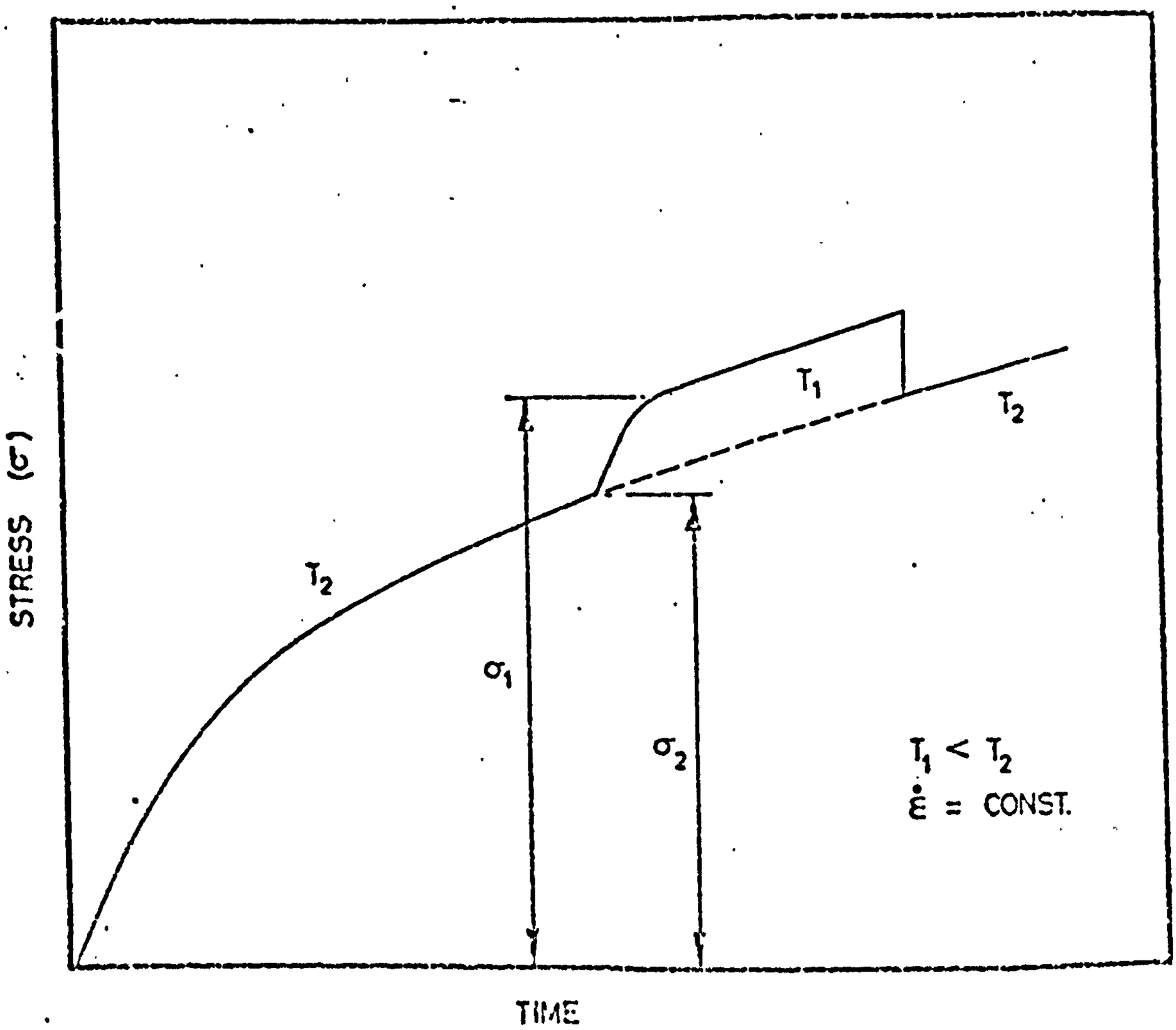


FIG. 2. THE TEMPERATURE CHANGE TEST.

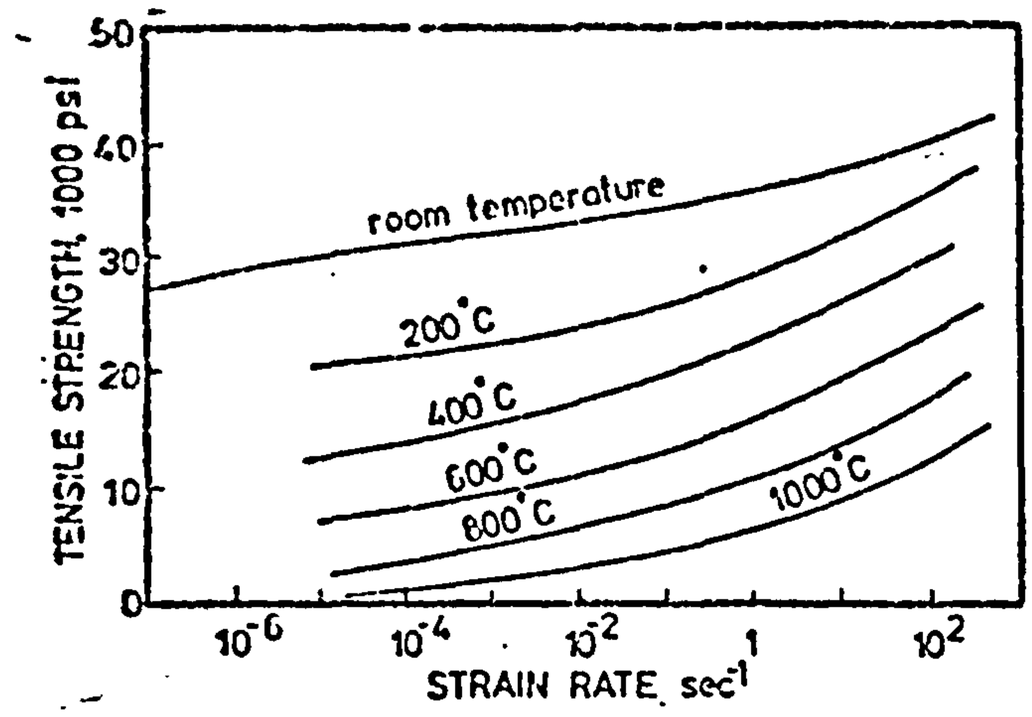


FIG.3. EFFECT OF STRAIN RATE ON THE TENSILE STRENGTH OF COPPER. (REF. 6.)

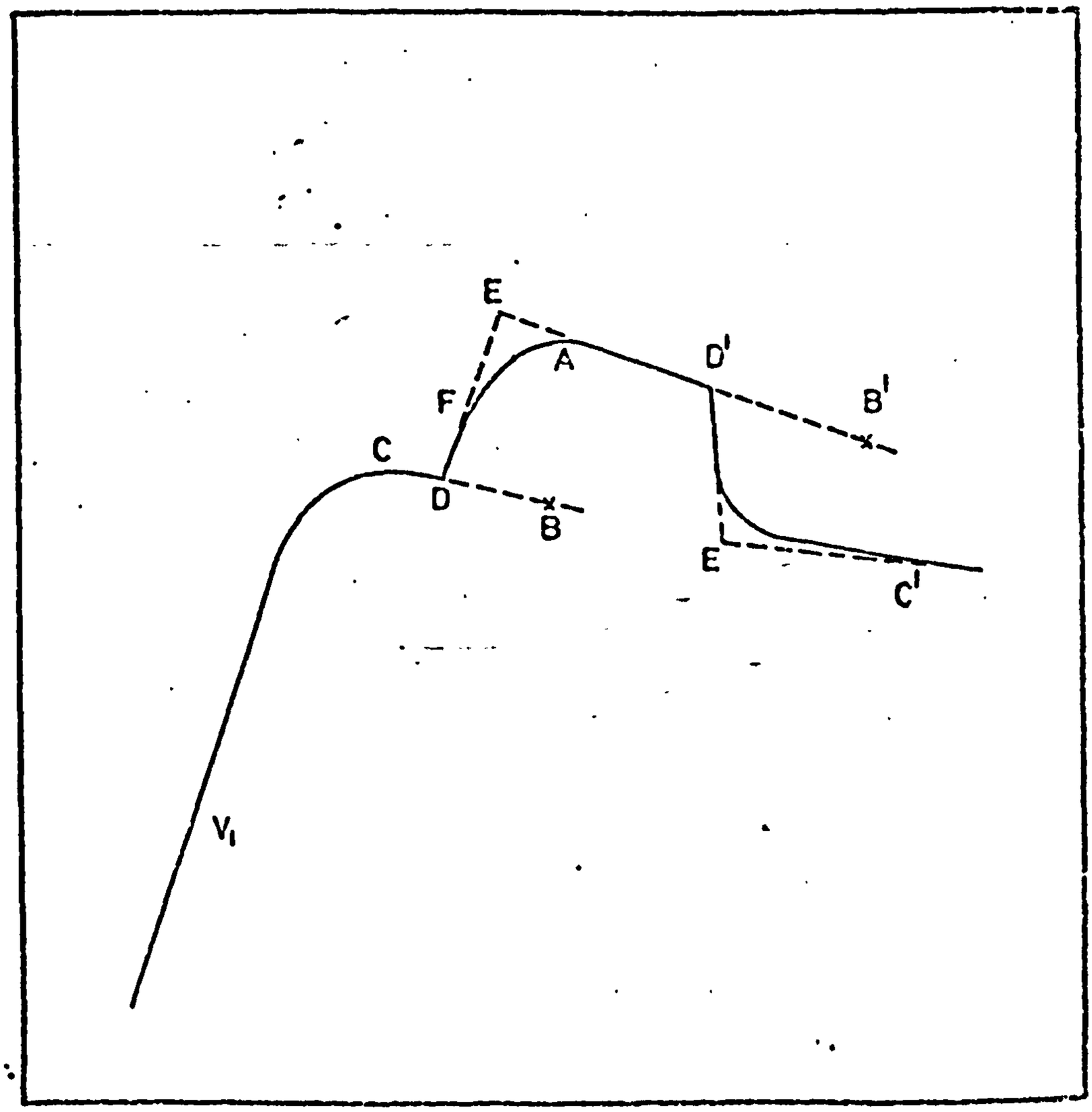


FIG.4. THE STRAIN RATE CYCLING TEST.

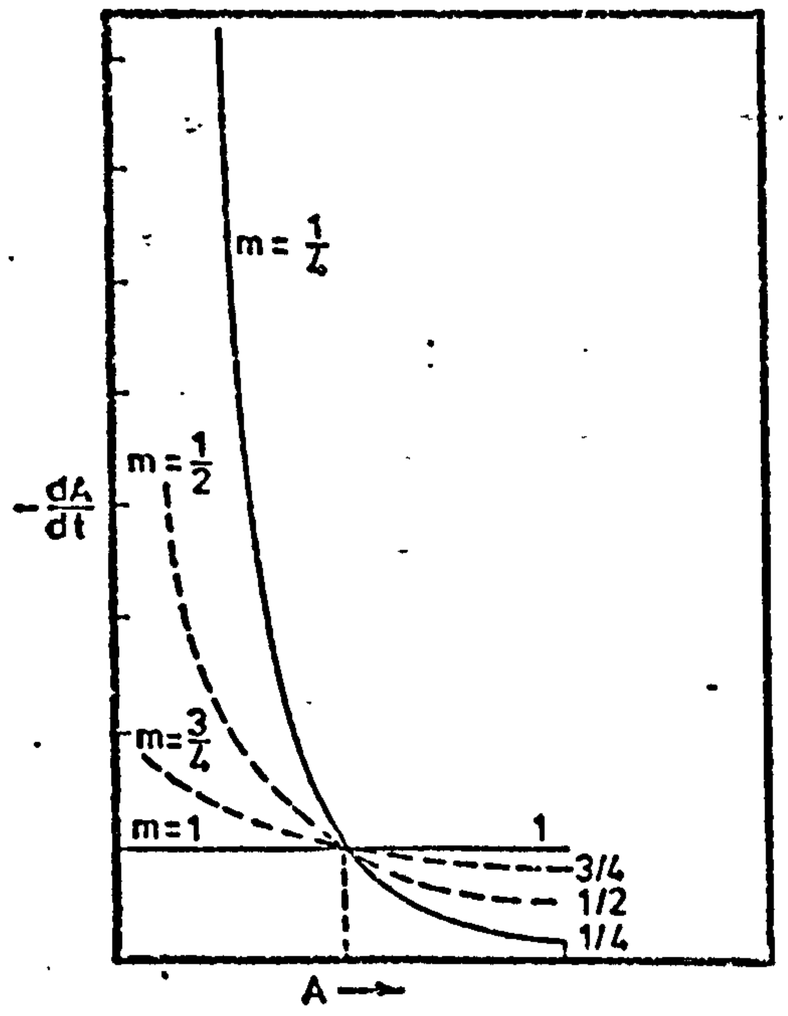
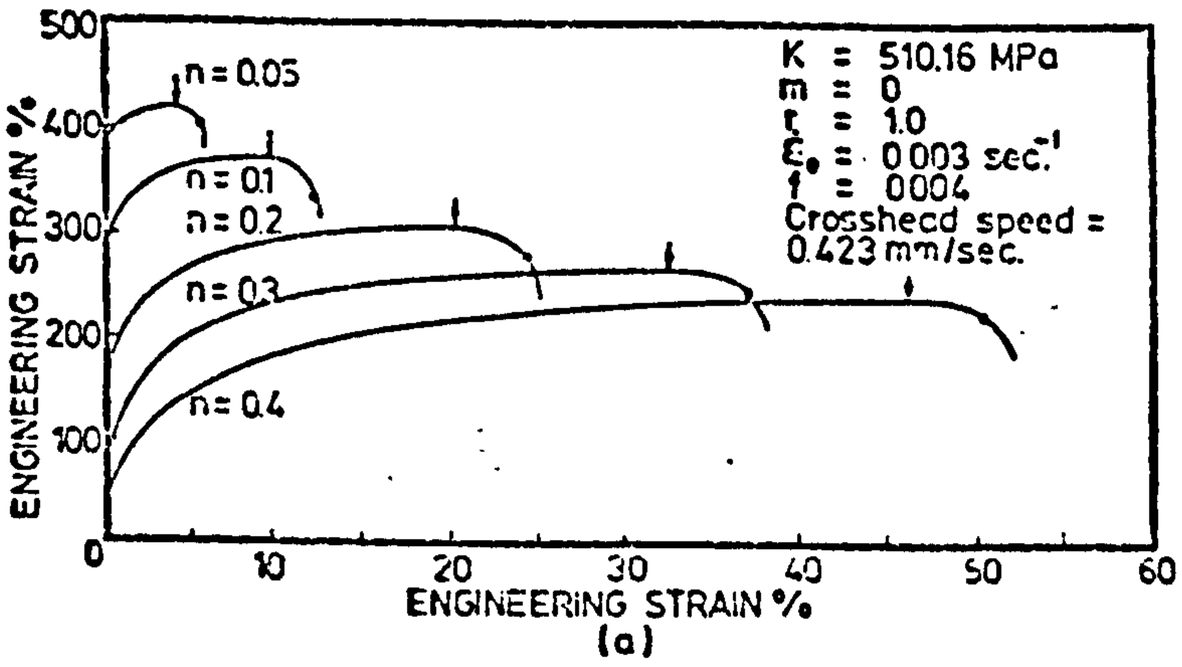
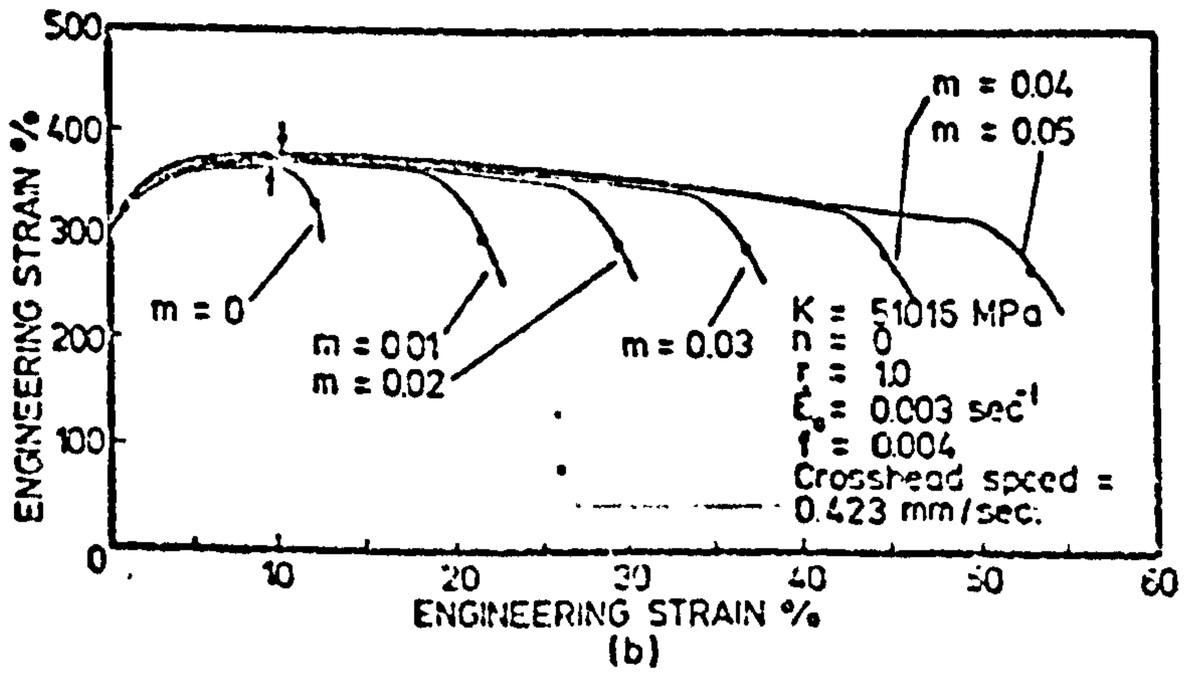


FIG. 5. RATE OF DECREASE OF AREA AGAINST CROSS-SECTIONAL AREA FOR DIFFERENT VALUES OF m. (REF. 19)





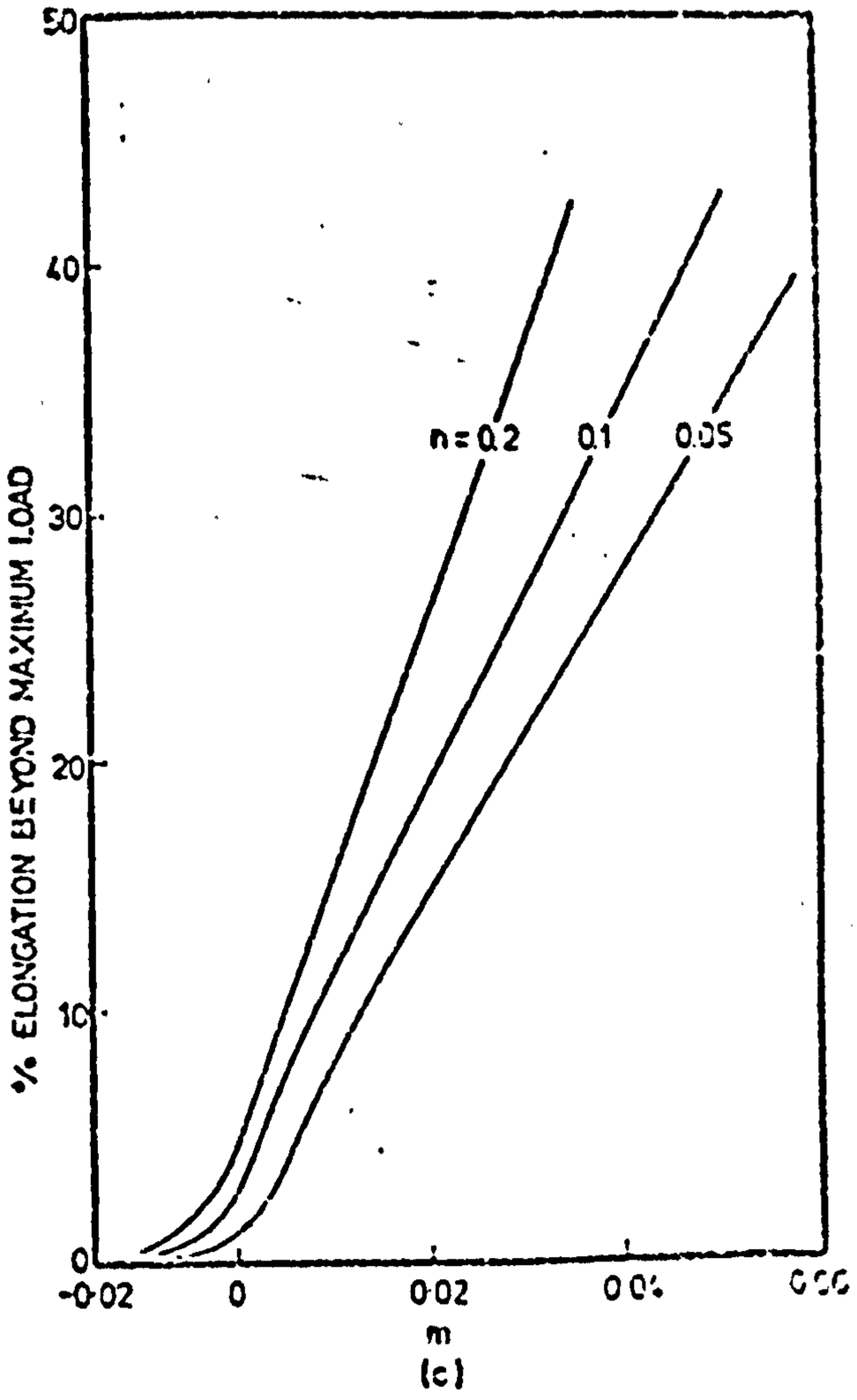


FIG. 6. EFFECT OF m AND n ON ELONGATION. (REF. 20)

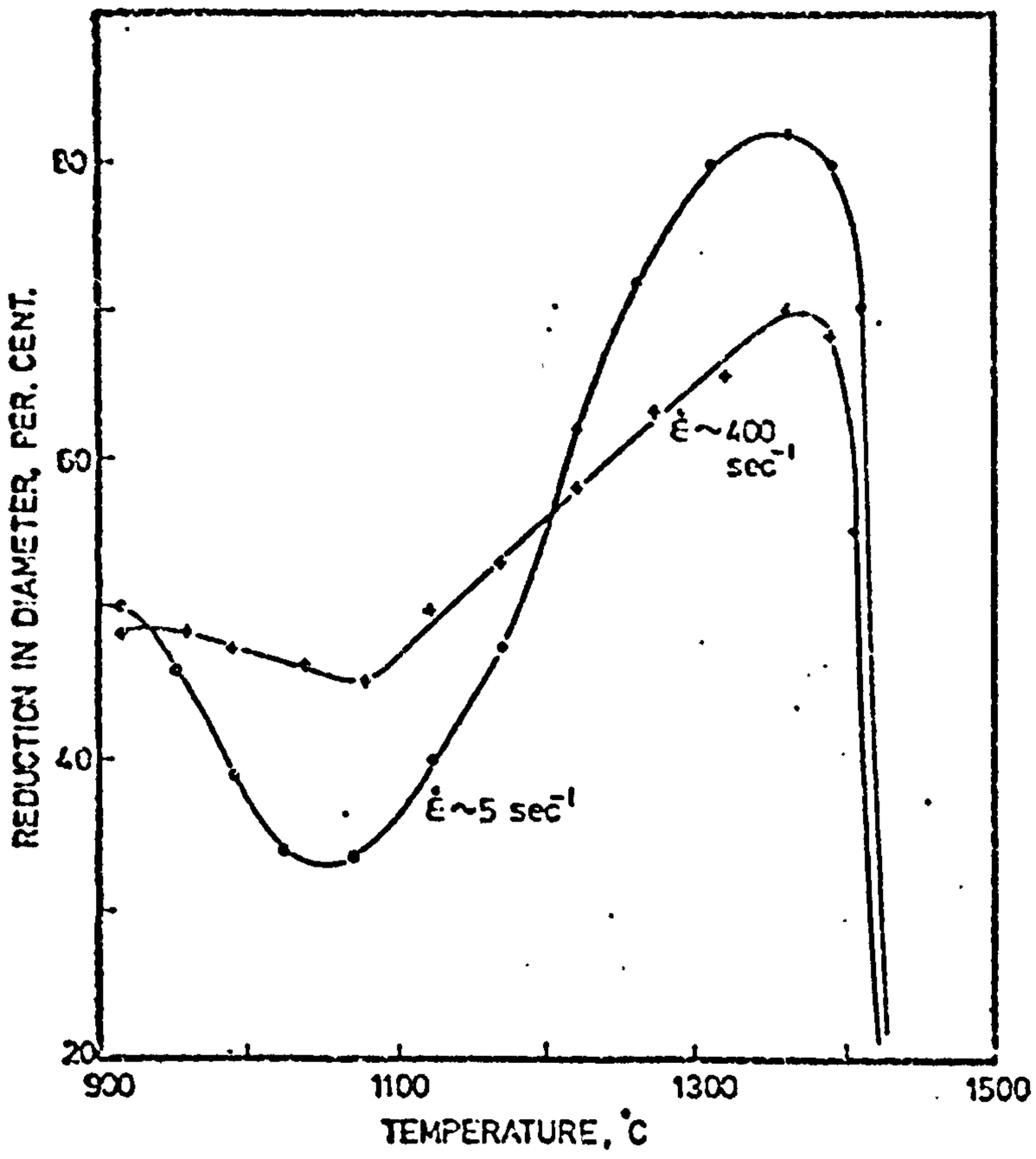


FIG.7. DUCTILITY OF A 0·14C, 0·56Si, 0·65Mn, 10·3Ni, 18Cr STEEL DEFORMED IN TENSION AT TWO STRAIN RATES. (REF.27)

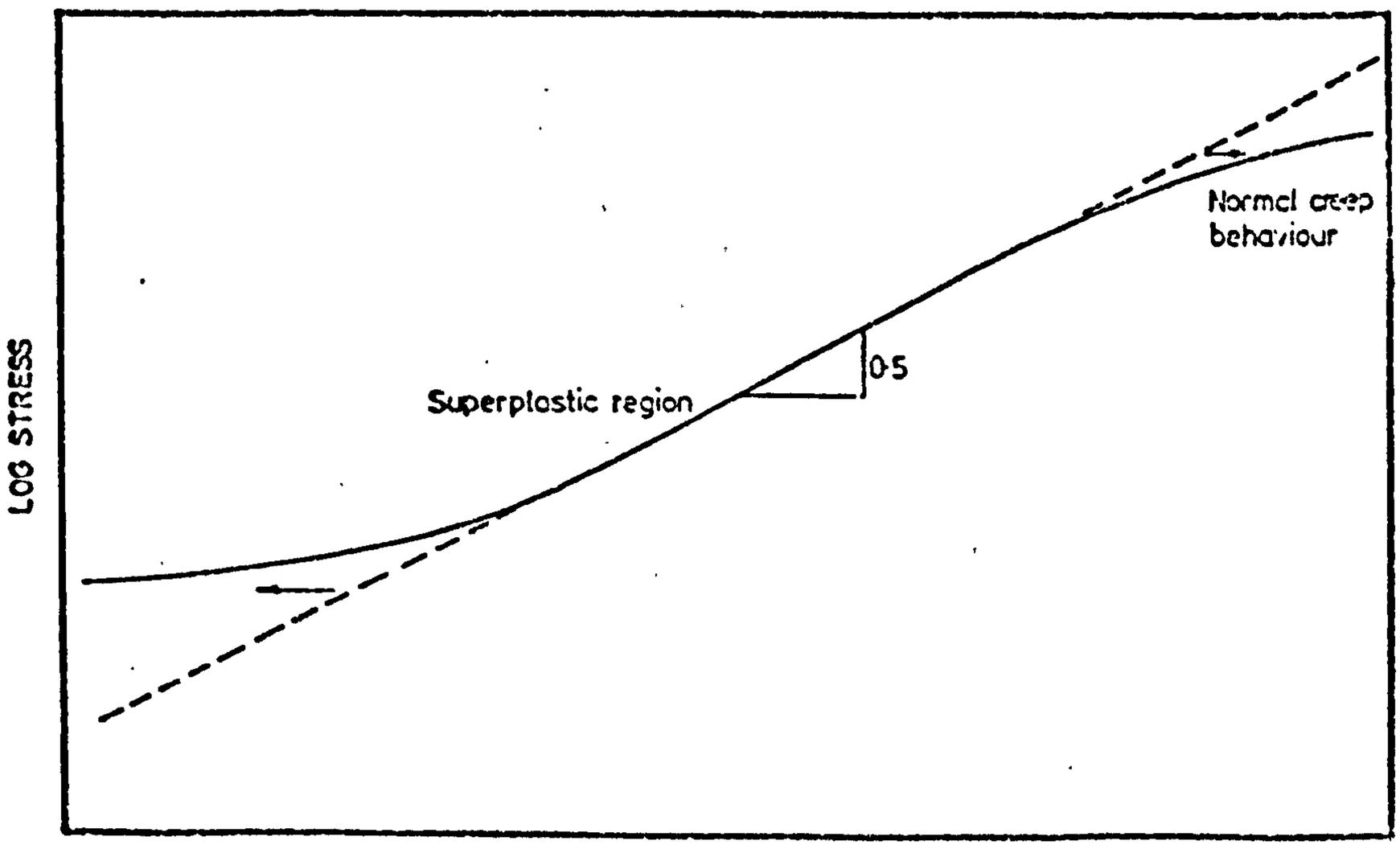


FIG.8. SCHEMATIC RELATIONSHIP BETWEEN STRAIN RATE AND STRESS. (REF. 28)



(a) (b) (c)

Figure 9 Microstructures of various regions in a superplastic alloy (Ref.28).

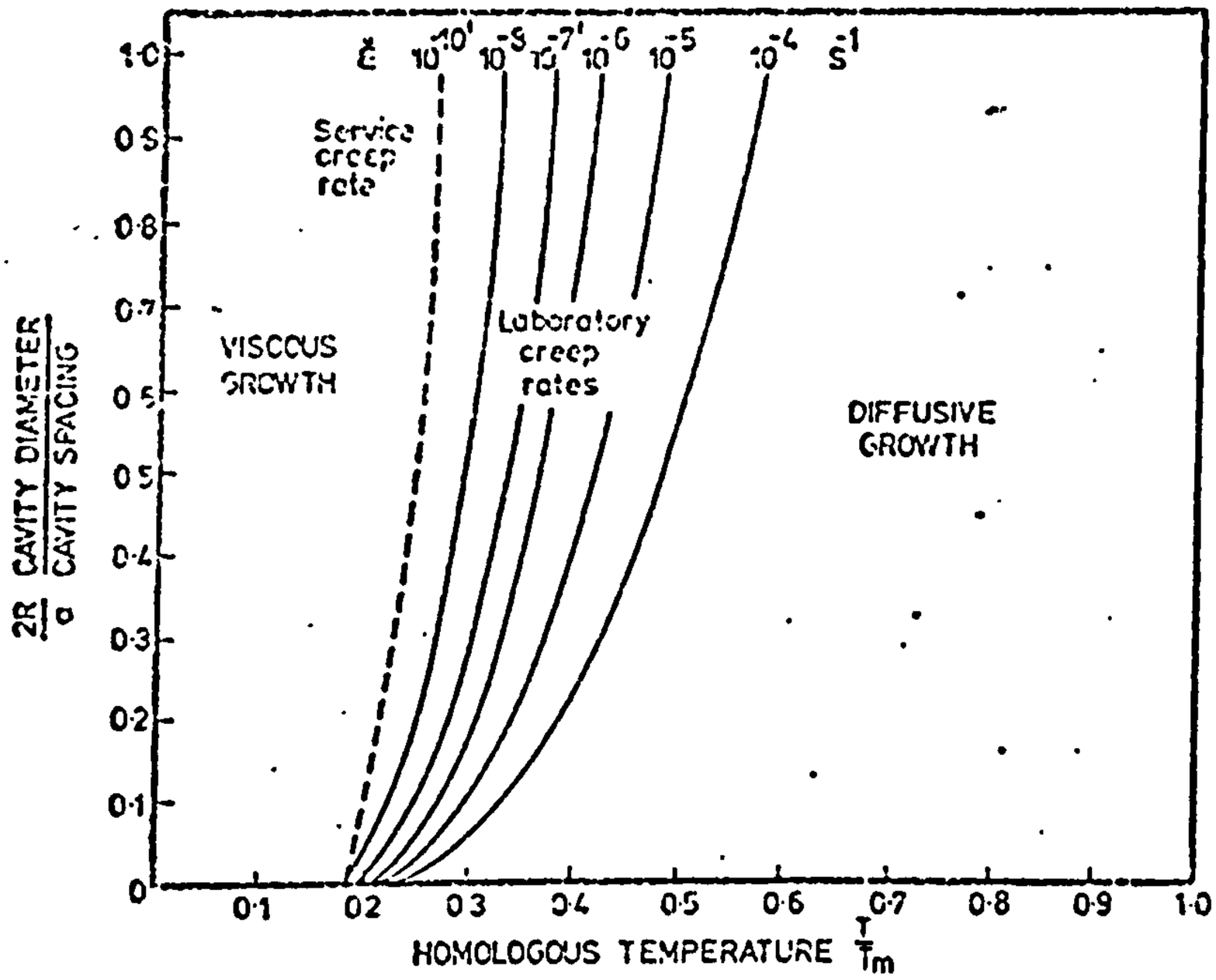


FIG.10. NON-NEWTONIAN VISCOUS AND DIFFUSIVE GROWTH (REF.51)

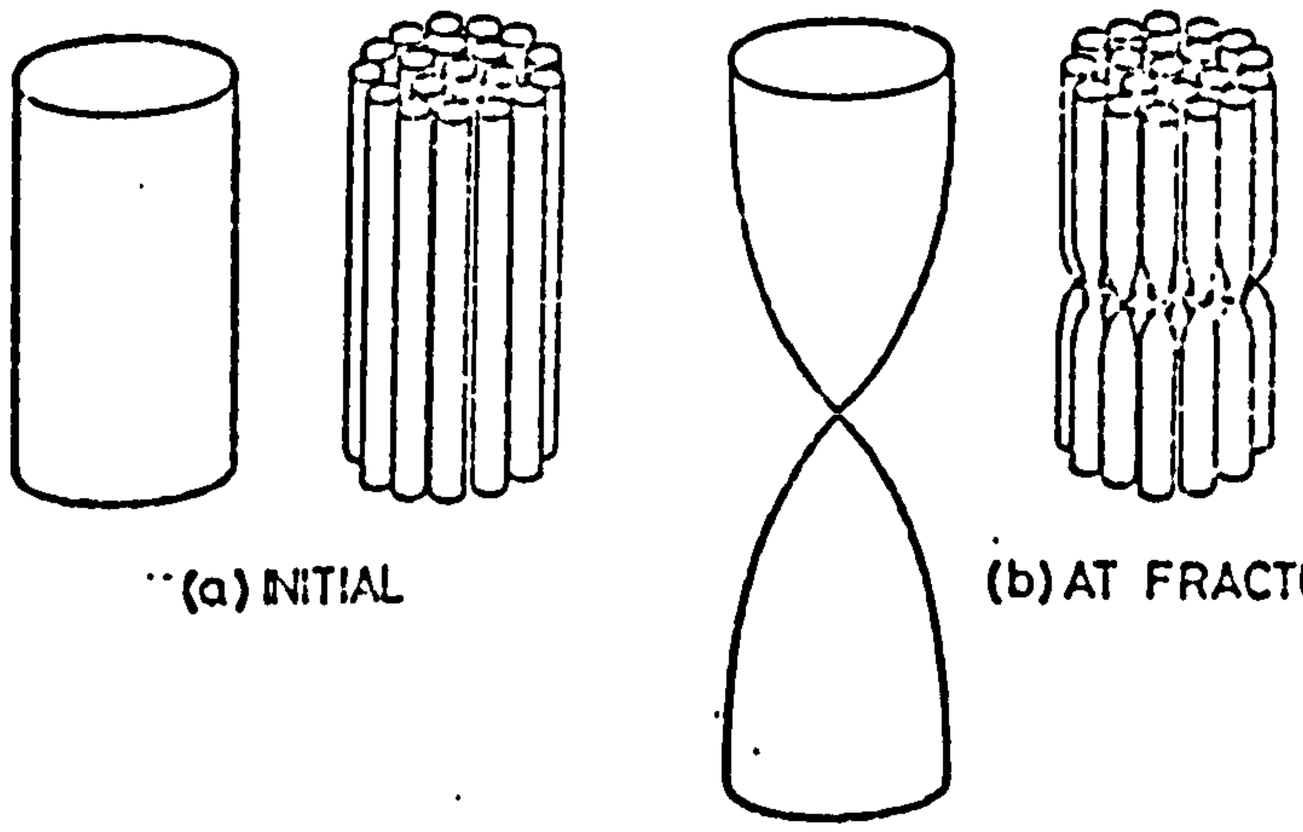


FIG.11. SCHEMATIC ILLUSTRATION OF FRACTURE OF A SOLID CYLINDER AND A 'CABLE' SPECIMEN. (REF.53)

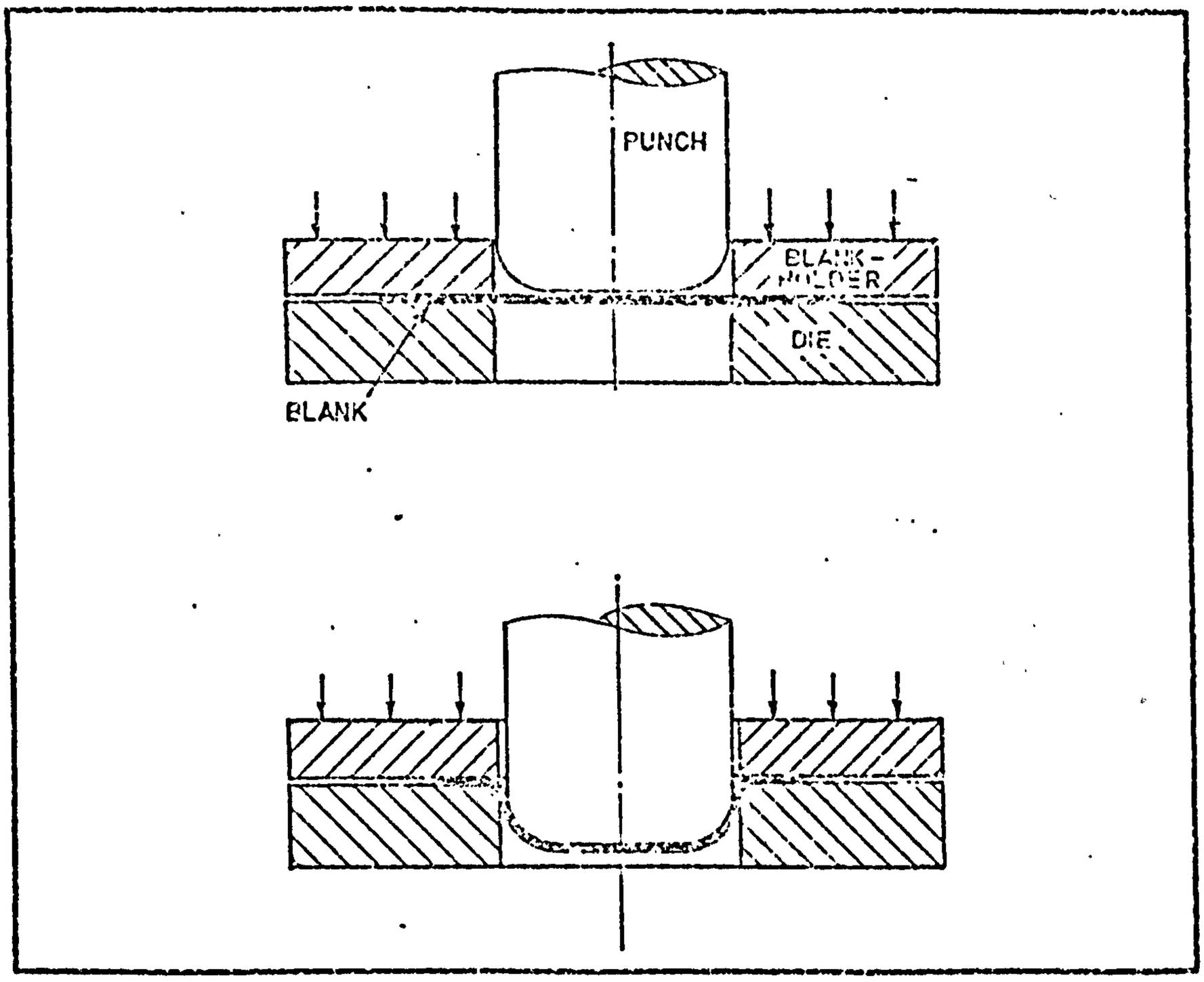


FIG. 12. DEEP DRAWING PROCESS

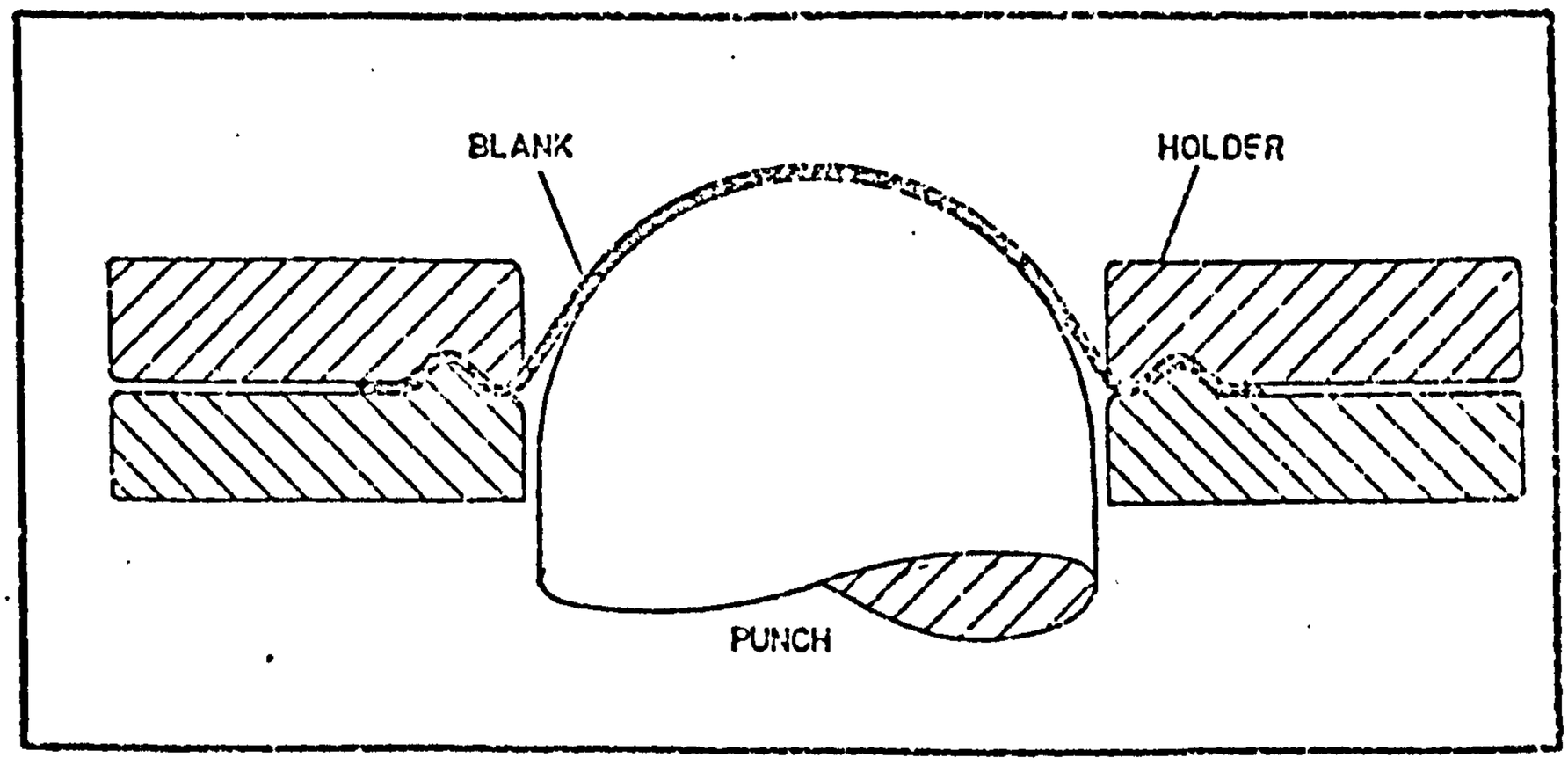


FIG.13. PUNCH - STRETCHING PROCESS.

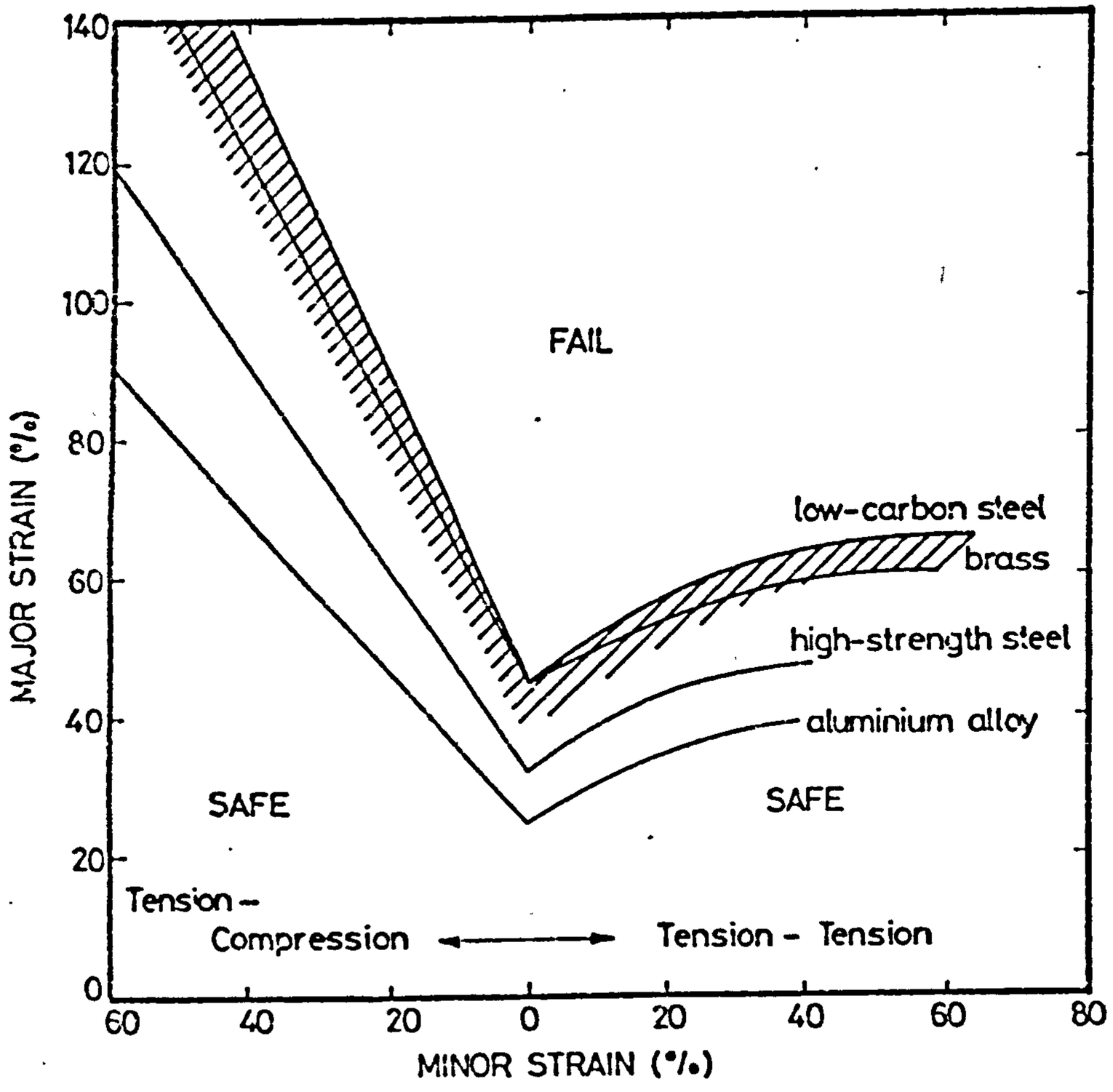


FIG.14. FORMING LIMIT DIAGRAM FOR DIFFERENT MATERIALS.

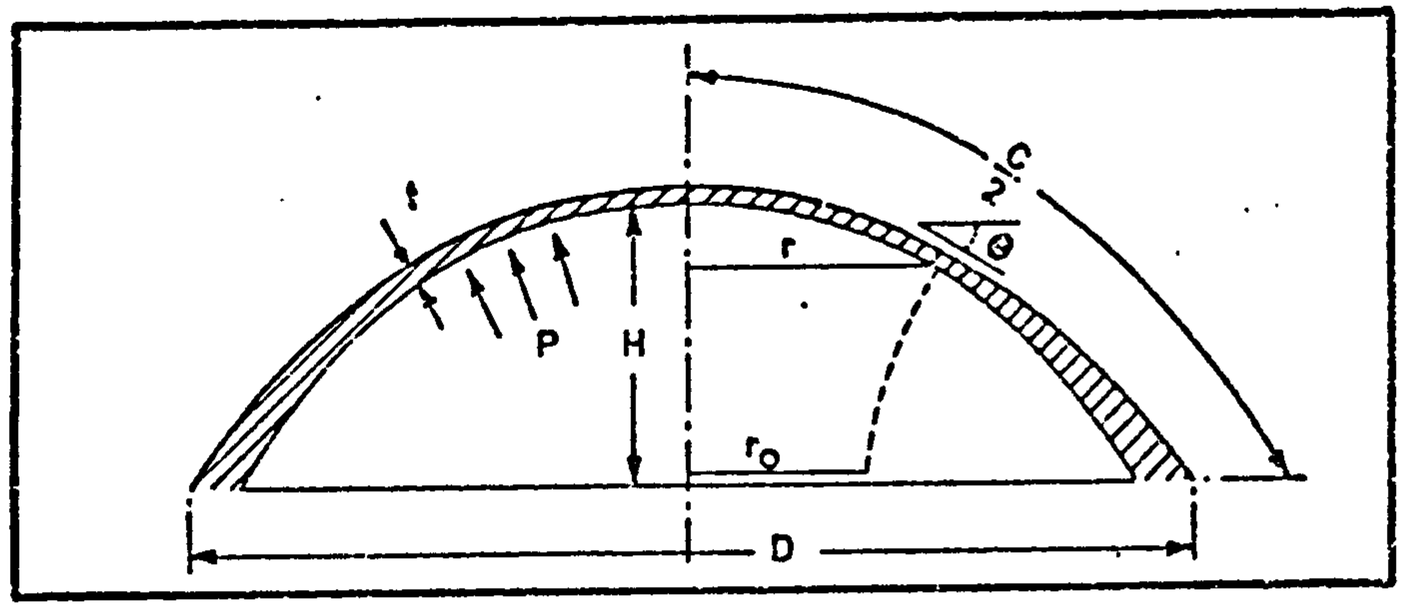


FIG.15. A SCHEMATIC DIAGRAM FOR BULGE PROFILE.

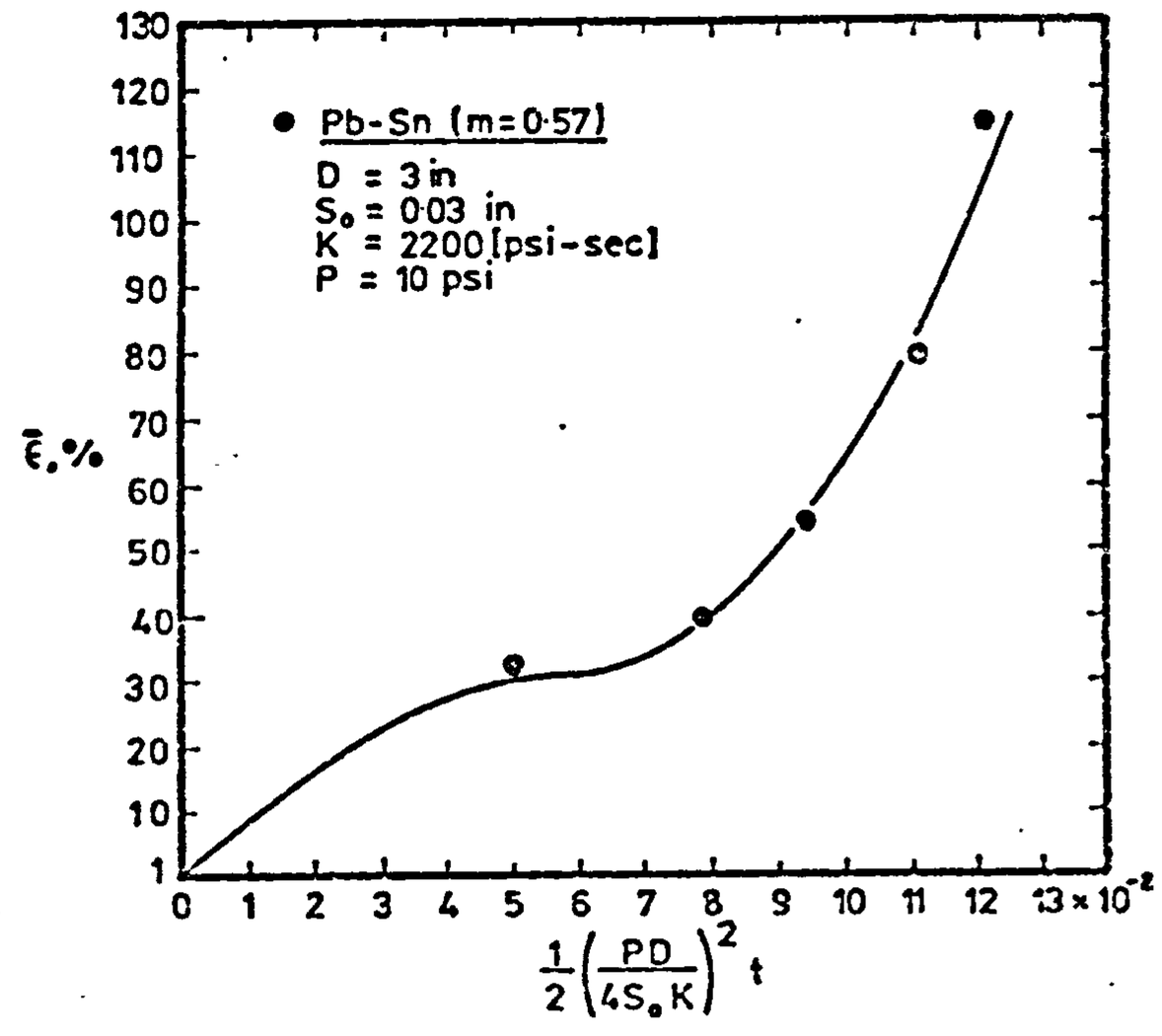
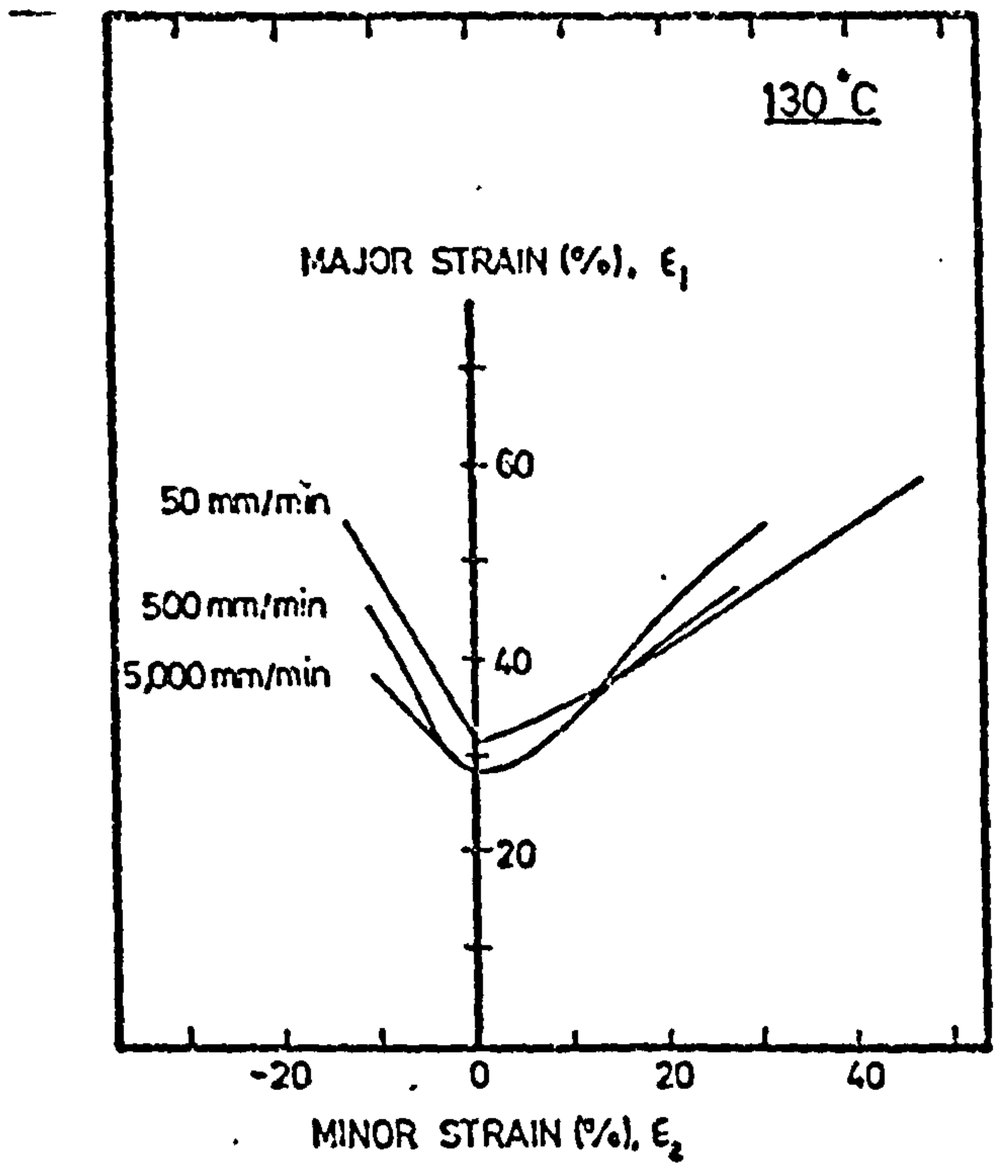


FIG.16. THE CALCULATED RELATIONSHIP BETWEEN MEAN TANGENTIAL STRAIN AND PRESSURE-COMPENSATED TIME. POINTS WERE OBTAINED EXPERIMENTALLY.



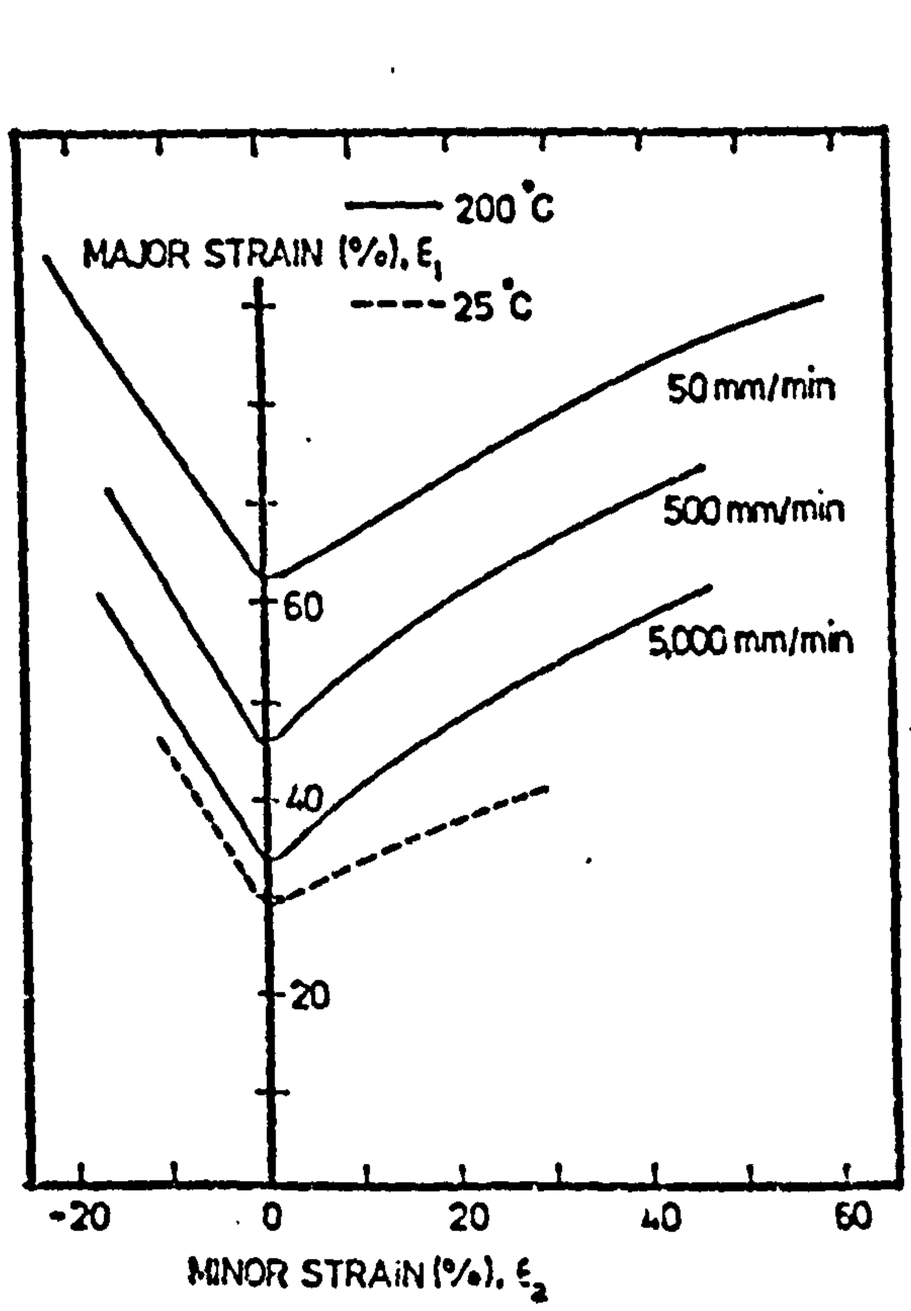


FIG.17. FLD's OF ALUMINIUM ALLOY AS A FUNCTION OF PUNCH RATE AND TEMPERATURE (REF.[88])

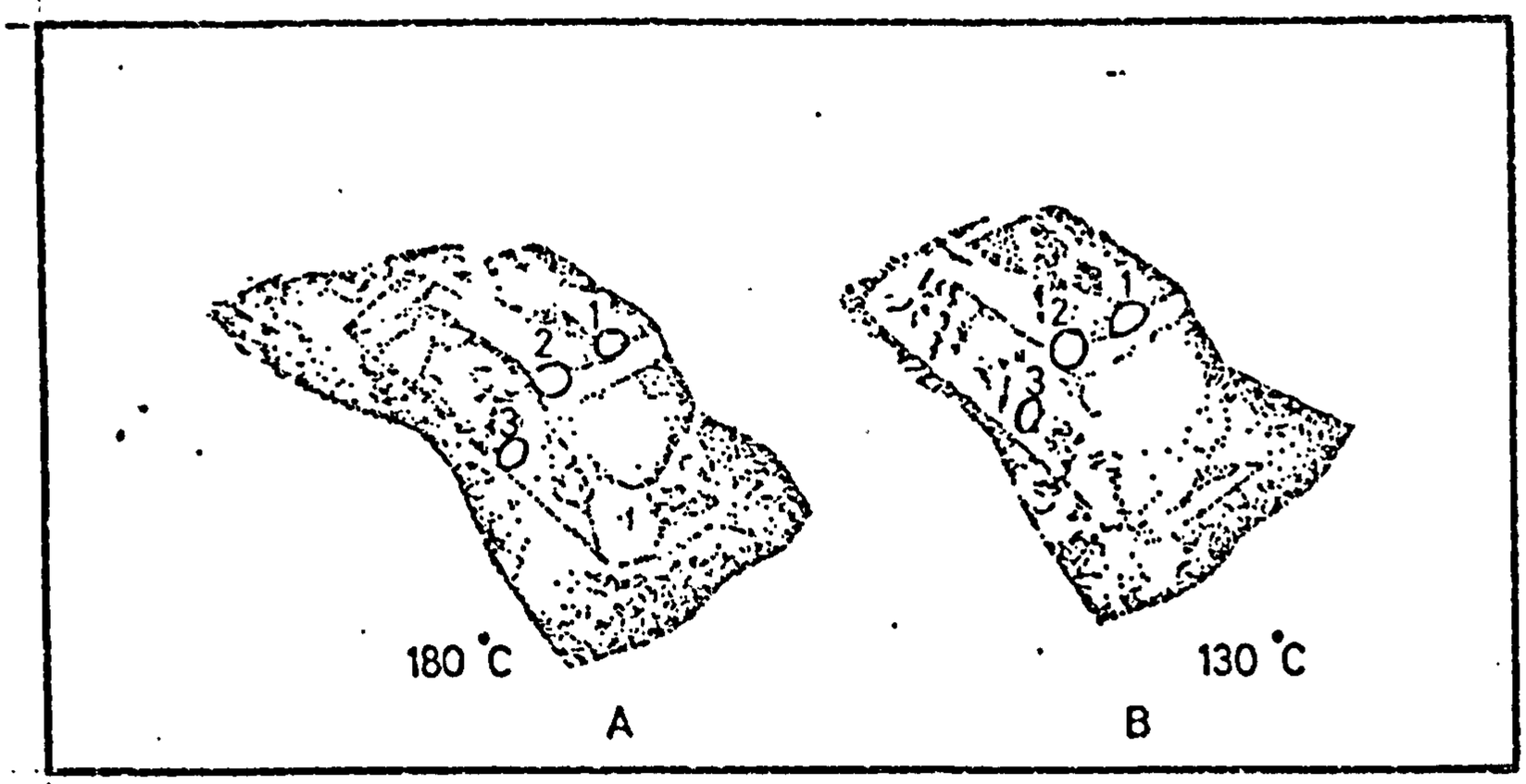


FIG. 18. OIL PANS FORMED AT VARIOUS TEMPERATURES SHOWING CRITICAL REGIONS 1, 2, & 3 (REF.89)

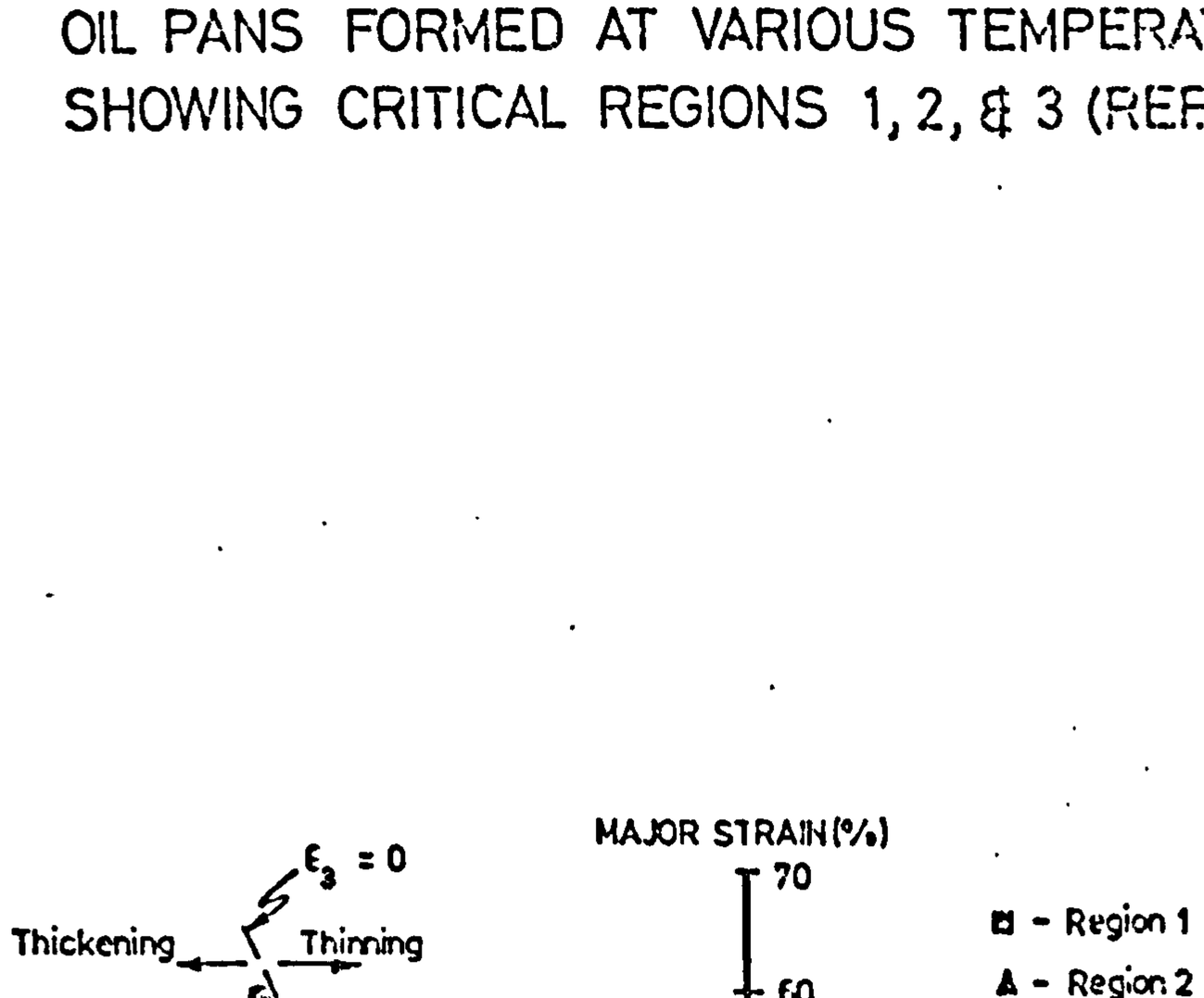


FIG.19. STRAINS IN CRITICAL REGIONS 1-3 OF AN OIL PAN SUCCESSFULLY FORMED AT 180 °C

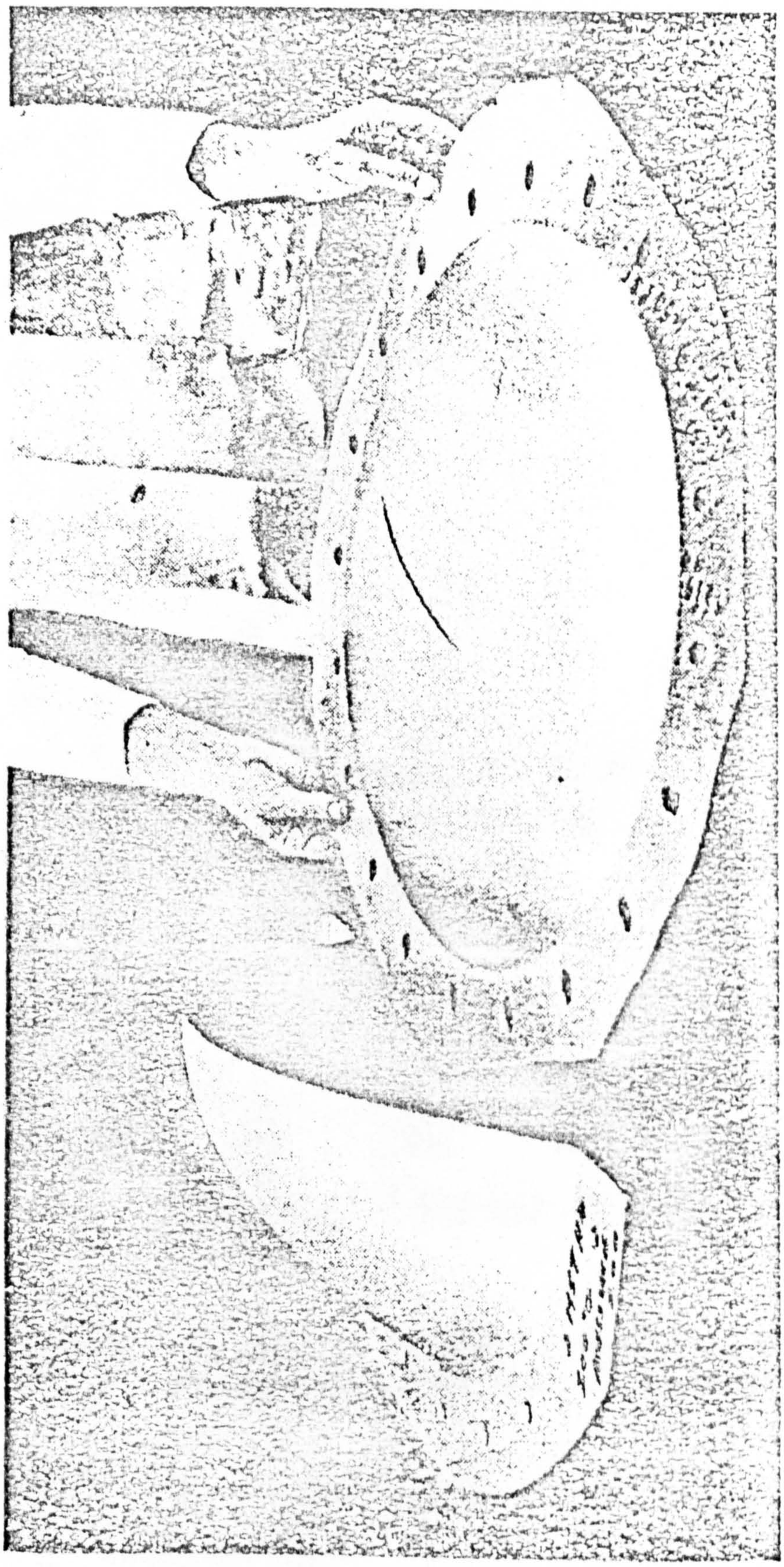


Figure 20 Typical hot hydraulic bulge test, carried out at 200°C, (Ref.90).

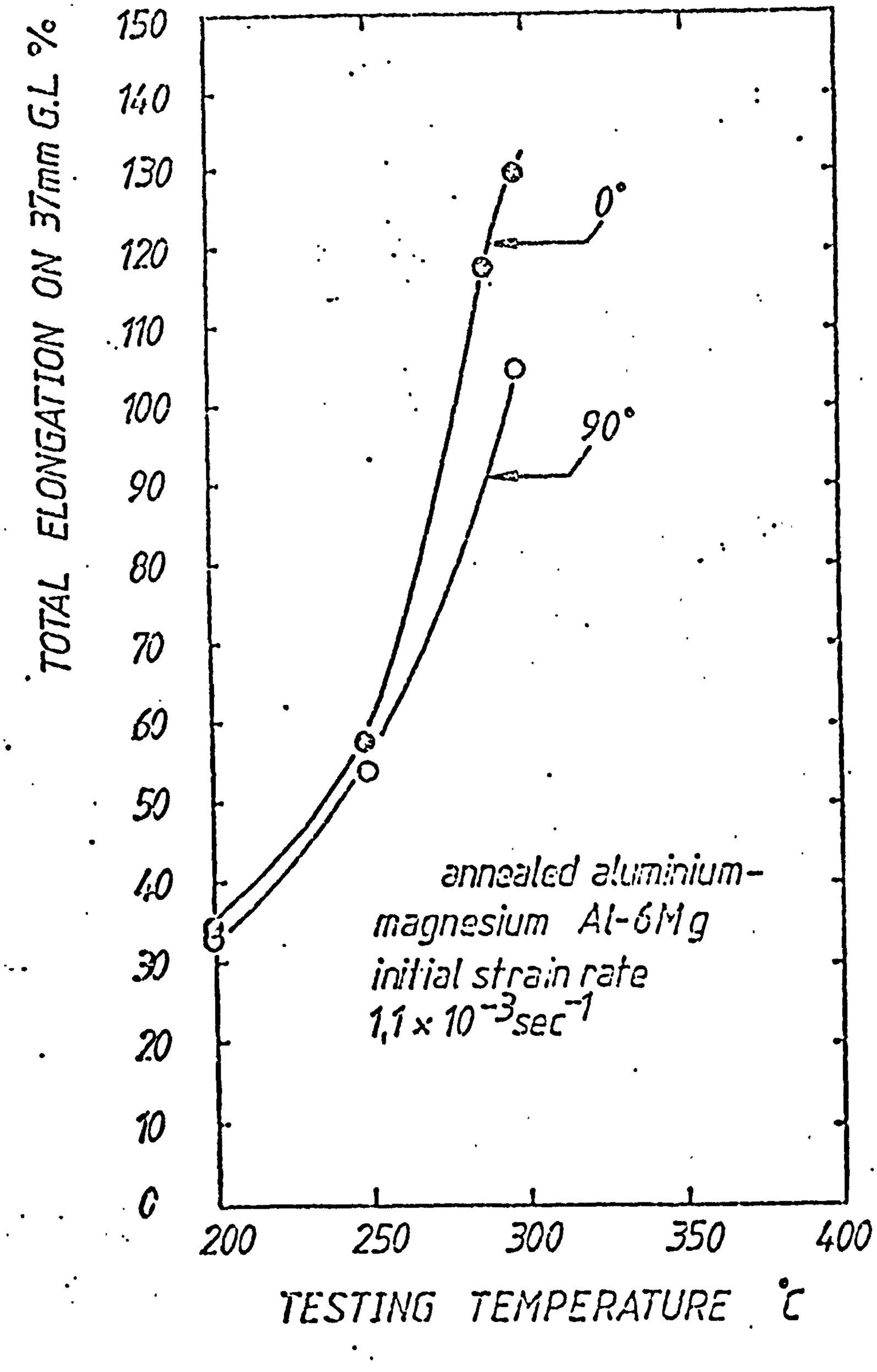


Figure 21 : The total elongation of longitudinal and transverse tension tests on annealed Al-6Mg. (Ref.100).

Chapter II

Materials and experimental techniques.

Chapter II

Materials and experimental techniques

2.1.Materials

Ten grades of commercial sheet aluminium/magnesium alloys containing between o and 6.6% magnesium as the major alloying element were used for this investigation. Our designation, the nominal composition, the hardness and sheet thickness are shown in Table 1. The chemical composition of 6 Mg and 4 Mg groups are given in Table 2.

2.2. Experimental techniques

The following tests were used to evaluate and understand the warm formability of the aluminium/magnesium sheets:-

(1) Uniaxial tensile tests
(2) Hot biaxial stretching using a solid punch and a gas bulge forming
(3) Microstructure examinations.

2.2.1. Uniaxial tests

Standard 50 mm x 12.5 mm gauge-length tensile specimens were machined, all in the original sheet rolling direction. The machined specimens were solution-annealed at temperatures and for the periods shown in Table 3, in an air circulation furnace, its temperature controlled to $\pm$ 5°C. The specimens were deformed to fracture in an Instron 5000 Kg tensile testing machine, using a range of testing temperatures (20° - 300°C) and cross head speeds (0.02 - 25 mm/min.). The heating of specimens during testing was carried out using an air circulating oven specially designed to fit on the Instron machine. Specimen temperature was directly measured with a thermocouple tied to the centre of the specimen. After the test temperature had been reached, the specimen was held for about 10 minutes before pulling. After fracture, the specimen was rapidly cooled in water. The tests were conducted from room temperature to 300°C.

Strain measurement was calibrated between strain in the gauge section and crosshead travel, using several specimens after given amount of cross head travel.

Measurements of the strain rate sensitivity index m from the equation $\sigma = K \dot{\varepsilon}^m$, were made by deforming several specimens at the rate & temperature investigated after given amounts of strain. Because m depends on strain all values were determined between engineering strains of 30 - 40%, this ensures that the effect of strain on all samples would be the same.

After deforming each sample to 30%, the cross-head rate was altered by a factor of two to obtain a value of m by using the equation:-

$$m = \frac{\log P_A/P_B}{\log V_2/V_1}$$

2.2.2. Hot pressing tests

The hot stretch-forming machine, using fully clamped blank and a 50 mm hemispherical punch, is shown schematically in figure (22). The punch, die plate and clamping plate were heated by electrical cartridge heaters, each heater consists of an outer Inconel cylindrical tube, inside which is a precisely wound and spaced resistance wire. For the die plate and clamping plate, the cartridges are inserted with a radial arrangement figure (23) into a stainless steel block 9 in. diameter and 2.5 in. thick.

In order to minimise the loss by conduction, the area of the stainless steel discs in contact with the press was reduced by the removal of an annular volume of metal from the underside of each disc. This volume was fitted with refractory Kaolin wall. The punch head was heated by a single, non-standard cartridge 9 in. long and 1 in. diameter, the details of these parts are given by Barrett (Ref.91.)

This test was carried out on Al/2.2% Mg and Al/6.6% Mg alloy sheets in three different tempers - hard rolled, partially annealed and fully annealed.

The sheet thickness of deformed cups, at various distances from the pole, was measured directly with a point-ended micrometer to find the strain gradients into the cups.

2.2.3. Hot bulging tests

Blanks 150 mm in diameter were bulge formed using the hot bulging rig shown in figure (24).

It was first decided to use the Mand hydraulic bulge tester, and heat the oil around the sheet by an electric coil, but local heating of the oil and sheet blank led to unsatisfactory results and so a gas employed.

The hot bulging consists mainly of a bottom die, with a central aperture diameter of 5 mm for the gas inlet and six studs, each 3 mm in diameter, for specimen clamping and a top die with a large central hole, as shown in figure (24).

The pre-holed sheet specimen is clamped between the two dies, and the whole unit is inserted in an air circulation oven. The unit is then heated until the desired operating temperature is reached as indicted by thermocouple located on the sheet specimen and at this point the chosen gas pressure is applied and bulging continues until fracture. Argon was the gas used.

After testing, bulge heights were measured, then the bulges were sectioned in the diametral plane, figure (91), to study the thickness distribution.

2.2.4. Microstructure examinations

The major techniques employed in surface study were optical metallography, transmission electron microscope and scanning electron microscope.

Optical microscope

After testing the specimens were rapidly quenched in water to minimize the structural changes immediately after testing. The grids on the specimen surfaces enabled samples to be cut which were deformed to different known strains.

Microstructures were obtained from samples of 50%, 100%, 200% and 250% elongations, additionally, camples were taken from grip ends to study and compare the effect of static annealing.

The samples were mounted, polished and etched in the usual ways, using orthophosperic acid as the etching solution.

Transmission electron microscopy

Samples were cut, near to the optical specimens of 200% elongation, using a spark machine to avoid the excessive deformation of mechanical cutting. This was done by making the sheet specimen the anode and the cutting tool (a 2 mm diameter cylinder) was made the cathode. A small gap about one millimeter was left between the cathode and anode, both electrodes were usually immersed in a dielectric such as Kerosene (Paraffin) to prevent a continuous discharge build up and to stabilize the spark (Ref.92.).

Material is removed when a spark is struck between the tool and the specimen. Deformation of the specimen is limited to the region close to the spark-melted area.

The disc specimens were then mechanically polished on both sides using emery papers and a mounting polisher, to reduce their thickness down to 120 μm ready for the final electropolishing thinning process to produce a final foil suitable for electron transmission microscopy. A Struer polishing machine with a photo cell was used for this purpose.

To produce a thin foil by electropolishing suitable for electron transmission, the criterion usually employed is that, as soon as a few tiny holes appear the areas near them are thin enough for examination. This is becuase it is normally difficult to measure a foil thickness of 200 - 2000 Å. However, if electropolishing is carried on after the appearance of the holes, they become rounded and the thin regions are lost. The decision when to stop polishing was made automatically by the functioning of a photo cell.

An electrolytic system of ethyl alcohol, perchloric acid and glycerol in the proportions 7:2:1 , were found suitable at 20°C to reveal the microstructure. A potential of 30 volts and a current of 0.1 amperes were employed. The thinned discs, with central holes, with appropriate areas for electron transmission examination were washed in ethyl alcohol before examination in the electron microscope.

Scanning electron microscopy

The fracture surfaces were first degreased by washing for 5 minutes in a bath of "Grammosole" placed on a vibrator. The specimens were then mounted on stubs and studied using the Cambridge Instruments Stereoscan MK.I.

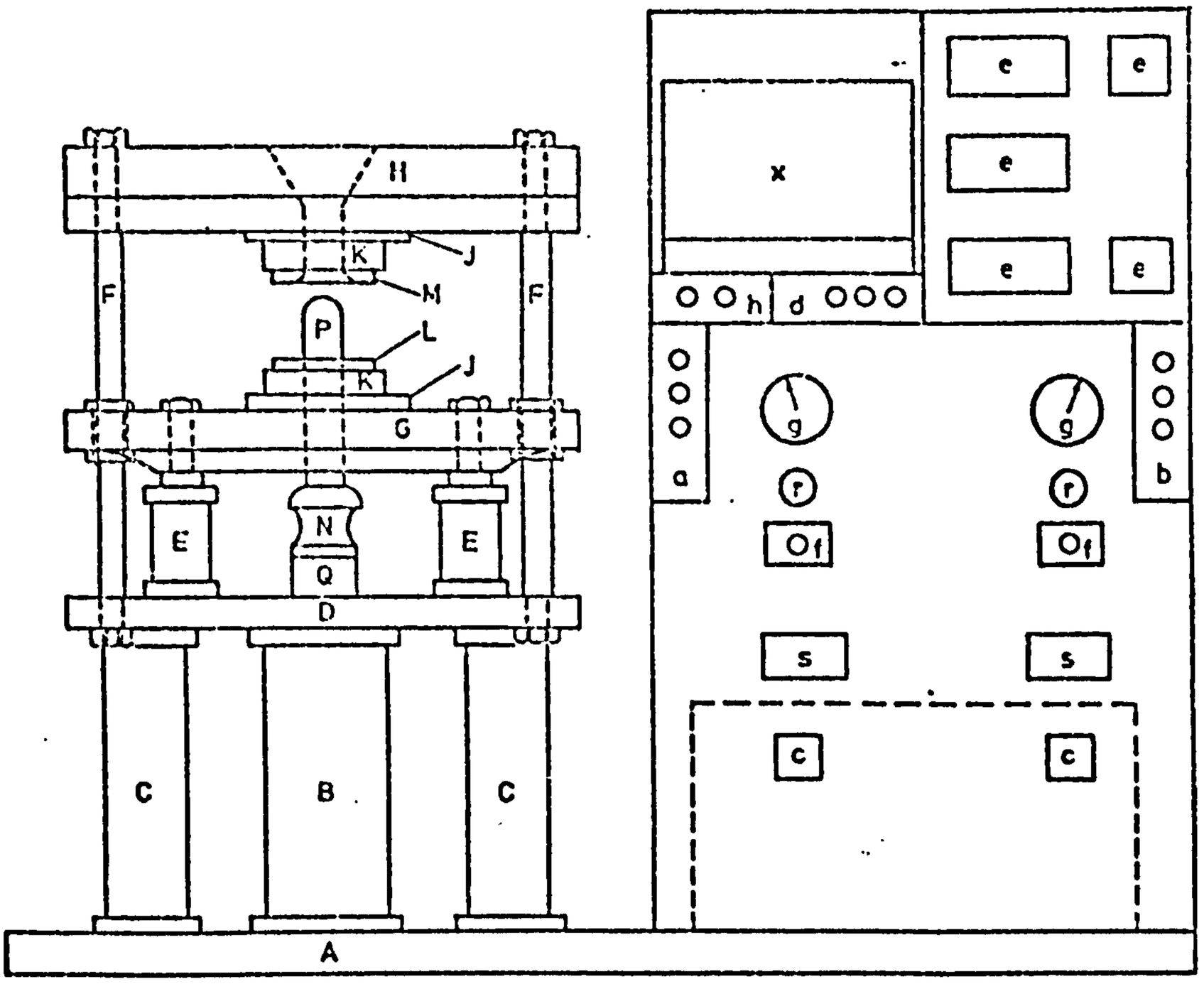


FIG. 22. A MACHINE FOR STRETCH FORMING & DEEP DRAWING SHEET MATERIALS AT ELEVATED TEMPERATURE. (REF 91)

Machine Assembly

A main base plate

B main ram

C spacer supports

D secondary base plate
E primary clampint rams

F vertical support rods
G intermediate moving plate
H fixed top plate
J intermediate water cooled plates
K hot plates

L clamping plate
M die plate
N load cell
P punch 50mm dia
Q ram piston.

Control Cabinet

a push button control (punch).
b push button control (clamp)
c pilot operated check valves
d mains 3 phase control
e proportional controllers (heating)
f flow control valve
g pressure gauges
h mains control (heating)
r pressure reducing valve

s solenoid operated directional valves
x flat bed X-Y recorder

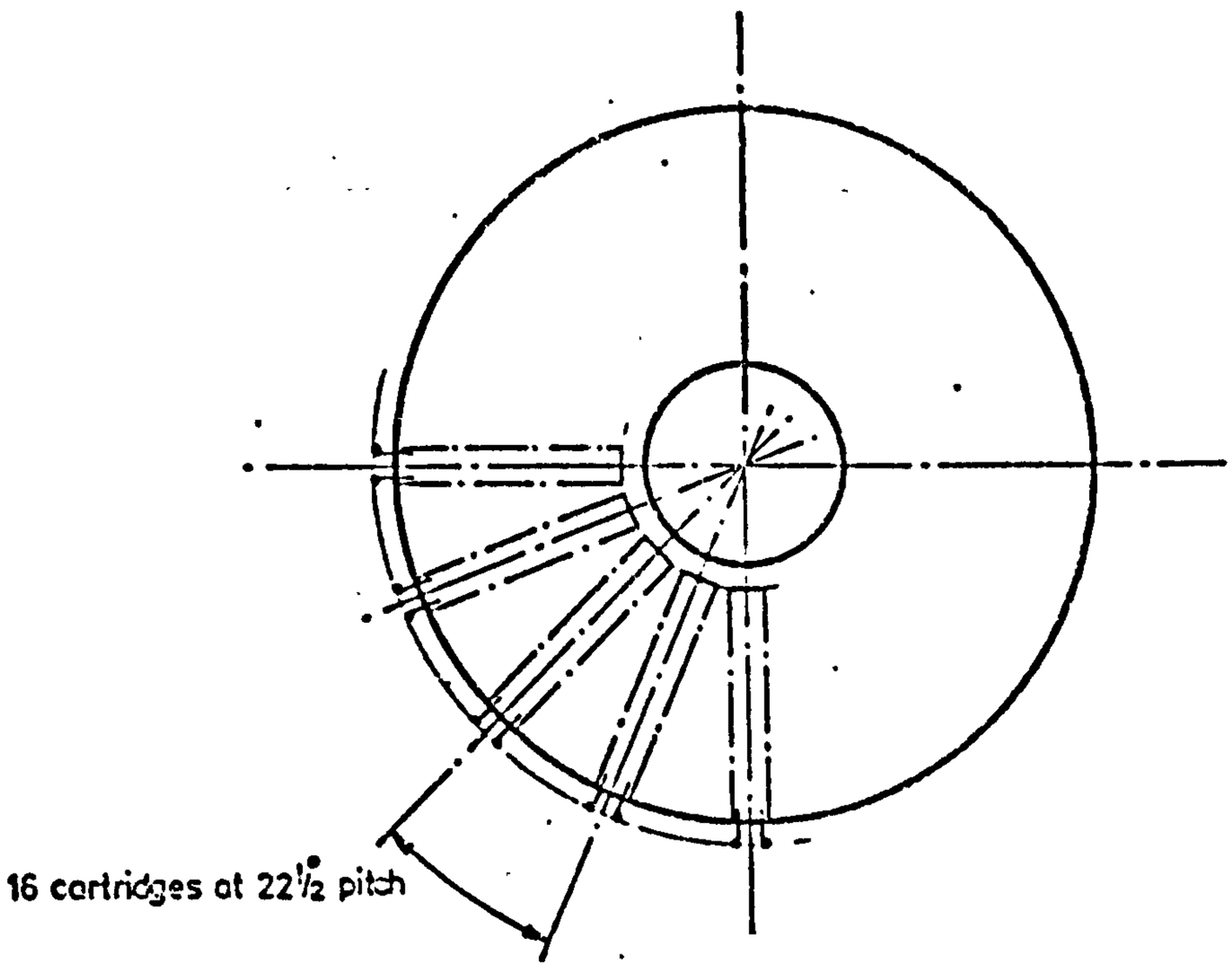


FIG. 23 SECTIONAL PLAN OF HOT PLATE SHOWING THE RADIAL ARRANGEMENT OF CARTRIDGE HEATERS.

TEXT BOUND INTO THE SPINE

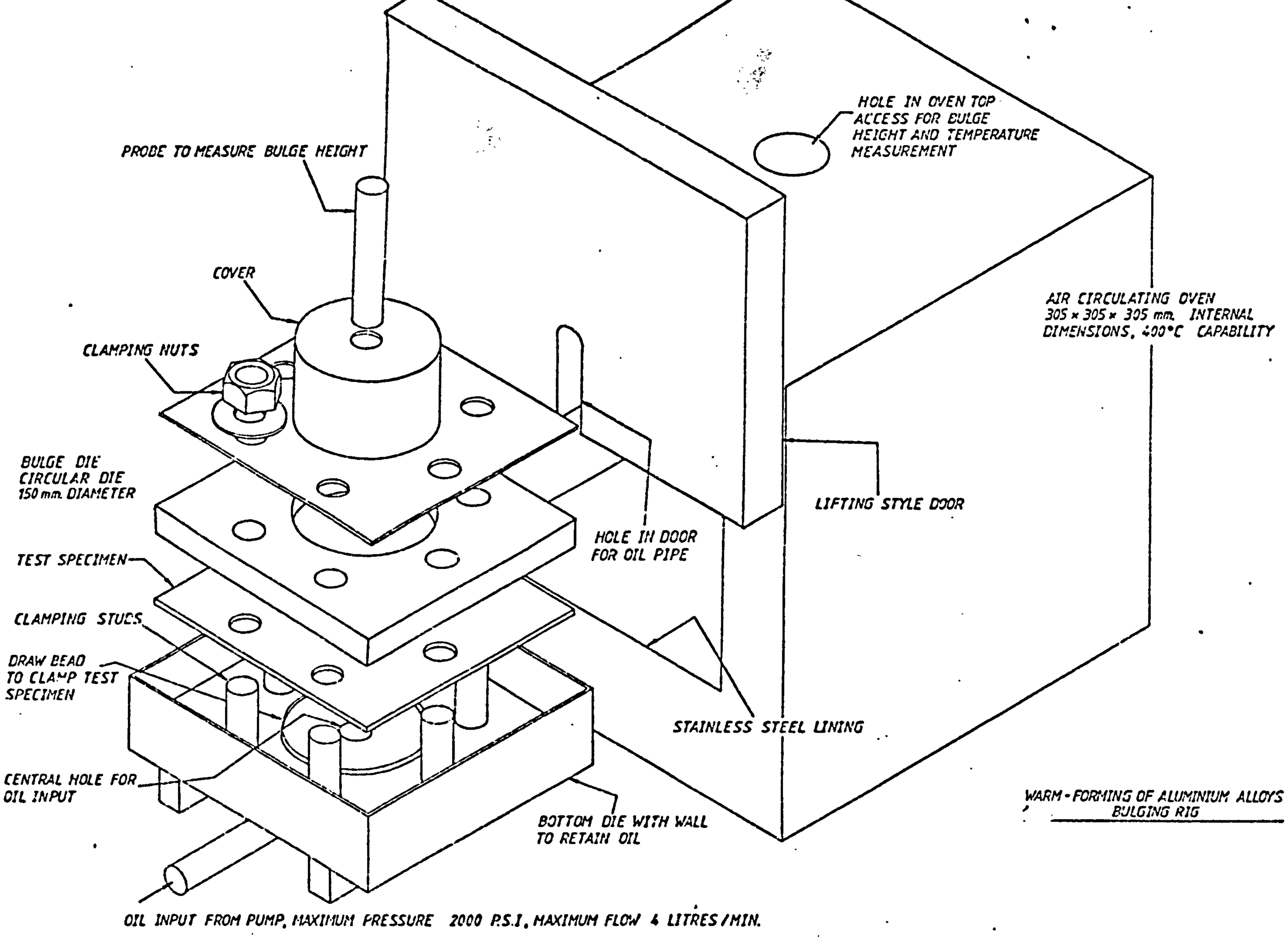


Figure 24 Schematic representation of hot bulge forming rig

Chapter III

Experimental Results.

Chapter III

Experimental results

Three distinct groups of results are shown in this chapter.

(1) Conventional uniaxial tensile test results

(2) Hot biaxial stretching test results from a solid punch and gas bulge formings/

(3) Metallographic examination for Al/6 Mg sheet.

3.1. Uniaxial tensile tests

Results of tensile tests are firstly given for each alloy composition independently, then the possible combination of different groups are also presented.

3.1.1. Commercial purity aluminium

Results using commercial purity aluminium (0 Mg) are given in figures (25) and (26). As shown in figure (25) the elongation present has little increased with increase in test temperature up to 200°C whereafter the elongation decreased again for all strain rates.

Decreasing the initial strain rate from 0.83 x 10^{-4} sec^{-1} to 4.67 x 10^{-4} sec^{-1} has produced little increase in the elongation present at testing temperatures up to 200°C, but on further heating the elongation properties have decreased again.

Plots of the strain rate sensitivity index $\underline{m}$ against testing temperature are shown in figure (26) for $\dot{\varepsilon} = 8.3 \times 10^{-3}$ sec^{-1}, $\dot{\varepsilon} = 1.67 \times 10^{-3}$ sec^{-1} and $\dot{\varepsilon} = 4.67 \times 10^{-4}$ sec^{-1}. The values of $\underline{m}$ are relatively small. However, the general feature shows the dependence of $\underline{m}$ on testing temperature and strain rate. Furthermore, at higher temperatures the $\underline{m}$ values show a little decrease. This trend is inconsistent with the elongation against temperature curve (Fig.26.)

3.1.2. Al - 2.2% Mg alloys

The results of this alloy are given in figures (27-32). Figures (27-30) show the effect of testing temperature on total elongation at different initial strain rates for all the three annealing conditions - 2 Mg(56), 2 Mg(73) and 2 Mg(74). These graphs indicate

that, the total elongations are significantly increased by a temperature rise of 300°C and/or decreasing strain rates (from 8.3×10^{-3} to 8.3×10^{-5} sec^{-1}).

The graphs show the strong dependence of m value on test temperatures and strain rate. Furthermore, the high m values for the half-hard condition is consistent with the curves of elongation versus temperature (figs.27-30).

3.1.3. Al - 3% Mg alloys

The results for this alloy are given in figures (33-34) for the annealed conditions.

As shown in figure 33, the elongation present has markedly increased with increasing the test temperature or decreasing the strain rate. At the highest temperature, 300°C and lowest strain rate 1.67×10^{-4} sec^{-1}, an elongation of ~170% was observed.

Plots of strain rate sensitivity index m against test temperature are shown in figure 34, for various strain rates. The values of m have increased in a way corresponding to the increase in elongation with temperature and strain rate curves.

3.1.4. Al - 4.4% Mg alloys

The results for these alloys are given in figures (35-44). Figures (35-38) show the effect of testing temperatures on total elongation at different initial strain rates for all the three different material conditions, 4 Mg(64), 4 Mg(84) and 4 Mg(134). These graphs indicate that the total elongations are strongly effected by temperature rise and decreasing strain rates. At the highest temperature, 300°C and lowest strain rate 1.67×10^{-4} sec^{-1}, an elongation of more than 200% was obtained from sheet in the hard-rolled condition.

In case of a fast strain rate - 8.3×10^{-3} sec^{-1} the fully annealed 4 Mg(64) is the most ductile at room temperature, figure (39). At slower strain rates this ductility has gradually decreased to lower values relative to the hand-rolled 4 Mg(134). At test temperatures higher than 150°C, the hard alloy became the most ductile.

Figure (39) shows typical deformed specimens of the 4 Mg(134) condition deformed at 300°C. The specimen on the left is an undeformed one, the other four specimens were deformed at 300°C and strain rates of 8.3×10^{-3}, 1.67×10^{-3}, 4.17×10^{-4} and 1.67×10^{-4} sec^{-1} respectively from left to right.

The specimen of the slowest strain rate 1.67 x 10^{-4} sec^{-1} was stopped at 200% before the fracture due to the size limitation of the oven used.

Figure (40) shows other typical deformed specimens of the 4 Mg(64) condition, deformed at different temperatures 20, 150, 200, 250 and 300°C respectively from left to right. All specimens were deformed at the same initial strain rate of 4.17 x 10^{-4} sec^{-1}.

The change of failure type can here be detected. The sheer fracture at low temperatures has changed to a fractured diffuse neck at higher temperatures (250°C and 300°C).

Figure (41) shows $\underline{m}$ value versus elongation for the three temper conditions [4 Mg(64), 4 Mg(84) and 4 Mg(134)] at various temperatures and strain rates. Again, high $\underline{m}$ values mean high elongation. The curves of Lee and Backofen (Ref.76) and Woodford (Ref.97) were replotted on this graph, to show the correlations between superplastic material and commercial Al - Mg alloy. They are in reasonable agreement with each other.

Figures (42-44) show the variation of elongation with the strain rate. Figure (42) shows elongation versus initial strain rate for the 4 Mg(64) alloy. For 250°C and 300°C, the values of elongation showed an optimum strain rate. The elongation decreases rapidly towards the higher end of the strain rate and smoothly towards the slower end of the strain rate.

At higher initial hardness [4 Mg(134) and 4 Mg(84)], the overall level of elongation is considerably higher than for the soft condition (figs.43,44) The optimum strain rate could not be achieved, probably because of limited strain rates available. However, the results show a rapid decrease in elongation towards the higher strain rate end.

3.1.5. Al - 6.6% Mg alloys

The results of these alloys are given in figures (45-54). The figures (45-48) show the effect of testing temperatures on total elongation at different initial strain rates for the three different material conditions, 6 Mg(84), 6 Mg(105) and 6 Mg(153). These graphs indicate that the total elongations are significantly effected by temperature rise and decreasing strain rates. This effect seems to be stronger than in the case of 2 Mg and 4 Mg.

At the highest temperature, 300°C, and the two lowest strain rates 1.67×10^{-4} and 4.17×10^{-4} sec^{-1}, elongations of more than 200% were achieved in 6 Mg(153) and 6 Mg(105). Again these two tests were stopped before fracture at 200% elongation due to the limited size of the oven used.

Generally, the decrease in strain rate or increase in temperature leads to a significant increase in total elongation. Values for annealed materials, that showed the higher elongation at room temperature showed lower elongations at > 200°C, figures (47,48).

Typical deformed specimens of 6 Mg alloys are shown in figures (49) and (50). Figure (49) shows the effect of strain rate on 6 Mg(105) deformed at 250°C and strain rates of 8.3×10^{-3}, 1.67×10^{-3}, 4.17×10^{-4} and 1.67×10^{-4} sec^{-1}, respectively from left to right. The effect of increasing temperature is shown in figure (50) which illustrates that there is a systematic increase in elongation with increasing temperature. A distinction can, however, be shown in the mode of fracture, which changes from, shear fracture to a diffuse neck as the temperature rises. Figure (50) shows 6 Mg(84) deformed at 25, 150, 200, 250 and 300°C.

The results of heat treatment process, i.e. water quenching and furnace cooling are shown in figure (51). The water quenched specimens showed higher values of elongation at temperatures more than 180°C. Figure (51) also clearly illustrates the variation of elongation with strain rate. At low strain rates (4.17×10^{-4} sec^{-1}) elongation is very high values, whilst at higher strain rates (4.17×10^{-2} sec^{-1}) the elongations became nearly the same for all testing temperatures.

Figure (52) shows the effect of temperature on $\underline{m}$ value for 6 Mg(153) alloy at three different strain rates. It will be seen that m = 0.34 for the lowest strain rate and the highest temperature.

Figure (53) shows elongations versus $\underline{m}$ - values for 6 Mg(84), 6 Mg(105) and 6 Mg(153), at various temperatures and strain rates. Higher $\underline{m}$ values mean higher elongations.

Figure (54) shows the variation of thickness along the central axis of uniaxial tension test specimens of 6 Mg(84) and 6 Mg(153) deformed to failure at 300°C. In addition, the variation in the hardness after forming is shown on the same graph. The final hardness was approximately the same in both alloys no matter what strain the metal is subjected to, or the degree of cold-rolled it started with.

Further tension tests on Al - 6 Mg, cold-rolled at various amounts, gave the data shown in figure (55) where it can be seen that there is an optimum degree of cold work, in this case about 30% cold reduction. However in these tests a change in thickness was unavoidable where cold working has been carried out by rolling and this has not been taken into account.

3.1.6. Results from all tests

From the results of all the tests on all these Al/Mg alloys, plots of elongation versus test temperatures are shown in figure (56), for the annealed conditions. This shows that the total elongation of 0 Mg(25) is not significantly affected by a temperature rise of 275°C but the other three alloys showed about a five-fold increase and the higher the magnesium content, the higher the elongation.

Figure (57) shows the effect of initial strain rate on total elongation. Again 0 Mg(25) is virtually insensitive, whilst the three Al/Mg alloys all show increases in elongation with decreasing strain rate.

Figure (58) shows the effect of initial hardness of 4 Mg and 6 Mg alloys on elongation percent. It can be shown that the initial hardness decreases the elongation at lower testing temperatures up to 200°C, whereas it increases the elongation at more than 200°C.

Figure (59) shows the relationship between elongation and m value for all alloys tested. This indicates the strong correlation between m and elongation.

Figure (60) shows the effect of nominal magnesium content on the maximum flow strength, defined as P_{max}/Ao where P_{max} is the maximum load in uniaxial tension, usually reached in these tests at strains $\leq 5\%$ and Ao is the original cross sectional area of the specimen. Here flow stress rises with addition of alloying elements as would be expected.

In figure (61), the fall in stress with temperature for 6 Mg in all conditions together with the results of Matsuki et al (Ref.85) for their superplastic Al/6 Mg alloy is shown.

This demonstrates that the warm forming deformation process requires considerably higher stresses than does genuine superplasticity even though a judiciously dotted line connects Matsuki's result to this result in a reasonably smooth manner.

3.2. Experimental results in biaxial stretch forming

Al/2.2% Mg and Al/6.6% Mg were chosen for some hot punch stretching and bulge forming tests to bridge the gap between laboratory tensile testing and production of pressings. Hot punch stretching tests using a 50 mm diameter hemispherical punch lubricated with PTFE film were carried out over a range of temperatures (20 - 300°C) and punch speeds (1.27 - 25 mm/minute) by courtesy of the Department of Industrial Metallurgy, University of Birmingham.

3.2.1. Results of Al/2.2% Mg alloys

The results for 2 Mg(56), 2 Mg(73) and 2 Mg(74) are presented in figures (62-66). Figure (62) shows the change in punch height at fracture h* with test temperature; the large increase in maximum cup height h*, between room temperature and any of the test temperatures (150 - 300) is apparent. Secondly, the strain rate effect, apparent in tensile test, is apparent here. Thirdly, as in the tension test, the initial, cold-rolled condition of the sheet is important. The data of figure (62) was replotted for both hard-rolled and annealed conditions in figure (63).

In cold-rolled metal, h* is low at low temperatures, however, the increase of h* with temperature is quite rapid and at the highest temperatures used (300°C), it becomes markedly higher than that of the equivalent condition in the annealed material.

The effect of temperature on the thickness distribution across the pole of the failed bulge in the annealed case 2 Mg(56) is shown in figure (64) as the temperature increases the pole strain and the general strain level rise and become a single, fairly flat, peak.

The effect of punch speed is shown in figure (65). As the speed is decreased, so h* and the general strain level increases and the peak of the strain gradient becomes flatter.

The influence of temperature and punch speed is further demonstrated in figure (66), here, the major strain (e_1 %) at the pole is plotted against the test temperature for three punch speeds used; a four fold increase in limit strain occurs when the test temperature is increased from 20 to 300°C.

The strain rate in the hemispherical punch stretching was assessed on the basis of time required to fracture as shown in table (4). Figure (67) indicates the relationship between cup height (h*) and strain rate; the range of strain rates used in tensile tests compared to that of punch stretching are also shown in figure (67).

3.2.2. Results of Al/6.6% Mg alloys

Results using 6 Mg(86), 6 Mg(105) and 6 Mg(153) are shown in figures (68-79).

Figure (68) shows the change in h* with test temperature. In agreement with the previous test on 2 Mg, h* increases from 150°C to 300°C.

Here the strain rate effect gave an optimum punch speed which depended on the prior annealing conditions. Generally, the annealed 6 Mg(86) showed the largest h* at 250°C, and at an intermediate punch speed of 5 mm/minute.

However, in 6 Mg(153), the increase in h* with temperature is rapid and affected by decreasing the punch speed, as in the tensile tests.

Figures (69,70 and 71) show the thickness and hardness variation across the pole of the the punch test specimens of 6 MG alloys in the three temper conditions, deformed at 300°C and a punch speed of 25 mm/minute. In the annealed conditions 6 Mg(84), the hardness in the highly strained polar region decreases to about H_v = 60, whereas both 6 Mg(153) and 6 Mg(105), the final hardness is approximately uniform, regardless the extent of deformation.

Figures (72-75) shows the effect of radial strain distribution as a function of temperature and punch speeds. As the temperature increases the pole strain and general strain level rises. The effect of temperature on thickness strain distribution across the pole of a cup is shown in figure (76), apparently the increase in h* is due to the increased polar strain at higher temperature. Figure (77) shows the influence of punch speed on h* and on the thickness strain distribution at 200°C.

Figures (78-79) shows typical 6 Mg hot pressings. Figures (78a) and (78b) show the elevation and plan of five cups tested at 25, 150, 200, 250 and 300°C and punch speed 5 mm/minute. The influence of temperature rise on the height is very clear.

Higher temperatures also tend to reduce the fracture length and change its direction relative to the rolling direction. At lower temperatures (50 - 150°C) the fracture was perpendicular to rolling direction, whilst at higher temperatures (200 - 300°C), the fracture is very small and in the rolling direction.

Figure (79) shows the elevation and plan of three cups 6 Mg(153) tested at the same temperature (250°C) and punch speeds of 25, 5 and 2.5 mm/minute. Slower punch speeds improved the depth of draw and also tend to decrease the fracture length.

3.2.3. A comparison between 2 Mg and 6 Mg hot pressings

A comparison between the strain gradients across the poles of fractured 50 mm cups, is shown in figure (80) for 6 Mg(86) and 2 Mg(54) at a test temperature of 300°C and a punch speed 25 mm/minute. The 6 Mg alloy gave a more uniform, higher strain level and deeper cup, than the 2 Mg alloy, the cup height was 30 mm for 6 Mg and only 25mm for 2 Mg alloy. This behaviour, however, was not apparent at the slower punch speed of 1.25 mm/min (and 300°C), as shown in fig. (81). Here, 6 Mg gave a slightly lower height (29.3 mm) than 2 Mg (29.7 mm).

Figure (82) shows the cup height at fracture for both 2 Mg and 6 Mg alloys as a function of punch speed and test tempertures. This gives us a broad picture of the forming behaviour of both alloys. In general, cup heights in 6 Mg are seen to be superior to those in 2 Mg over the temperature range 20 to 300°C. This superiority is most noticeable at 25 mm/min. where, at the same temperature, h* for 6 Mg is approximately 20% greater than 2 Mg.

Relationships between cup height, h*, and the corresponding tensile elongation and $\underline{m}$ value are shown in figures (83) and (84) for both alloys and a combination of these figures is given in figure (85). These graphs indicate the general connection between h*, $\underline{m}$ value and total elongation. It is apparent that $\underline{m}$ is the dominant parameter in controlling the ductility and cup height, high $\underline{m}$, giving high h*.

3.2.4. Results of hot bulging tests

Thickness distribution across the poles of hot bulges are shown in figures 86,87 and 88 for the three different alloys 0 Mg(25), 2 Mg(56) and 6 Mg(84) respectively. All tests were carried out at 300°C using a gas pressure of 1.03×10^6 Pa (150 p.s.i.).

Figure (86) shows that the minimum thickness for 0 Mg alloy is 0.9 mm, which is much larger than that for the 2 Mg alloy (0.38 mm) and 6 Mg alloy (0.33 mm). This result is emphasized is figure (89) where true thickness strains, $\xi = \ln to/t$, are plotted as a function of current distance from the pole. Here the strain level of 6 Mg is higher and more uniform than those of 0 Mg and 2 Mg, with a maximum true stain of 1.22 for 6 Mg, 1.07 for 2 Mg and 0.52 for 0 Mg.

Specimens of 6 Mg were tested at 250°C, 300°C and 350°C, and a constant pressure of 1.03 x 10^6 Pa, plots of thickness strain against projected diameter of the bulge are shown in figure 90. The maximum strain obtained increases as the test temperature increases to 350°C, but the bulges at the lowest temperature (250°C) show more uniform strain distribution.

The rupture time decreased rapidly as the test temperature increased. At 350°C, the rupture time was 5 minutes, at 300°C 20 minutes and at 350°C 80 minutes. In each test, the measurement of bulge heights as a function of time showed that bulging rate is high at the beginning and end of the test and slow in the intermediate stage

Figure 91 shows a typical complete bulge before sectioning. Figure 92 shows the effect of increasing magnesium content on the bulge height of a test temperature of 300°C and 1.03 x 10^6 Pa.

3.3. Discussion

3.3.1. Uniaxial tensile tests

The aim of this work was to investigate the ductility of an Al/Mg alloy series at elevated temperatures. Uniaxial tensile tests were carried out, since they are the easiest tests to give a ready indication of a metal's ductility.

The results show that with the Al/Mg alloy series 0 - 6.6% Mg, the alloys with the higher Mg content have higher ductility as the test temperature increases to the so called warm-forming temperature ($\lesssim 0.5\ T_m$).

The two most important parameters governing ductility are the strain rate and the test temperature, but the initial temper is also relevant.

The change in dimensions of the test piece during extension means that the strain rate is continually changing, unless a controlled rate of cross-head movement is used and a further change in strain rate occurs with the onset of necking, which usually begins at an elongation of about 10%, generally much less than the total strain achieved ($\sim$200%).

The ductility dependance on temperature and strain rate presented in this work, shows that the higher temperature and slower strain rate always give higher ductility in all materials tested except 0 Mg which was not significantly affected by increasing the test temperature. in fact, at temperatures >250°C, the elongation decreased. This is probably due to grain growth, which would adversly affect the ductility. Fleck et al (Ref.93) has shown that tensile elongation at elevated temperatures shows a dependence on grain size.

Tests on alloys containing Mg at elevated temperatures showed a large increase in ductility; elongation of ~160% in 2 Mg alloy and > 200% in 4 Mg and 6 Mg alloys were easily obtained, approaching the lower limit of superplastic materials. The general effect of solid solution alloying is the increase strength, as shown in figure (60) where increasing Mg leads to an increase in the flow stress of the alloy. Also, alloying generally decreases ductility; but this effect is more pronounced in materials where recrystallisation is the softening process (Ref. 94), in view of the more marked effect of alloying on recrystallisation than on recovery (Ref.95). This will be discussed later, when examining the deformation mechanism operating from an analysis of the results of optical and electron microscopy.

With regard to initial alloy temper conditions, it was found that the soft temper was most ductile at test temperatures up to 200°C, whereafter the hard temper showed better results. The reason for this behaviour could be the greater dispersion of the second phase in a hard temper than in an annealed alloy. There is some evidence that ductility can be improved by having a dispersion of fine coherent particles which restrain grain growth and restrict crack propagation (Ref. 96). The same explanation could be applied in the observed higher ductility of as-quenched alloys than the annealed alloy, see figure (51), for here the rapid cooling supresses the precipitation of the β phase so that the alloy exists at room temperature in a supersaturated condition; then fine dispersion of β phase precipitates during heating.

The effect of strain rate sensitivity m was very strong in these tests. The m value increased with an increase in the test temperature or a decrease in the strain rate and a good correlation has been shown to exist between m value and elongation figure (59). A similar relationship is shown in most superplastic materials (Ref. 97) and this emphasizes that m is an important parameter in warm forming in a similar way to superplasticity. m describes the capacity of the metal to resist necking; a high m value giving an increased resistance to neck growth. Physically this is due to the local increase in strain rate in the developing neck causing an increase in the stress necessary to continue necking, the higher the strain rate the greater the increase in stress. The applied stress is then isufficient to propagate the neck without the remainder of the specimen continuing to deform plastically. Such limited neck growth has been confirmed by several observations, in particular those of Morrison and Wray (Ref.98,99) who showed; in superplastic materials, that several necks could slowly grow simultaneously before one finally predominated.

3.3.2. Biaxial press-stretching at elevated temperatures

Uniaxial tests have shown large elongations at elevated temperatures, so it is expected that cup heights in biaxial tests would also be enhanced.

High m values would be expected to produce a more uniform strain distribution and this was seen as in the tensile tests, at slow strain rates and/or high temperatures.

The strain rate in the hemispherical punch stretching can be assessed on the basis of time required to fracture (t_f) and the thickness strain at the pole (ε_t).

Then $$\dot{\varepsilon} = \frac{\varepsilon_t}{t_f} \qquad (1)$$

$$t_f = h^*/V \qquad (2)$$

where h^* is the cup height and
V is the punch speed

Then $$\dot{\varepsilon} = \frac{\varepsilon_t V}{h^*}$$

Table 3 shows the strain rate calculations according to the above analysis. Figure (67) shows the effect of strain rate on cup heights. This indicates that strain rate has a large influence on cup height - the slower the strain rate the higher is the cup height, h^*. This behaviour is very similar to that of the tensile tests of the same alloy, i.e., it was found that h^* was also dependent on strain rate and temperature. A large increase in h^* was achieved as the temperature was increased or the strain rate decreased. However the strain rate used in tensile test was slightly slower than that of hot pressings, see figure (67).

As in the tensile tests, the initial temper of the sheet was important, i.e., 2 Mg(73) gave a larger h^* than did 2 Mg(56).

The biaxial hot pressing of 6 Mg alloys did, however, show some contradictions to the tensile test results. For example, h^* was not strongly dependent on strain rate. It seems that there is an optimum strain rate and temperature for each temper condition. This may be due to the planar anisotropy - high in cold worked alloys - which caused the cups always to fracture along the rolling direction, especially in the high temperature tests. Most tensile tests in this work have been carried out in the rolling direction, however a small number of tests by Painter (Ref. 100) in the traverse direction have shown lower elongation in the transverse direction particularly at temperatures $> 250°C$ (figure 21). Thus it could be that tensile elongation in the transverse direction is the controlling factor for h^*.

The variation in cup heights at fracture showed that at temperatures up to 250°C, 6 Mg(84) gave deeper cups, than the other two alloys 6 Mg(105) and 6 Mg(153). At temperatures between 250°C and 300°C, all conditions gave similar results. This suggests that the temperature at which 6 Mg(153) is better, would be more than 300°C. Since no maximum height h* was obtained for 6 Mg(153) whilst 6 Mg(84) showed maximum at 250°C then decreased at 300°C, see figure (67).

Comparing the thickness strain distribution of 2 Mg and 6 Mg alloys at a punch speed of 25mm/min. and 300°C, annealed 6 Mg(84) gave a more uniform strain distribution and deeper cup than 2 Mg, but at a punch speed of 1.25 mm/min. the situation was reversed.

In general, though, the stretching behaviour of 6 Mg alloys is better than 2 Mg, it shows in general a 20% increase in cup height above that for 2 Mg, particularly at the highest punch speed.

A comparison between the tensile m value and h* indicates that the m value can be used to assess the deformation behaviour under biaxial conditions, with higher m values giving higher cups.

3.3.3. Biaxial bulge stretching at elevated temperatures.

The experiments discussed here demonstrate the potential of hot bulge forming using compressed gas for 0 Mg(25), 2 Mg(56) and 6 Mg(153) alloys. These alloys were bulged to fracture at the same temperature 300°C, and a pressure of 1.03×10^6 Pa see figure 89. The polar thickness strains observed in 6 Mg alloy were higher than those for 2 Mg and 0 Mg, 6 Mg also showed higher bulge height 6.,2 cm. compared to 2 Mg, 5.2 cm. and 0 Mg 3.7.

The instantaneous strain rate varies during deformation, although a theoretical treatment by Cornfield and Johnson (Ref.101) predicted that for a metal with m value ≥ 0.3 the surface area strain-rate, $\frac{dA}{dt}$ for a bulge under constant pressure is approximately constant when h^*/D is between 0.1 and 0.45. Some experimental verification of this was made by Cocks et al (Ref.102) using a superplastic copper alloy, they found that, broadly, the strain rates during bulging were high at the beginning ($h^*/D < 0.1$) and at the end ($h^*/D > 0.45$) but roughly constant during the majority of the deformation, as predicted by theory. Greater deformation was achieved, however, when a more constant strain rate was used by varying the pressure during the test. In the present tests the ratio of bulge height(h^*) to base diameter (D) was between 0.25 and 0.41 and a constant gas pressure was used.

For the 6 Mg alloy tested at various temperatures 250, 300 and 350°C and the same pressure, the thickness strain, figure 89, was higher for higher temperature tests. Although the bulge heights were approximately the same, 6.2 cm at 250°C, 6.2 cm at 300°C and 6.5 at 350°C, the strain distribution is more uniform at the lower temperature, figure 90. In fact the bulging time to rupture at 250°C was much longer (80 minutes) relative to tests at 300°C (20 minutes) and at 350°C (5 minutes), all tests being carried out at the same pressure.

Thus a compromise may be necessary in which a temperature-pressure combination is selected to produce the optimum bulge profiles and reduce the bulging time for a specific manufacturing operation. However, the bulging can be done at higher temperature, where the high dome profilesare required and thickness uniformity is not critical.

3.4. Metallography of Al/6 Mg alloys

It has been shown that the whole range of commercial aluminium/magnesium alloys show enhanced ductility over the temperature range 150 - 300°C e.g., tensile elongations of >200%, were obtained in Al 6 Mg. In this section, the results of metallographic investigations optical, scanning and transmission microscopy are presented in an attempt to explain the enhanced plasticity of Al 6 Mg in particular.

3.4.1. Optical microscopy

The microstructures of 6 Mg(153) and 6 Mg(84) are shown in figures (99 - 107) for low deformation temperature tests, up to 300°C while figures (108 - 113) shows the microstructures of the same alloy at high deformation temperatures, up to 500°C.

In figure (99), the as received 6Mg(153) shows elongated grains [20 x 36 μm], whereas uniform equiaxed grains are observed in 6 Mg(84) 26 μm .

Figure (100) shows the undeformed grip ends of a tensile specimen deformed at 300°C and strain rate of 1.67×10^{-4} sec^{-4}; little significant difference is seen between these two microstructures and corresponding room temperature conditions. However a small amount of grain growth has occurred in both cases.

Figures 101 - 104 reveal the changes in microstructure of alloys deformed to different elongations 50%, 100%, 200% and 250% respectively. Both tempers show the development of small grains. These small grains are all equiaxed and predominantly appear in the grain boundaries of the original elongated grains.

The figures also show that the average grain size decreased sharply to 13 μm in 6 Mg(153) at 250%. 6 Mg(84) showed a less sharp decrease in grain size, to ~20 μm at 200%; an increase in grain size was observed after deformation to 250%, but this was near to the final fracture.

Another observation is the development and the increase in degree of cavitation as deformation continued, as figures (95 _ 98). There was a somewhat greater tendency for cavitation in 6 Mg(84) alloy than in 6 Mg(153) alloy.

The extent of cavitation with deformation, temperature and strain rate is shown in figures (99 - 101). Comparison of figure (99 and 100) for specimens deformed at 250°C and 300°C respectively indicates that the growth of cavity is favoured by deformation at the higher temperature. Both tests were at $\dot{\varepsilon} = 1.67 \times 10^{-4}$ sec^{-1}.

Figure (101) shows the effect of an increase in strain rate to 1.67×10^{-3} sec^{-1} on this phenomenon. The number and size of the cavities decreases with increase in strain rate. A common feature is the spreading of cavities along the whole gauge length with more severe cavitation in the vicinity of the fracture.

Some further experiments were made on 6 Mg(84), in which deformation temperatures were increased to 500°C and $\dot{\varepsilon} = 1 \times 10^{-3}$ sec^{-1}. It should be noted that these high temperature tensile tests were carried out in Nene, 50KN tensile machine, fitted with split furnace, recently purchased by the Institute. Results of mechanical properties of these tests are shown in Table 5.

Figures (102, 103, 104 and 105) show the microstructure of specimens deformed at 300, 400, 450 and 500°C respectively. In each figure, (a) represents the undeformed grip ends of the tensile specimens, whereas (b) and (c) reveal the changes at elongations 100 and 200% respectively.

From the photographs of grip ends, where the total deformation time is about ~50 minutes, it can be seen that a small increase in grain size, to 25 μ at 400°C, had occurred, compared to the value 22 μm obtained at 300°C.

At a deformation temperature of 450°C, new grains have appeared, such new grains have grown bigger at 500°C, suggesting that static recrystallisation might start at ~450°C.

An examination of the structure of deformed specimens shows the formation of new small grains at 400°C and 450°C. Whereas at 500°C they become fairly large giving a more homogenous grain size. At 400°C and 450°C these new grains are equiaxial and mainly occur in the grain boundaries of the original large and deformed grains. This is clear from figure (106) where structures of 200% elongations are magnified to 800 for all the four different temperatures.

Figure (107) shows an unetched specimen tested at 500°C to show the extent of cavitation throughout the whole gauge length, it is clear from all the microstructures figs (102 - 107) that the degree of cavitation increases as deformation or temperature increased.

3.4.2. Scanning electron microscopy

Scanning electron micrographs illustrating the fracture surfaces of 6 Mg(153) and 6 Mg(84) are shown in figure (108). The fracture surface, in general, revealed predominately ductile fracture with extensive cavities, subjected to considerable plastic deformation.

The size and concentration of cavities decreased as the deformation temperature decreased, see figure (108 a and b) at 300°C and compare with figure (108 c and d) at 250°C. This behaviour is similar to that observed by optical microscopy.

A characteristic feature of the 6 Mg(153) fracture surface is the sharp-edged fractures with relatively thin walls, whereas 6 Mg(84) shows rounded edge fractures with thicker walls.

3.4.3. Transmission electron microscopy

Transmission electron micrographs taken from both gauge lengths and grip ends of the tensile specimens are shown in figures (109 - 116). The gauge length samples were cut from regions of 200% elongation measured from grids printed on the specimen surface before deformation.

Grip-end structure of 6 Mg(84) and 6 Mg(153), where the total deformation time is about 3 hours, are shown in figures (109 and 110) respectively. The tests were carried out at strain rate of 1.67×10^{-4} sec^{-1}.

Figure (109 a) shows polygonized subgrains of ~6 μm in size in the specimen tested at 250°C and a larger subgrain size (~ 8μ), at 300°C in figure (109 b).

Figure (110 a) shows tangles of dislocation at 250°C and a tendency for cell formation at 300°C, in figure (110 b).

The structures of samples taken from the deformed gauge length of the tensile specimens of 6 Mg(84) at 250°C and a strain rate of 1.67×10^{-4} are shown in figure (111) for 6 Mg(153) in figure (112). In both cases the deformation produced marked changes from those seen in the corresponding grip ends. Fairly uniform, equiaxed subgrains develop in both alloys. The sizes of these subgrains appear to be smaller (~0.9 μm) in 6 Mg(153) than in 6 Mg(84) alloys (~ 6 μm).

The new small subgrain indicated by an arrow in figure (112 b) has probably grown from a triple point, at the expense of the large original subgrains.

Increasing the deformation temperature to 300°C produced a larger subgrain structure in both materials, see figures (113 and 114.). Again 6 Mg(153) shows smaller subgrains (1.5 μm) than 6 Mg(84) ($\sim$10 μm).

Increasing the strain rate to 1.67×10^{-3} sec^{-1} at the same temperature, 300°C produces significant changes in dislocation structure in both materials figures (115 and 116).

6 Mg(153) shows dislocations accompanied by dislocation loops as in (b) or two-family dislocations as in (c) or a hexagonal dislocation network as in (d). All these dislocations seemed to be moved by stress unitl they have been trapped at cell boundaries.

Dislocations may also be generated by the presence of a second phase (Fig. 116 b). In the case of 6 Mg(84) (Fig. 115.), the structure shows mainly long, straight dislocations, as in (a) and (b). The dislocation densities, here are smaller than 6 Mg(153). Figure 115 (c) and (d) show a forest of dislocations trapped by subboundaries. Two sets of dislocations are clearly shown in (d), probably indicating an incompletely developed network.

3.5. Discussion

3.5.1. Optical metallography

Two important features emerge from the study of the microstructures of the 6 Mg alloys. They are:

(1) the limited grain distortion even after 250% elongation.

(2) the formation of cavities throughout the gauge-length of the specimens.

The detailed behaviour depends on many factors, however, such as the degree of deformation, the initial temper conditions, the strain rate and the temperaturs.

The microstructure of 6 Mg consists of a solid solution and a $\beta(Mg_2 Al_3)$ precipitate, mainly in the grain-boundaries. (The phase diagram for Al-Mg is shown in figure 117). There appears to be more β-phase in grain-boundaries of 6 Mg(84) than in 6 Mg(153) and this is probably due to the nearer-to-equilibrium condition of the annealed alloy. On slow cooling, precipitation of the β-phase starts at a temperature just below the solvus line at points of easy nucleation, e.g., grain boundaries. On continued slow cooling, the grain-boundary precipitate continues to grow through diffusion of solute from the matrix to the existing precipitate particles. At the same time, the solute concentration in the matrix is continually reduced and the solution never becomes greatly supersaturated. So, more β phase is likely in 6 Mg(84) than 6 Mg(153).

The lack of microstructure distortion found after warm-forming is distinctly different from that observed after conventional room temperature deformation, which is usually accompanied by severe grain deformation. Measurements of strain from grain-shape changes gave a value of 10-15% for the slow strain rate at 300°C. This is very much less than the grid strain of 250% measured on the surface of the specimens. This difference suggests the possibility that the subgrain structure changes rather than grain structure itself, however, grain-boundary sliding may also be important. An attempt to estimate the magnitude of grain-boundary sliding has been made by Rachinger (Ref.103), among many others. Working with aluminium strained at 50% and 300°C, he observed no appreciable change in the shape of the grains and concluded that this was due to grain-boundary sliding. This should not be taken as generally illustrative, however, since Rachinger's results are capable of alternative interpretations (Refs.104,105) which have predicted a lower magnitude for the grain-boundary component.

It has also been suggested that deformation occurs by shear and rotation of the grains relative to one another; here the average grain should then maintain its original shape. Some experimental results however, bearing directly on grain-boundary shearing (Ref. 106) showed it should not be considered as simple sliding of one grain over another, but rather as plastic deformation, which occurs in material alongside the boundaries proper. Also it is recognised that the greatest amount of plastic deformation usually occurs in the regions adjoining grain-boundaries, where recovery consequently starts, in these regions of high strain energy. Thus, during deformation at elevated temperatures, the regions adjacent to the grain-boundary will, on this theory, first undergo softening due to recovery, long before the material in the centre of the grain. This softening of the metal next to boundaries permits additional deformation to occur in this region, which appears as what is commonly called grain-boundary shear. However, optical microscopy cannot show whether recovery occurs or not. This aspect will be discussed in Section 3.5.2.

Generally, the worked grains contain high densities of dislocations, which are increasingly polygonized as the temperature of deformation and the stacking-fault-energy of the metal rise. The grains observed in the deformed alloy are longer than the observed recrystallised grains and correspond in size to the initial grains. From these results it is concluded that the obviously worked regions had not recrystallised in the course of deformation and had not been subsequently re-worked.

The appearance of small new recrystallised grains on the grain-boundaries of deformed grains is quite clear, particularly at higher deformation temperatures. These small grains start to appear at high temperature (400°C, $\dot{\epsilon} = 1 \times 10^{-4}$ sec^{-1}), see figure (106), or at 300°C and $\dot{\epsilon} = 1 \times 67 \times 10^{-4}$ sec^{-1}, figure (97). These tiny grains are mainly equiaxed (undeformed) and it is suggested that they formed after deformation had ceased. Furthermore, it is unlikely that these small recrystallised grains cover regions where recrystallisation had occurred during deformation, since they are found in contact with, and occasionally in the centre of, a worked grain which had not recrystallised.

A microstructure consisting of undeformed recrystallised grains in a matrix of the elongated initial grains is not compatible with a recrystallisation mechanism of steady-state hot working (Refs.107-110) which should give rise to a microstructure containing grains which had recrystallised and then been reworked, because, to maintain a constant flow stress, recrystallisation must occur consecutively in dispersed small regions which then harden while recrystallisation proceeds elsewhere. If, as is believed, recrystallisation takes place only after

deformation has ceased, dynamic recovery is probably the mechanism of warm forming up to 450°C.

Recrystallisation was observed at 500°C, figure (116d), with distortion of the new recrystallised grains; this probably occurred during deformation.

Further evidence for these views is shown in subgrain examination by electron microscopy and from activation energy determination, both discussed later (Section 3.5.2. and 3.6.).

Another important feature is the cavitation exhibited during the warm deformation of this alloy. In both temper conditions, cavities were easily visible using both optical and scanning microscopy. The cavities were formed throughout the deformed region but not in the grip ends of tensile specimens. The size and distribution of the cavities increased as the elongation or temperature increased and as the strain rate decreased. Interestingly, in annealed material 6 Mg(84) the cavity concentration seemed higher than in 6 Mg(153) figure (99).

The reason for this cavitation is not yet fully understood, however, the cavities seem to start at grain-boundaries, particularly at triple junctions where the stress concentration would be relatively high. Because of the similarity between superplasticity, creep and warm-forming, it seems likely that those materials that cavitate in creep or superplastic deformation will also cavitate during warm-forming, although Matsuki et al (Ref. 111) who studied superplasticity in a specially produced Al/6 Mg alloy did not mention cavitation, even at elongations of $\leq 855\%$ at 525°C and $\dot{\varepsilon} 3.3 \times 10^{-4}$ sec^{-1}. More recently, Taplin and Smith (Ref. 112) did report cavitation during the deformation of certain Al/Mg alloys.

3.5.2. Transmission electron microscopy

From the results of transmission electron microscopy, it can be seen that the characteristic feature of the warm-formed structure was the development of small subgrains. These subgrains were observed in the gauge length of tensile specimens after deformation (200% elongation) rather than in their grip ends.

The examination of these subgrains reveals that they were made up of a regular network of dislocations, figures 111 and 112; this suggests that dynamic recovery is the main softening process occurring during deformation.

At higher deformation temperatures, more extensive networks and less dislocation tangles are observed, figures 113 and 114. In fact figure 114 shows almost no dislocations present inside relatively large subgrains, indicating almost complete dynamic recovery. Increasing the test temperature from 250°C to 300°C led to an increase in subgrain size by 160%. Subgrain sizes of (0.9μm and 6μm) at 250°C and (1.4μm and 10μm) at 300°C for 6 Mg(84) and 6 Mg(153) respectively were obtained.

A relationship between subgrain sizes and applied stress suggested in (Ref. 113) is:-

$$\sigma = Kd^{-x}$$

whereas (K) is constant, (x) is about 1.5 for Al/Mg (d) is subgrain size and σ is the applied stress.

Using this equation in our case, then:-

6 Mg(84)

$$\frac{d_{300}}{d_{250}} = \left(\frac{\sigma_{300}}{\sigma_{250}}\right)^{-1/x} = \left(\frac{9,829}{16,70}\right)^{-1/1.5} = 1.427$$

and

6 Mg(153)

$$\frac{d_{300}}{d_{250}} = \left(\frac{\sigma_{300}}{\sigma_{250}}\right)^{-1/x} = \left(\frac{8,085}{12,800}\right)^{-1/1.5} = 1.358$$

Where d_{300} and d_{250} are subgrain sizes at 300°C and 250°C respectiveiy and σ_{300} and σ_{250} are the corresponding applied stresses These calculated subgrains

are slightly lower than the measured values of about 1.6μm. The boundaries between subgrains consist of walls of dislocations of one sign which arrange themselves into so-called.low-angle boundaries. In this way the strain fields of adjacent dislocations partly cancel each other, for the tensile strain in the region below the extraplane of one dislocation overlaps the compressive strain field of the next lower dislocation. In addition to lowering the strain energy, the rearrangement of edge dislocations into low-angle boundaries has a second effect; this is the removal of general lattice curvature.

This rearrangement of dislocations is accomplished without much change in the total number of dislocations present. Hence the small subgrains observed in 6 Mg(153) (0.9 μm - 1.4μm) compared to 6 Mg(84) (6 - 10μm) can be attributed to the greater original number of dislocations, due to cold-rolling. A soft annealed metal can have dislocation densities of the order of 10^6 to 10^8 cm^{-2}, and heavily cold-worked metals can have $\sim 10^{12}$ cm^{-2}. Accordingly, the subgrain sizes of 6 Mg(153) were relatively smaller than 6 Mg(84), both at low (250°C) and high (300°C) temperatures.

On the whole, the subgrains observed in the warm-formed structures were still equiaxed after 200% elongation. Since optical microscopy showed the original grains developed some shape changes, then the subboundaries must be able to relocate their position by rotation or by some continuous disintegration and reformation as suggested by McQueen el al (Ref.114). This migration of subboundaries could also lead to the isolation of cracks which might arise from the original grain boundary and hence crack propagation would be slowed down (Ref. 115).

Alternatively, these small subgrains can be regarded as the fine-grained structure usually necessary for superplasticity. It should be mentioned here, that the necessity of a fine grain for superplasticity was dictated, in particular, by a requirement to prevent a substructure forming inside grains (Ref. 116). Other workers (Refs.117,118) however, showed that superplasticity can occur in large-grained materials and mentioned that the superplasticity in their case was not dependant on the intrinisic grain structure.

At 300°C, the effect of increasing the strain rate to 1.67×10^{-3} sec^{-1} on the dislocation substructure was appreciable. The dislocation networks form in a different distribution, and dynamic recovery appears to be incomplete, adding to the evidence that dynamic recovery, is the controlling softening process. Examination of the dislocation substructures formed at high strain rates revealed that irregular helical dislocations were formed initially. Figure (116a) followed by the formation of a regular network consisting of parallel dislocations or hexagons; the dislocations seem to be all screw type. Figure (116c) shows the parallel type and figure (116d)

The driving stress for dislocations to assemble in_ to a stable dislocation network can be calculated according to (Ref. 119), from the following equation:-

$$|\tau_d| = \frac{Gb}{4\pi(1-\nu/2)h}$$

where G is the bulk modulus (3.7×10^6 psi) for Al
ν poisson's ratio (0.34)
b Burger's vector (1.2×10^{-8} in)
h the mesh size of the dislocation network.

Taking h = 400 Å (figure 116d), then the driving stress for network formation = 2522 p.s.i.

The ratio of driving stress to applied stress ($\sim$ 15,000 p.s.i.) will be 0.17. Thus the applied stress is available for assembling dislocations into stable networks by cross-slip. In other words, cross slip is the controlling dislocation mechanism during dynamic recovery.

This conclusion was confirmed later on by calculating the activation energy for recovery see sec. (3.6.) The ratio obtained here (0.17) is comparable with that of 0.14 obtained by Lee (Ref. 120) working on pure aluminium at 300°C. The difference is probably due to the influence of solute atoms, in 6 Mg, on dislocation motion.

Another parameter that can be obtained from measurements on stable dislocation networks in the subgrain rotation angle, α . This angle can be estimated by means of the following equation, (Ref. 121):-

$$\alpha = 2 \sin^{-1}(b/2h) \simeq b/h$$

where the terms are as described above. This gives a relatively high angle subboundary of 23 minutes in this case. The calculation is for a specimen deformed at a relatively fast strain rate where it has been shown that a smaller fraction of dynamic recovery takes place. This structure actually represents the transition from a partially recovered structure with tangles of dislocations, to dislocation-free sugbrains and regular small-angle boundaries, at low angles, the spacing between dislocations will be large, as shown from figures 111-114.

In summary, the systematic observation of dislocations and subboundaries formed during warm deformation confirm and strengthen the view that dynamic recovery is the prime softening process. This is in accord with the optical metallography, where no dynamic recrystallisation was observed. The formation of a regular mesh of dislocation networks provides evidence that the rate-controlling mechanism is the cross slip of screw dislocations.

3.6. Determination of activation energy

In this part, activation energies were obtained from tensile deformation data in an attempt to clarify the role of dynamic recovery and/or obtain other deformation processes in warm-forming. In this way, the contributions to the total deformation process of various mechanisms can be isolated and studied. (Ref.120).

3.6.1. Activation energy for tensile deformation

At each deformation temperature and at a constant strain, the true stress (σ) varies with strain rate ($\dot{\varepsilon}$) in accordance with the relationship:-

$$\sigma = K \dot{\varepsilon}^m \qquad (1)$$

where K is a constant and m is the strain rate sensitivity index, given from the slope of the straight line $(\partial \log \sigma / \partial \log \dot{\varepsilon})_{T,\varepsilon}$, see figure (118). The variation of Ln σ with $1/T$ is shown in figure (119).

To obtain activation energies for deformation from the experimental data, a local slope $\partial \ln \sigma / \partial (1/T)_{\varepsilon, \dot{\varepsilon}}$ was determined at 50°C intervals. With these values of m and local slopes, the activation energy for deformation, ΔH_d, was determined from the following relation (Ref.122).

$$A \sigma^{1/m} = \dot{\varepsilon} e^{(\Delta H_d / RT)} \qquad (2)$$

or

$$\Delta H_d = \frac{R}{m} \left[\frac{\partial \ln \sigma}{\partial (1/T)} \right]_{\varepsilon, \dot{\varepsilon}} \qquad (3)$$

where A is a constant and R is the gas constant.

Figure (120) shows the variation of ΔH_d with temperature and two activation energies are apparent: a ΔH_d value of 21 $\pm$ 3.5 K cal/mole (88 $\pm$ 13 K Joule/mole) at the lower temperature range and ΔH_d of 25.2 $\pm$ 3.2 k cal/mole (105 $\pm$ 13 K joule/mole) at the higher temperatures. It appears that a high strain rate will shift the curve to a lower activation energy. This feature of the curve is similar to that obtained on pure aluminium by Lee et al (Ref.120); their results are shown on the same graph. Pure aluminium shows a higher energy level than Al/Mg alloy. This is probably due to alloying additions and the high flow stresses of the Al/Mg alloys.

3.6.2. The activation energy for dynamic recovery

In the temperature range considered in this work, dynamic recovery is the most likely process affecting dislocation motion. It is difficult to conclude accurate results about dislocation mechanisms by the measurement of activation energy, since the Q for self-diffusion in pure Al is very similar to the Q for Mg diffusing in Al and so it is necessary to obtain a more sensitive parameter than Q.

A method (Refs.123,124) of calculating the amount of recovery occurring at a given temperature at constant strain involves separating the flow stress into its reversible and irreversible components. This is necessary since a decrease of flow stress with temp (see figure 119) can result from either a decrease in elastic constants (reversible) or from recovery (irreversible). If the irreversible decrease in flow stress ($\Delta\sigma_{irr}$) is normalized to flow stress (σ_1) at a sufficiently low temperature, where recovery does not occur, the relative friction of dynamic recovery (f_r) at constant strain can be calculated as follows:-

Since $\Delta\sigma_{rev}$ arises primarily from the change of elastic modulus with temperature, then:-

$$\Delta\sigma_{rev} = \sigma_h \left[(E_1/E_h)-1\right] \qquad (4)$$

where σ_h is the flow stress at strain (ε) and temperature (T_h)-see figure (121)-and E_1 and E_h are the Young's modulus at temperature T_1 and T_h respectively. then the irreversible change of flow stress $\Delta\sigma_{irr}$ is given by:-

$$\Delta\sigma_{irr} = \sigma_1 - \sigma_h\,(E_1/E_h) \qquad (5)$$

where σ_1 is the flow stress at the same strain ε and temperature T, see figure (121). The parameter $\Delta\sigma_{irr}/\sigma_1$, which is a quantitative measure of dynamic recovery (Ref. 124) can be obtained from:-

$$\frac{\Delta\sigma_{irr}}{\sigma_1} = 1 - \left(\frac{\sigma_h}{\sigma_1}\right)\left(\frac{E_1}{E_h}\right) \qquad (6)$$

Taking T_1 = 25°C as the reference deformation temperature in this work, it should be noted that the temperature for no recovery was taken (Ref.120) as -73°C for pure Al, but this is not expected to introduce much error, since recovery in Al alloys at 25°C is negligibly small.

The relative fraction of dynamic recovery (f_r) is defined from equation 6 as:-

$$f_r = \frac{\Delta\sigma_{irr}}{\sigma_1} = \left(1 - \frac{\sigma_h}{\sigma_1}\right)\left(\frac{E_1}{E_h}\right) \qquad (7)$$

Here, the values of f_r are obtained by substituting measured values of flow stress and published data of Young's modulus, figure (122), (Ref.125) at various temperatures.

The relative fraction of dynamic recovery increases with deformation temperature but decreases as initial strain rates increase (figure 122). This variation in f_r is understandable, because more thermal energy and time are available for the process of dynamic recovery as the deformation is increased and the strain rate is lowered.

The relative fraction of dynamic recovery data, f_r, as a function of temperature, for pure Al, (Ref. 120) are plotted on the same graph. It is noted that the dynamic recovery of 6 Mg(153) alloy greatly depends on temperature compared to pure Al; where temperature is not significant. While at temperatures >200°C, the 6 Mg alloy approaches the same value as that for pure Al. The fraction of dynamic recovery occurring in both materials decreases with strain rate.

The differential of f_r with respect to time t,

$$\dot{f}_r = \frac{df_r}{dt}$$

is considered to represent the rate of dynamic recovery and moreover, as dynamic recovery is believed to be a thermally-activated process, its f_r can be described as:-

$$\dot{f}_r = \frac{df_r}{dt} = Ae^{(-\Delta Hr/RT)} \qquad (8)$$

where A is the pre-exponential factor
ΔH_r the activation energy for dynamic recovery
R the gas constant, and
T the absolute temperature of deformation.

The time t, necessary to achieve a strain ε at an initial strain rate $\dot{\varepsilon}_0$, is given by:-

$$t = \varepsilon/\dot{\varepsilon}_0 \qquad (9)$$

upon obtaining the values of $\dot{f} = df_r/dt$, the activation energy for dynamic recovery ΔH_r was determined to be 17.3 $\pm$ 3 k cal/mole (72 $\pm$ 13 KJoule/mole) from the slope of the plot of ln $\dot{f}_r$ versus (1/T), figure (130).

This value of ΔH_r approaches the values which gives the theoretical activation energy for cross-slip as reported by Schoeck and Seger (Ref. 126) to be ΔH_c = 16 - 25 k cal/mole (70 - 105 K Joule/mole).

3.7. Discussion

The activation energy for deformation shown in figure (120) have a two-stage appearance, a lower-level activation energy (88 ± 13 k Joule/mole) and a higher level of activation energy, (105 ± 13 K Joule/mole). Both of these correspond with the activation energy where the cross slip of screw dislocations is the main controlling mechanism (118 k Joule/mole). (Ref.127).

Table 6 summarizes the activation energy values reported in aluminium for various deformation processes. The difference between experimental activation energy for dynamic recovery reported in this work (72 ± 13 k Joule/mole) and static recovery 118 k Joule/mole, reported in (Ref.128) appears to be significant in Al/Mg alloys. The kinetics and degree of softening however are appreciably greater (Ref.130) for dynamic recovery; this is in agreement with its lower activation energy.

The theoretical values for the cross-slip of screw dislocations (70 - 150 k Joule/mole) are those for dynamic recovery and so it appears reasonable to conclude in our case that this is the controlling mechanism.

Observation made in the TEM confirm and strengthen these conclusions.

Chapter IV

General Discussion and Conclusions.

Chapter IV

4.1. General discussion and conclusions

(1) The ductility of the Al/Mg alloys is enhanced by raising the temperature.

The increase in ductility depends on strain rate and temperature. Values of more than 200% elongation were achieved in 4 Mg and 6 Mg alloys at temperatures less than 300°C (0.68 T_m) and at a true initial strain rate of 1.67×10^{-4} sec^{-1}.

(2) The general effect of magnesium content is to decrease the ductility at room temperature, but increase it at elevated temperatures, though, in the case of 0 Mg the ducility decreases at still higher temperatures. This effect arises from the influence of magnesium on the substructure of the alloy.

(3) At room temperature ductility decreases with increasing deformation, but at elevated temperatures, this behaviour is reversed but depends on strain rate, deformation temperature and magnesium content.

(4) The stress required for warm forming is considerably higher than that for genuine superplasticity. This is because the temperatures used are relatively low and flow stress is temperature dependent.

(5) The m value is the most important parameter in increasing the ductility.

As in the case of superplastic deformation, there is a close relationship between m value and elongation. In general, elongation to failure increases with increasing value of m. A value of m $\simeq$ 0.3 was obtained.

(6) A large value of m means higher cup height in both 2 Mg and 6 Mg alloys.

From a practical view-point such correlation could be useful in predicting the cup height from the m value determined from a simple tensile test.

(7) 6 Mg alloys showed higher cup heights than 2 Mg alloys.

The effects described for uniaxial tensile are broadly followed in the punch-stretching experiments, showing that biaxial behaviour can be predicted from uniaxial data, as is the case in conventional sheet metal forming. Cup height at fracture, h*, increases with increasing temperature.

(8) The initial temper and punch-speed have a great influence on 2 Mg thanon 6Mg in punch stretching.

For the2Mgalloy,higher cup heights are obtained by increasing the temperature, decreasing the punch speed and at higher temperature by using the hard temper sheet. For 6 Mg, punch speeds between 1.25 and 25mm/min had little effect and using a hard temper was no better than an annealed one at temperatures up to 300°C.

(9) The extent of warm bulging is greatly influenced by magnesium content, bulging temperature and bulging pressure.

The effect of magnesium shown in tensile tests is also clear in bulge stretching experiments, 6 Mg alloys show deeper bulges and larger thickness strains than did 2 Mg and 0 Mg. For a given alloy (6 Mg) and pressure (1 MPa), bulging can be carried out at a higher temperature (350°C) in a relatively short time (5 minutes) with more thickness strain. From a practical point of view, bulging can be done at higher temperatures if the final thickness uniformity is not critical.

(10) Optical microscopy shows that dynamic recrystallisation cannot be the softening process during deformation.

The microstructure reveals very small equiaxed grains predominantly near to the worked grain boundaries. Due to the equiaxity of these grains, it is believed that they formed when deformation had ceased.

(11) The cold-rolled alloy showed fin grain sizes than the annealed material.

This must be due to the degree of cold worked and dispersion of the second phase, which restrains grain growth and restricts crack propagation and hence postpones fracture.

(12) Cavitation is observed in the whole gauge length of the specimens, but not in the grip ends.

It is believed that the cavities form originally at triple points and in grain boundaries. For a given elongation, slower strain rates and higher temperatures favour larger cavities, suggesting that diffusion is the rate controlling mechanism for cavity growth. Again, for a given elongation, the amount of cavitation is smaller in 6 Mg(153) than in 6 Mg(84).

(13) During the early stages of deformation, a fine subgrain structure is formed which persists until fracture.

Subgrains were formed as a result of deformation at 250°C and 300°C. These subgrains, which result from the tensile test indicate that dynamic recovery, which occurs during deformtion is responsible for the enhanced ductility of Al/Mg alloy.

(14) Smaller subgrains were found in the hard rolled alloy 6 Mg(153) than in the annealed one 6 Mg(84).

This is attributed to the larger initial dislocation density associated with cold-rolled materials.

(15) Subgrains remain equiaxed, while grains elongated.

This is due to the ability of subboundaries to relocate their position by rotation or disintegration and reformation of dislocations under the applied load.

(16) Formation of regular-mesh dislocation networks at higher strain rates.

This structure provides evidence that cross-slip occurs during the dynamic recovery process.

(17) The subgrain size increases with increasing deformation temperature, again 6 Mg(153) shows smaller subgrain size than 6 Mg(84).

(18) Two levels of activation energy are observed betwen room temperature and 300°C. The activation energy at lower temperatures (88 $\pm$ 13 k Joule/mole) and also the larger activation energy (105 $\pm$ 13 k Joule/mole) at higher temperatures are known to be associated with the cross-slip of screw dislocations.

(19) The relative fraction of dynamic recovery increases with deformation temperature but decreases as the strain rate increases.

This variation occurs because more thermal energy and time are available for the process of dynamic recovery as the deformation temperature is increased and strain rate is lowered.

(20) The measured activation energy for dynamic recovery is similar to the theoretical values of activation energy calculated for cross-slip of screw dislocations and therefore this is the rate controlling process for dynamic recovery.

4.2. Recommendations for future work

1. A more detailed study of the influence of higher magnesium contents (up to 35%) should yield a useful information on its role in warm forming operations and perhaps offer new products.

2. A detailed study of the cavitation reasons and the mechanisms operating. This might shed some light on one of the most serious disadvantages of the current series of alloys.

3. An investigation into the effect of other alloying additions on ductility, strength and properties of Al/Mg. This could yield a more useful alloy.

4. More experiments are required on the hot bulging process at various pressures and temperatures.

5. Design and prove a hot pressing and hot bulging machine on an industrial scale with a good temperature control and minimal heat losses.

Table (1) Designation and Properties of Al/Mg Alloy Sheet

No.	Alloy	Designation	Sheet thickness mm	Hardness Hv
1	Annealed commercial purity aluminium	OMg (25)	1.50	25
2	Annealed aluminium 2% magnesium	2Mg (56)	1.15	56
3	Cold-rolled aluminium 2% magnesium	2Mg (73)	1.15	73
4	Cold-rolled aluminium 2% magnesium	2 Mg (74)	1.15	74
5	Annealed aluminium 3.4% magnesium	3Mg (67)	1.15	67
6	Annealed alumnium 4.4% magnesium	4Mg (64)	1.00	64
7	Cold-rolled aluminium 4.4% magnesium	4Mg (184)	1.00	84
8	Cold-rolled (80%) aluminium 4.4% magnesium	4Mg (134)	1.00	134
9	Annealed aluminium 6.6% magnesium	6Mg (84)	1.20	84
10	Cold-rolled aluminium 6.6% magnesium	6Mg (105)	1.20	105
11	Cold-rolled (40%) aluminium 6.6% magnesium	6Mg (153)	1.20	153

Table 2; Chemical composition of 6 Mg and 4 Mg alloys.

Alloy	Mg	Cr	Si	Fe	Cu	Mn
6 Mg	6.6	0.19	0.07	0.06	0.09	0.15
4 Mg	4.4	-	0.15	0.31	-	-

Table 5; Tensile properties at high deformation temperatures.

Test Temp. (^{o}C)	Max. Strengh. N / mm^2	Total Elongation %	$\underline{m}$ Value
300	98	139	0.18
400	38	15o	0.24
450	18	158	0.31
500	10	155	0.34

Table (4)

Process	Activation Energy K Joule/mole	Reference
Dynamic Recovery	94 $\pm$ 14	Underwood (Ref.120)
Dynamic Recovery	72 $\pm$ 13	This work
Tensile deformation	92 $\pm$ 12	Underwood (Ref.120)
Tensile deformation	88 $\pm$ 13	This work
Cross-slip (theoretical)	67 - 105	Schoeck & Seeger (Ref.126)
Cross-slip (theoretical)	117	Friedel (Ref.127)
Dislocation climb	150	Astrom (Ref.128)
Static recovery	117	Astrom (Ref.128)

Table 3; Strain rate determination of 2 Mg hot pressing.

Alloy	Test Temp °C	Punch Speed V" /min	Cup Height h* in	Pole thick t in.	True Strain $\varepsilon_t = \ln t_o/t$	Strain Rate $= \frac{\varepsilon_t V}{h^*}$ sec^{-1}
2Mg(56)	150	0.05	0.991	0.0165	1.047	8.8×10^{-4}
2Mg(73)			0.921	0.0158	1.09	9.9×10^{-4}
2Mg(56)		0.2	1.000	0.0158	1.09	3.6×10^{-3}
2Mg(73)			0.912	0.0152	1.13	4.1×10^{-3}
2Mg(56)		1.0	0.949	0.0122	1.35	2.37×10^{-2}
2Mg(73)			0.871	0.0174	0.99	1.9×10^{-2}
2Mg(56)	200	0.05	1.058	0.0100	1.55	1.22×10^{-3}
2Mg(73)			1.018	0.0122	1.35	1.10×10^{-3}
2Mg(56)		0.2	1.045	0.0105	1.50	4.80×10^{-3}
2Mg(73)			0.967	0.009	1.65	5.7×10^{-3}
2Mg(56)		1.0	0.959	0.0146	1.17	2.03×10^{-2}
2Mg(73)			0.949	0.0145	1.176	2.07×10^{-2}
2Mg(56)	250	0.05	1.012	0.0068	1.93	1.6×10^{-3}
2Mg(73)			1.112	0.0095	1.60	1.2×10^{-3}
2Mg(56)		0.2	1.005	0.0098	1.57	5.2×10^{-3}
2Mg(73)			1.064	0.0085	1.71	5.4×10^{-3}
2Mg(56)		1.0	1.005	0.0078	1.8	2.98×10^{-2}
2Mg(73)			0.951	0.007	1.5	2.70×10^{-2}
2Mg(56)	300	0.05	1.162	0.0082	1.75	1.25×10^{-3}
2Mg(73)			1.213	0.0075	1.90	1.30×10^{-3}
2Mg(56)		0.2	1.068	0.0085	1.71	5.3×10^{-3}
2Mg(73)			1.157	0.0085	1.71	4.9×10^{-3}
2Mg(56)		1.0	0.984	0.0115	1.41	2.38×10^{-2}
2Mg(73)			1.083	0.0042	2.4	3.72×10^{-2}

References

1. FINSH, D.M, WILSON, S.P. and DORN, J.E. Trans. A.S.M. 36, 1946, P254.

2. TAYLOR, B. HEIMBUCH, R.A. and BABCOCK, S.G. "Proceedings of the second Int. Conf. on Mech Behaviour of Materials". A.S.M. (1976), P2004.

3. AYRES, R. Met. Trans. A, volume 8A, 1977, P487.

4. ALDER, J.F. and PHILLIPS, V.A. The effect of strain rate and temperature on the resistance of Al, Cn and steel, J. Inst. Met. 83, 80 (1954-55).

5. WRAY, P.T,J. Appl. phys. 1970, Vol.41, P3347.

6. DIETER, E.D. Mechanical Metallurgy, 2nd Ed., McGraw-Hill, 1976, P351.

7. BACKOFEN, W.A., TURNER, I.R. and AVERY, D.H. Trans. Quart. A.S.M. 57 (1964), P980.

8. NAZIRI and PEARCE, R. J. Inst. Metals, 97 (1969) P326.

9. HEDWORTH, J. and STOWELL M.J. J. Mat. Sci. 6 (1971) P1061.

10. HEDWORTH, J. and STOWELL M.J. J. Mat. Sc. Vol.6, (1971) P1061.

11. CUTLER, C.P. Unv. of Cambridge, Ph.D. Thesis (1971).

12. MORRISON. W.B. Trans. A.I.M.E. 242 (1968) (2221).

13. MORRISON. W.B. Trans. Quart. A.S.M. 61 (1968) 423.

14. GREEN. S.J., LANGON. J.J., LEASIA, J.D. and YANG.W.H. Met. Trans. Vol.2, 1971 P1813.

15. AYRES. R.A. Met. Trans. A. 84, 1977, P488.

16. HOCKETI. T.E. Trans. A.I.M.E., 239, 1967, P969.

17. RAI. G. Met. Trans. 6A, 1975, P305.

18. ROSSARD. C., Review, Met., 1966, 63, (3), 225.

19. BACKOFEN. W.A., TURNER. I.R. and AVERY. D.H. Trans. Amer. Soc. Met. 1964, 57, 980.

20. GHOSH. A.K. Met. Trans. A, 8A, 1977. P1224.

21. LATHAM. D.J. Ph.D. Thesis, Unv. Birmingham 1963.

22. LATHAM. D.J. and COCKCROFT. M.J. Nat. Eng. Lab. Ref.216, 1966.

23. ROBBINS.J.L., WAGENNAAR and O.C. SHEPARD J. Mater. 1967, 2, 271.

24. JONAS. J.J., SELLARS C.M. and TEGART W.J.M. Met. Rev. 1969, 14, (130), 1.

25. McQUEEN. H.J. Int. Rep. PM-M-67-7, Phys. Met. Div., Canada, April (1967).

26. STÜWE. H.P. Acta. Met. 13, 1337 (1965).

27. SELLARS C.M. and TEGART W.J. Int. Met. Reviews 158, vol.17, 1972.

28. JOHNSON R.H. Metallurgical Reviews, 1976, 15, 115.

29. FELBECK D.K. PRENTICE-HALL, Inter. Inc. London, 1968, P581.

30. PACKER. C.M., JOHNSON R.H. and SHERBY O.D. Trans. A.I.M.E. 242 (968) 2485.

31. JOHNSON.R.H. PACKER. C.M., ANDERSON. L. and SHERBY.O.P., Phil. Mag. 18 (1968), 1309.

32. STOWELL. M.J., WATTS. B.M., OWEN. D.G.E. and BACKIE.B.L. Institue of Metals Meeting on Recrystallisation, London, 1973.

33. GRIMES. R., STOWELL.M.J. and WATTS. B.M. Metals Society Meeting on "Alloy composition and microstructure Control in relation Processing", London (1975).

34. NAESS. S.E. and MERK. G., SCAND. J. Metallurgy, 1 (1972) 308.

35. FIRTH. M. and WILLIAMS W.M. Canada. Met. Quart, 8 (1969) 331.

36. RYUM. N. JIM, 94, 1966, 191.

37. GREENWOOD J.N. J. Iron Steel Inst. 171 (1952) 380.

38. IDEM, BULL. Inst. Met 1 (1952) 120.

39. GREENWOOD J.N., MILLER D.R. and SUITER. T.W. Acta Met. 2 (1954) 250.

40. GREENWOOD. J.N. J. iron steel Inst. 176 (1954) 268.

41. PERRY. A.J. J. of Mat. Sc. 9, 1974, 1016.

42. BALLUFFI R.W. and SEIGLE L.L. Acta Met. 3, 1955, 170.

43. MACHLIN E.S. Trans. Met. Soc. AIME 206 (1956) 106.

44. REID. B.J. and GREENWOOD J.N. Trans Met. Soc. AIME 212 (1958) 503.

45. GREENWOOD J.N., MILLER.D.R. and SUITER.T.W. Acta Met. 2 (1954) 250.

46. GIFKINS. R.D. Acta Met. 4 (1956) 98.

47. PRESLAND A.E.B. and HUTCHINSON R.I., J. Inst. Met. 90 (1961-62) 239.

48. IDEM, 5th Inter. Conf. on Electron Microscopy (Academic Press, New York, 1962), J-15.

51. TAPLIN D.M.R. and BARKER L.J. Acta Met. 14, 1966, 1527.

52. LANDON T.G. and TAPLIN. D.M.R. S.M. Archives, vol.2., issue 3, 1977.

53. ROGERS H.C. Ductility, A.S.M., 1967 (ed. H.W.PAXTON.).

54. FUJITA F.E. Acta. Met. 6 (1958) 543.

56. TAPLIN D.M.R. J. Australian Inst. Met. 10. (1965) 336.

57. COCKS G.J. and TAPLIN D.M.R. Scripta Met. 3 (1969) 623.

58. BONISZEWESKI and N.F. EATON, Met. Sci. J. 3 (1969) 103.

59. TIPLER. H.R., TAYLOR. L.H. and HOPKINS. B.E. ibidd 4 (1970) 167.

60. HOLCOMB. R.T. and BACKOFEN. W.A. Sheet Met. Ind., vol.43., 1966, P479.

61. JOHNSON W. and MAMALIS A.G. Hellemic steel publications Co. S.A. 1978. P20.

62. DILLAMORE. I.L., SMALLMAN R.E., and WILSON. D.V. 9th Commonwealth Mining & Met. Cong. 1969.

63. WILSON. D.V. and BUTLER. R.D. J. Inst. Met., Vol.90, 1961-62, P473.

64. DILLAMORE. I.L., MELLA. P. and HAZEL. R.J. J. Inst. Met., 100, 1972, P50.

65. HEYER R.H. and NEWBY. SAE 680094, 1968.

66. AL-NAIB. T.Y.M. and DUNCAN. J.L. Int. J. Mech. Sci., 1970, 12, 463.

67. HAWKINGS. R. and BELK. J.A. Met. Tech. 1976, P516.

68. OSHITA. T. and TAKEI. H. J. Japan Inst. Metals, 1972, 36, 1081.

69. HILL. R. phil. Mag. 41, 1133 (1950).

70. D.W. WOO. Int. J. Mech. Sc. 6, 303, 1964.

71. B. STORAKERS. Int. J. Mech. Sci. 8, 619, 1966.

72. GHOSH. A.K. Sheet Met, Int. J. Mech. Sci, 19, 457, (1977).

73. SWIFT. H.W. J. Mech. Phys. solids 1, 1 (1952).

74. S.P. KEELER and W.A. BACKOFEN. Trans. ASM 56 (1963).

75. KEELER. S.P. Sheet Met. Ind. 42, 683, 1965.

76. LEE. D. and BACKOFEN. W.A. Trans. Metall. Soc. AIME., 239, 1967, 1034.

77. PEARCE.R. SIM, 48 (1971) 943
WOODTHORPE. J. and PEARCE. R. SMI, 46 (1969) 1061.

78. PAINTER.M.J. and PEARCE. R. Met. Tech (1975), 62.

79. PEARCE. R. and GANGULI. D. J. Inst. Met., 100, 1972, 289.

80. DILLAMORE. J.L. British Steel Co. CDL/MT/9/1974.

81. BACKOFEN. W.A., AVERY. D.H. and TURNER I.R. Trans. Am. Soc. Metals 57, 980, 1964.

82. FIELD. D.S. Jr., IBM JL Res. Dev., 9, 134, 1965.

83. JOVANE. F. Int. J. Mech. Sci., 1968, 10, 403.

84. HOLT. D.L. Int. J. Mech. Sci., 1970, 12, 491.

85. WOO. D.M. Int. J. Mech. Sci. 6, 303, 1964.

86. TAYLOR. B., HEIMBUCH. R.A. and BABCOCK.S.G. "Proceeding of the Second Inst. cont. on Mech. Behaviour of Materials". ASM, 1976, 2004.

87. AYRES. R.A. Met. Trans. A. 8A (1977) 487.

88. AYRES. R.A. and WENNER.M.L. General Motors Research Lab. Warren, MI 48090.

89. AYRES. R.A., LANNING. H.W., TAYLOR. R., HEIMBUCH. R. and BRAZIER. W.G. Society of Automotive Eng., 780180, 1978.

90. WILLIS. J. Progress Report 2, Alcan Lab., Ltd., Banbury 1978.

91. BARRET. D.J. Sheet Met. Ind. 53 (1976) 174.

92. GOODHEW. D.J. "Specimen preperation in mat. science". 1973, ed. A.M. Blauret.

93. FLECK. R.G. Acta Met. 23, 1975.

94. TEGART.W.J. McG.
R. 35720, Seminar by the Am. So. for metals, Oct. 1967.

95. WHITE. F.E. Ph.D thesis, Unv. of Paris, 1967.

96. LEWIS. G.P. M. Met Thesis, Unv. of Sheffield, 1963.

97. WOODFORD. D.A. Trans. ASM, 62, (1969) 291.

98. MORRISON. W.B., Trans. Quart A.S.M., 61, (1968) 423.

99. WRAY. P.J. J. Appl. phys. 41, 1970, 3347.

100. PAINTER. M.J. and PEARCE. R. Unpublished work at Cranfield Inst. of Technology.

101. CORNFIELD. G.C. and JOHNSON. R.H. Int. J. Mech. Sci. 12, 1970, 479.

102. COCKS. G.J., ROWBOTTOM. G. and TAPLIN. D.M.R. Metals Tech. 7 (1976) 174.

103. RACHINGER. W.A. J. Inst. of Metals, 81, 33 (1952).

104. McLEAN. D. Grain boundaries in met. Oxford Unv. Press, London, 1957.

105. CONARD. H. "Mech. behaviour of Mat at elevated Temp". McGraw-Hill-Inc., New York, 1961.

106. RHINES. F.N., BOND, W.E. and KISSEL. M.A. Trans ASM, 48, 169, 1956.

107. SELLARS. C.M. and TEGART. W.J. Mem. Scient. Revue Metall, 63, 1966, 731.

108. HARDWICK. D. and TEGART. W.J. J. Inst. Met. 90, 1961-2, 17.

109. HARDWICK. D. and TEGART. W.J. Mem. Sc. Revue 58, 1961, 869.

110. SELLARS. C.M. and TEGART. W.J. Acta Met. 14, 1966, 1136.

111. MATSUKI. K., UETANI. Y, YAMADA. M. and MURAKAMI. Y. Met. Sci, J, 10, 1976, 235.

112. TAPLIN. D.M.R. and SMITH. R.F. Fracture 1977, vol.2, Unv. of Waterloo Press.

113. McQUEEN. H.J. Canad. J. Physics. 1967, 45, 1225.

114. McQUEEN. H.J. , WONG. W.A. and JONES. J.J. J. Inst. of Met. 1967, 95, 129.

115. COTNER. J.R. J. Inst. of Met. 1969, vol. 97.

116. HAYDEN. H.W., GIBSON. R.C., BROPHY. J.H. Metall. 24, 8, 847, 1970.

117. LIKHACHEV. V.A., MYSHLYAEV, OLEVSKI. S.S. and CHUCHMAN. Acta. Met. 22, 1974, 829.

118. GRIFFITHS. P. and HAMMOND. C. Acta. Met. 20, 1972, 935.

119. KUHLMANN - WILSDORF. D. and NINE. H.P. J. Appl. phys. 38, 1967, 1683.

120. LEE. E.U., KRANZIEIN. H.H. and UNDERWOOD. E.E. Mater. Sci. Eng. 7, 1971, 348.

121. FRANK. F.C. Rep. of the conf. on Defects in crys. solids held at Univ. of Bristol. The physical society, London, 1955, P159.

122. CONRAD. H. in J.E. DORN (ed.). Mechanical Behaviour of Met. at elevated temp. McGraw-Hill, New York, 1961, P149.

123. COTRELL. A.H. and STOKES. K.J. Proc. Roy Soc. London, A233 (1955) 17.

124. BULLEN. F.P. and HUTCHISON. M.M. Phil. Mag., 7, 1962, 557.

125. PINE. M. The review of scientific instruments, v.23, 1957, P643.

126. SCHOECK. G. and SEEGER A. Report of the conf. on defects in cryst-solids held at Unv. of Bristol, The physical society, London 1955, P340.

127. FRIEDEL. J. Physiques des Solides, Sorbonne, Paris, 1950, P220.

128. ASTROM. Arch. Fysik, 10, (1955), 147.

129. SHEHATA. F., PAINTER. M.J. and PEARCE. R. J. of Mech. working technology, 2, 1978, 279.

130. JONAS.J.J.,McQUEEN.H.J.and WONG.W.A., Deformation under hot working ,Iron steel Inst. No 108, 1968 P.49.

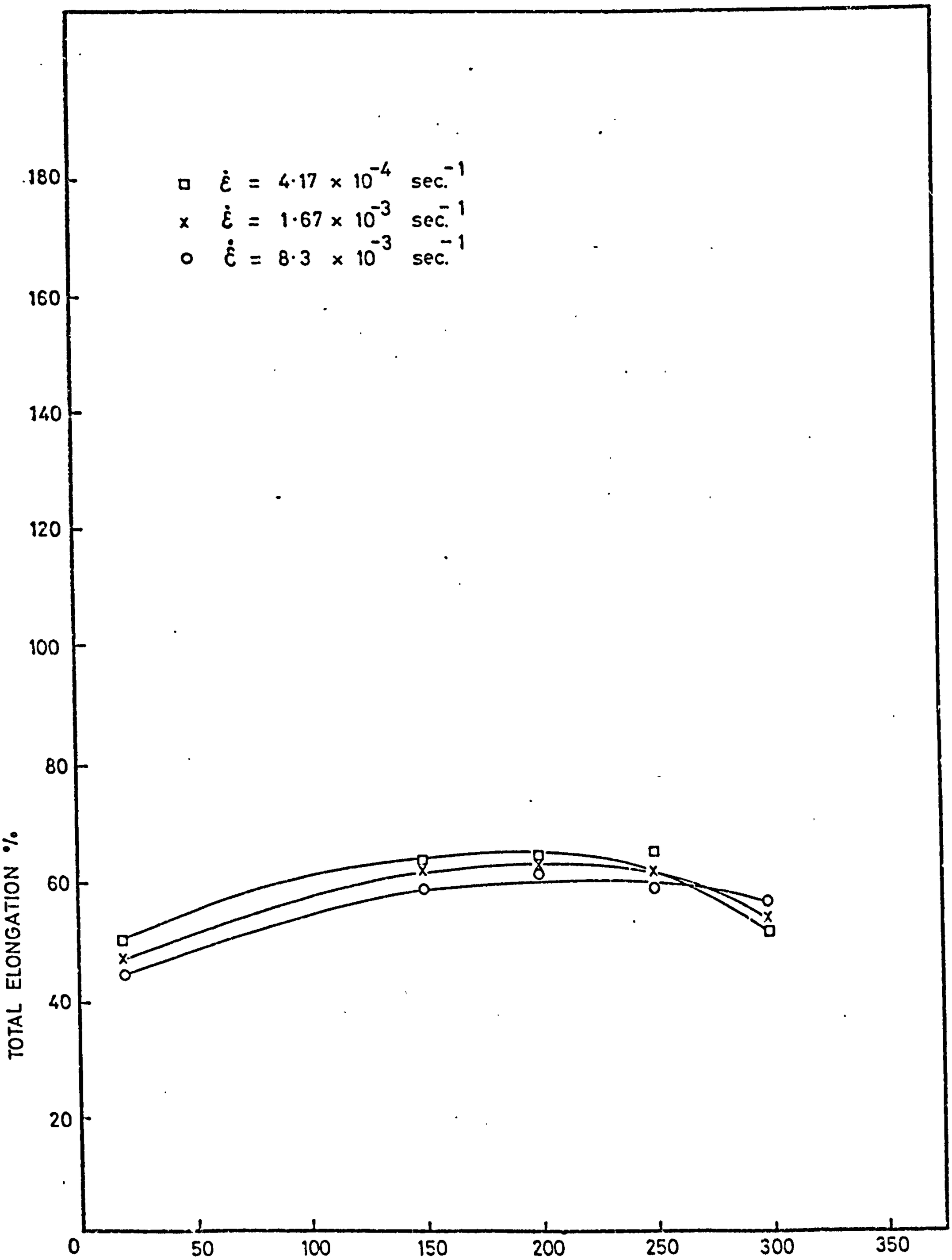


FIG.25. VARIATION IN TOTAL ELONGATION WITH TESTING TEMPERATURE ON 0Mg (25) AT VARIOUS STRAIN RATES.

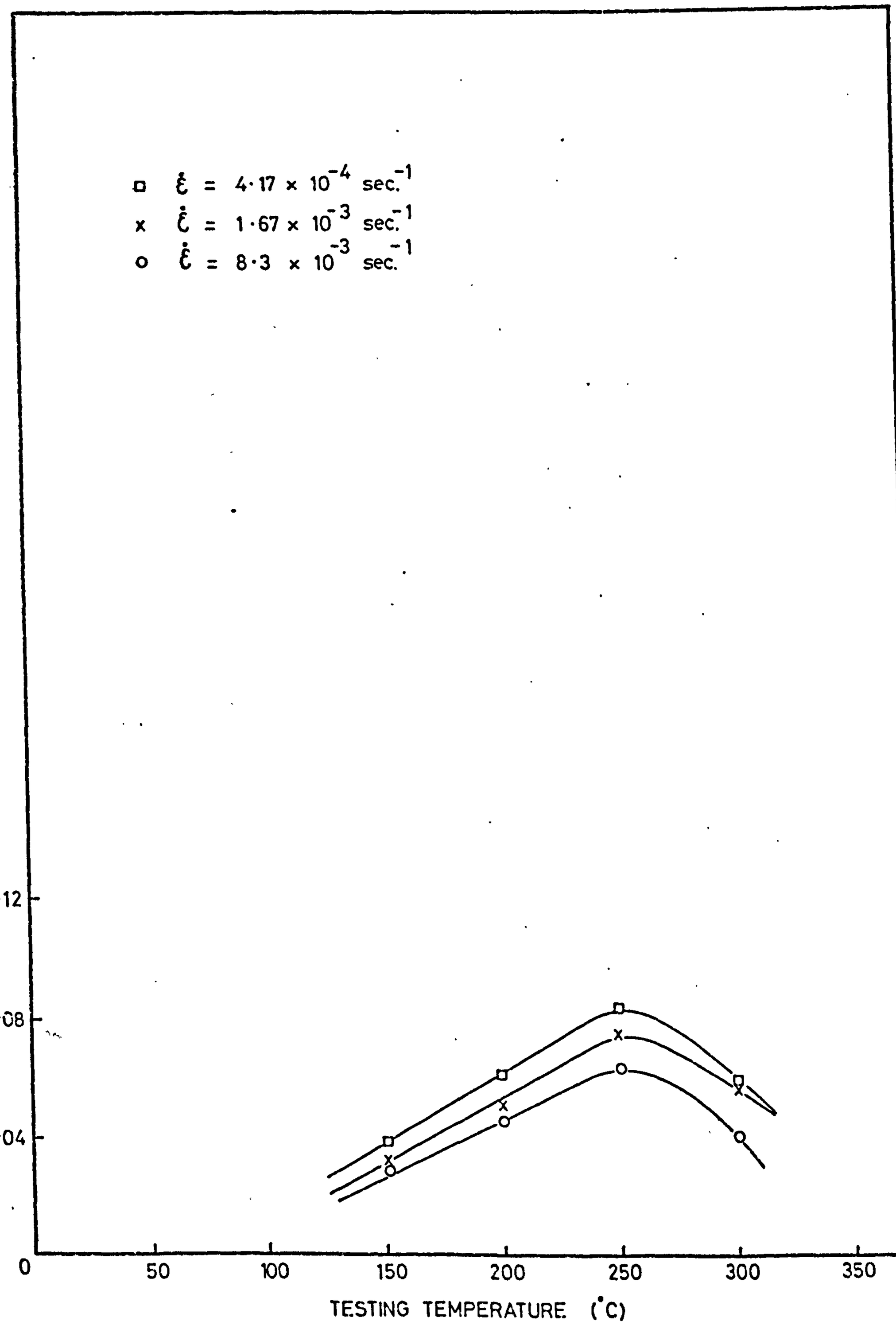


FIG. 26. EFFECT OF STRAIN RATE ON m VALUE FOR 0Mg (25) OVER A RANGE OF TEMPERATURES AND STRAIN RATES.

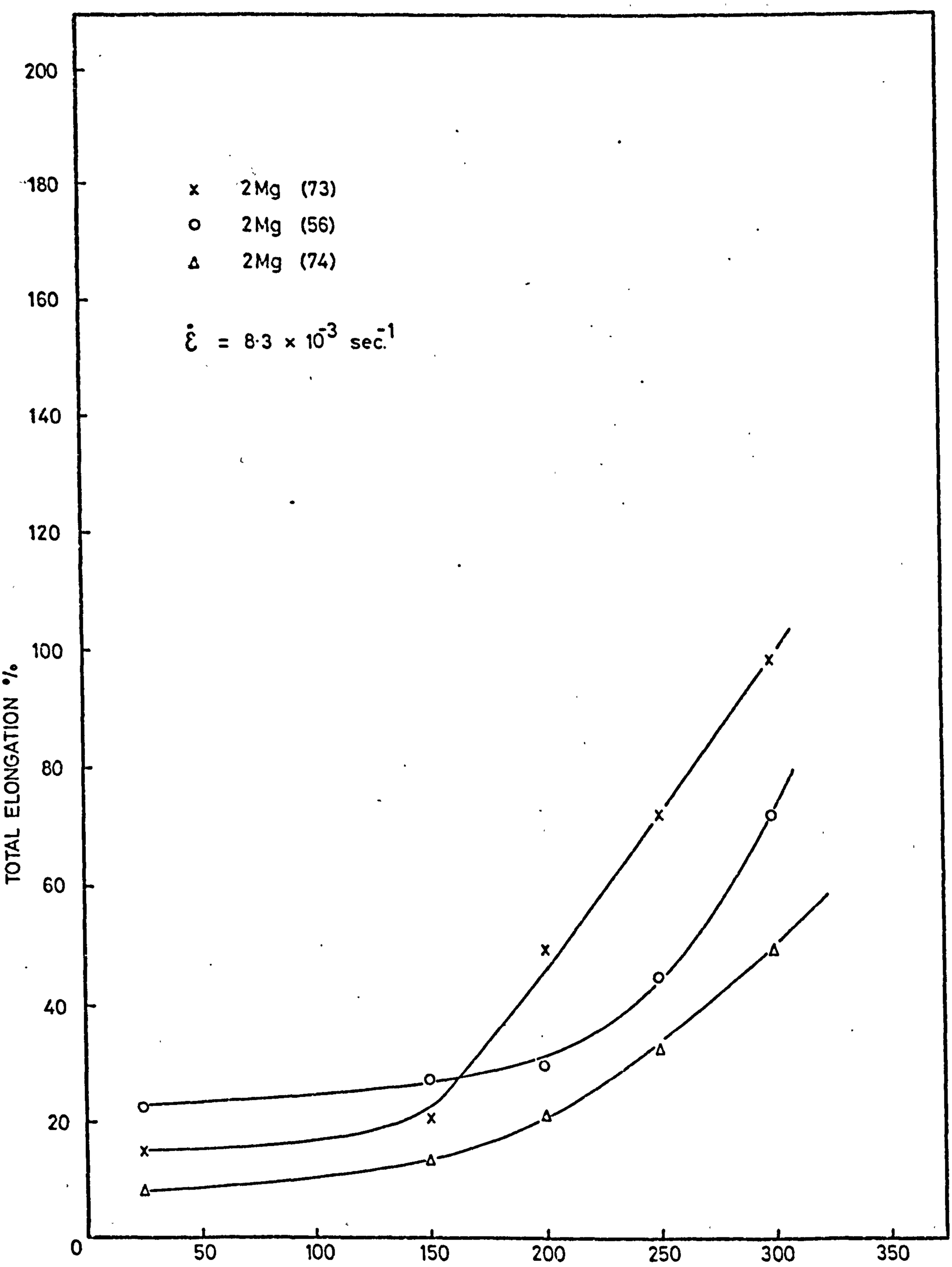


FIG. 27. EFFECT OF INITIAL SHEET TEMPER ON TOTAL ELONGATION FOR 2Mg ALLOY AT INITIAL STRAIN RATE $8{\cdot}3 \times 10^{-3}$ $sec.^{-1}$ AT VARIOUS TEMPERATURES.

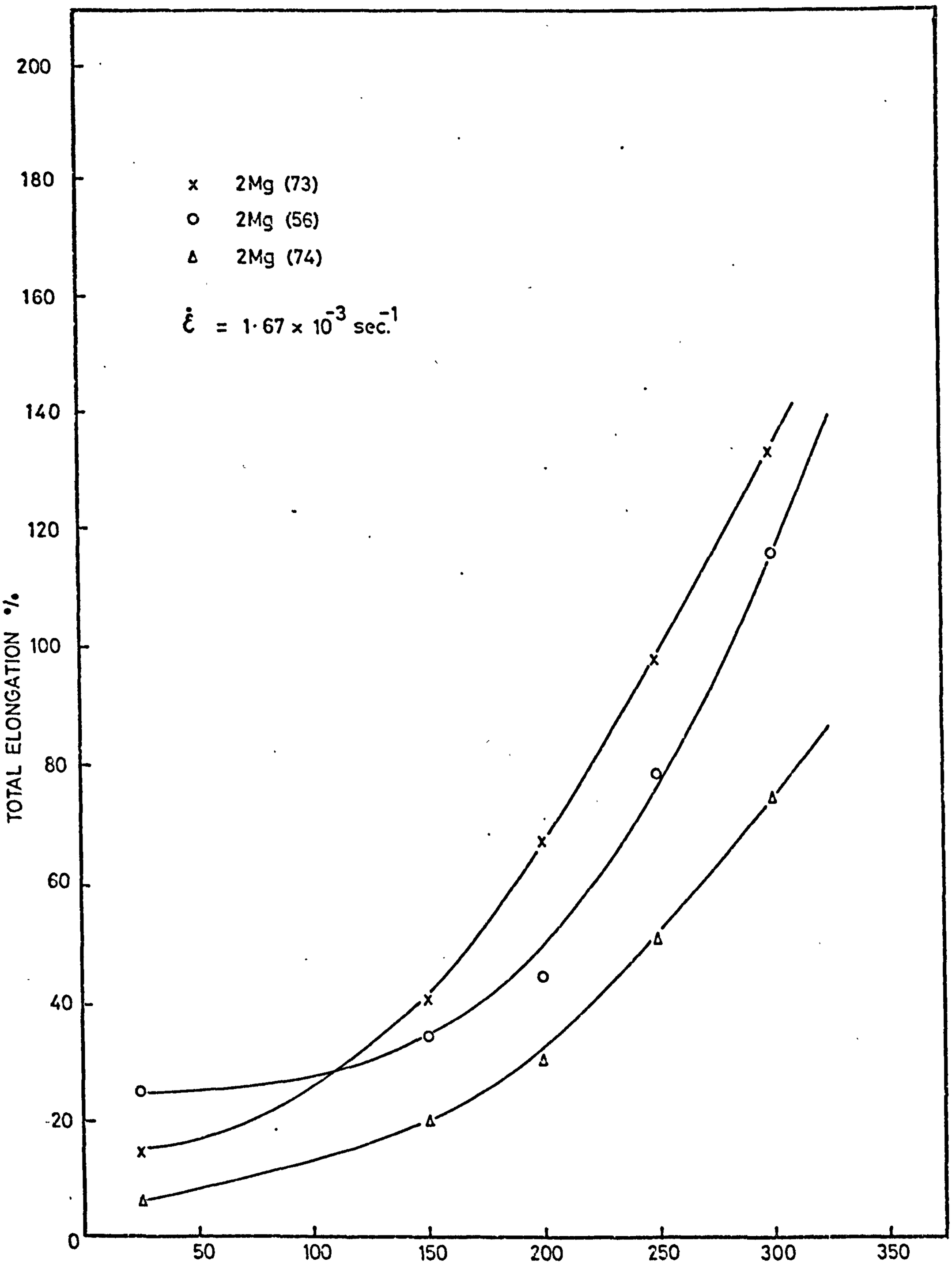


FIG. 28. EFFECT OF INITIAL SHEET TEMPER ON TOTAL ELONGATION FOR 2Mg ALLOY AT INITIAL STRAIN RATE OF 1·67 x 10^{-3} sec.$^{-1}$ AT VARIOUS TEMPERATURES.

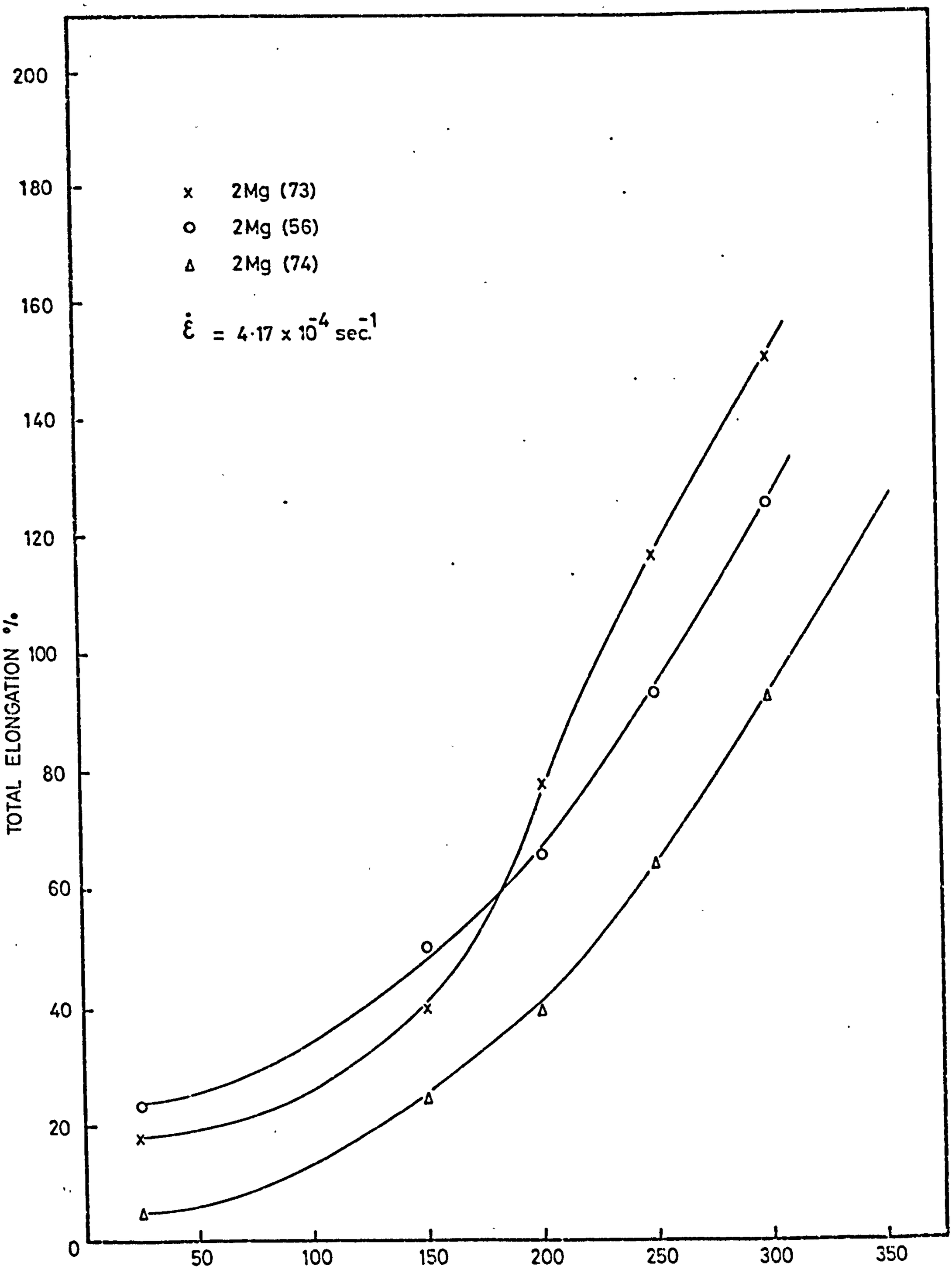


FIG. 29. EFFECT OF INITIAL SHEET TEMPER ON TOTAL ELONGATION FOR 2Mg ALLOY AT INITIAL STRAIN RATE OF $4{\cdot}17 \times 10^{-4}$ $sec.^{-1}$ AT VARIOUS TEMPERATURES.

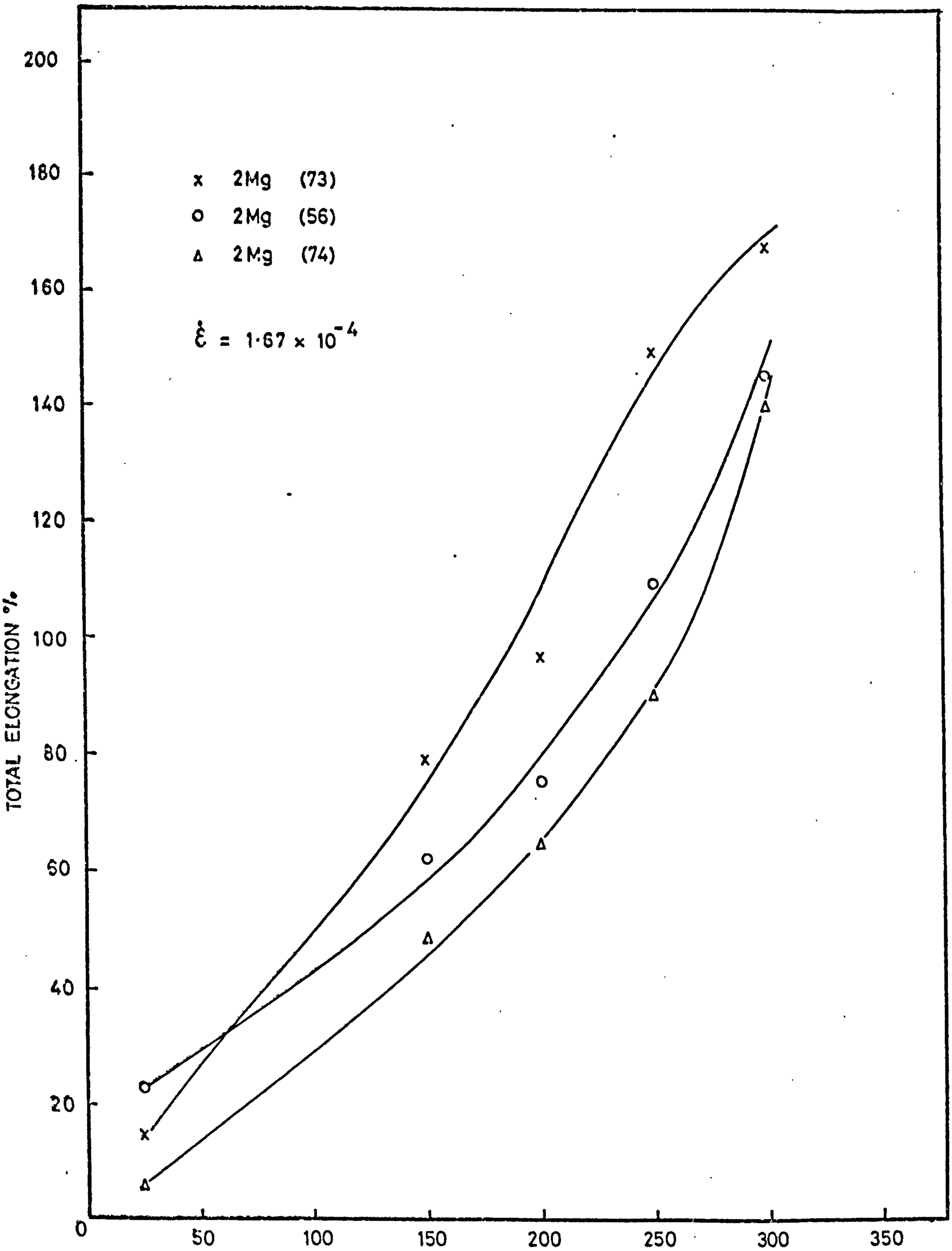


FIG. 30. EFFECT OF INITIAL TEMPER ON TOTAL ELONGATION FOR 2Mg ALLOY AT INITIAL STRAIN RATE OF $1{\cdot}67 \times 10^{-4}$ Sec^{-1} AT VARIOUS TEMPERATURES.

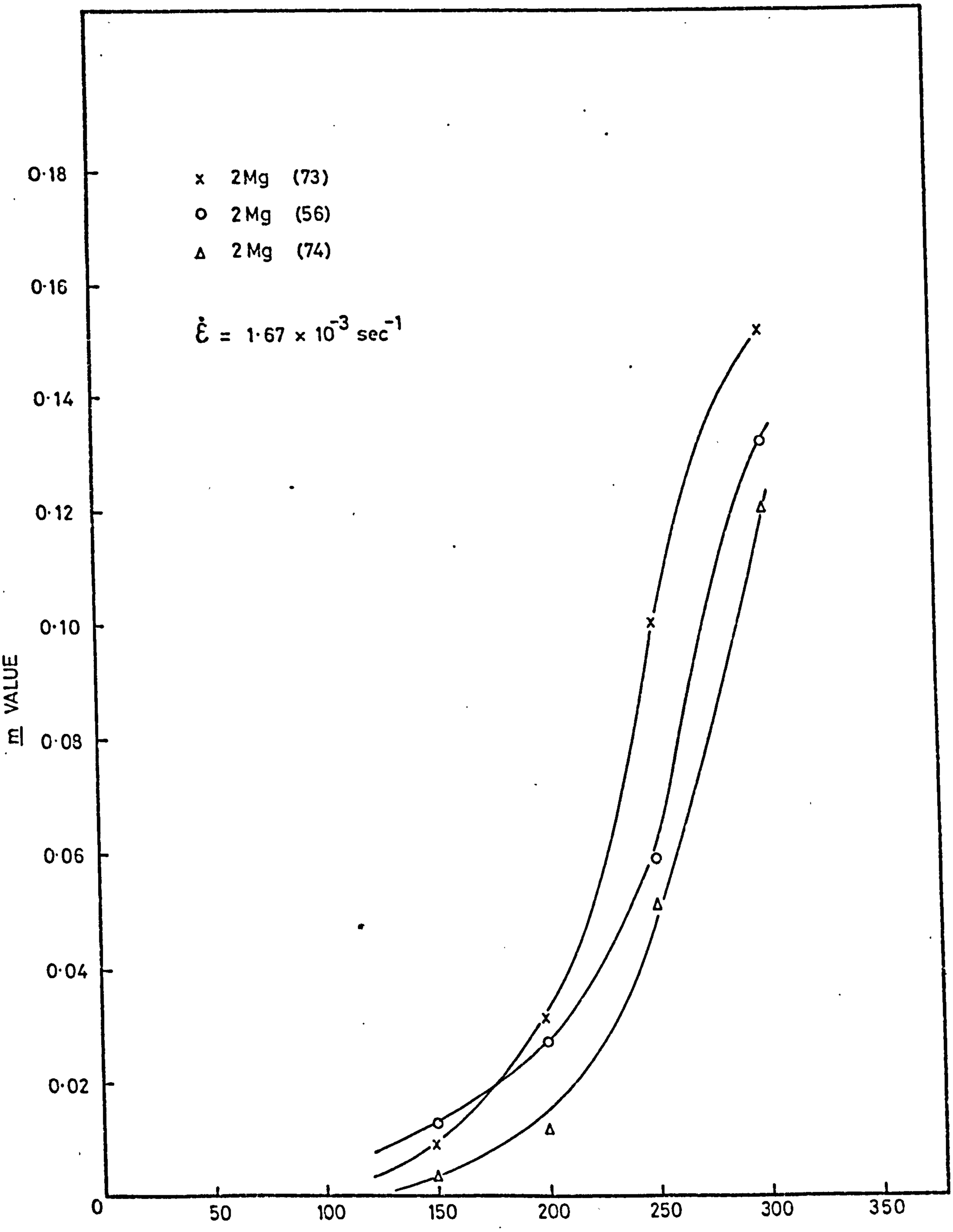


FIG. 31. EFFECT OF TEMPERATURE ON m VALUE FOR VARIOUS TEMPER CONDITIONS AT INITIAL STRAIN RATE OF 1.67×10^{-3} Sec^{-1}

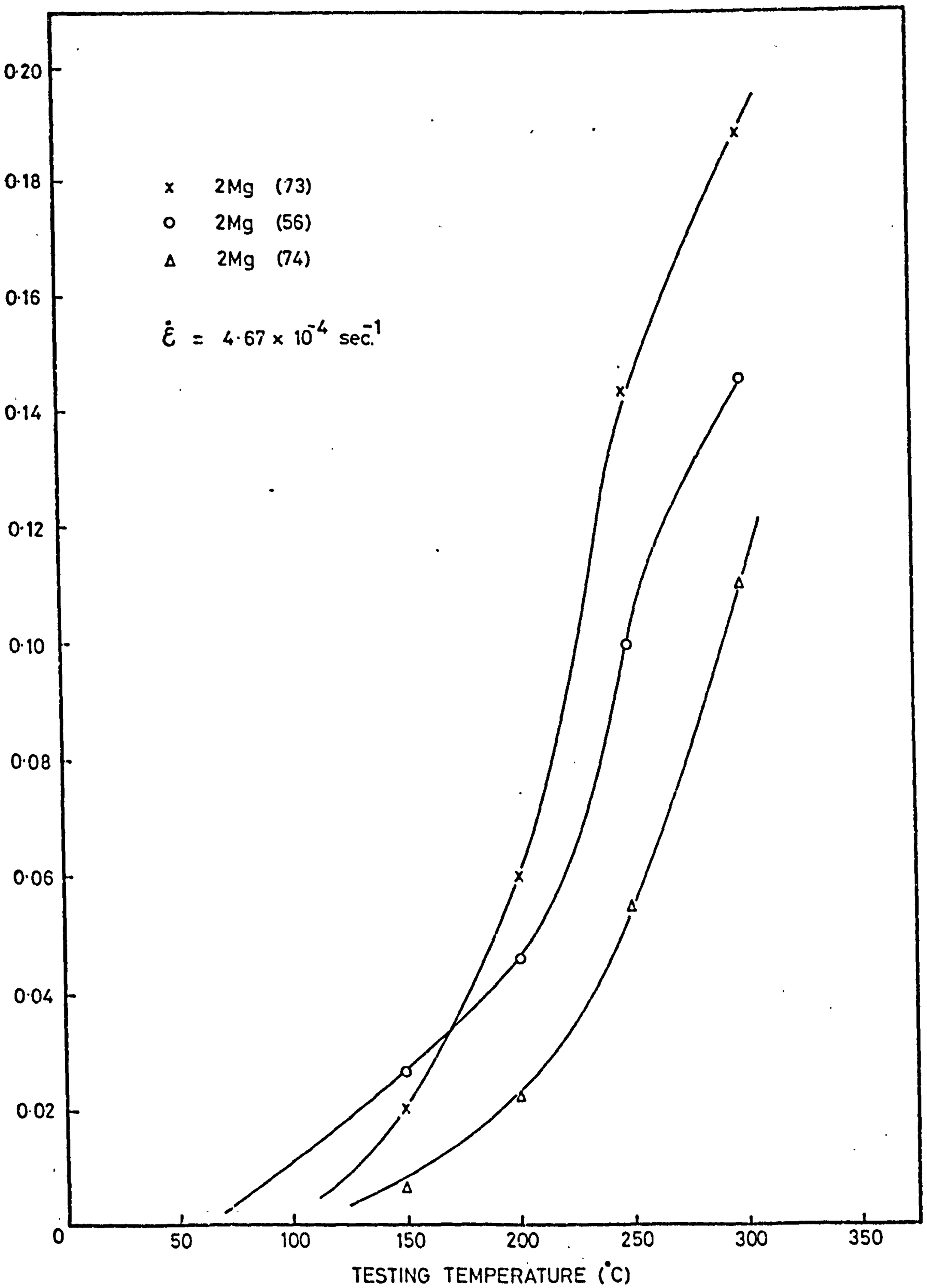


FIG.32. EFFECT OF TEMPERATURE ON m VALUE FOR VARIOUS TEMPER CONDITIONS AT INITIAL STRAIN RATE OF $4{\cdot}67 \times 10^{-4}$ Sec^{-1}

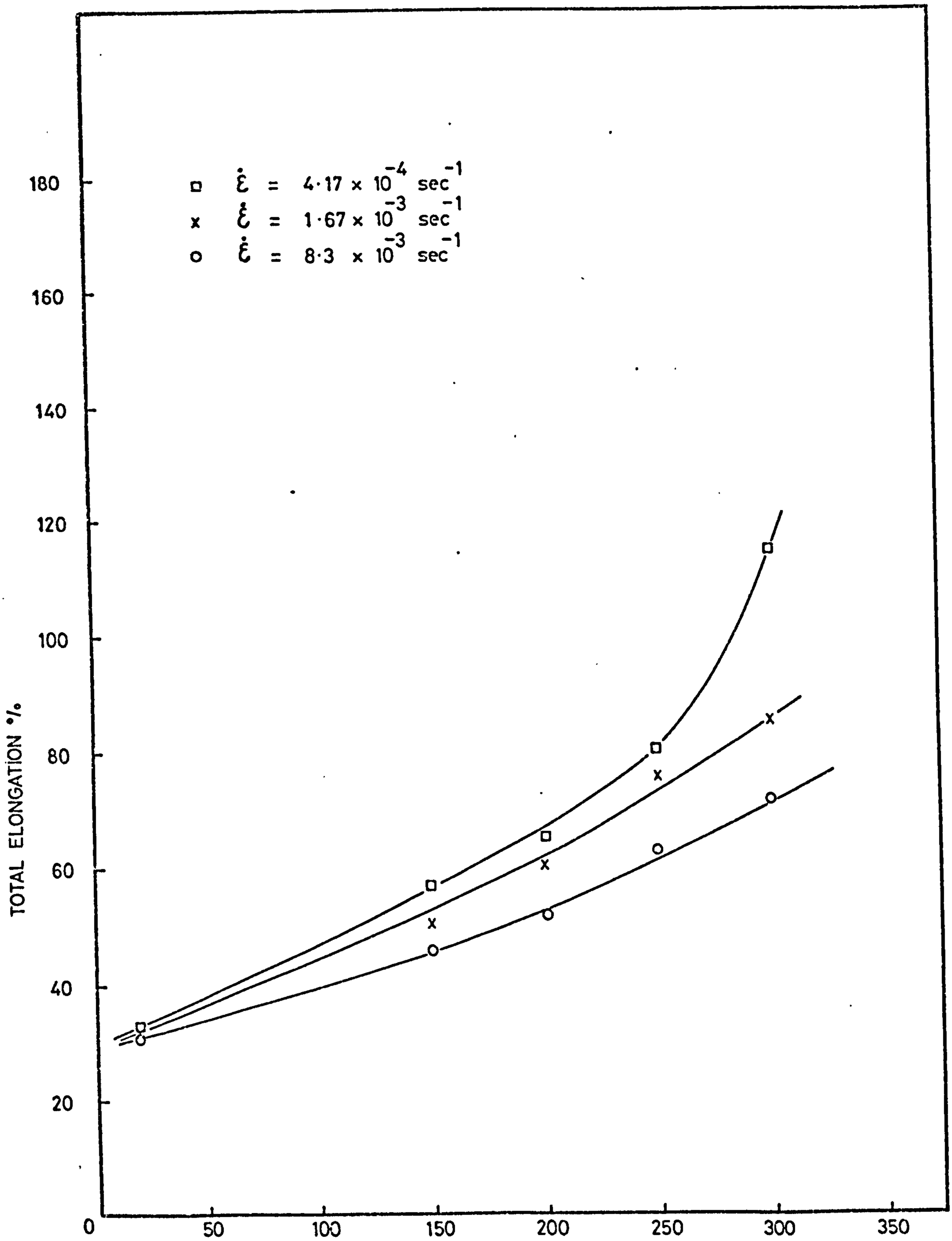


FIG. 33. VARIATION IN TOTAL ELONGATION WITH TESTING TEMPERATURE ON 3Mg (62) AT VARIOUS STRAIN RATES.

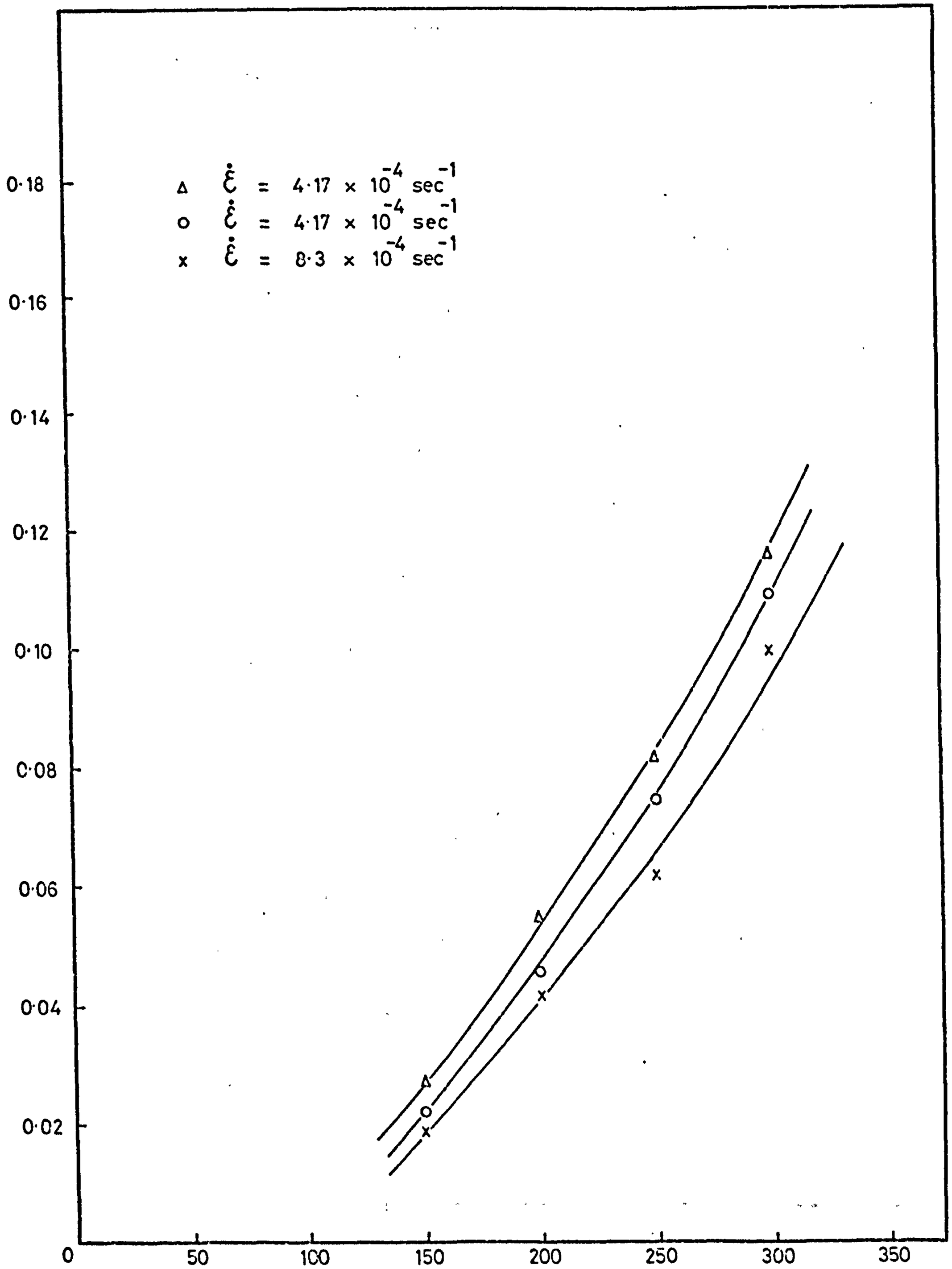


FIG.34. EFFECT OF STRAIN RATE ON m VALUE FOR 3Mg (62) OVER A RANGE OF TEMPERATURES AND STRAIN RATES.

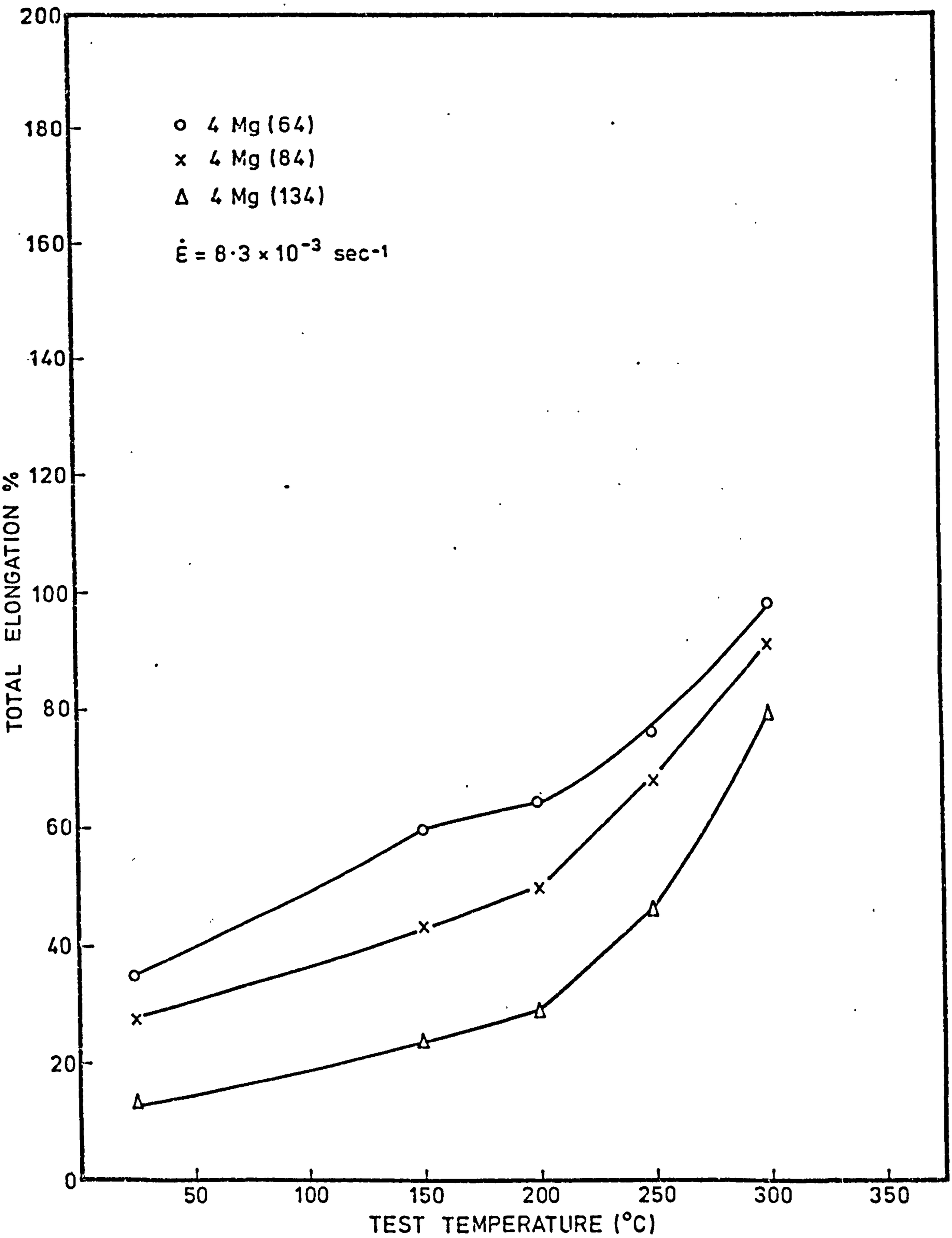


FIG. 35. EFFECT OF INITIAL SHEET HARDNESS ON ELONGATION FOR 4 Mg ALLOY AT VARIOUS TEMPERATURES AT AN INITIAL STRAIN-RATE OF $8{\cdot}3 \times 10^{-3}$ sec^{-1}

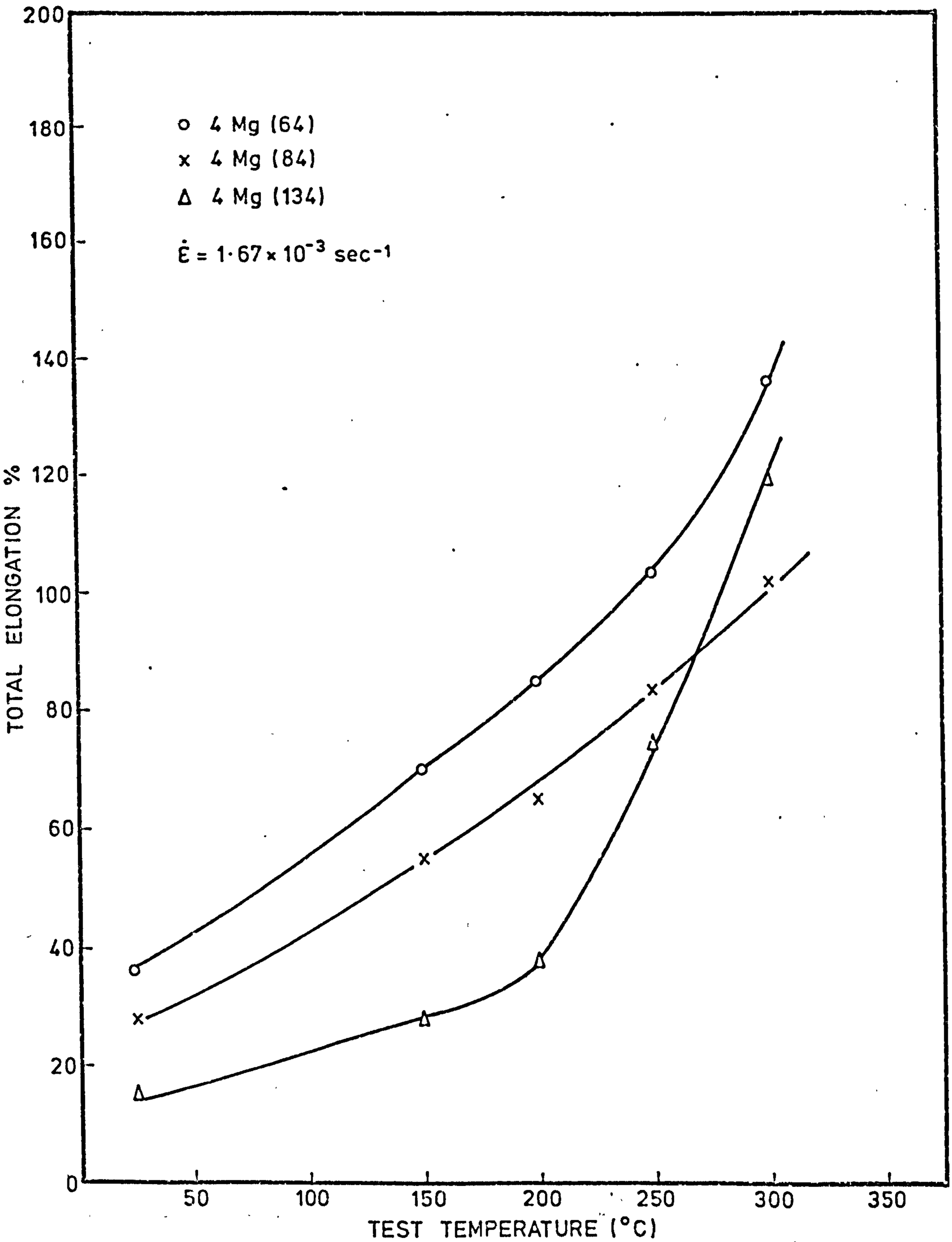


FIG. 36. EFFECT OF INITIAL SHEET HARDNESS ON ELONGATION FOR 4 Mg ALLOY AT VARIOUS TEMPERATURES AT AN INITIAL STRAIN-RATE OF $1{\cdot}67 \times 10^{-3}$ sec^{-1}

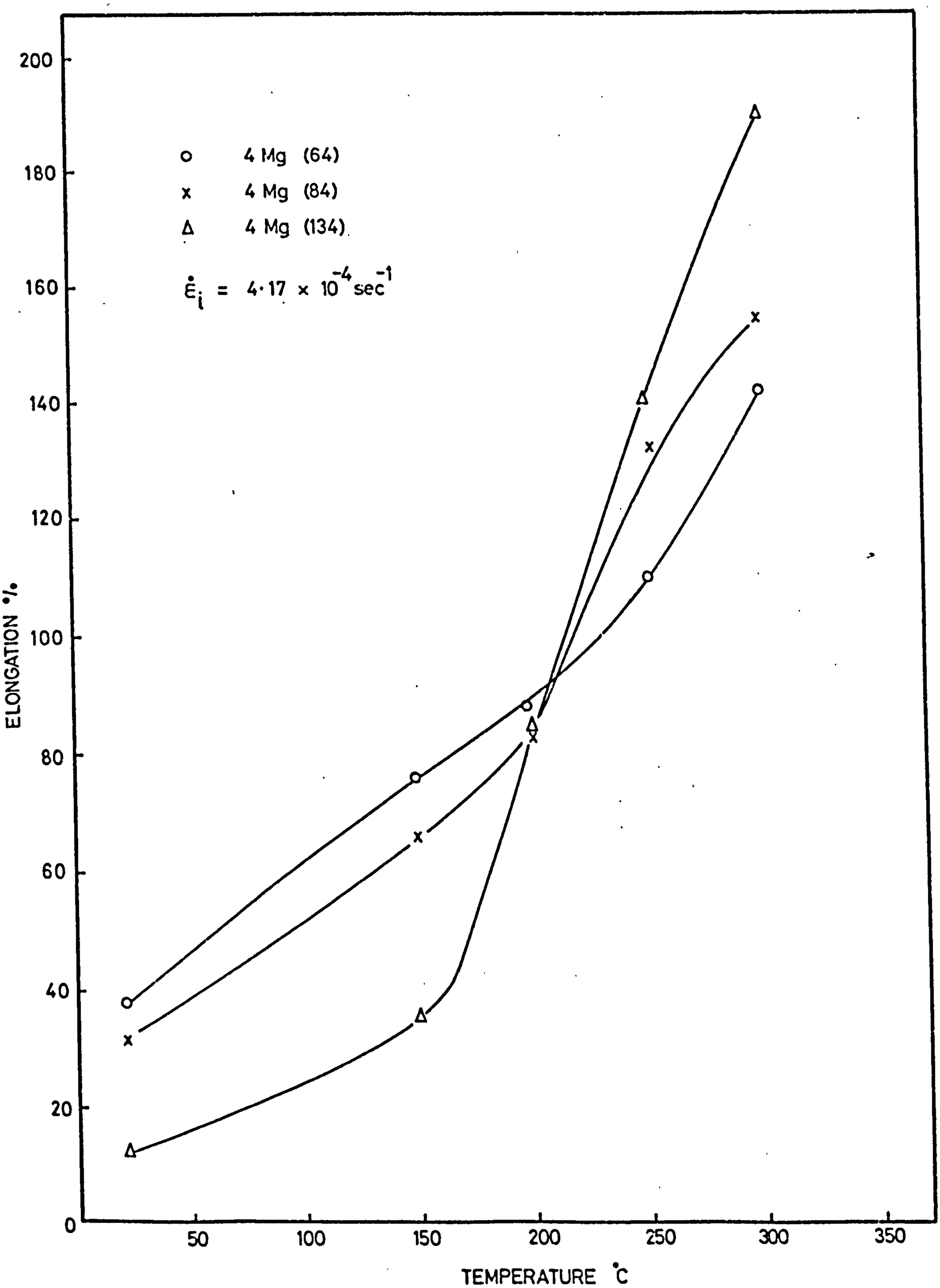


FIG.37. EFFECT OF INITIAL SHEET HARDNESS ON ELONGATION AT VARIOUS TEMPERATURES AND ON INITIAL STRAIN RATE OF $4{\cdot}17 \times 10^{-4}\ sec^{-1}$

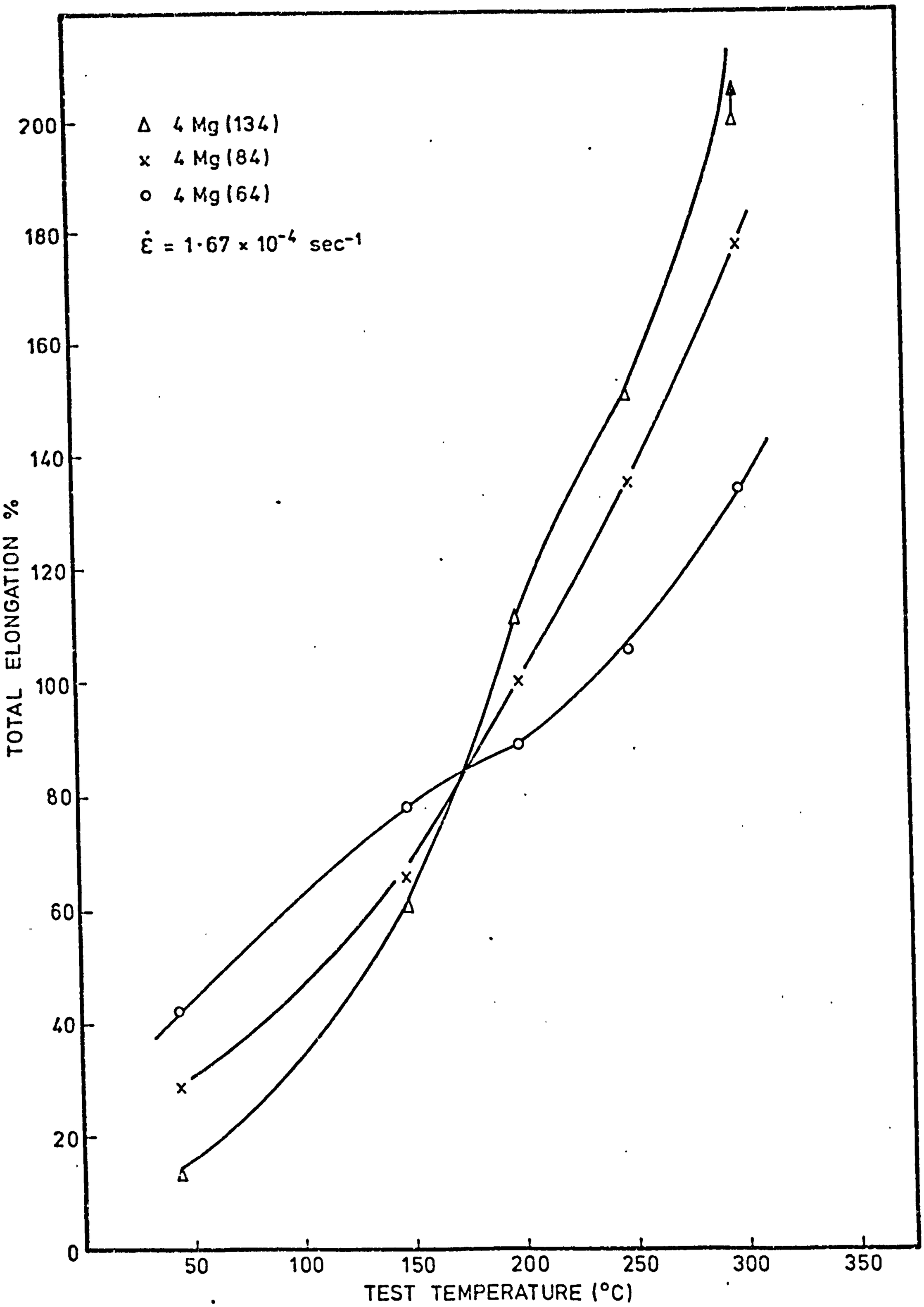


FIG. 38. EFFECT OF INITIAL SHEET HARDNESS ON ELONGATION AT VARIOUS TEMPERATURES AT AN INITIAL STRAIN-RATE OF $1{\cdot}67 \times 10^{-4}$ sec^{-1}

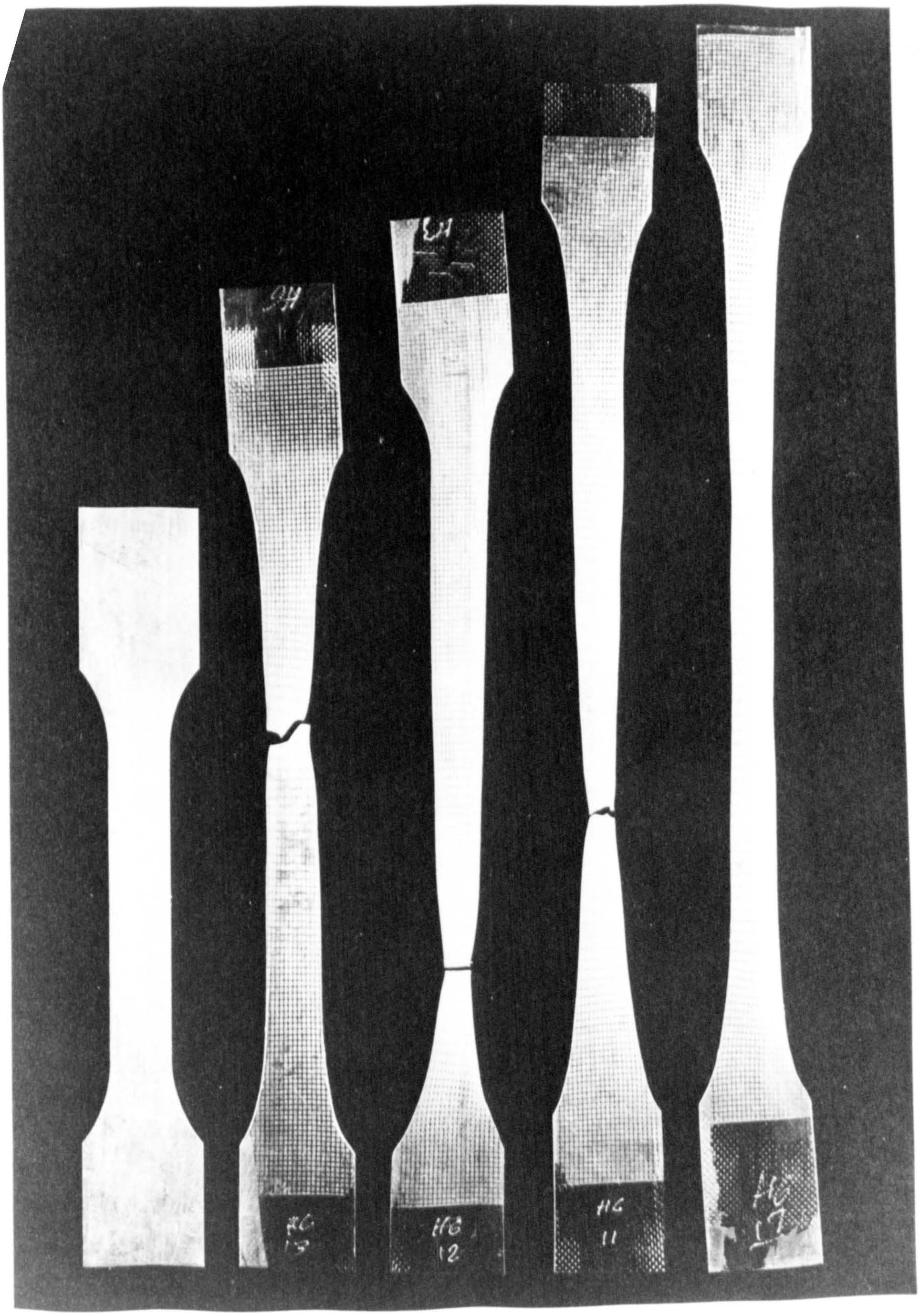


Fig. 39 Effect of strain rate on elongation for 4Mg(134) deformed at 300°C and initial strain rates of 8.3×10^{-3}, 1.67×10^{-3}, 4.17×10^{-4} and 1.67×10^{-4} sec^{-1} from left to right

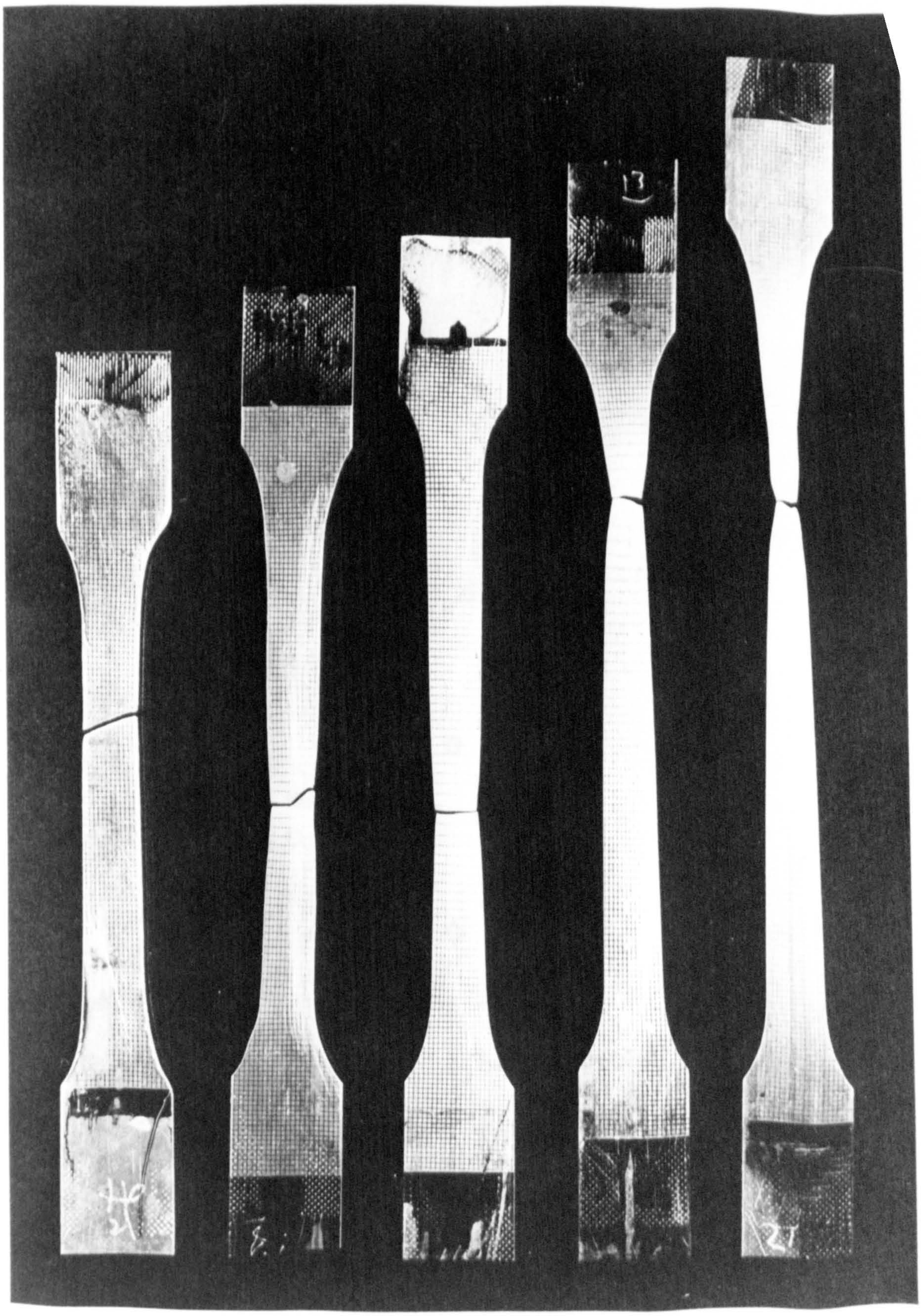


Fig. 40 Effect of test temperatures on elongation for 4 Mg(134) at 20°C, 150°C, 200°C, 250°C and 300°C from left to right.

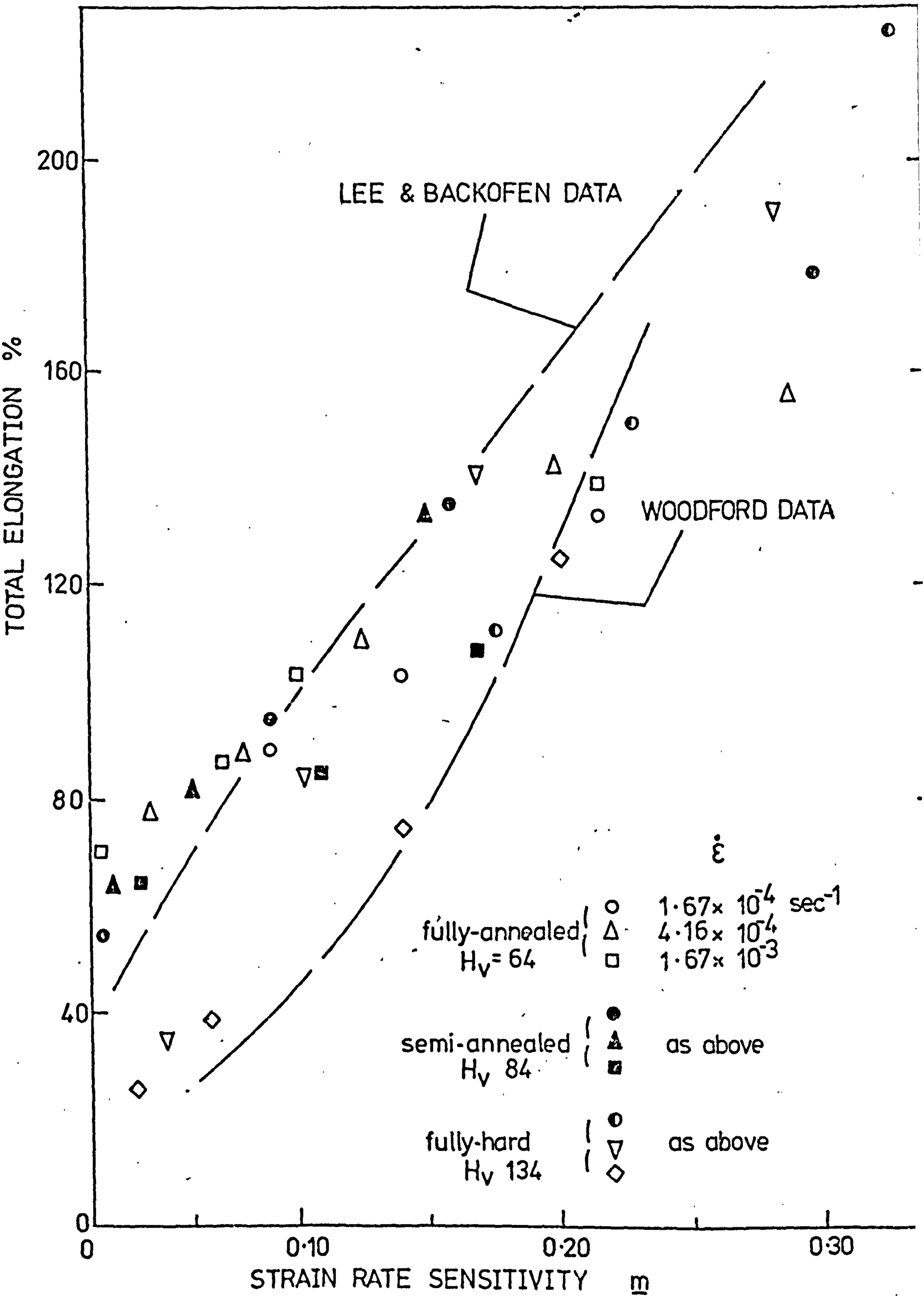


FIG.41. TOTAL ELONGATION ON 4Mg ALLOY AT VARIOUS TEMPERATURI AND STRAIN RATE VERSUS m VALUE.

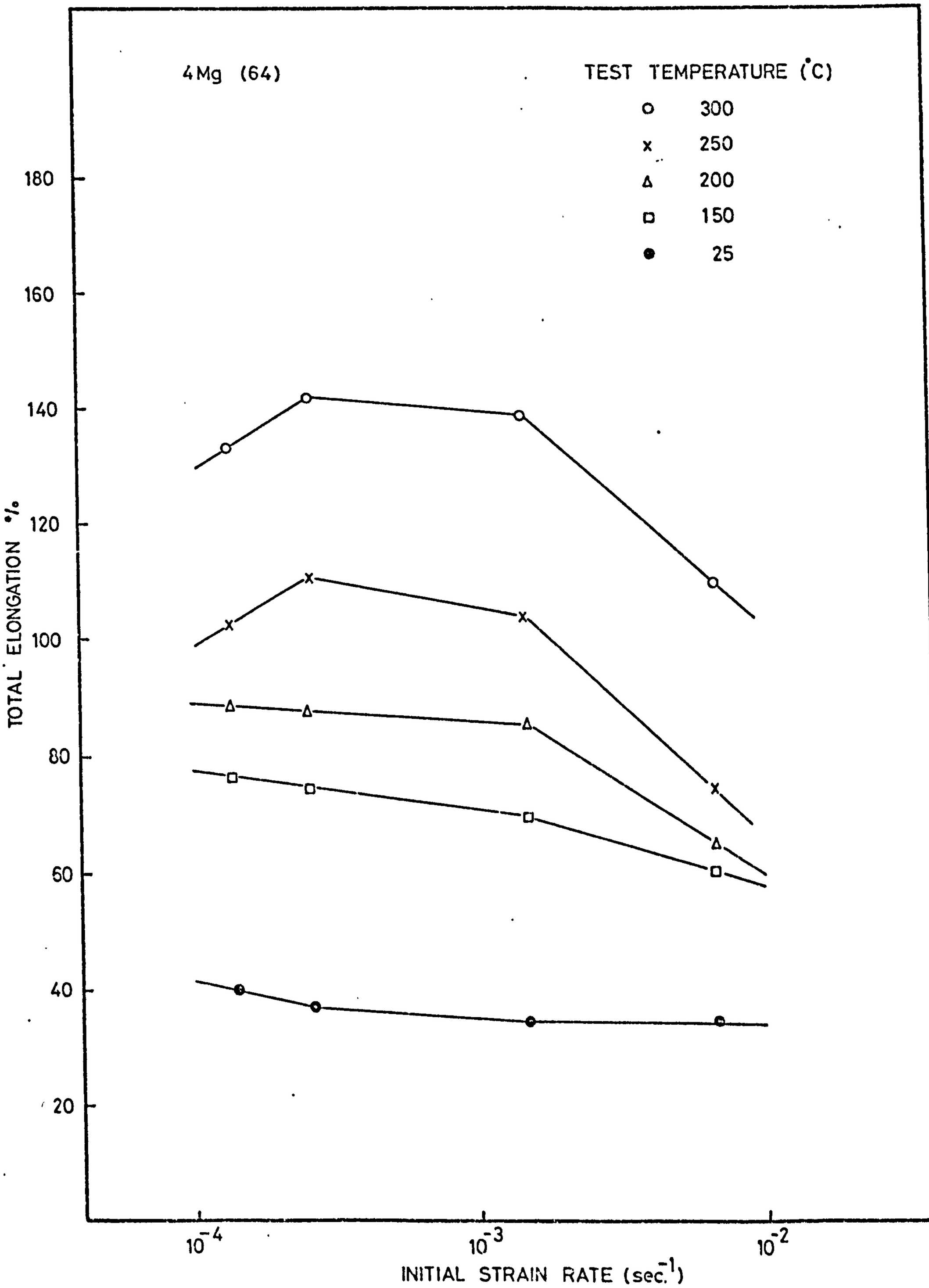


FIG.42. EFFECT OF INITIAL STRAIN RATE ON TOTAL ELONGATION FOR 4Mg (64) AT VARIOUS TEMPERATURES.

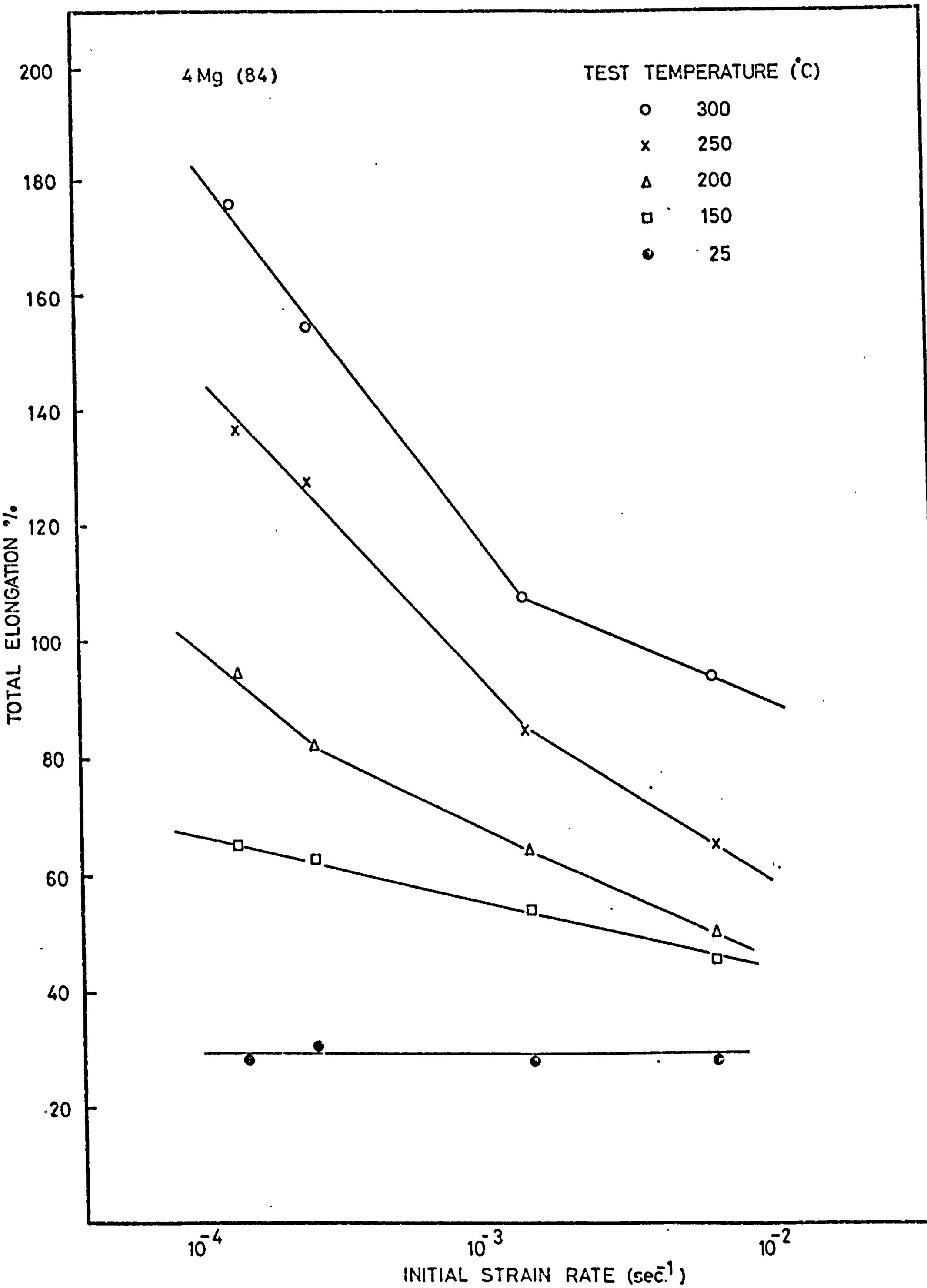


FIG. 43. EFFECT OF INITIAL STRAIN RATE ON TOTAL ELONGATION FOR 4Mg (84) AT VARIOUS TEMPERATURES.

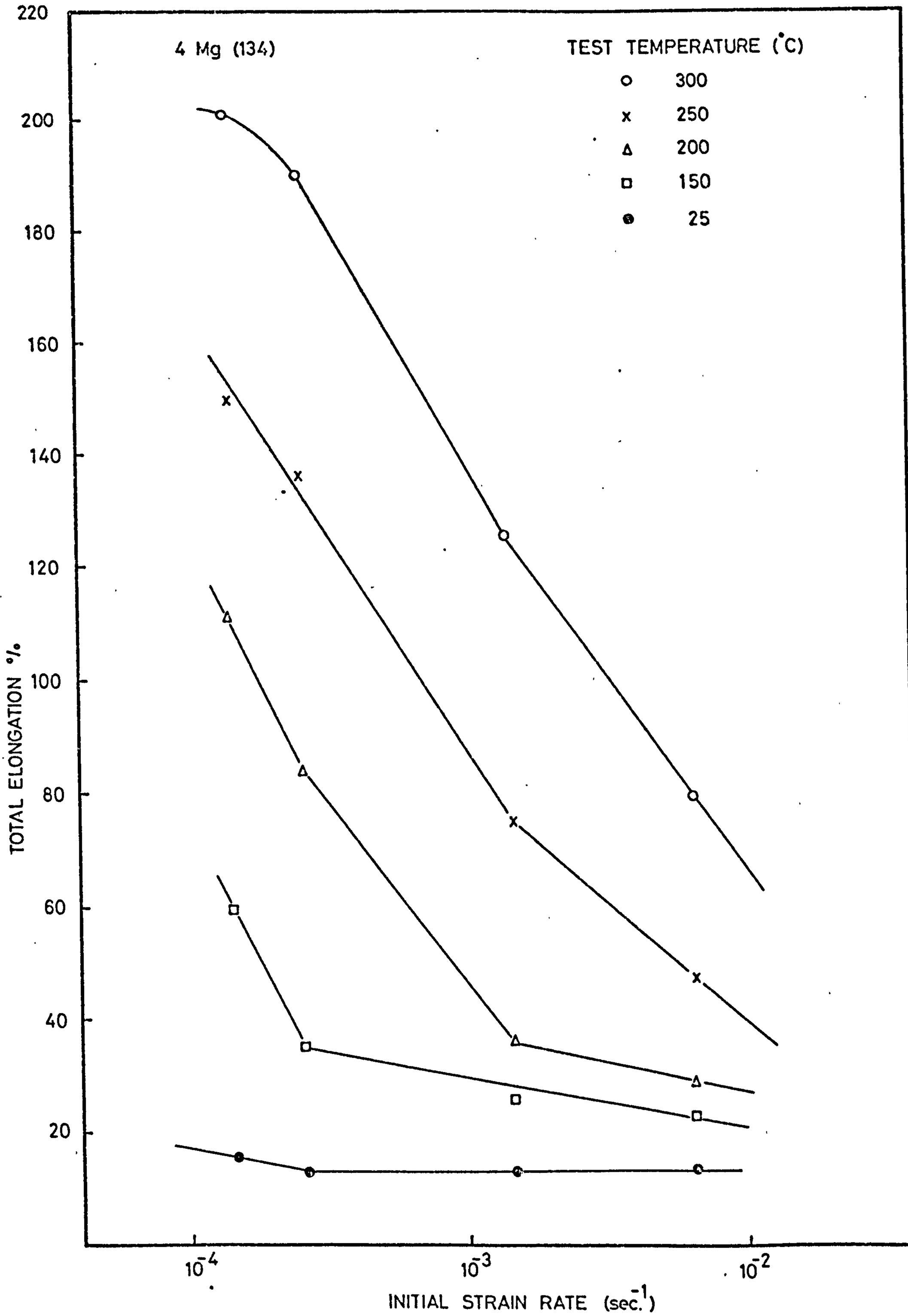


FIG. 44. EFFECT OF INITIAL STRAIN RATE ON TOTAL ELONGATION FOR 4 Mg (134) AT VARIOUS TEMPERATURES.

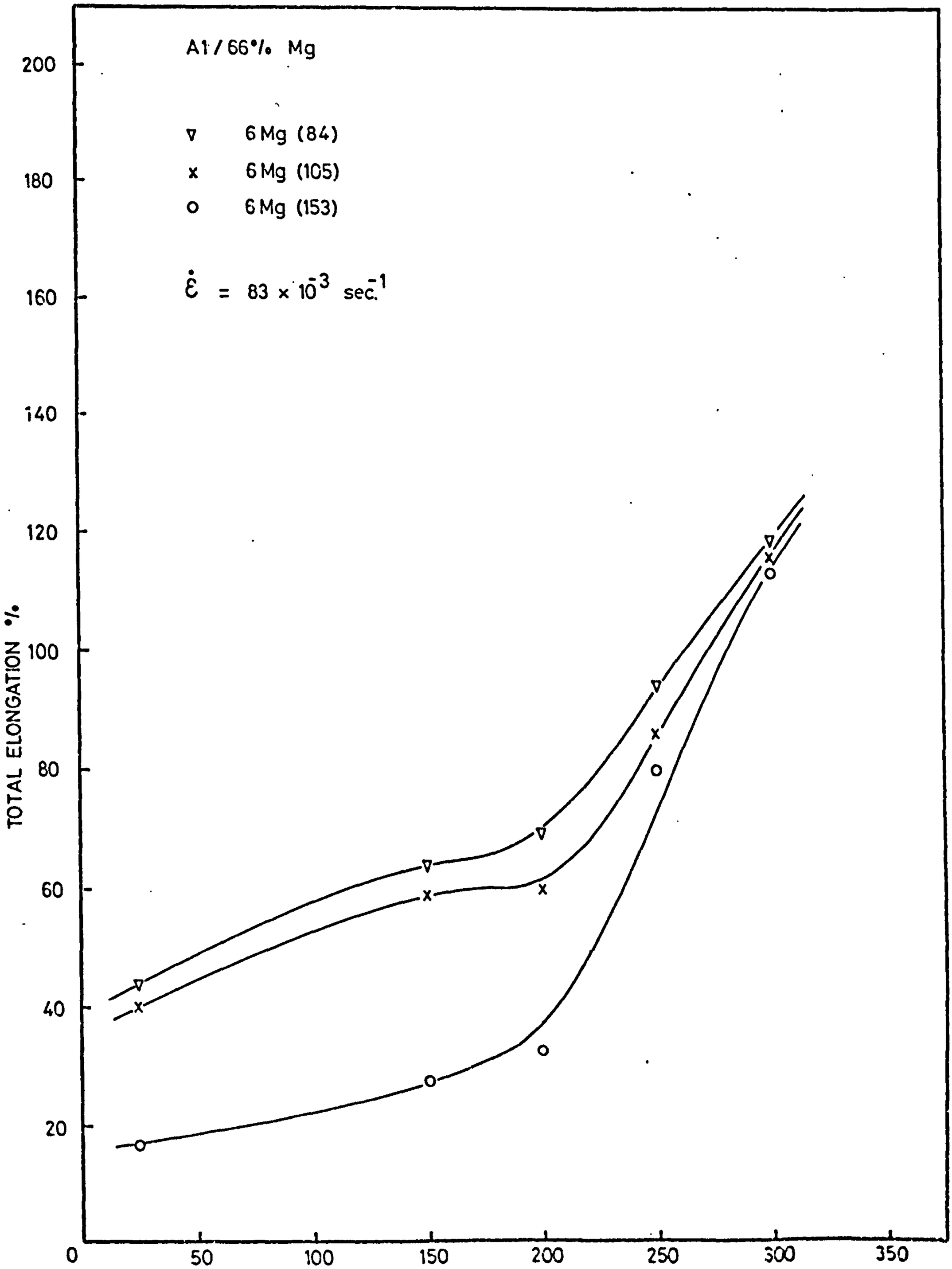


FIG.45. EFFECT OF INITIAL SHEET HARDNESS ON TOTAL ELONGATION AT VARIOUS TEMPERATURES AT AN INITIAL STRAIN RATE OF $8{\cdot}3 \times 10^{-3}$ $sec.^{-1}$

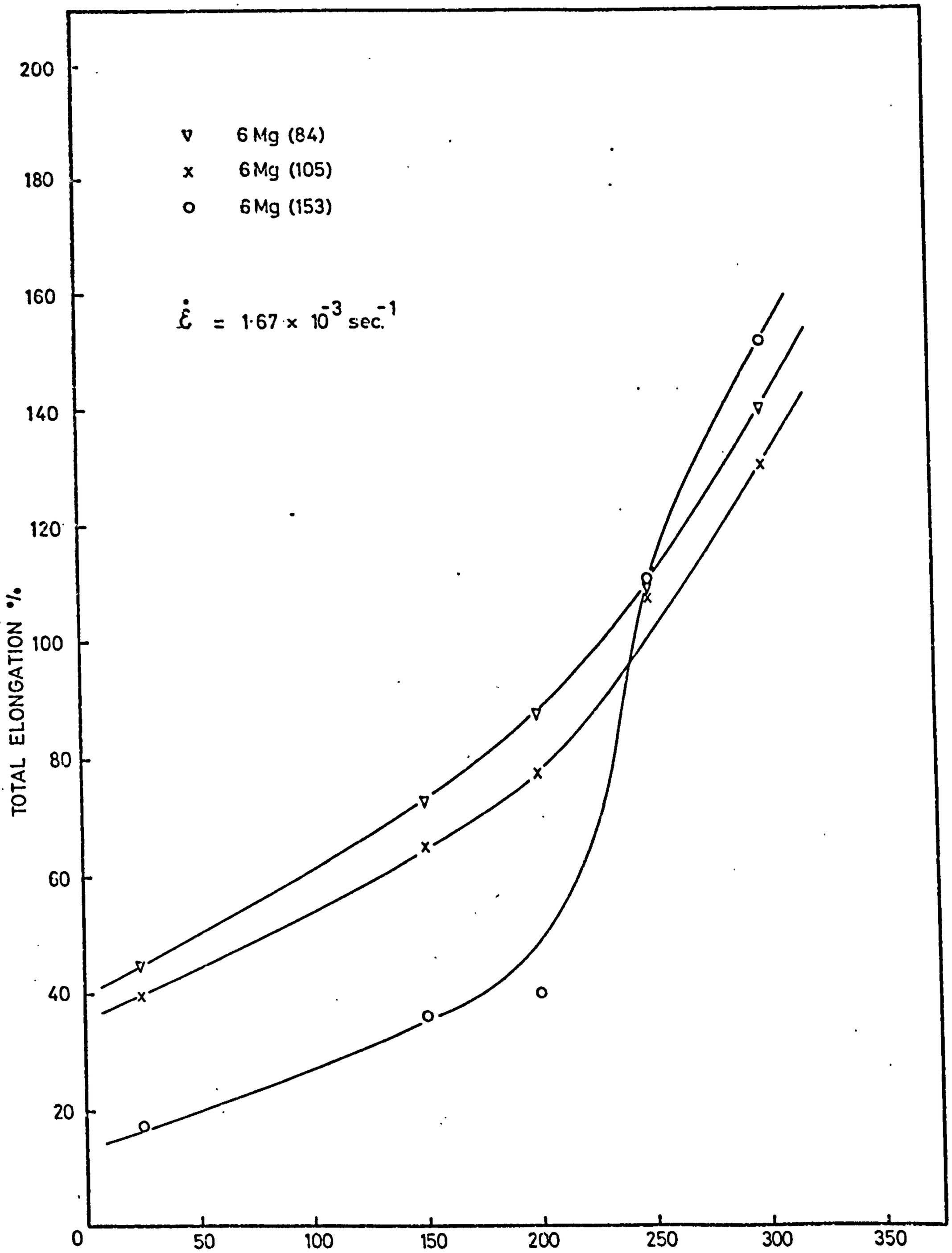


FIG.46. EFFECT OF INITIAL SHEET HARDNESS ON TOTAL ELONGATION AT VARIOUS TEMPERATURES AT AN INITIAL STRAIN RATE OF 1·67 × 10^{-3} sec.$^{-1}$

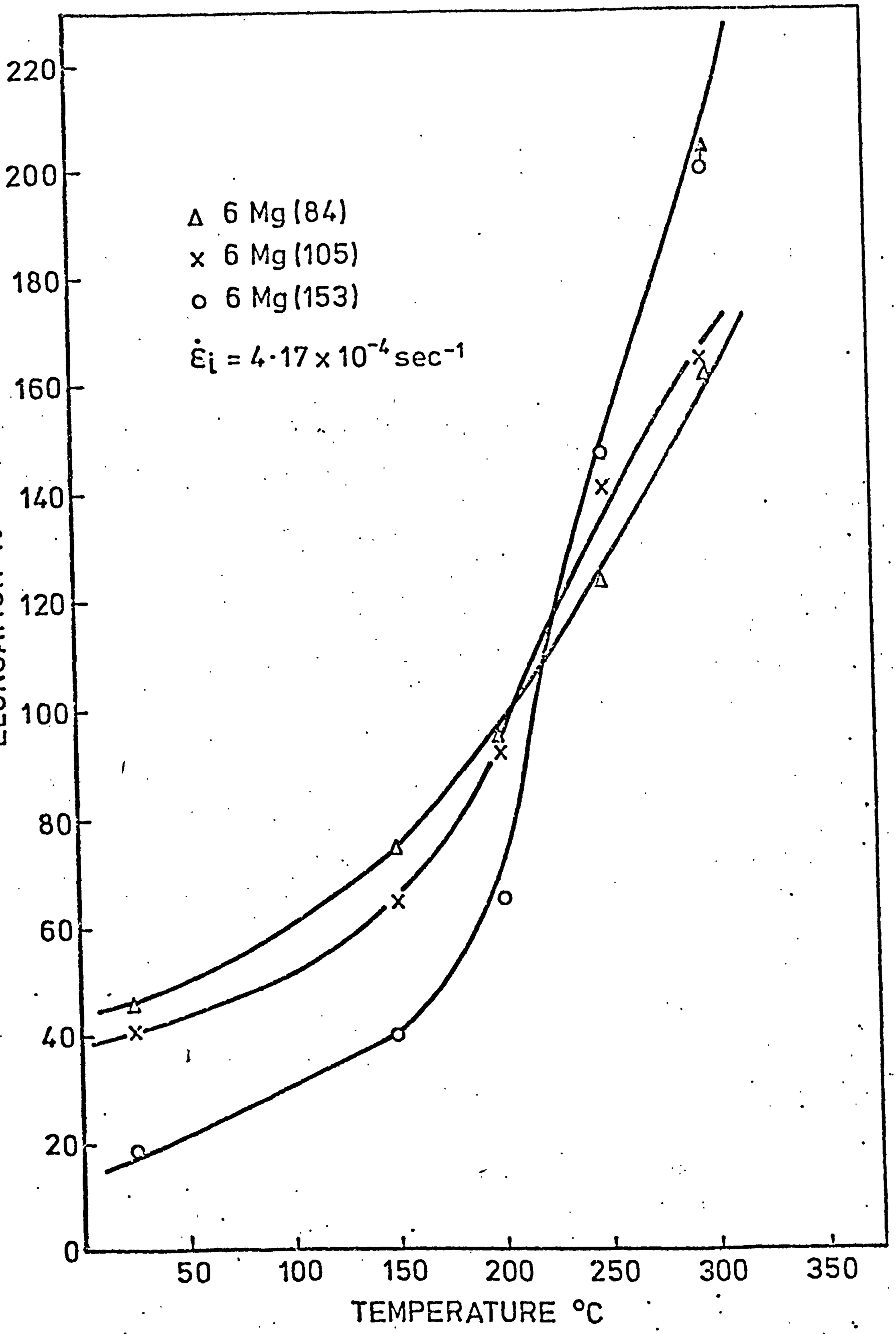


FIG. 47. EFFECT OF INITIAL SHEET HARDNESS ON TOTAL ELONGATION AT VARIOUS TEMPERATURES AND

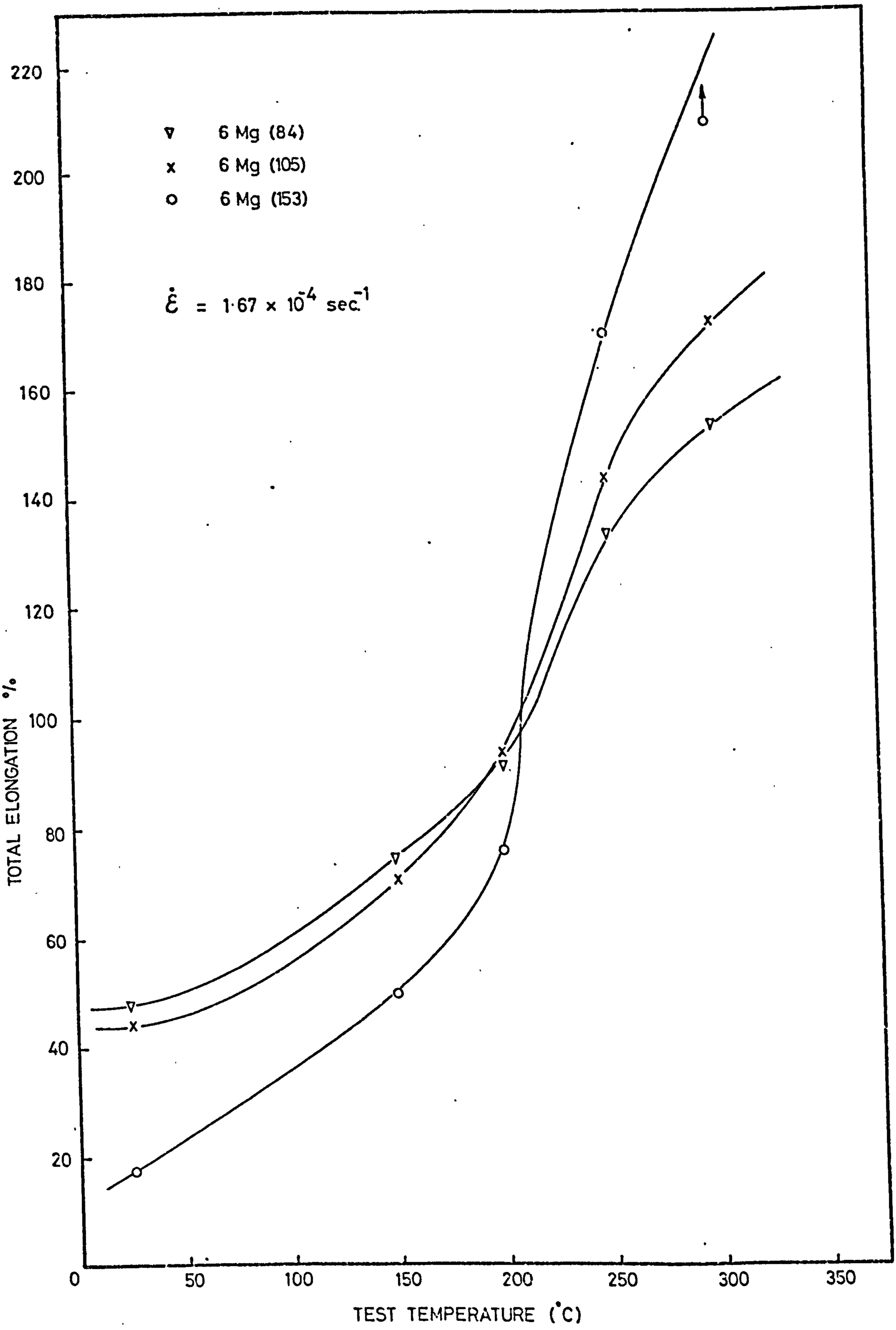


FIG.48. EFFECT OF INITIAL SHEET HARDNESS ON TOTAL ELONGATION AT VARIOUS TEMPERATURES AT AN INITIAL STRAIN RATE OF $1 \cdot 67 \times 10^{-4}$ sec.$^{-1}$



Fig. 49 Effect of strain rate on elongation for 6 Mg(105) deformed at 250°C and initial strain rates of 8.3×10^{-3}, 1.67×10^{-3}, 4.17×10^{-4} and 1.67×10^{-4} sec^{-1} from left to right.



Fig. 50 Effect of test temperature on elongation for 6 Mg(84) at 20°C, 150°C, 200°C, 250°C and 300°C from left to right.

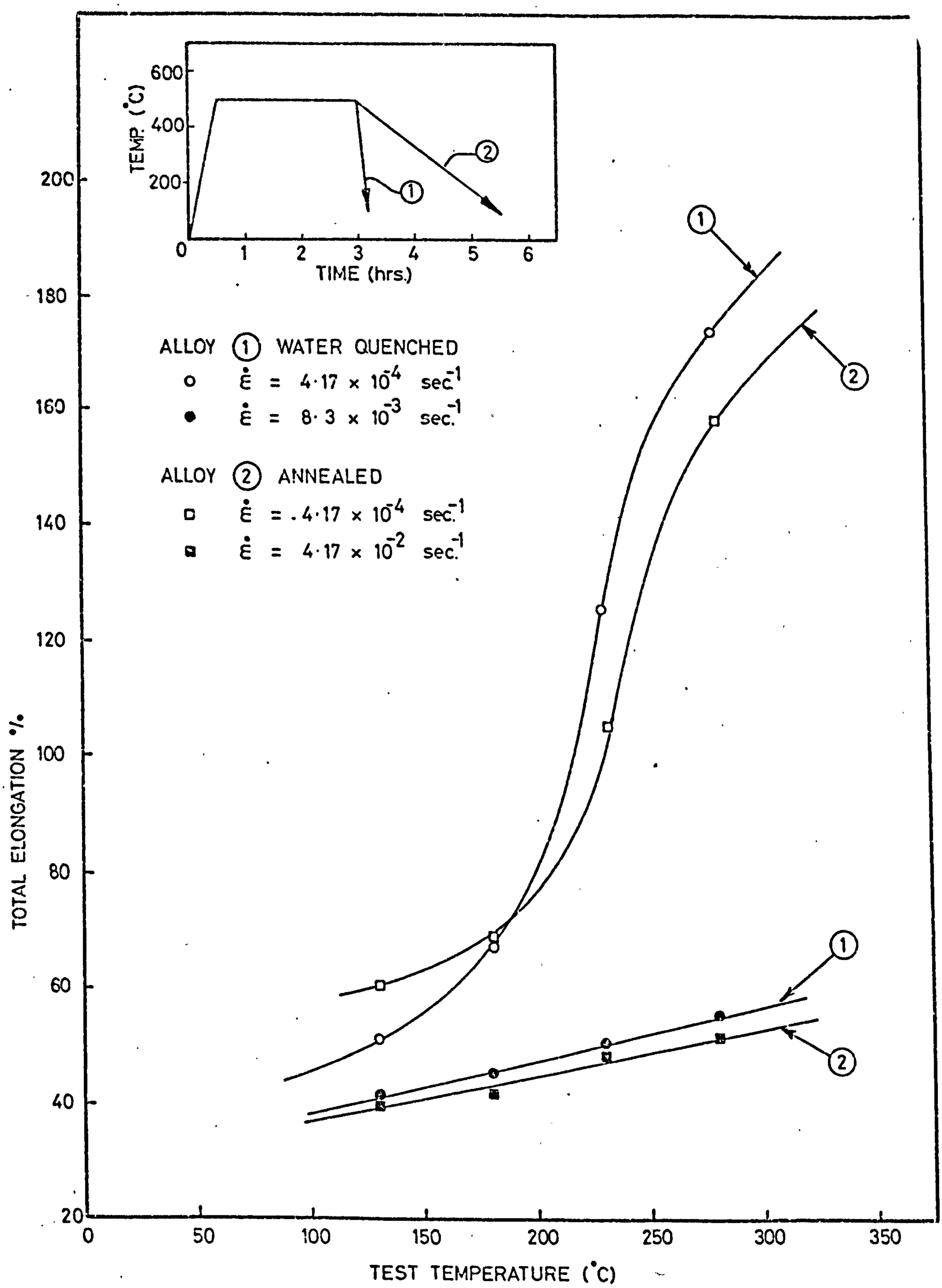


FIG. 51. INFLUENCE OF WATER QUENCHING AND ANNEALING ON TOTAL ELONGATION AT VARIOUS TEMPERATURES FOR 6 Mg ALLOY.

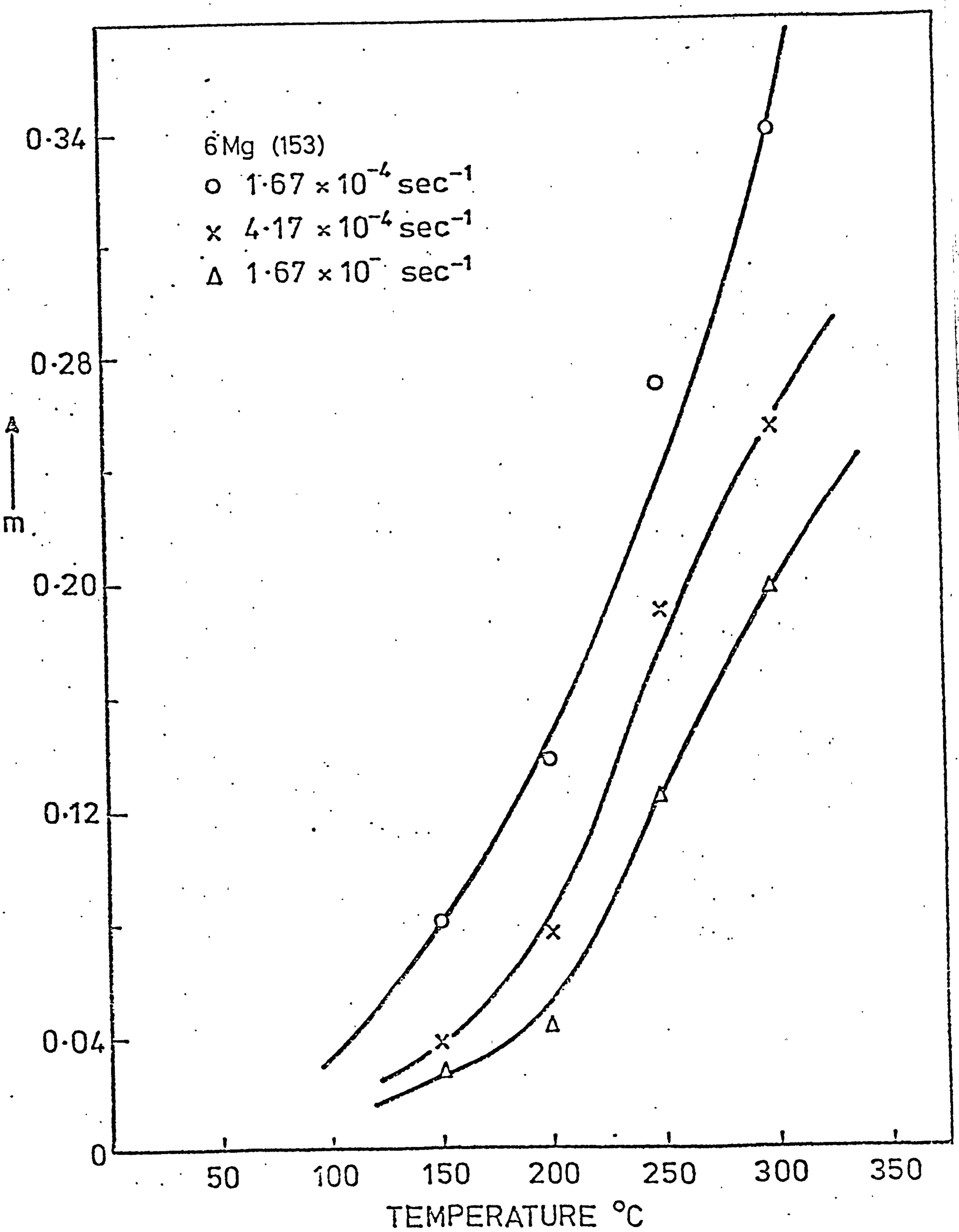


FIG.52. EFFECT OF TEMPERATURE ON m VALUE FOR 6Mg (153) AT VARIOUS STRAIN RATES.

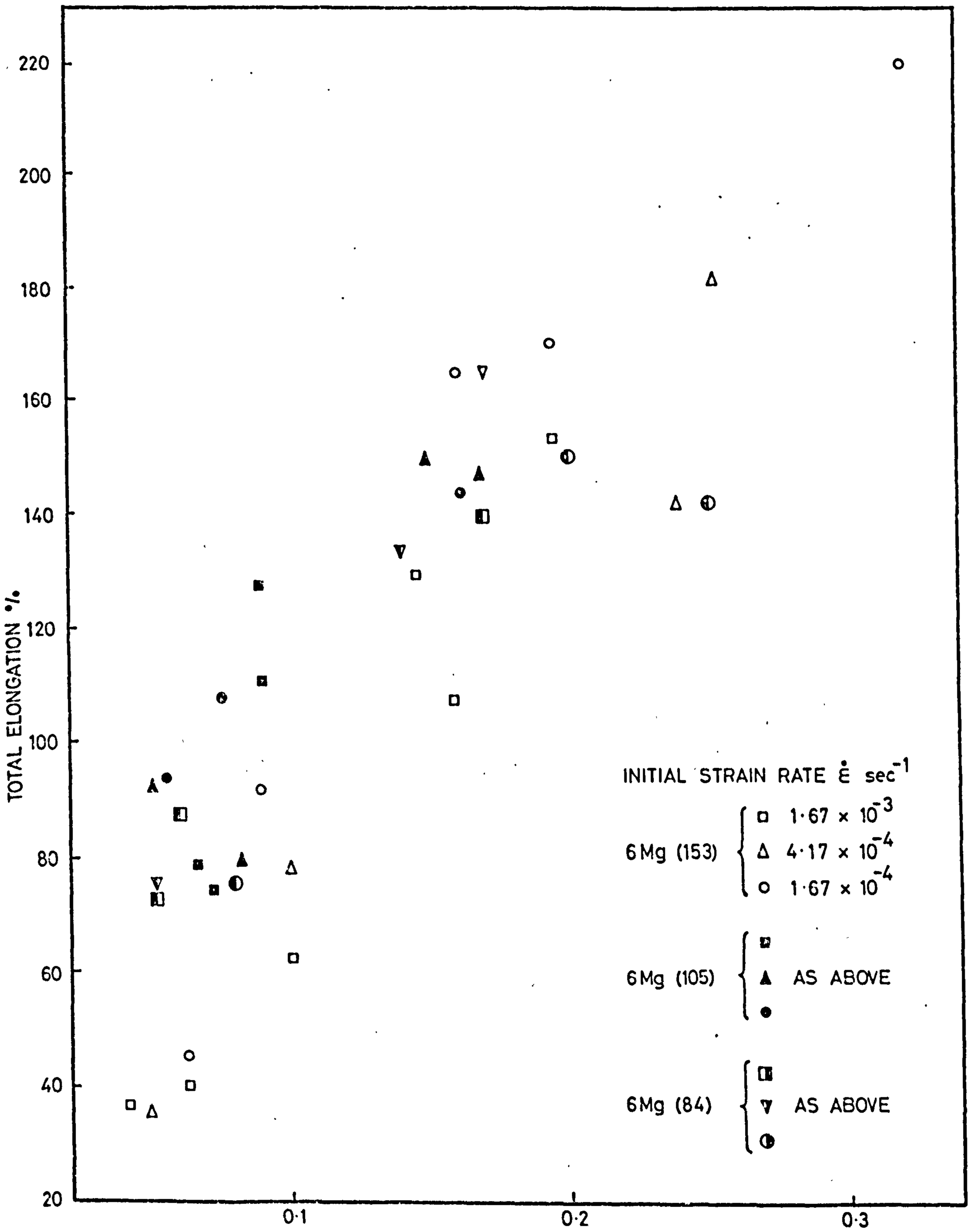


FIG.53. RELATIONSHIP BETWEEN m AND ELONGATION FOR 6 Mg ALLOYS AT VARIOUS STRAIN RATES.

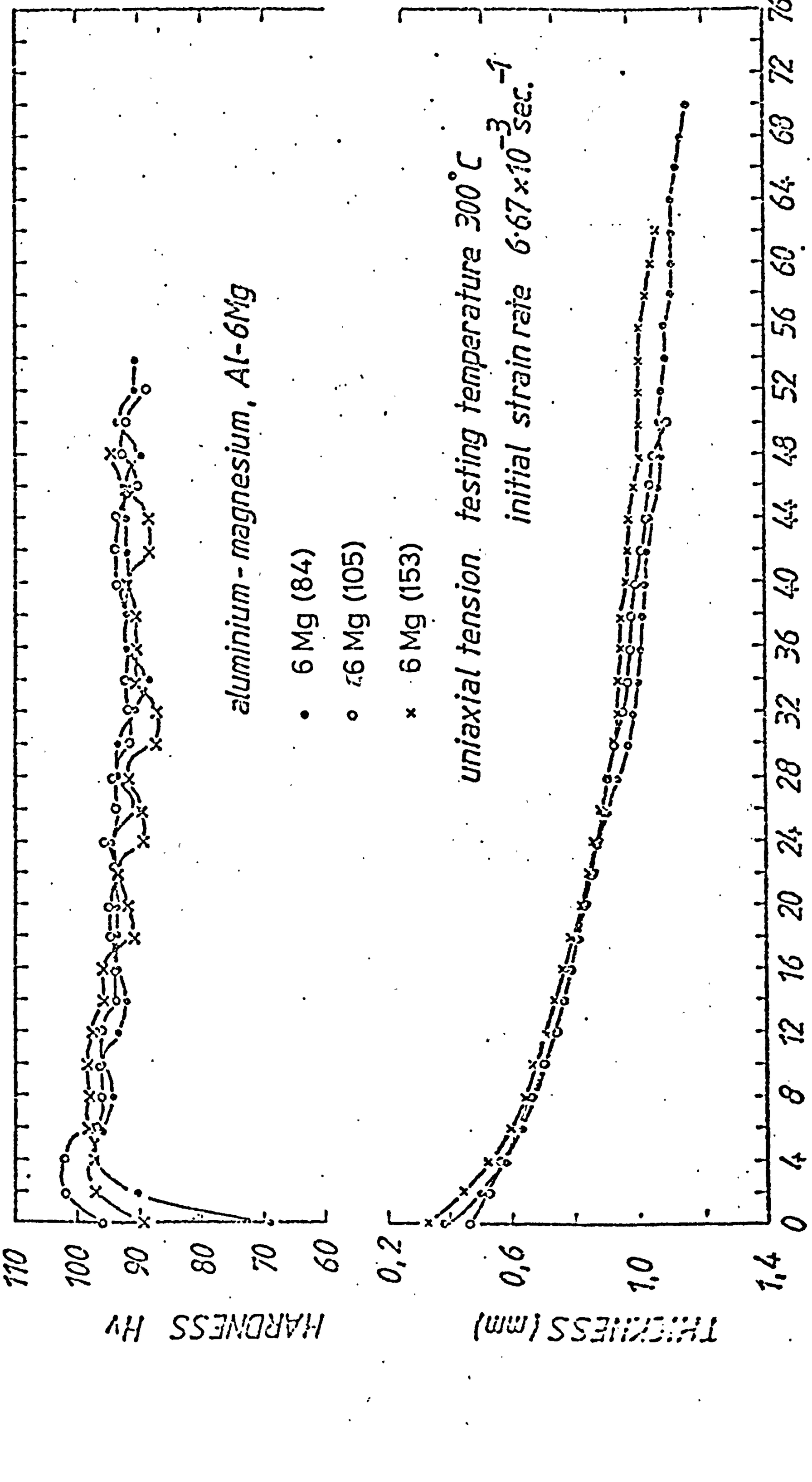


Figure 54 : The variation of hardness after uniaxial deformation at 300°C for cold-rolled and annealed Al-6Mg.

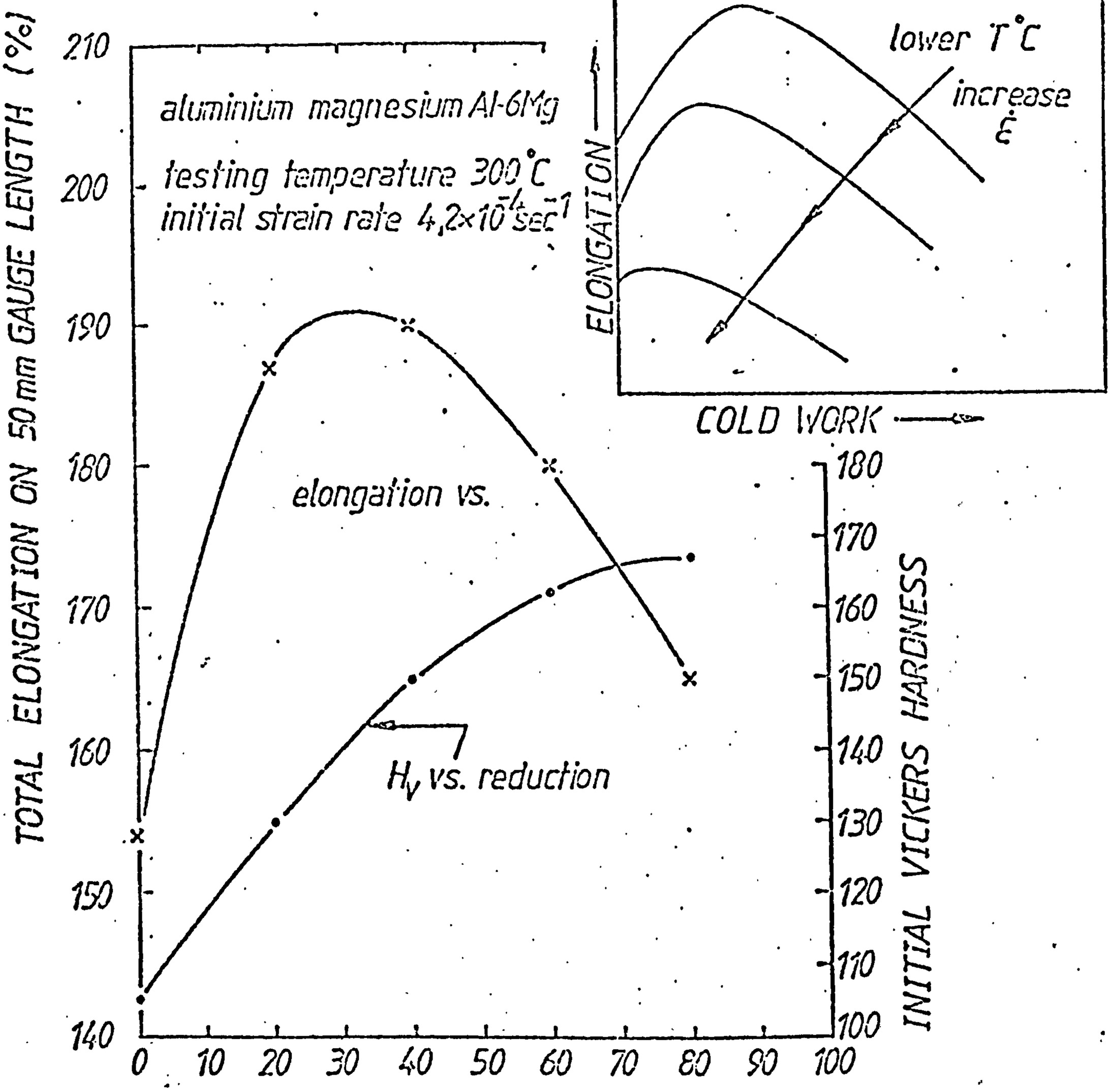


Figure 55; The influence of prior-cold-work on the total elongation during tension testing at elevated temperatures.

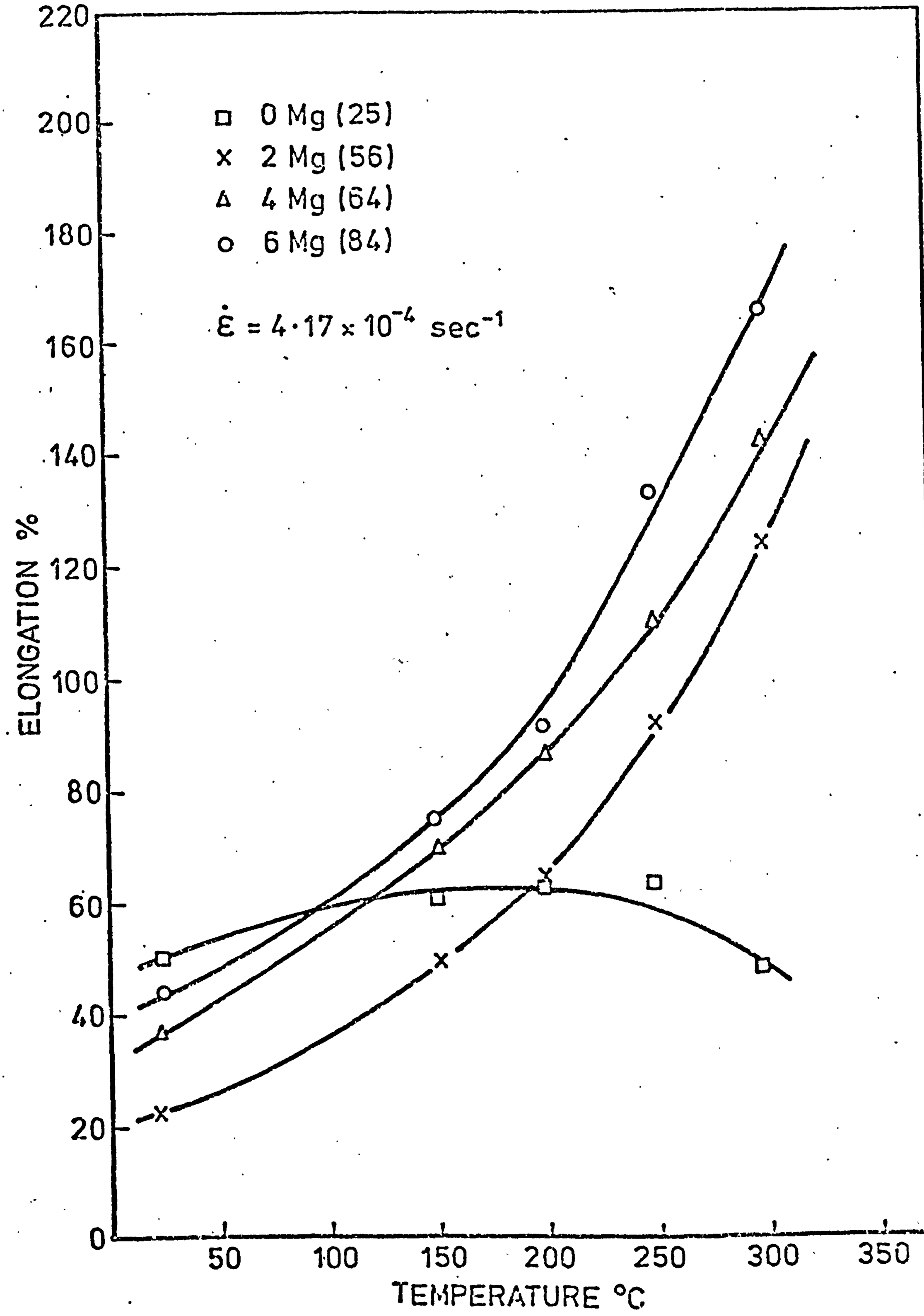


FIG.56. EFFECT OF MAGNESIUM CONTENT ON ELONGATION AT VARIOUS TEMPERATURES

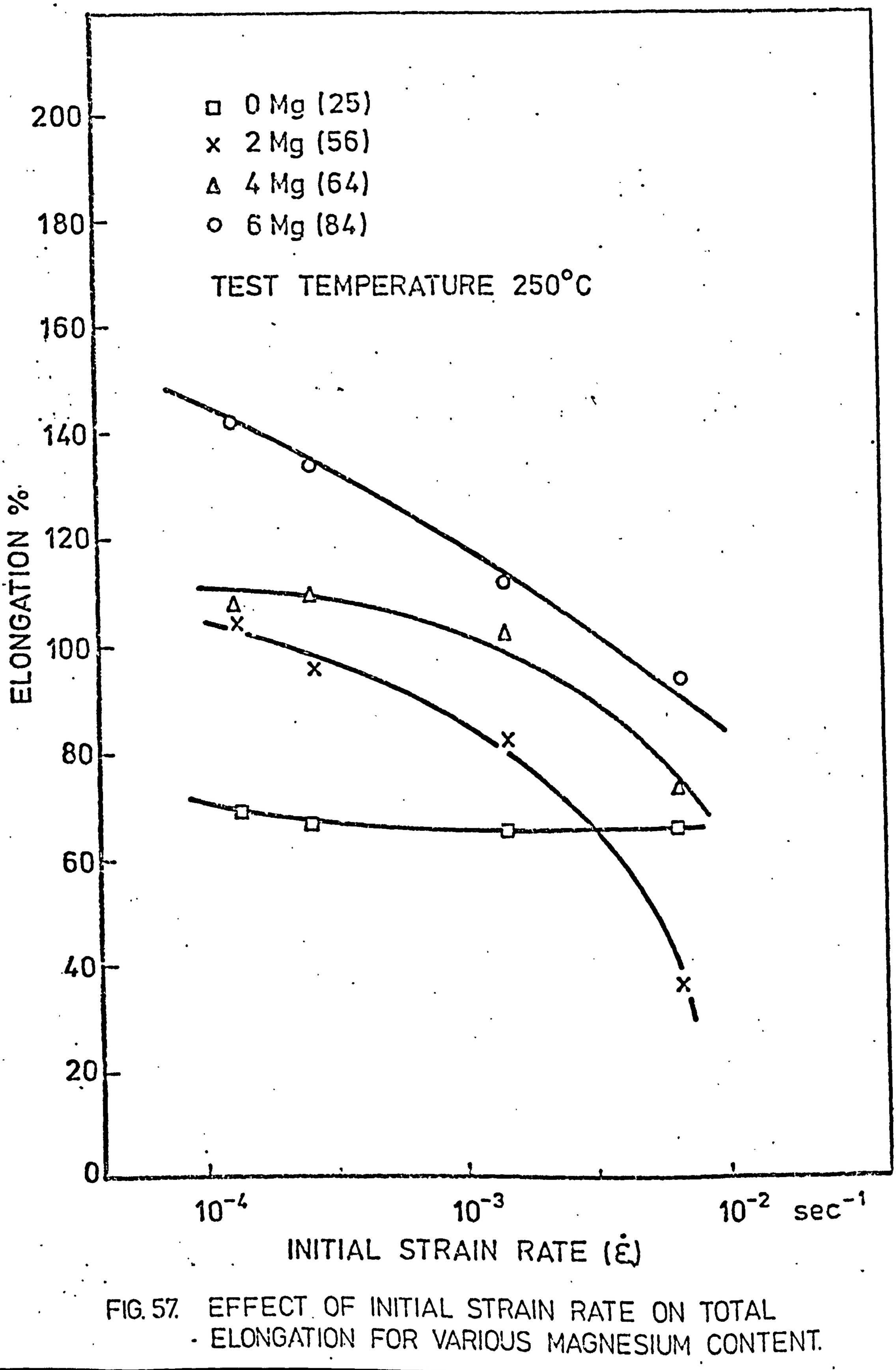


FIG. 57. EFFECT OF INITIAL STRAIN RATE ON TOTAL ELONGATION FOR VARIOUS MAGNESIUM CONTENT.

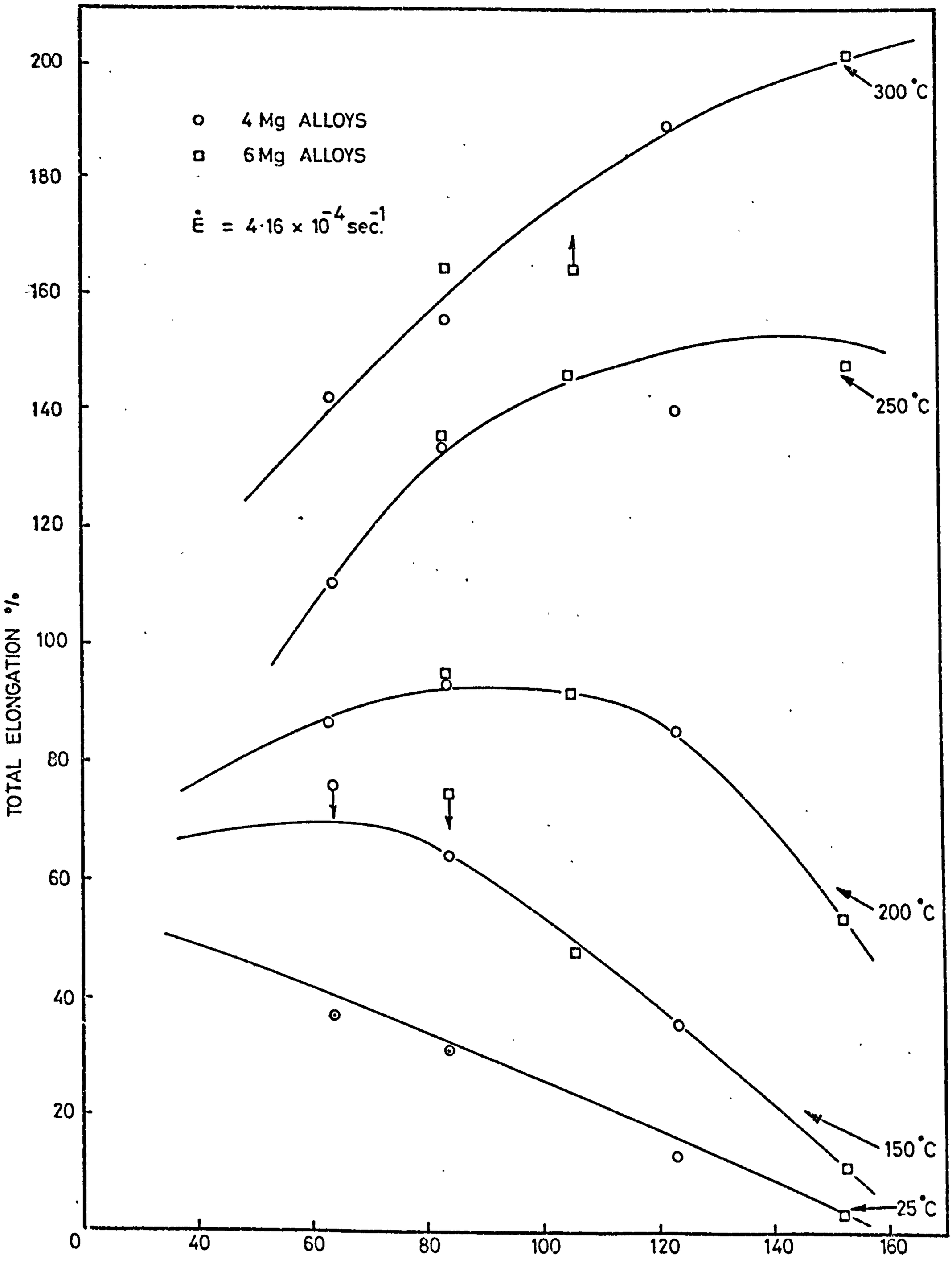


FIG. 58. INFLUENCE OF INITIAL SHEET HARDNESS ON THE TOTAL ELONGATION FOR 4Mg AND 6Mg ALLOYS AT VARIOUS TEMPERATURES.

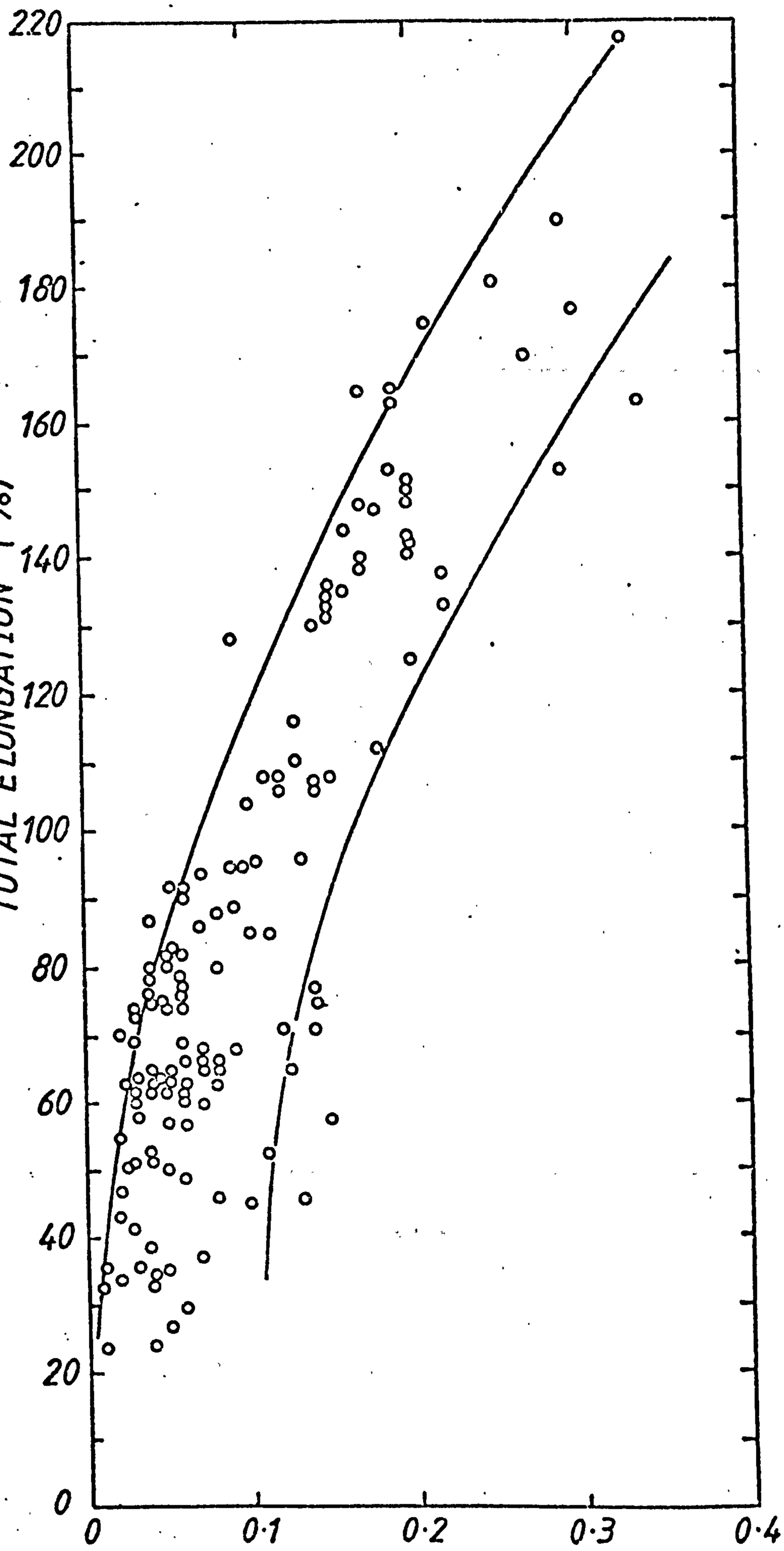


FIG.59. RELATIONSHIP BETWEEN m AND ELONGATION FOR ALL ALLOYS TESTED.

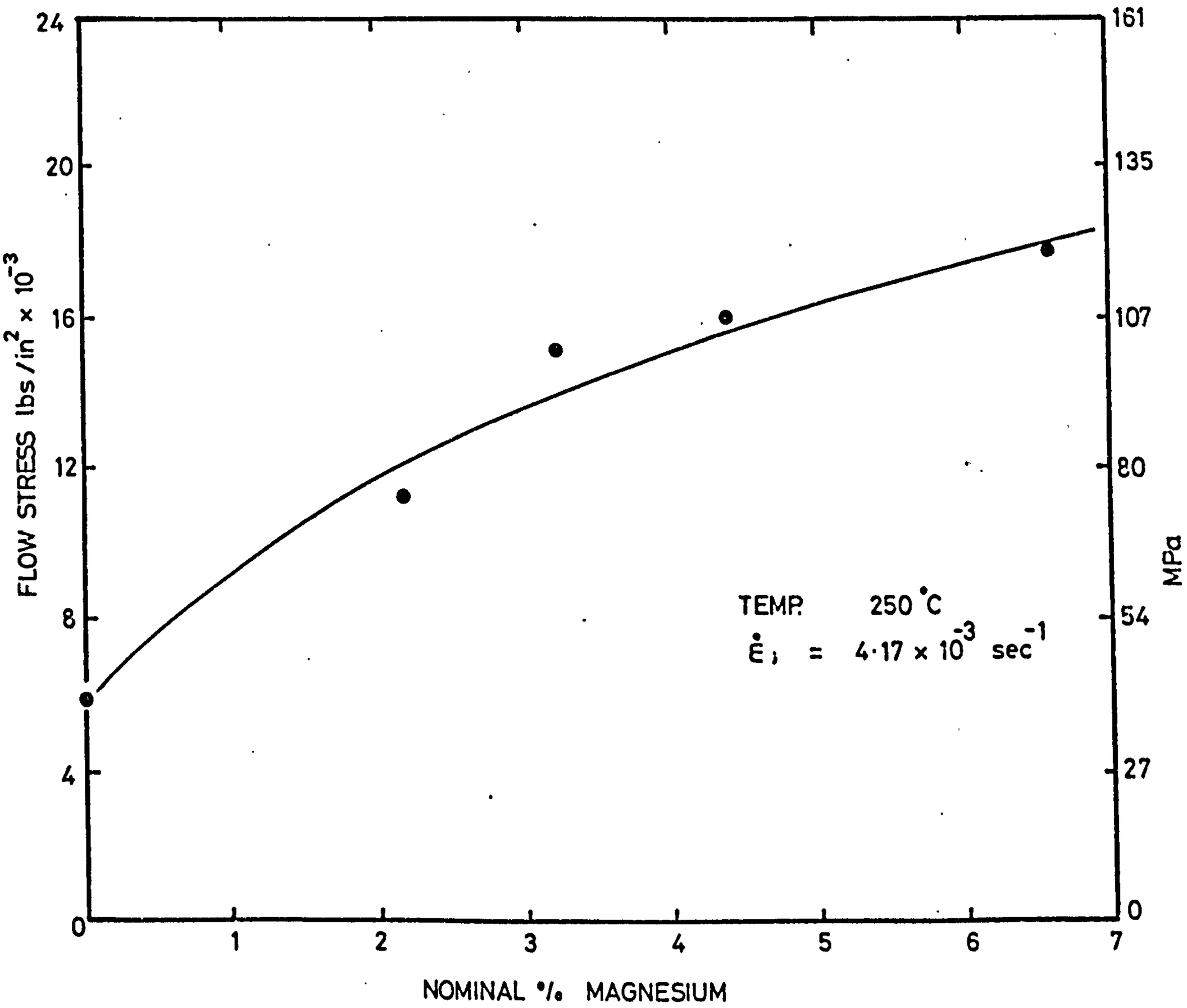


FIG.60. EFFECT OF MAGNESIUM CONTENT ON THE MAXIMUM FLOW STRENGTH AT 250 °C AND STRAIN RATE $4{\cdot}17 \times 10^{-3}$ sec^{-1}

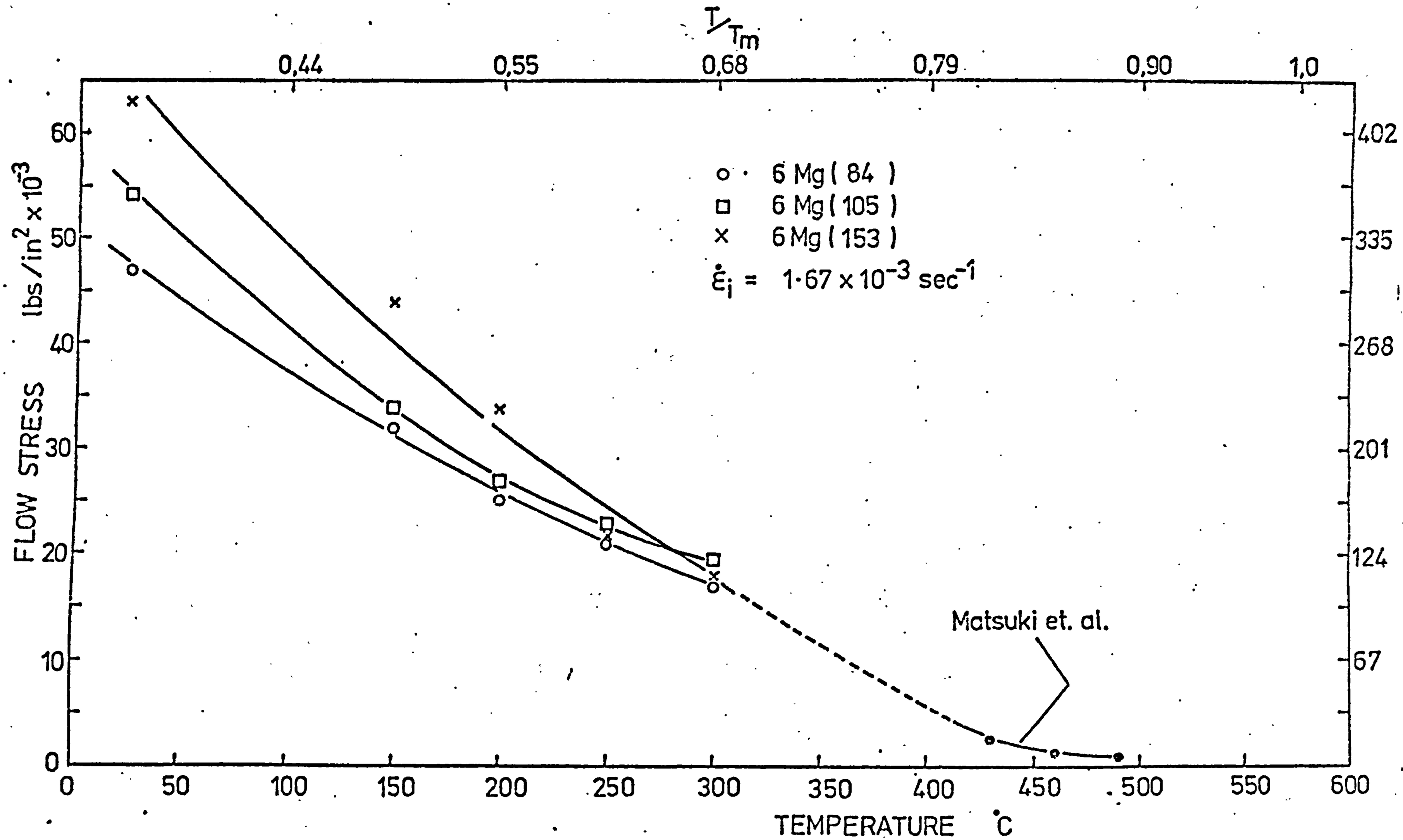


FIG. 61. FLOW STRENGTH VERSUS TEMPERATURE FOR 6Mg ALLOY TOGETHER WITH RESULT OF MATSUKI (REF. 85)

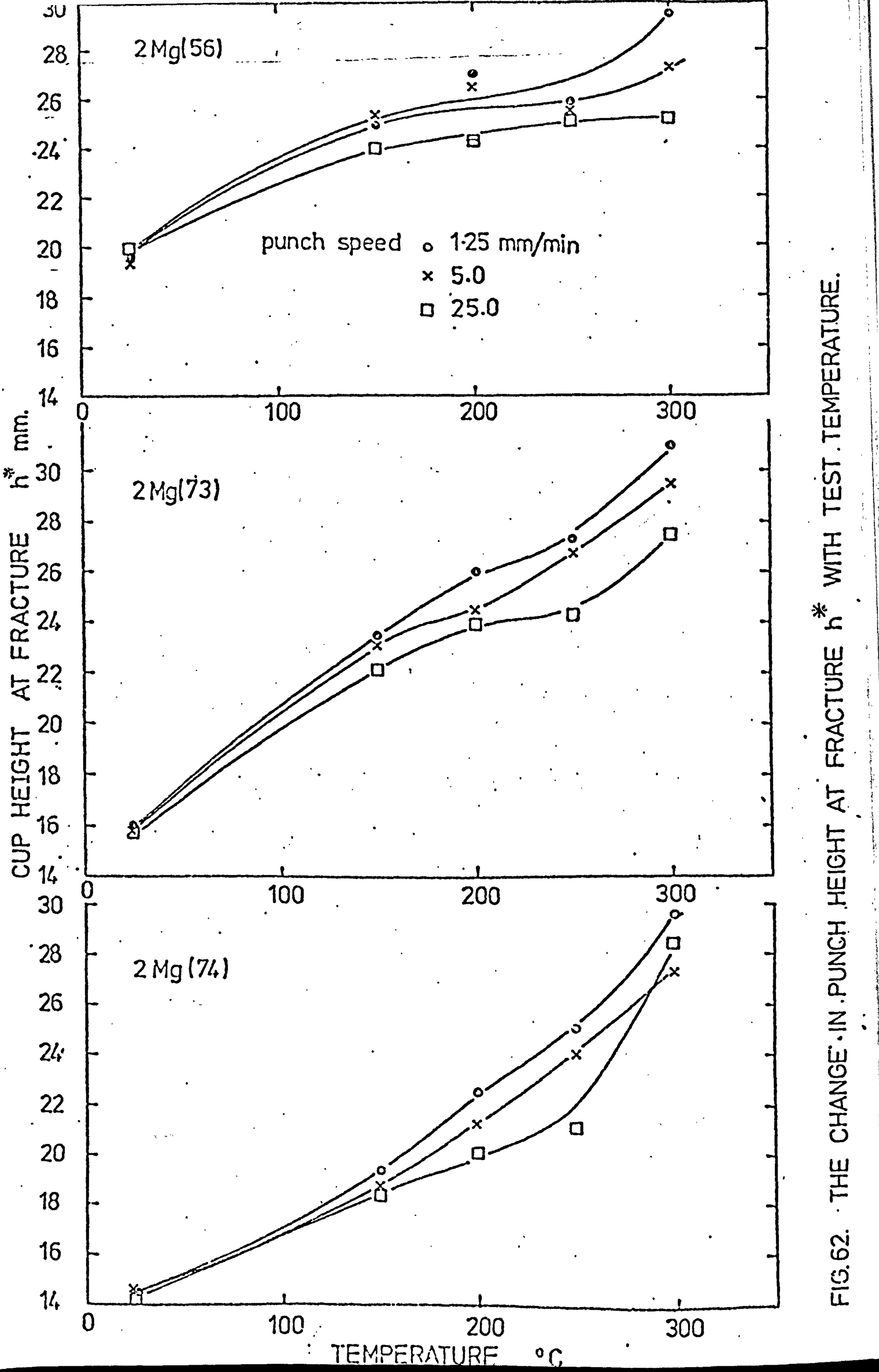


FIG.62. THE CHANGE IN PUNCH HEIGHT AT FRACTURE h* WITH TEST TEMPERATURE.

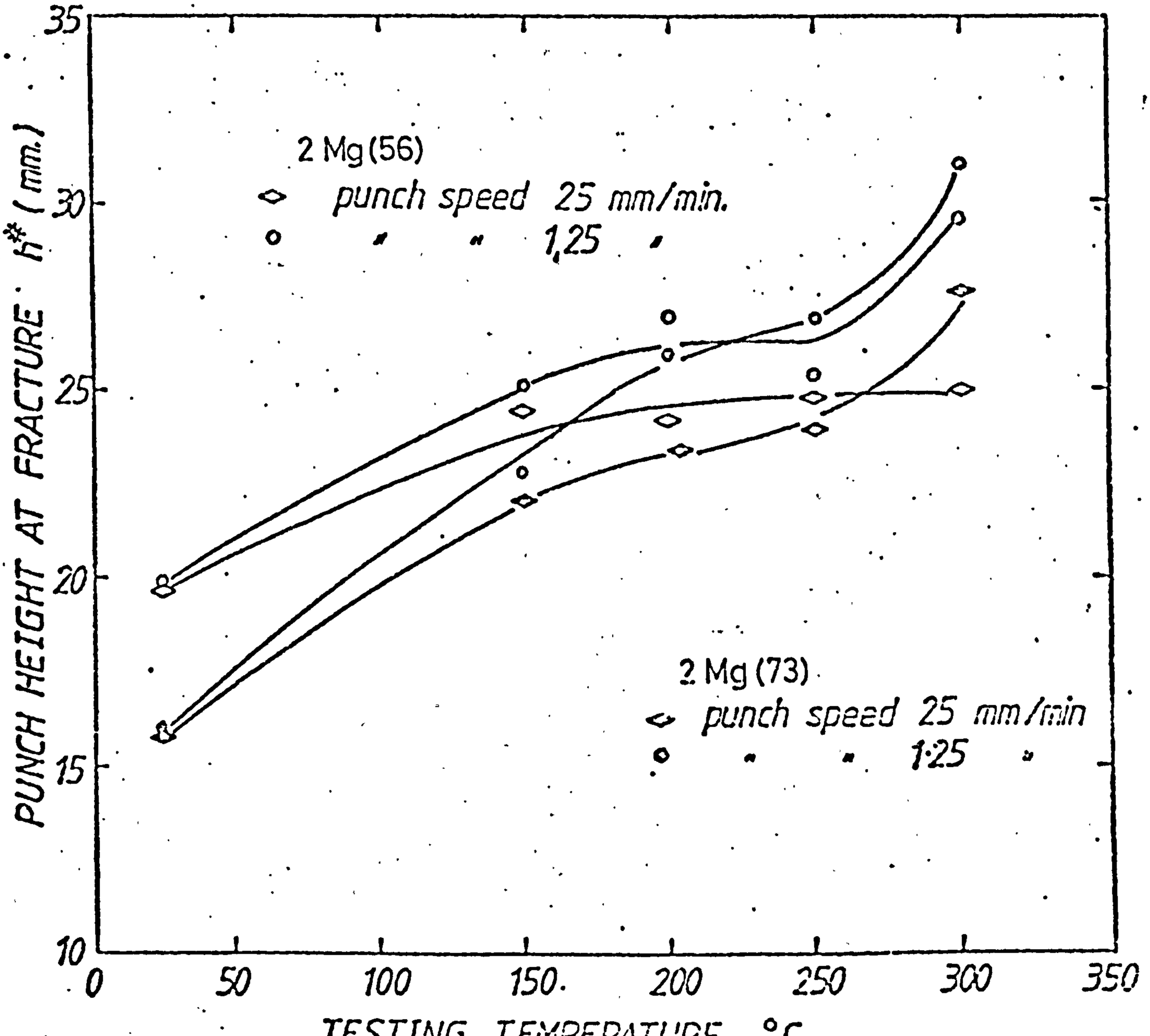


Figure 63 The effect of temperature on the limiting bulge height h^* for hemispherical punch stretching tests on Al-2Mg, carried out at different temperatures and punch speeds.

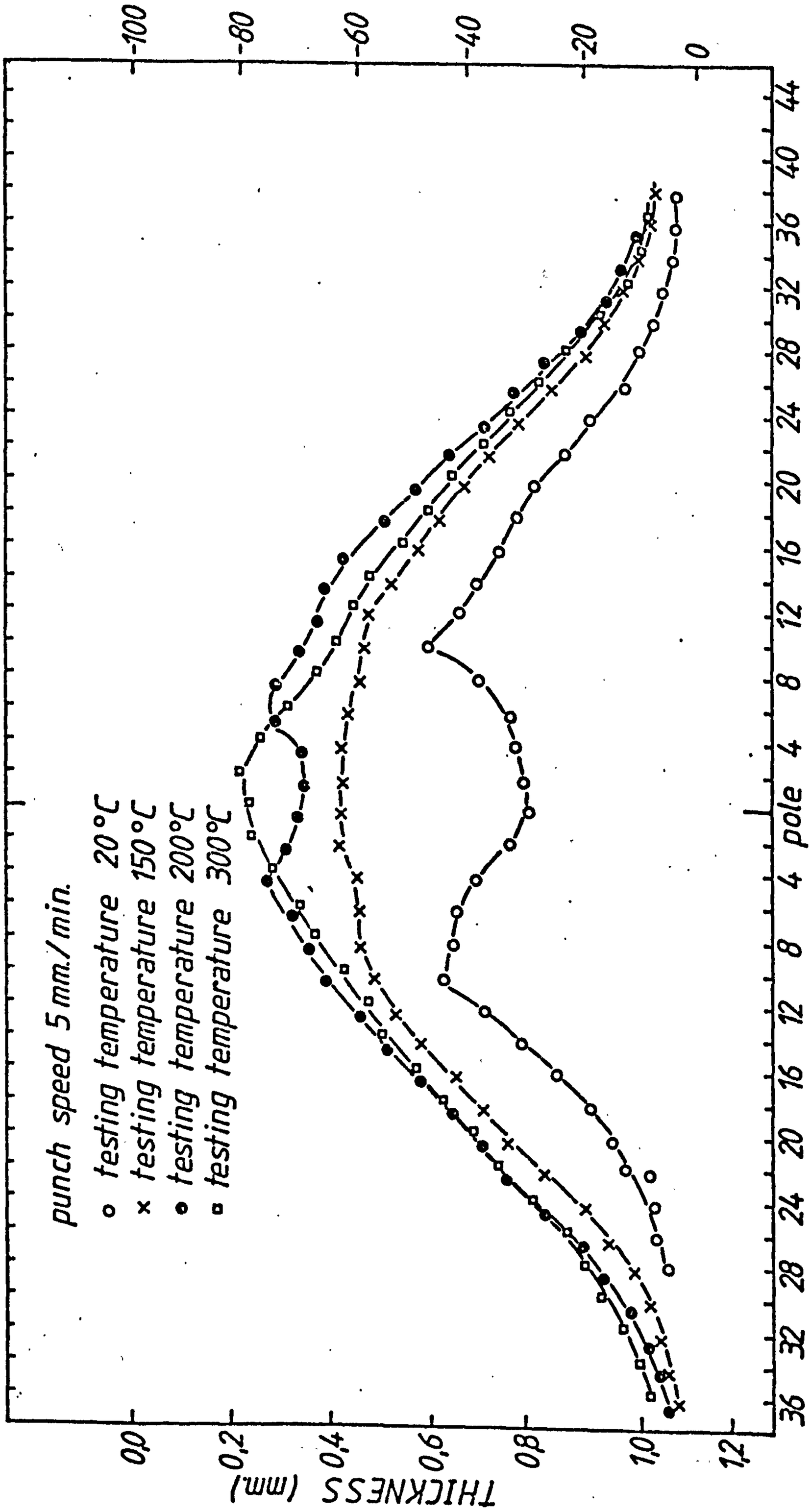


Figure 64 The effect of temperature on the strain gradient across the pole of a fractured bulge, stretch formed with a 50 mm diameter hemispherical punch and PTFE film as a lubricant, 2 Mg(56) alloy.

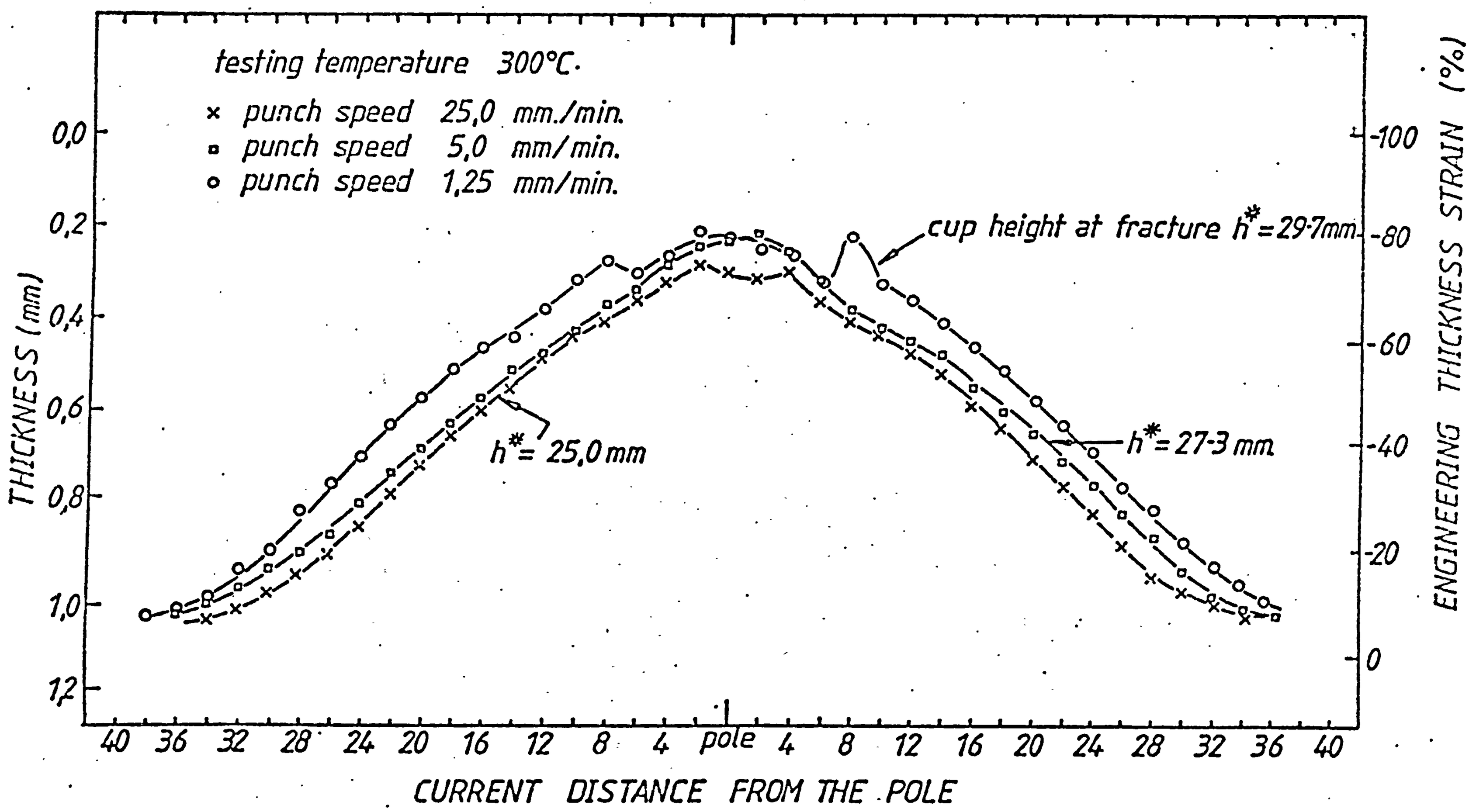


Figure 65· The effect of punch speed on the strain gradient across the pole of a fractured bulge, stretch formed at 300°C using a 50 mm. diameter hemispherical punch lubricated with PTFE film, for 2 Mg(56) alloy.

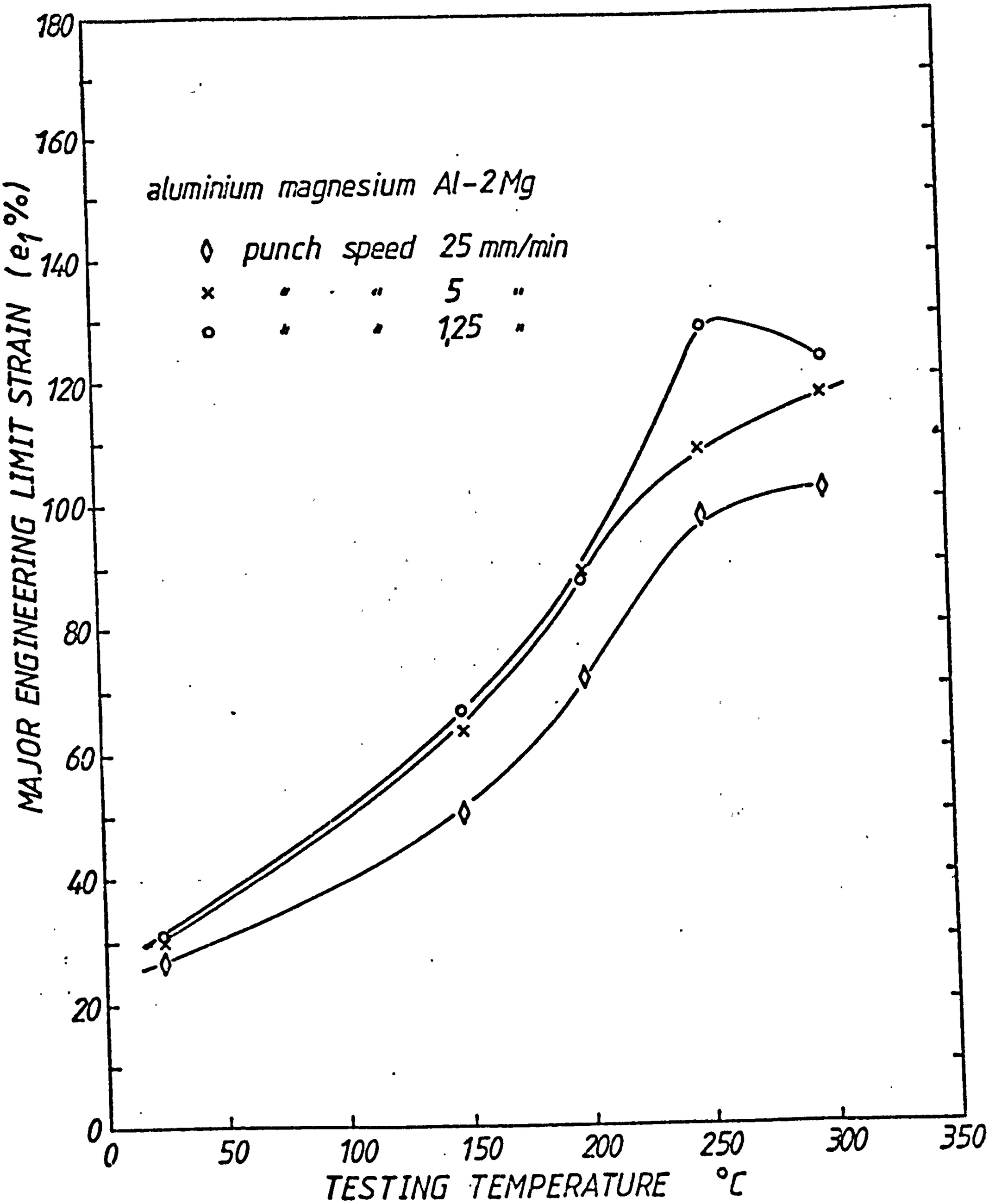


Figure 66 The effect of testing temperature on the major limit strain (e_1%) at the pole of a bulge, stretch formed using a 50mm diameter hemispherical punch and PTFE film as a lubricant, 2 Mg(56).

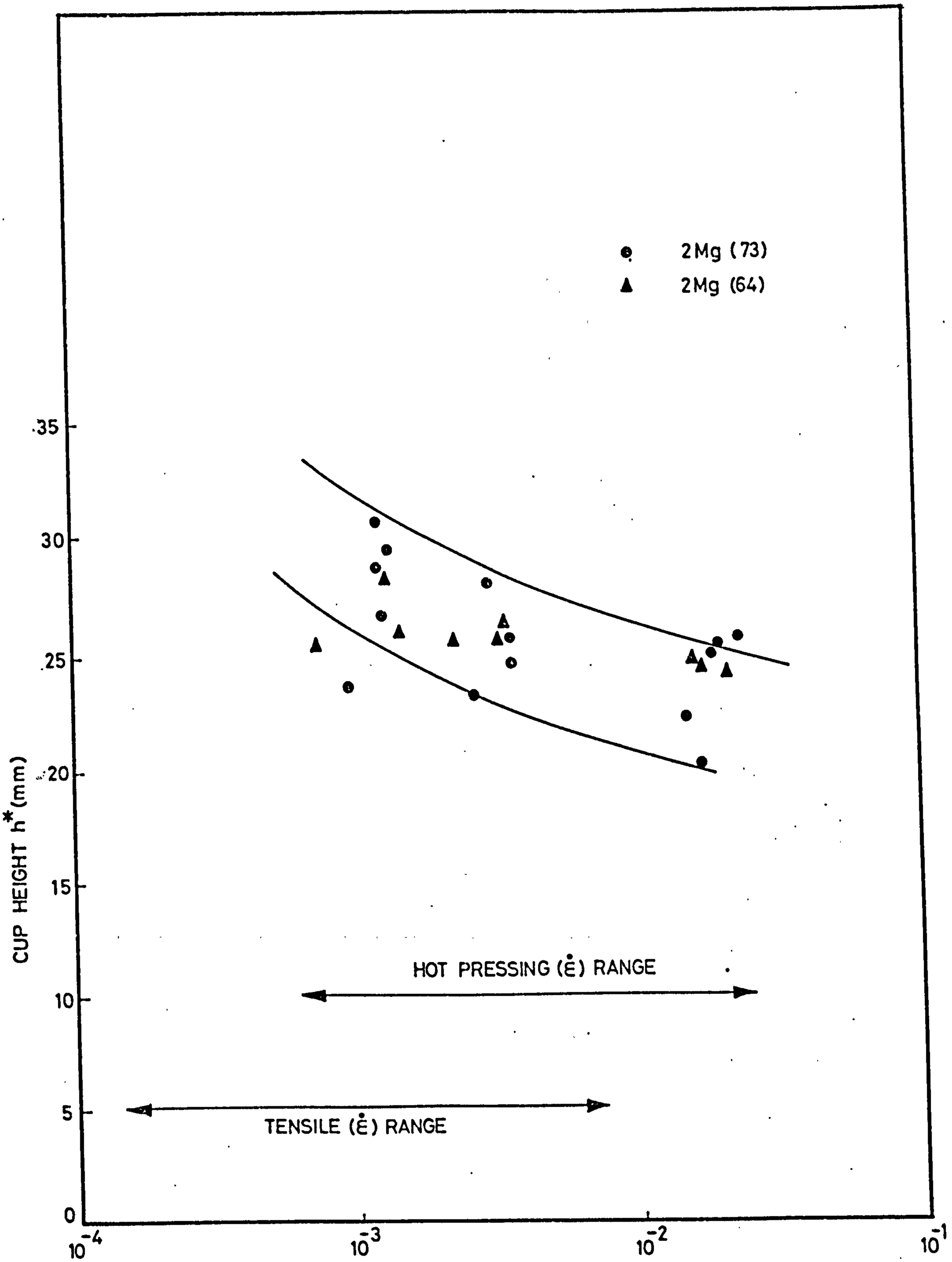


FIG:67. THE EFFECT OF STRAIN RATE ON CUP HEIGHT h^* FOR 2Mg AT VARIOUS TEMPERATURES.

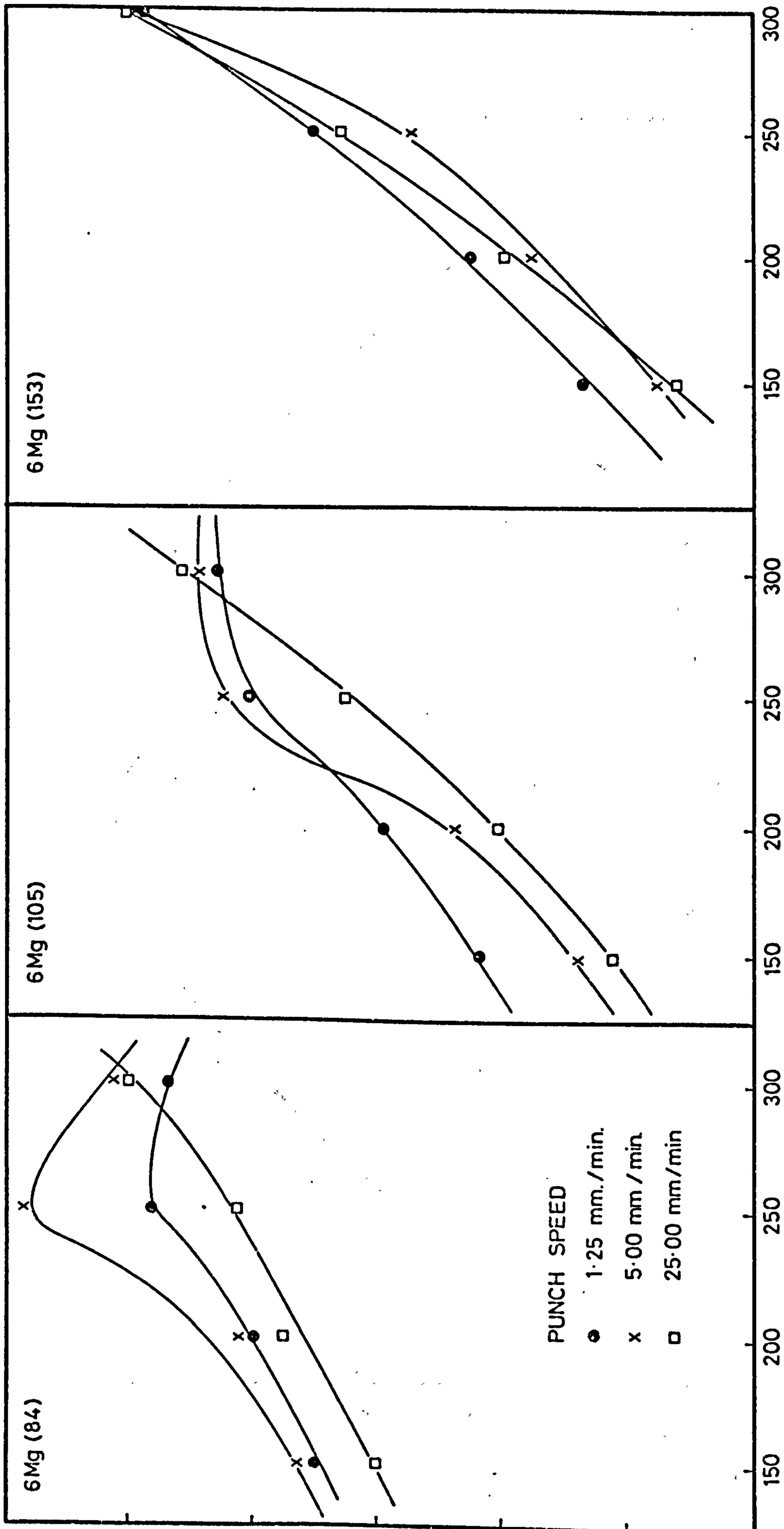


FIG. 68. CUP HEIGHT VERSUS TEMPERATURE FOR 6Mg ALLOYS TESTED AT DIFFERENT PUNCH SPEEDS.

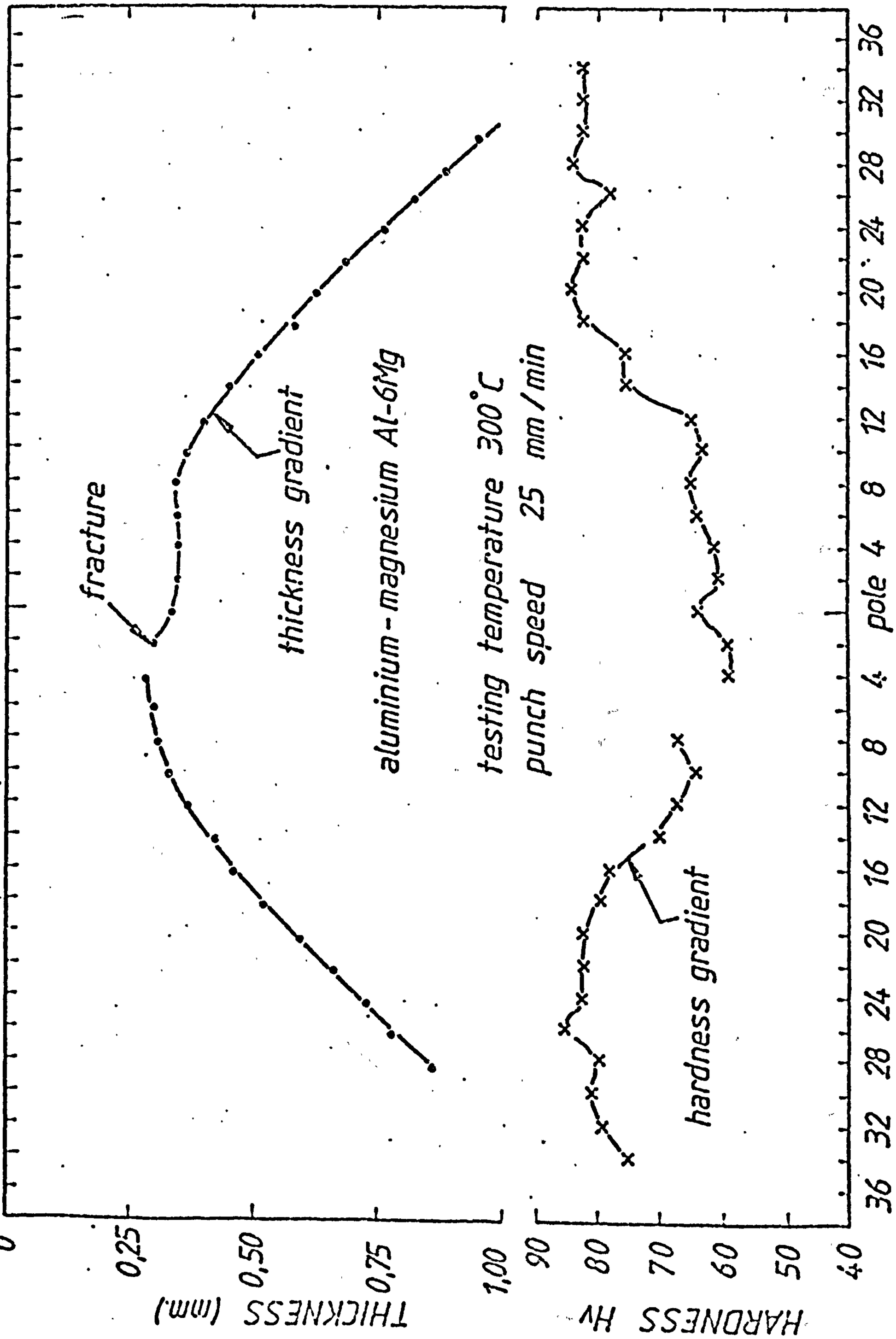


Figure 69 : The variation in hardness across the pole of a fractured 50mm diameter hemispherical cup; for 6 Mg(84).

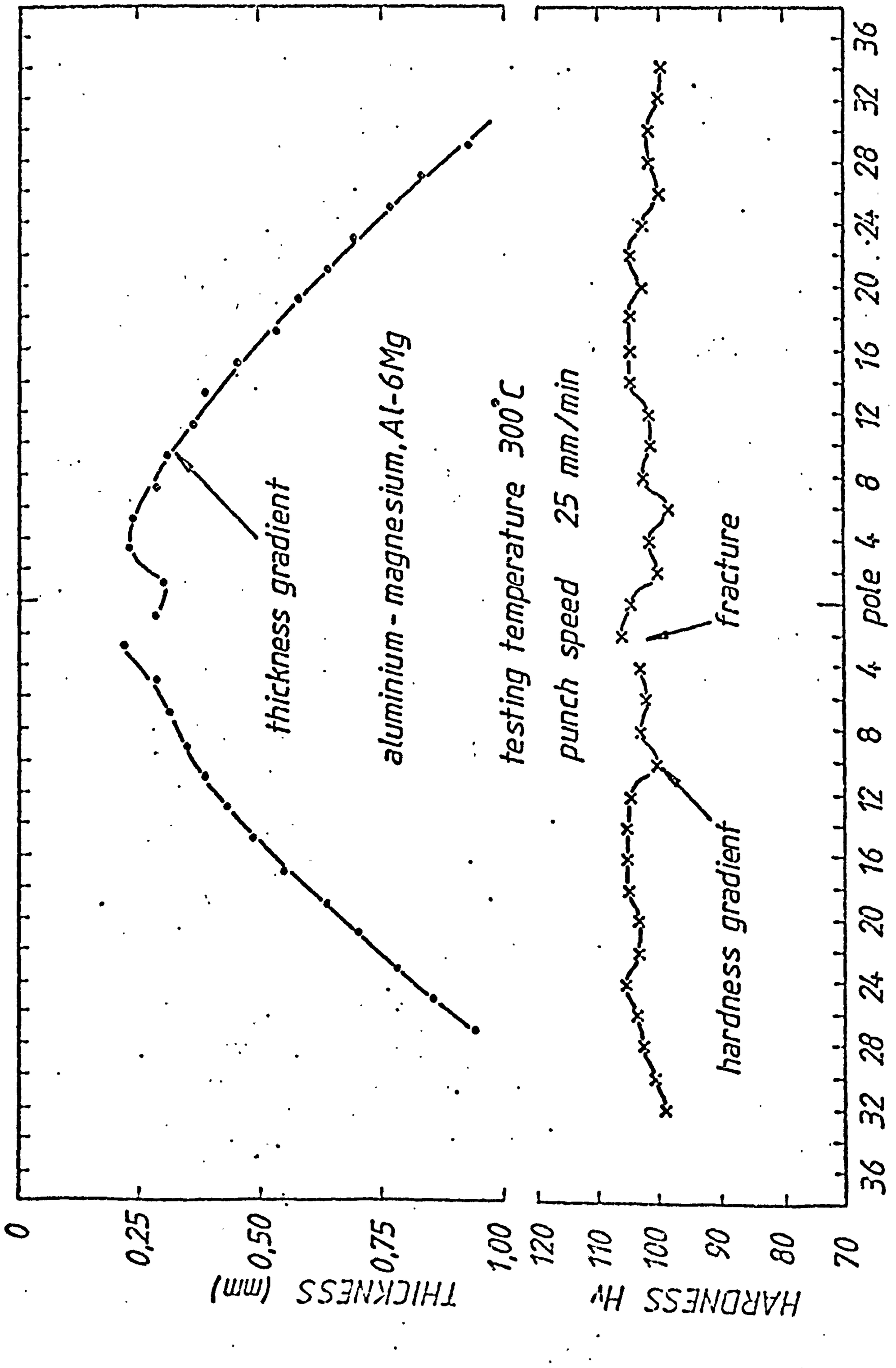


Figure 70 : The variation in hardness across the pole of a fractured 50mm diameter hemi-spherical cup; For 6 Mg(105).

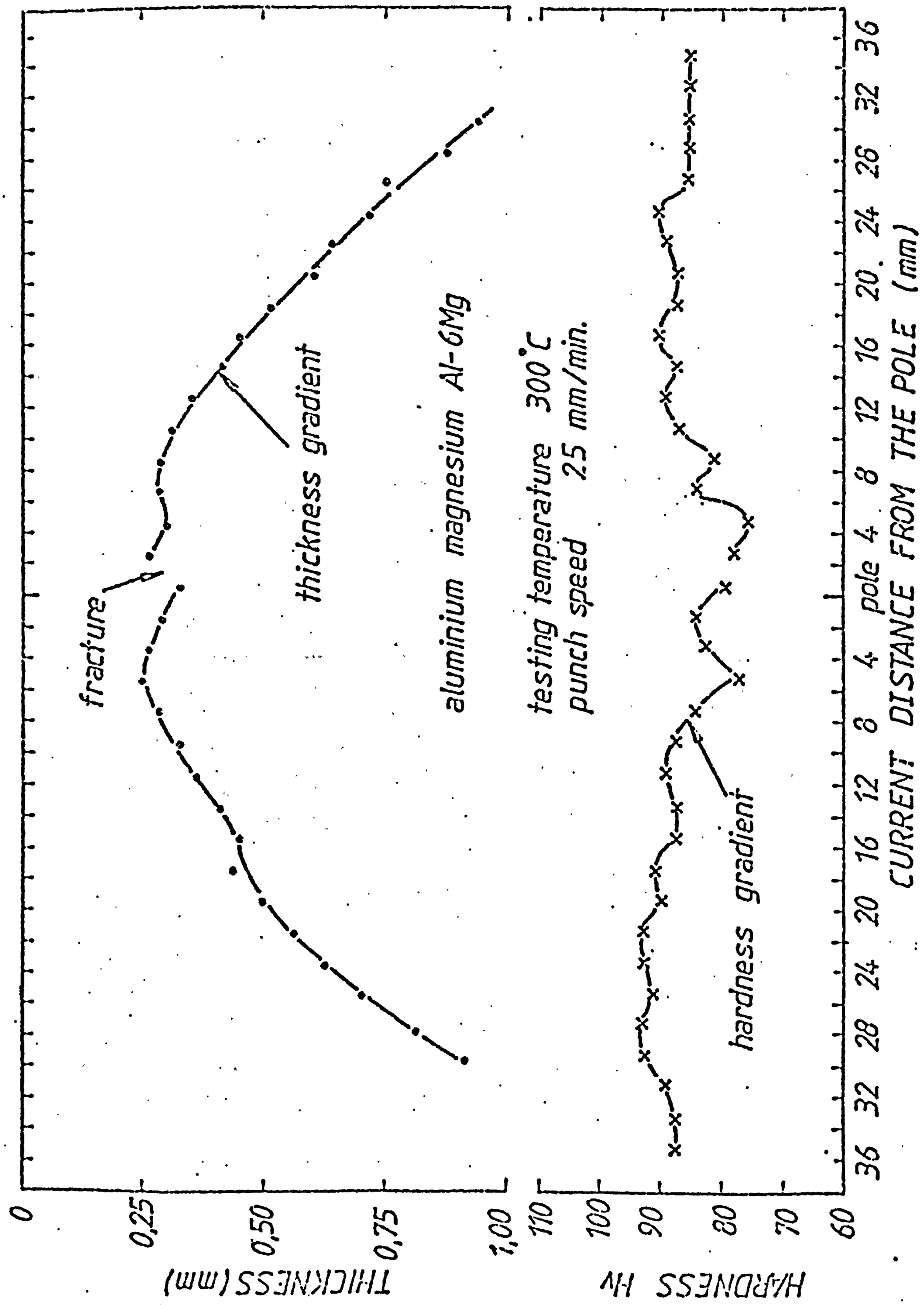


Figure 71 : The variation in hardness across the pole of a fractured 50mm diameter hemispherical cup; 6 Mg(153).

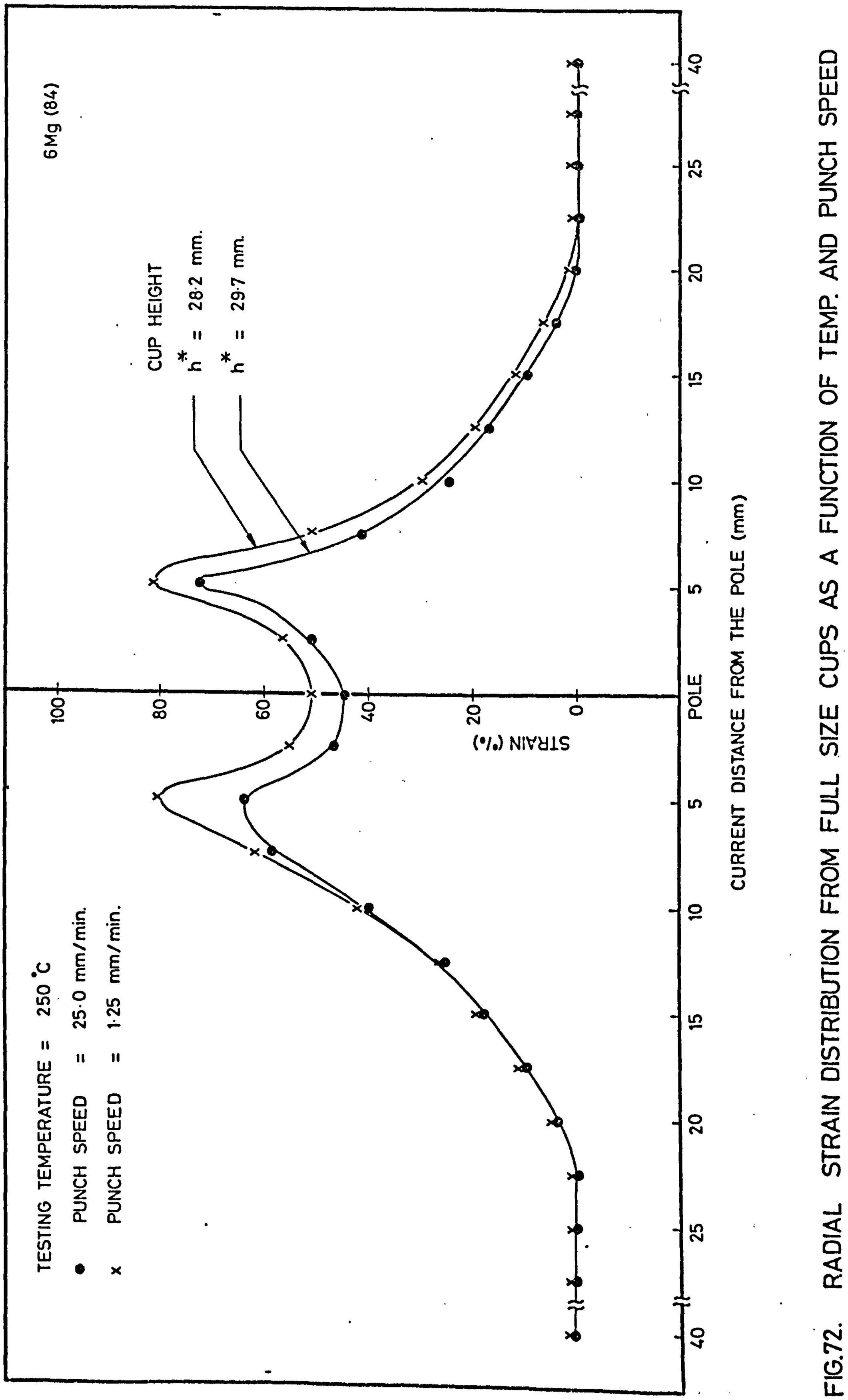


FIG.72. RADIAL STRAIN DISTRIBUTION FROM FULL SIZE CUPS AS A FUNCTION OF TEMP. AND PUNCH SPEED FOR 6Mg (84) AT 250 °C.

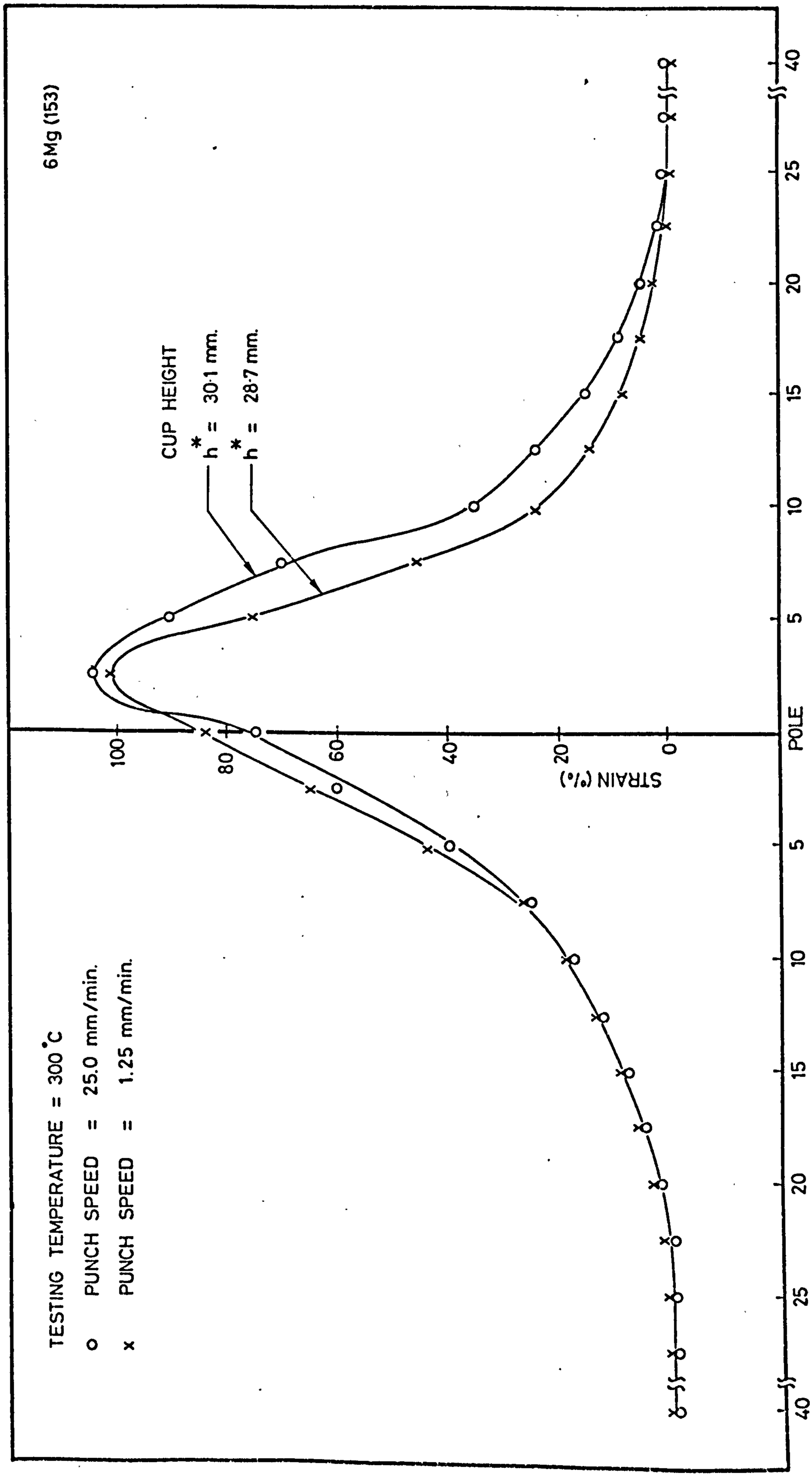


FIG. 73. RADIAL STRAIN DISTRIBUTION FROM FULL SIZE CUPS AS A FUNCTION OF TEMP. & PUNCH SPEED. FOR 6Mg (153) AT 300 °C.

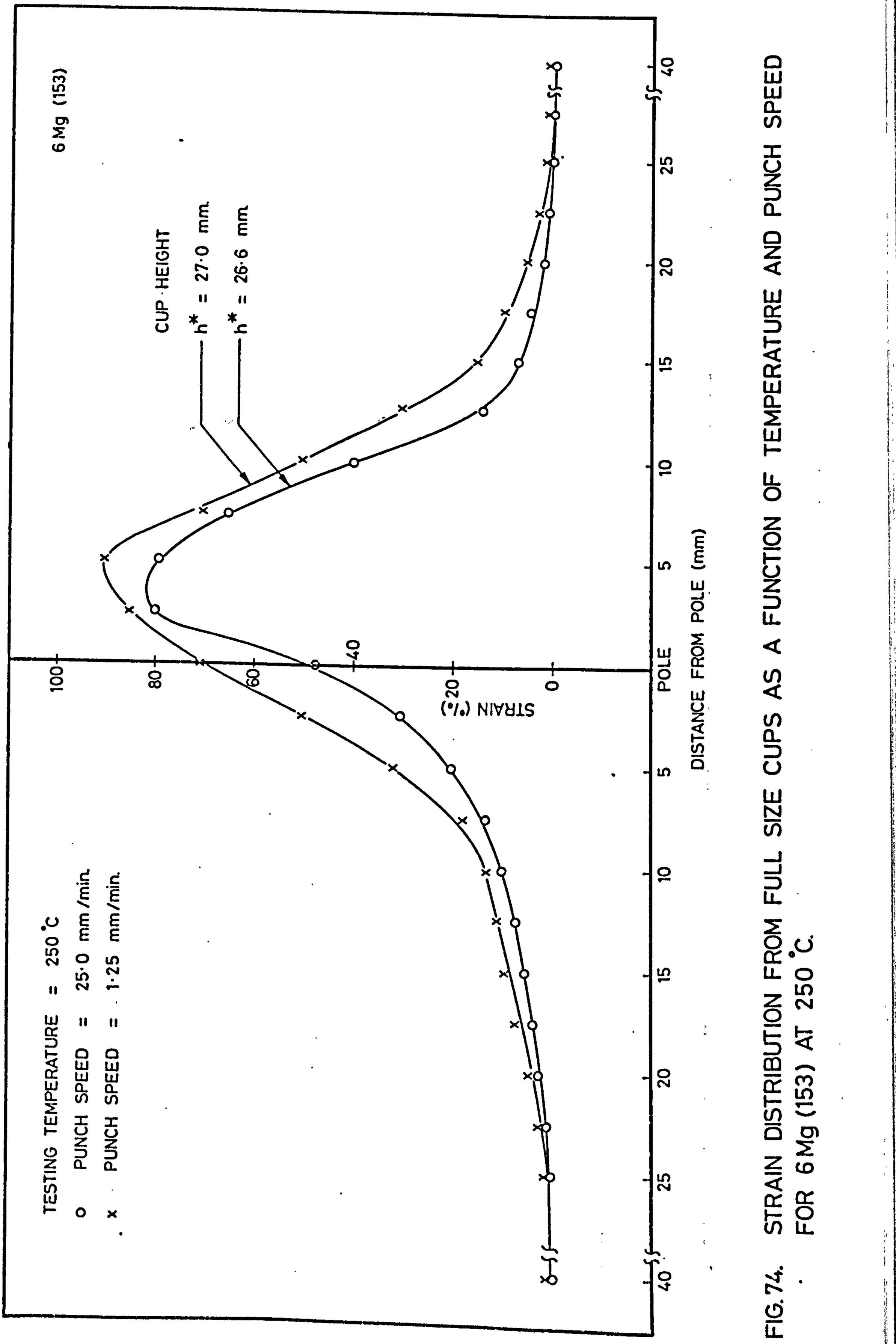


FIG. 74. STRAIN DISTRIBUTION FROM FULL SIZE CUPS AS A FUNCTION OF TEMPERATURE AND PUNCH SPEED FOR 6 Mg (153) AT 250 °C.

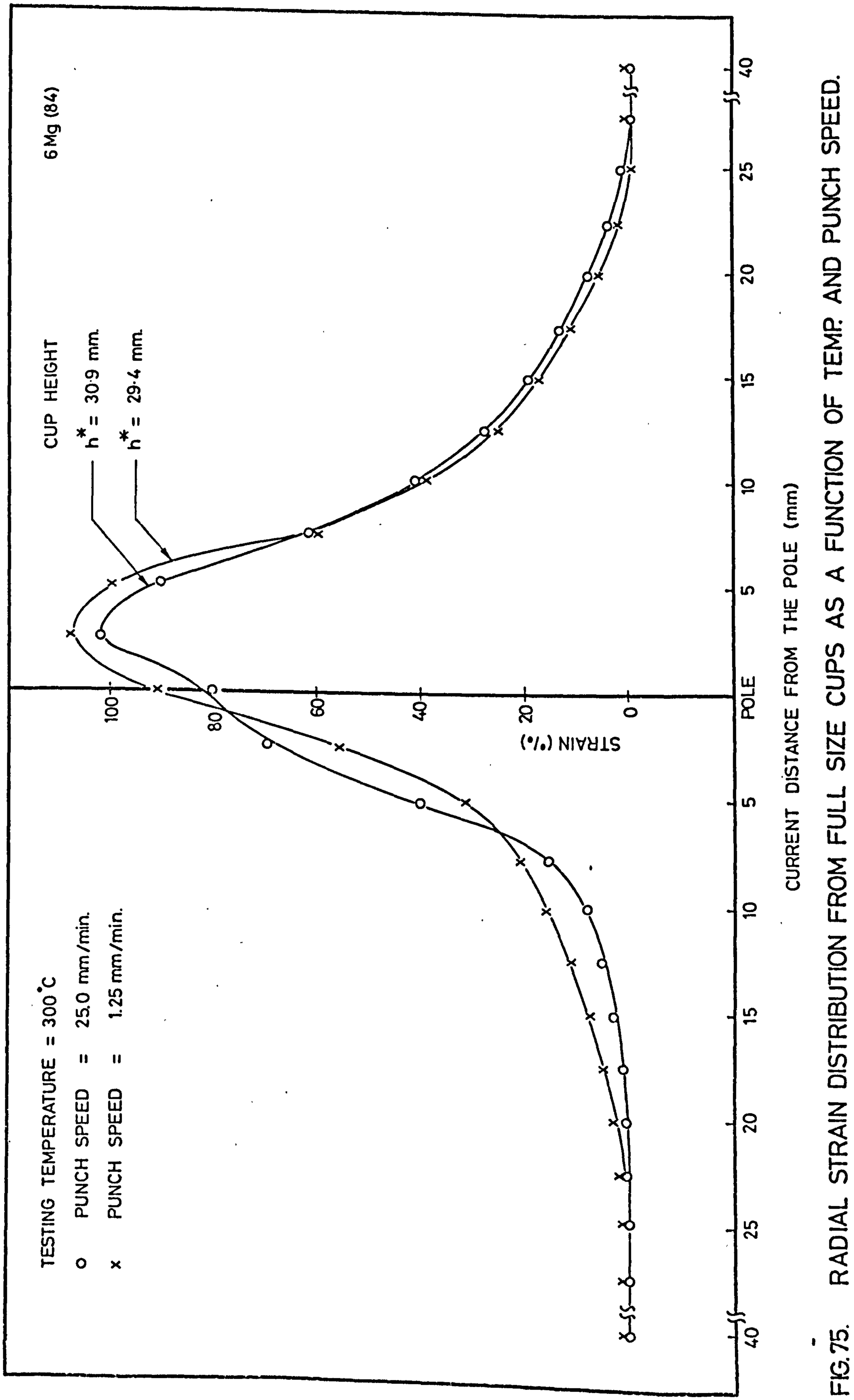


FIG.75. RADIAL STRAIN DISTRIBUTION FROM FULL SIZE CUPS AS A FUNCTION OF TEMP. AND PUNCH SPEED. FOR 6Mg (84) AT 300 °C.

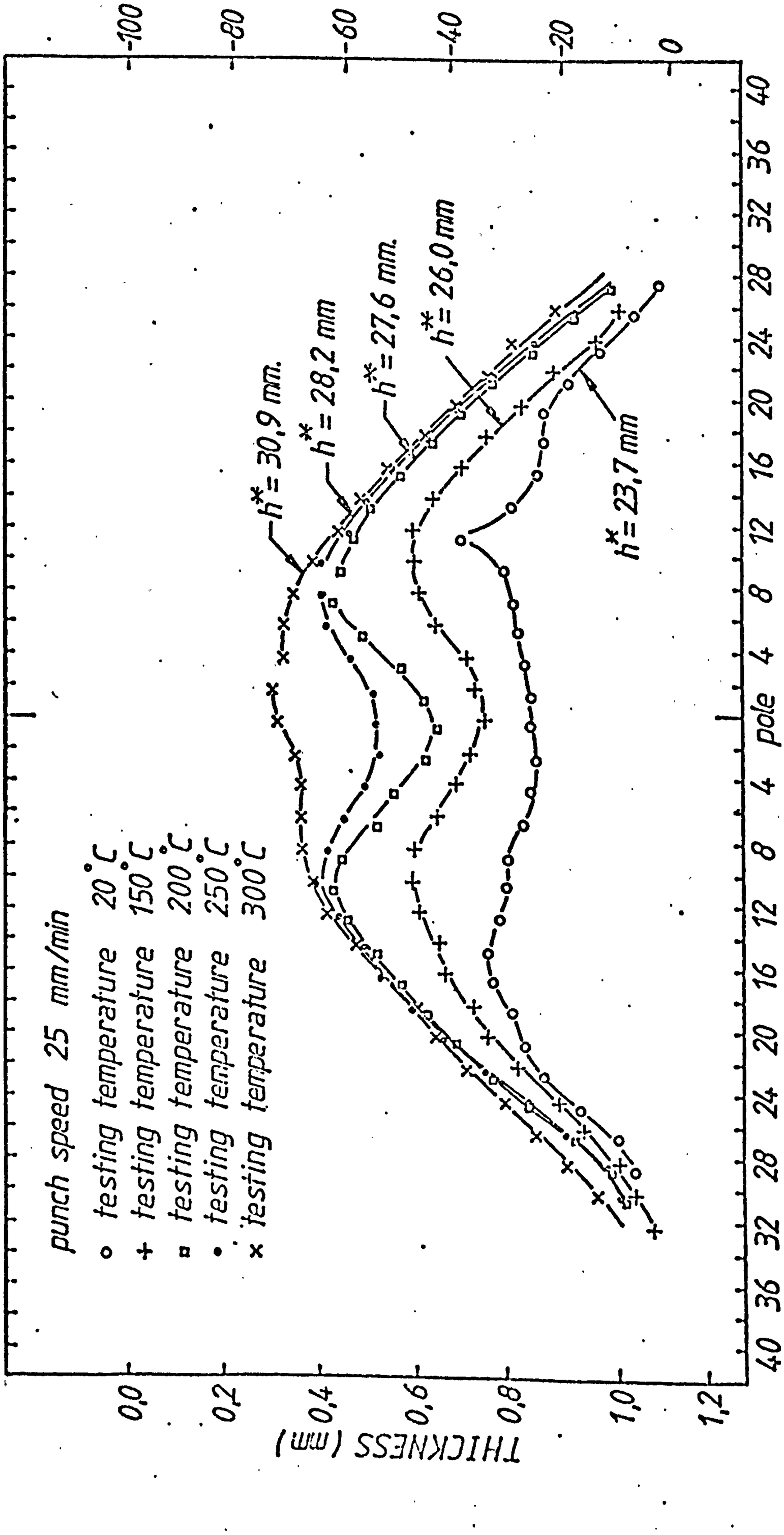


Figure 76: The effect of testing temperature on the strain gradient across the pole of a fracture bulge, stretch formed at a punch speed of 25mm/min using a 50mm diameter hemispherical punch lubricated with P.T.F.E. film; for 6 Mg(84).

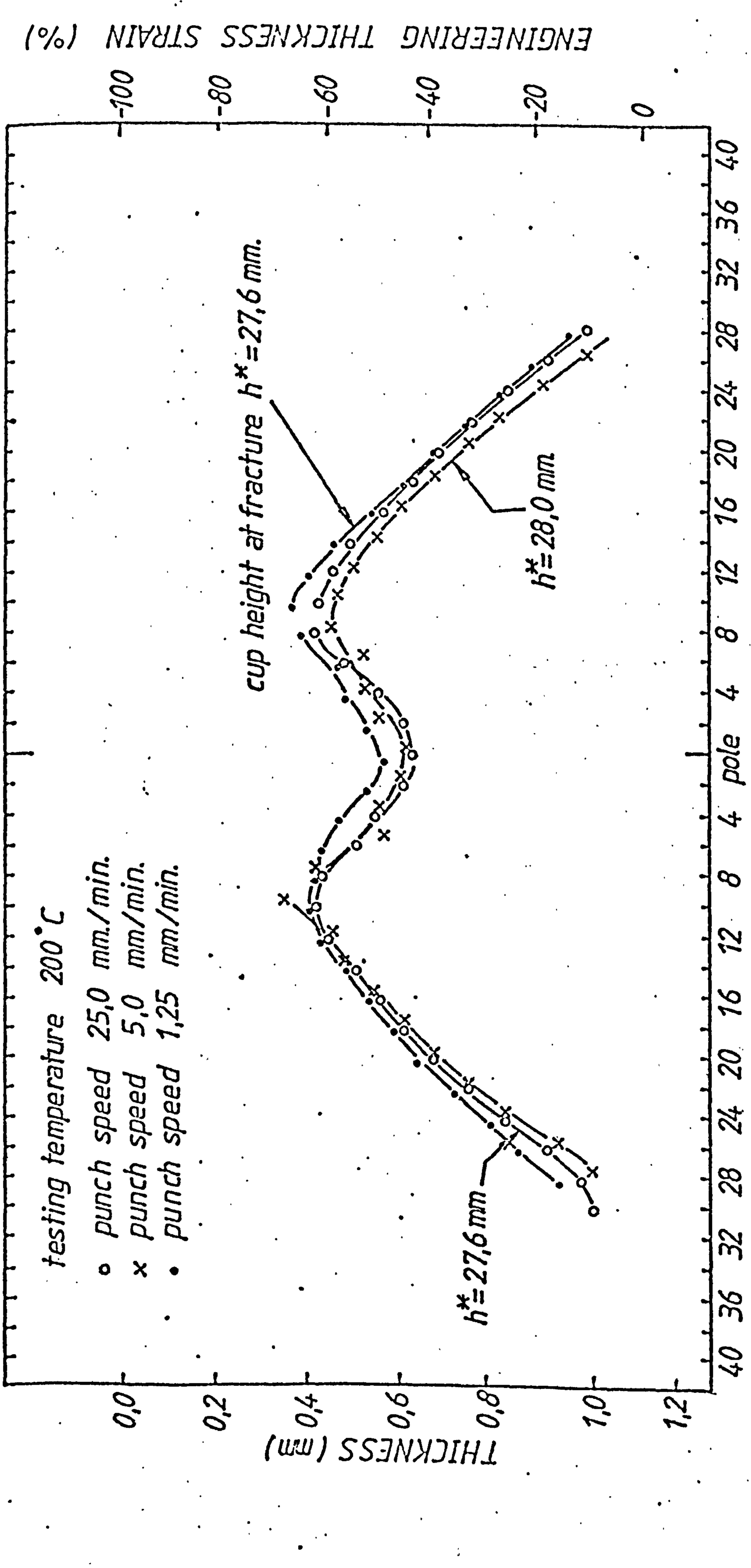


Figure 77: The effect of punch speed on the strain gradient across the pole of a fractured bulge, stretch formed at 200°C, using a 50mm diameter hemispherical punch lubricated with PTFE film for 6 Mg(84).

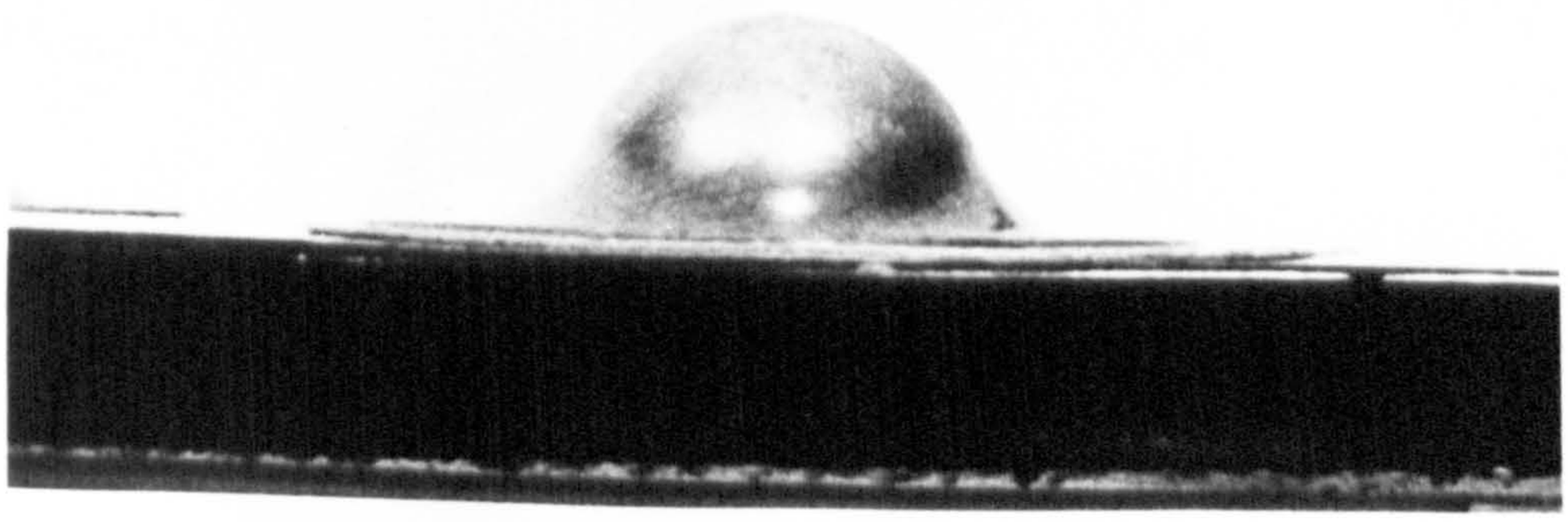


25°C



150°C

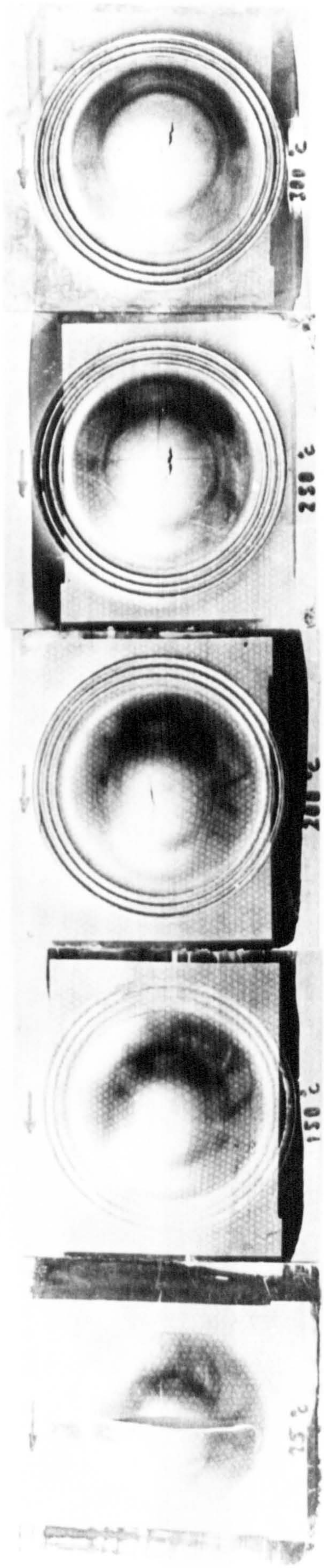
200°C



250°C

300°C

Fig. 78(a) Typical 6 Mg(153) hot pressings at various temperatures (elevation view).



Typical 6 Mg(153) hot pressings deformed at various temperatures (plan view).

Fig. 78(b)

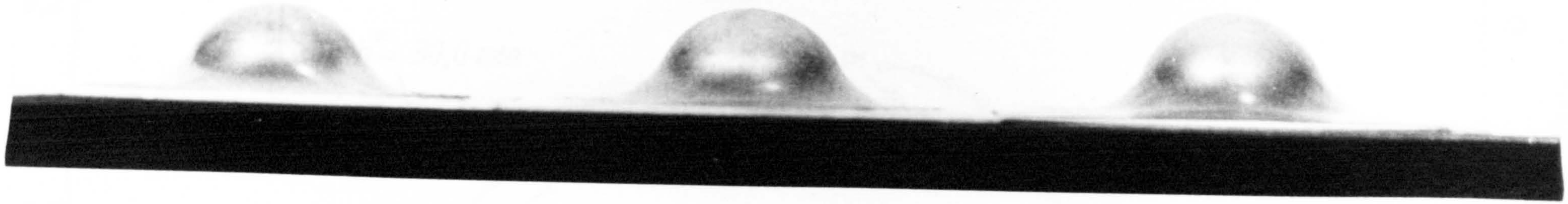


Fig. 79 The effect of punch speeds on cup height of hot pressings at 250°C for 6 Mg(84), punch speeds are 25, 5 and 2.5 mm/min, from left to right.

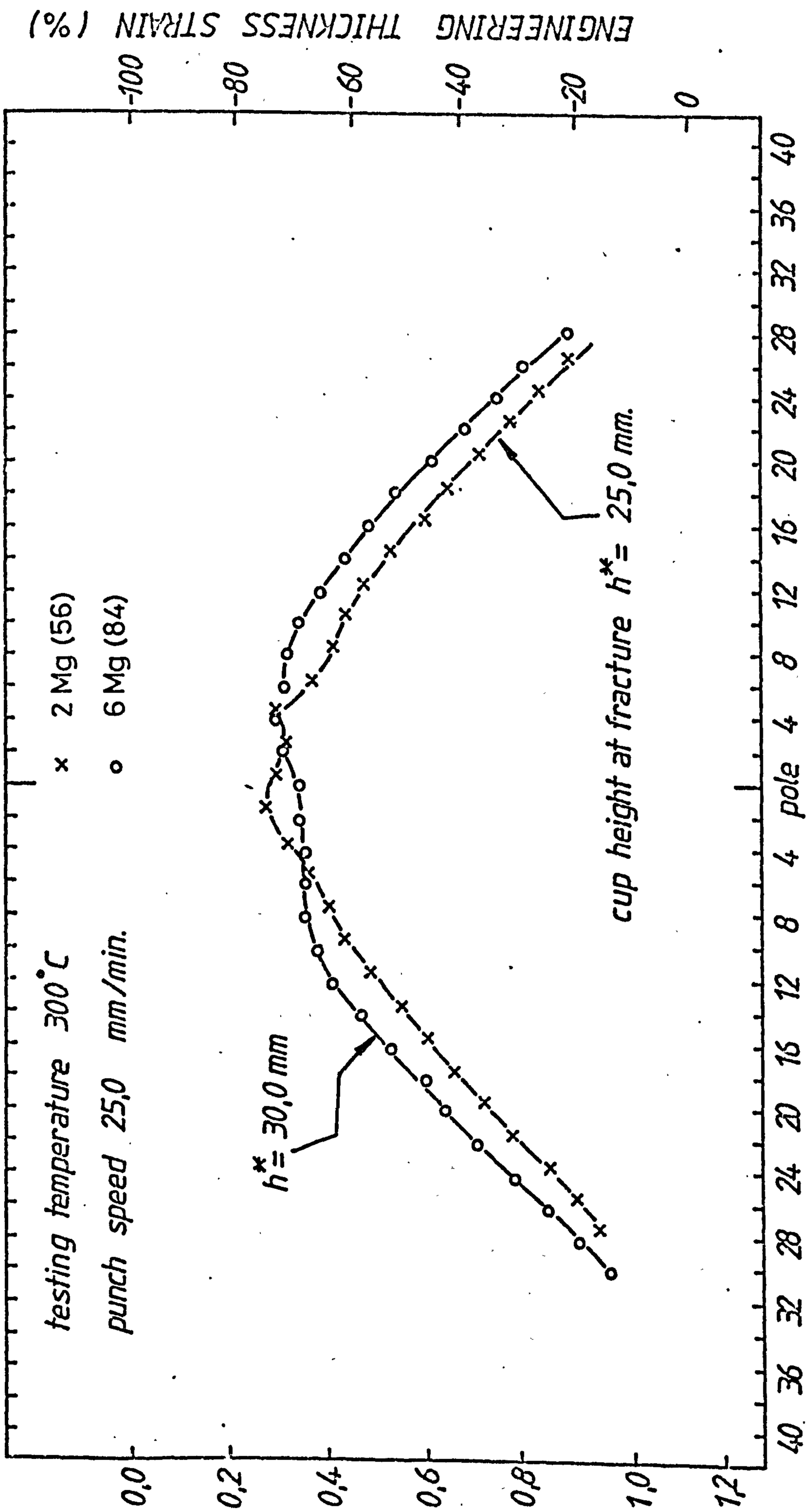


Figure 80 A comparison between the strain distribution across the pole of fractured 50 mm diameter hemispherical punch on 2 Mg(56) and 6 Mg(84).

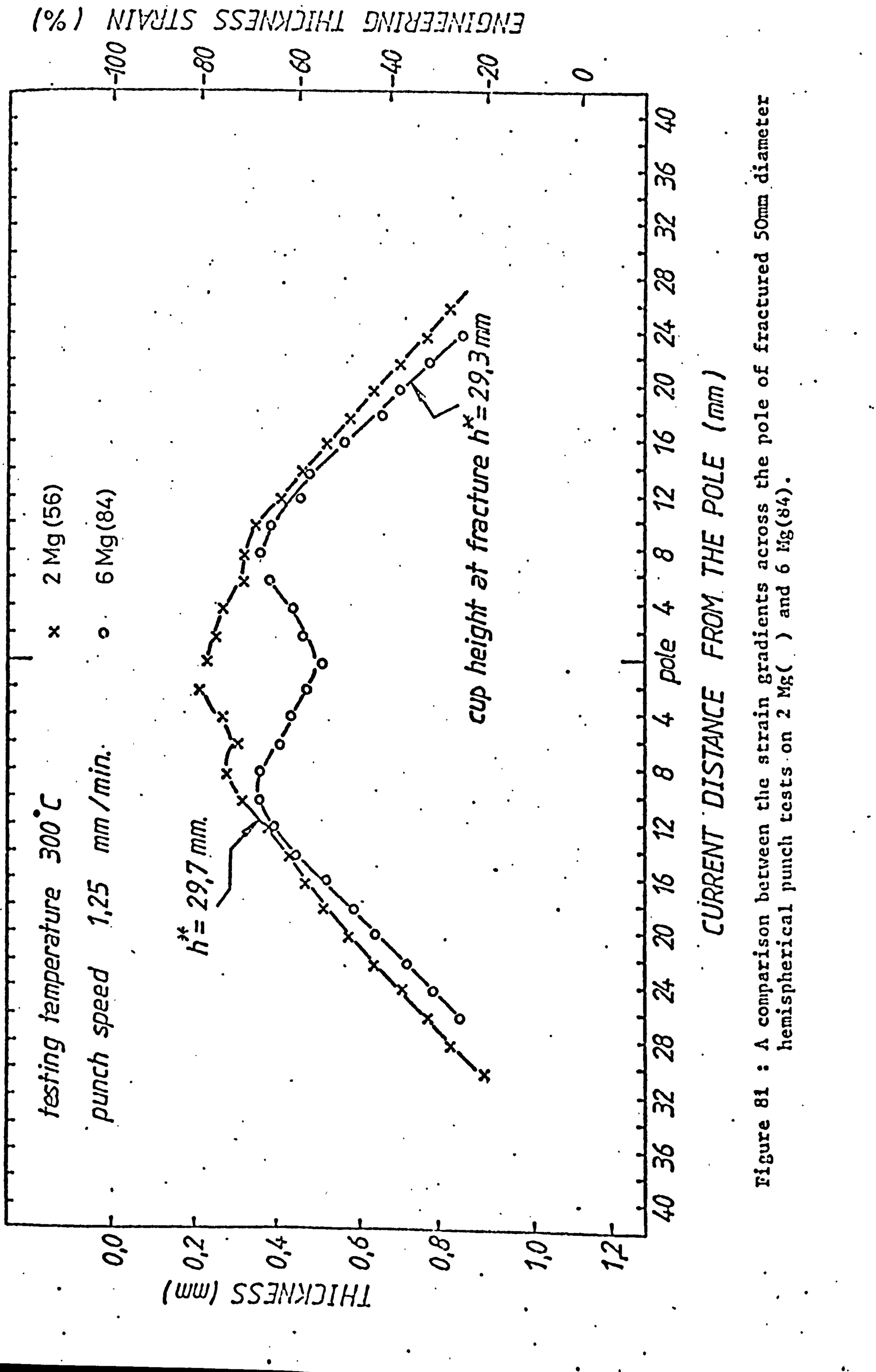


Figure 81 : A comparison between the strain gradients across the pole of fractured hemispherical punch tests on 2 Mg( ) and 6 Mg(84).

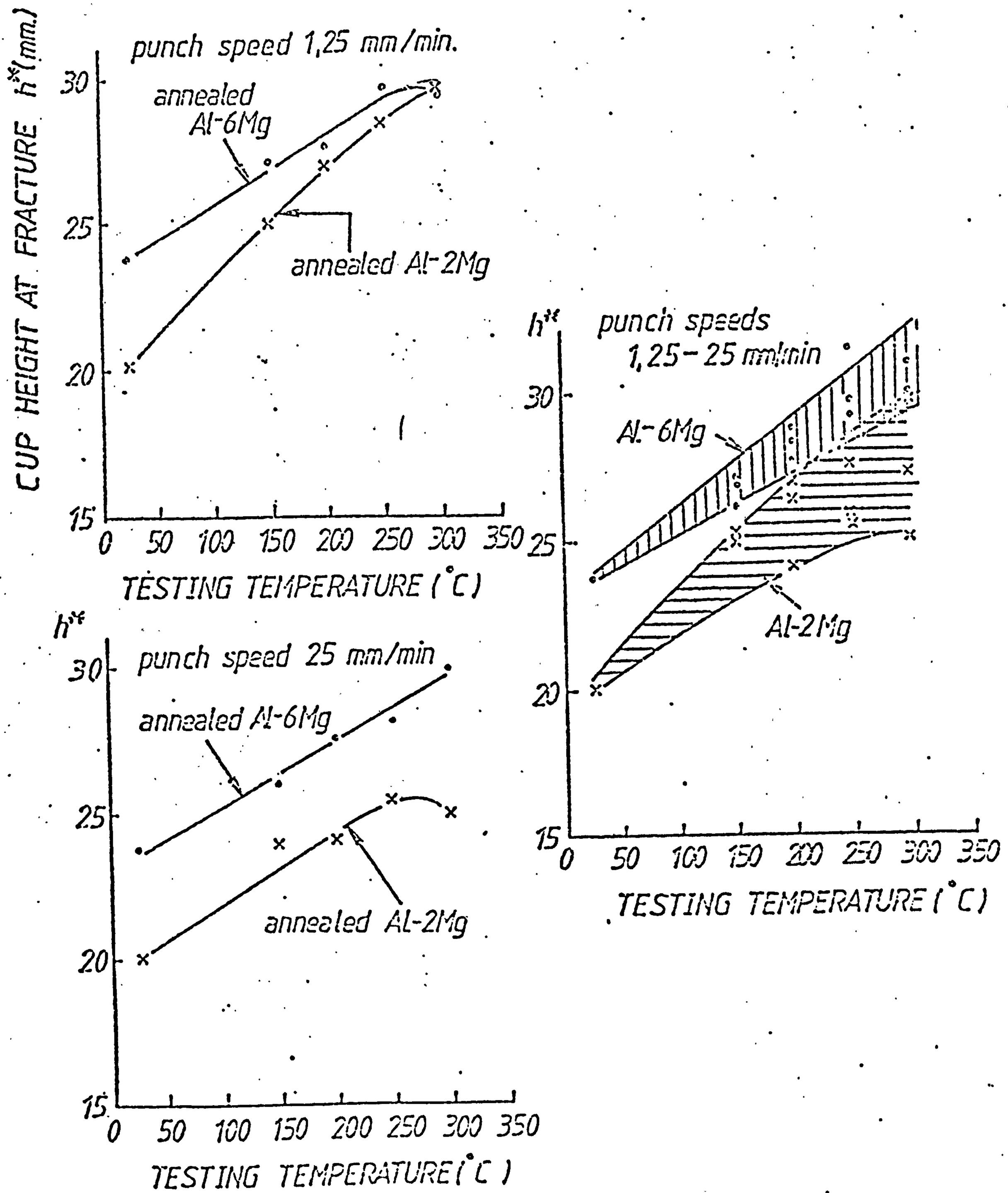


Figure 82 : A comparison of the stretch forming behaviour of 2 Mg(64) and 6 Mg(84) for different punch speeds.

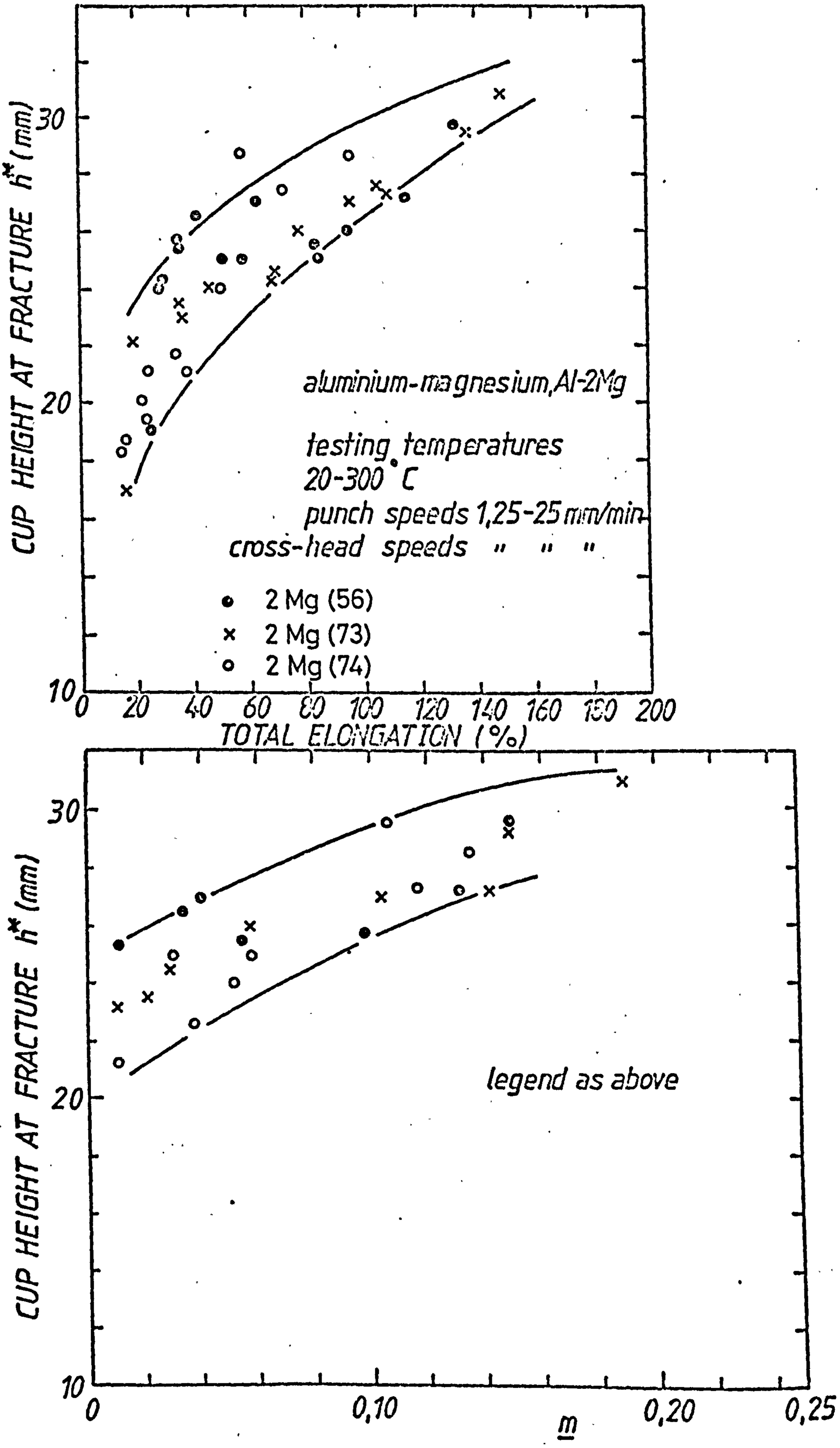
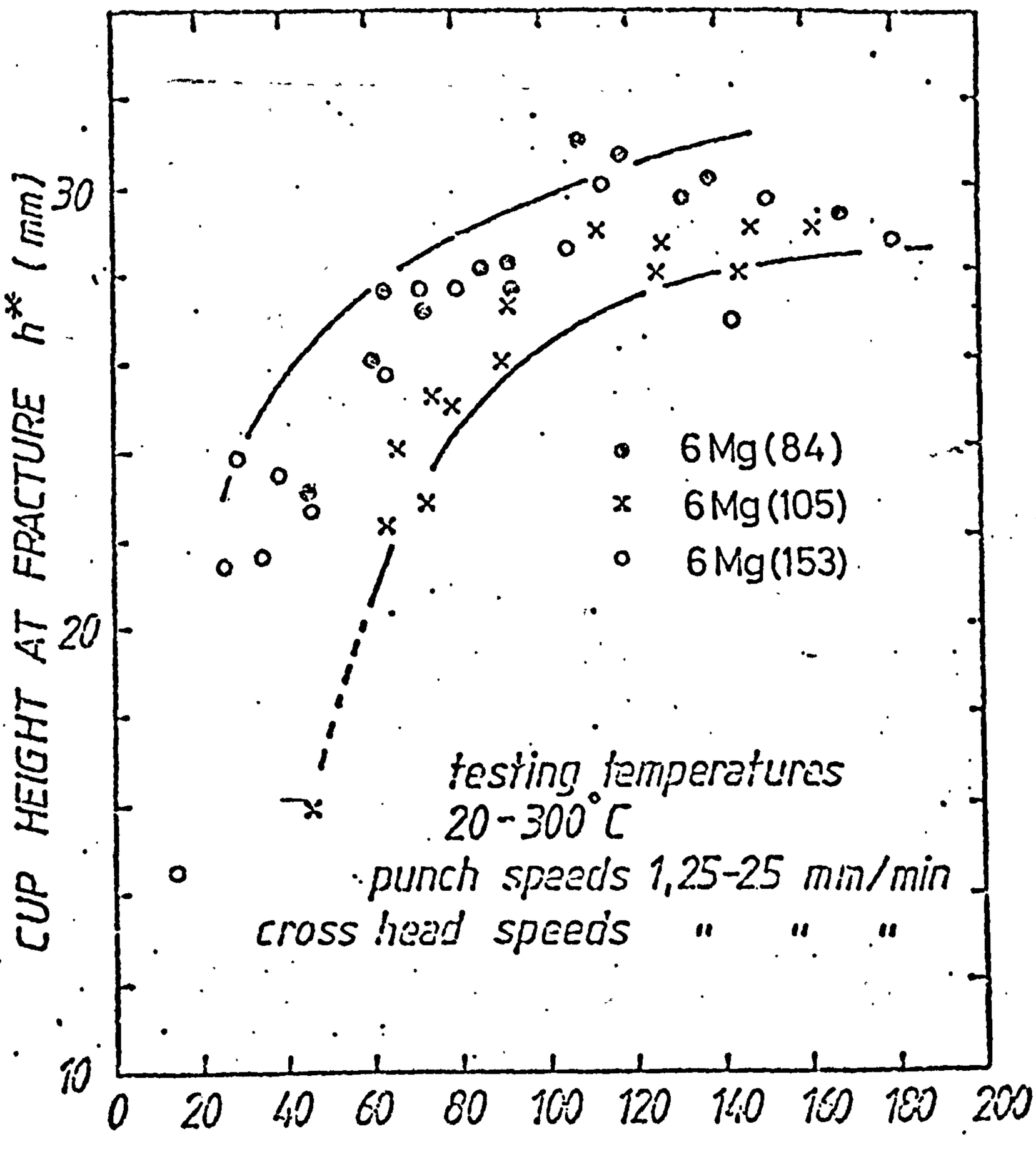


Figure 83 The relationship between the cup height at fracture h* and tensile parameters, elongations and m values.



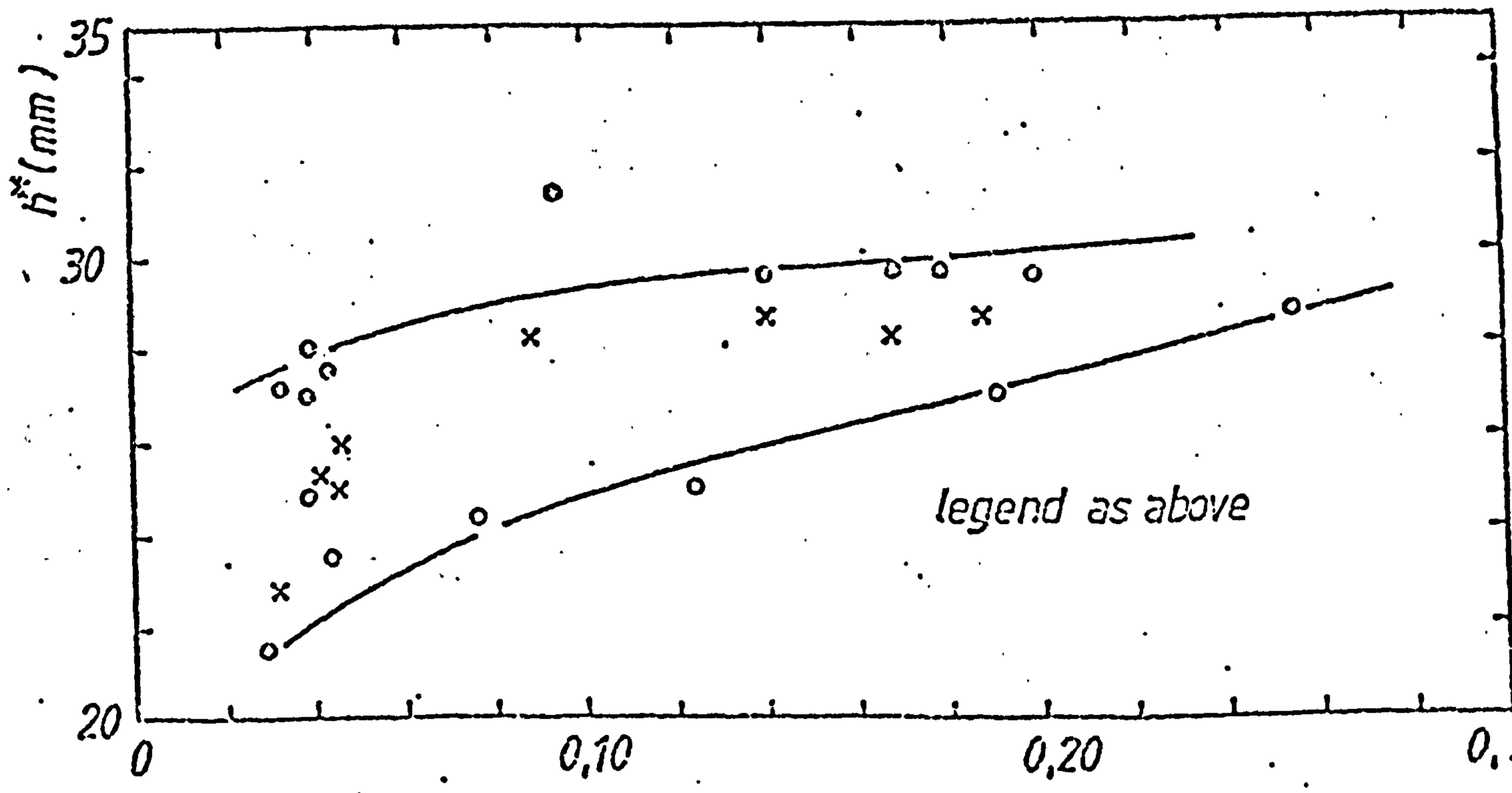
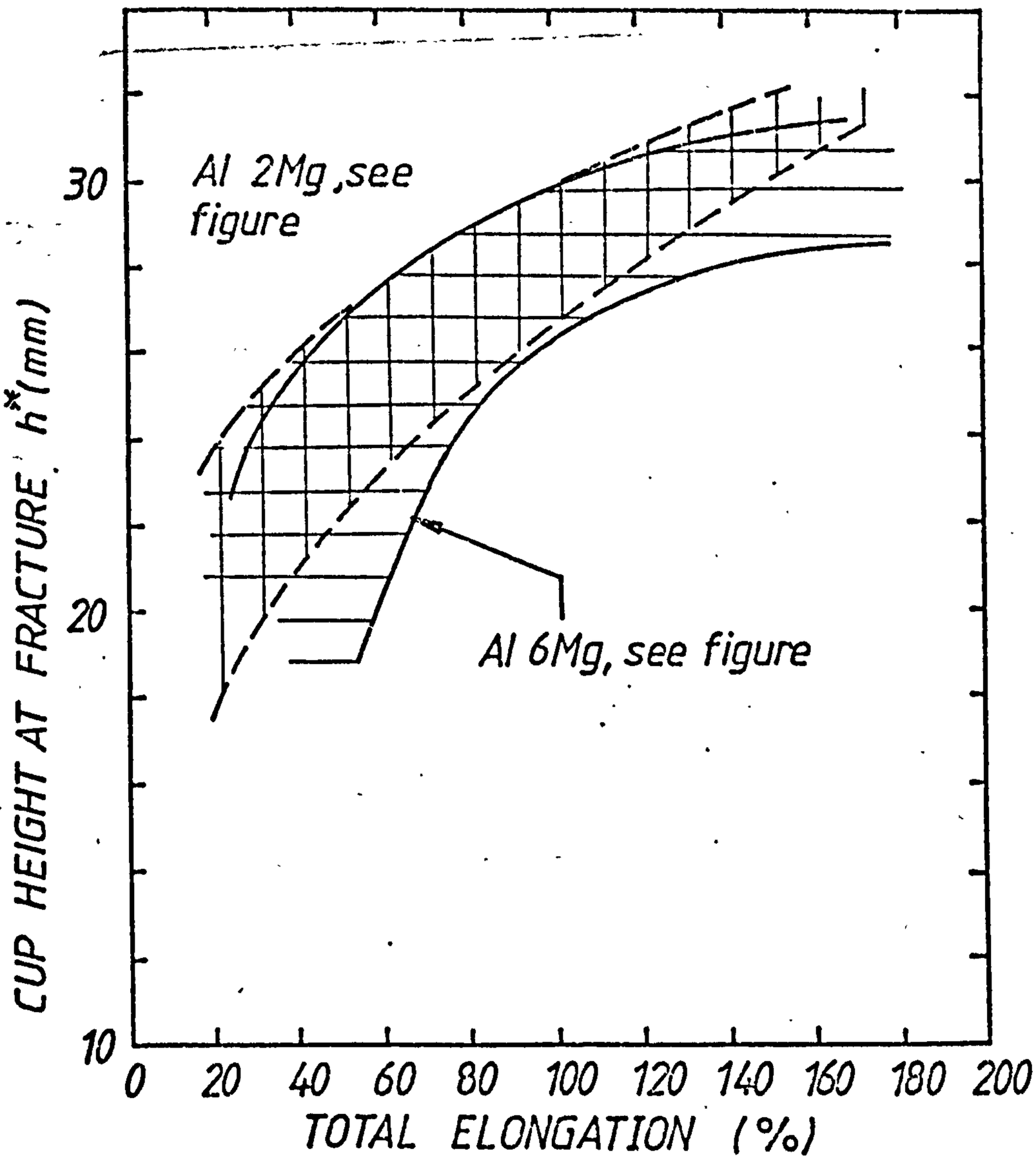


Figure 84 : The relationship between the cup height at fractore h^x and the uniaxial tension test parameters, the total elongation e_T and the coefficient of strain rate sensitivity $\underline{m}$ for annealed and cold-rolled Al-6%Mg.



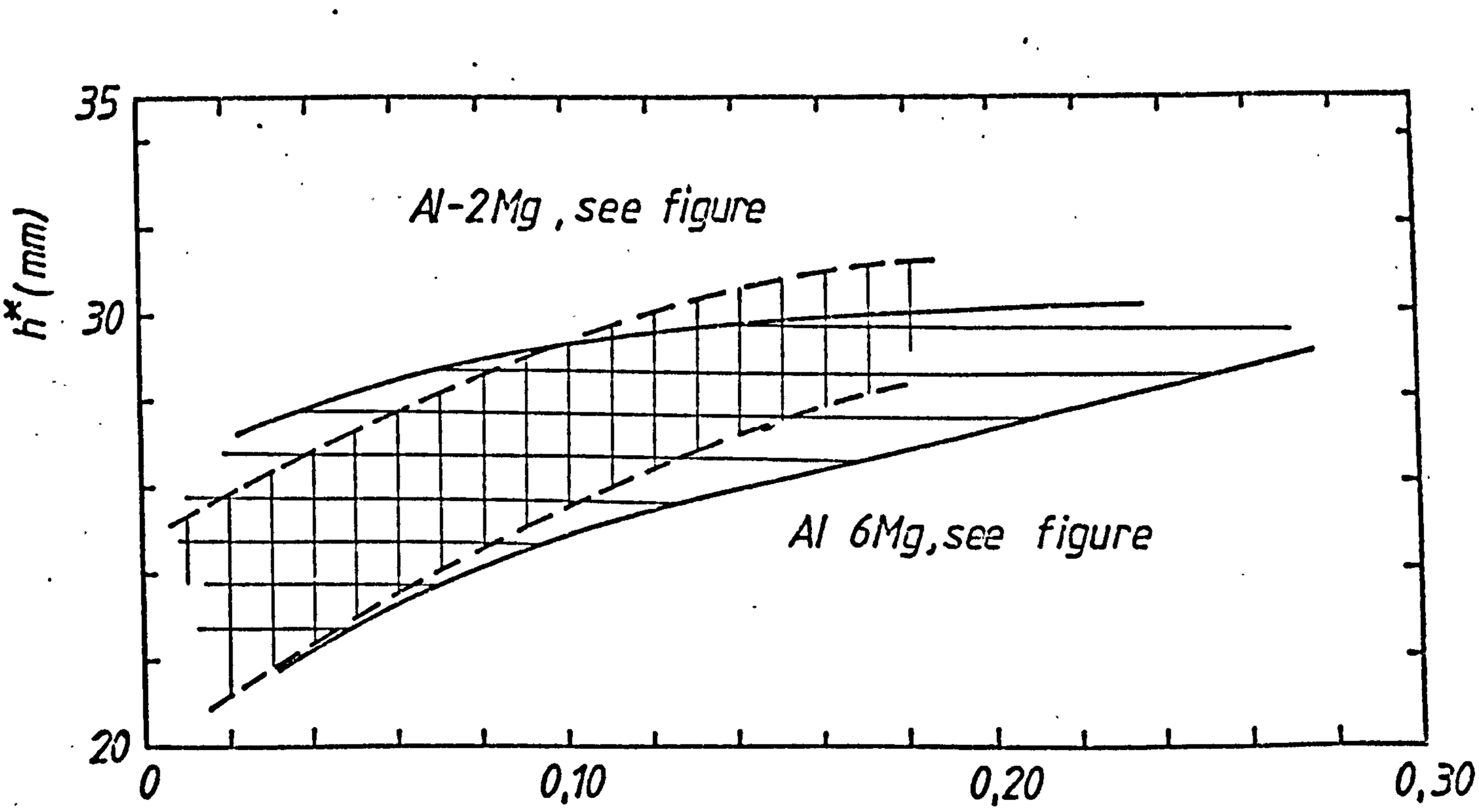


Figure 85 A combination of figures 83 and 84

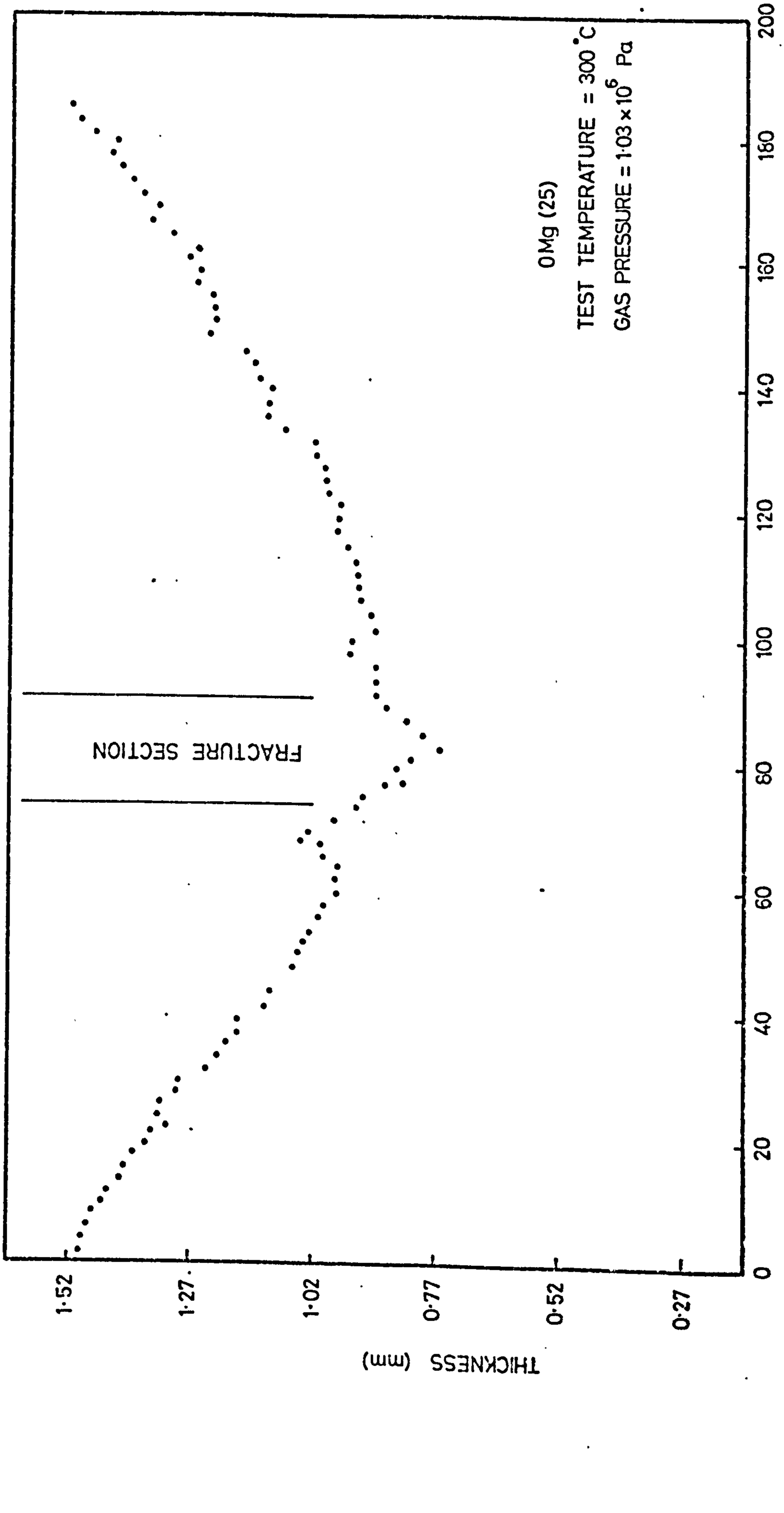


FIG. 86. THICKNESS DISTRIBUTION ACROSS THE POLE OF THE BULGE FOR 0Mg (25) ALLOY AT CONSTANT GAS PRESSURE 1·03 x 10^6 Pa AT 300 °C.

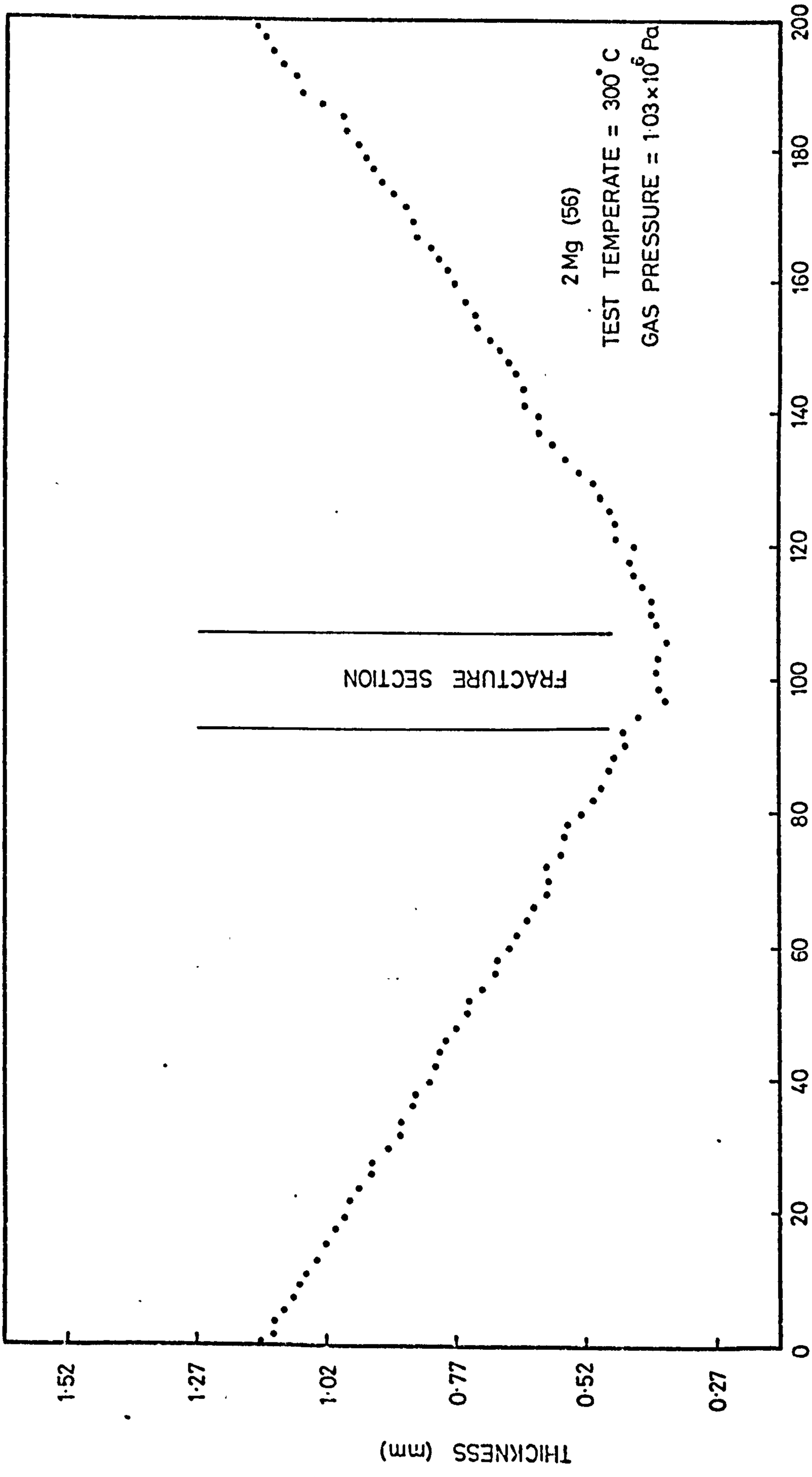


FIG. 87. THICKNESS DISTRIBUTION ACROSS THE POLE OF THE BULGE FOR 2Mg (56) ALLOY AT CONSTANT GAS PRESSURE $1{\cdot}03 \times 10^6$ Pa AT 300°C.

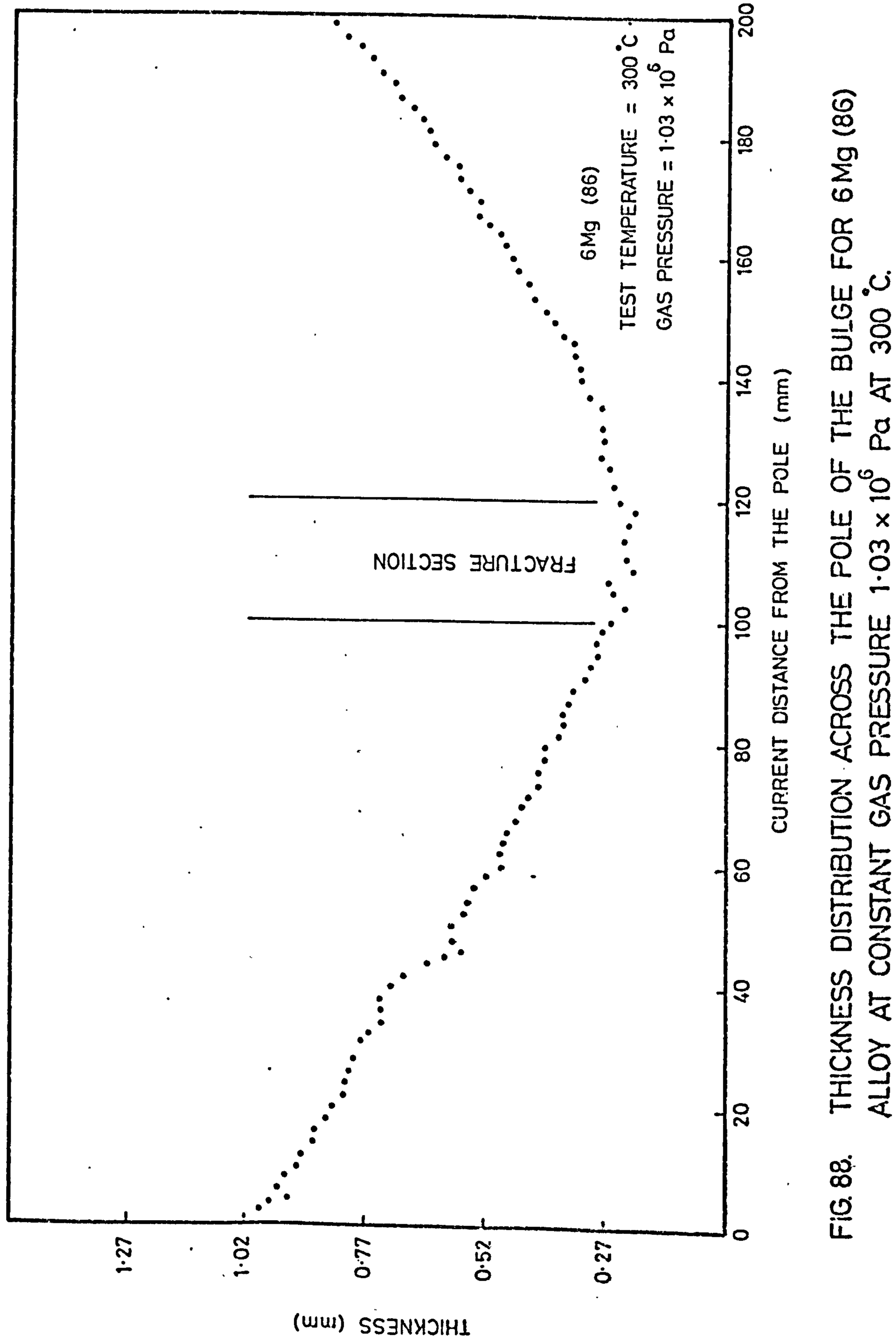


FIG. 88. THICKNESS DISTRIBUTION ACROSS THE POLE OF THE BULGE FOR 6Mg (86) ALLOY AT CONSTANT GAS PRESSURE $1{\cdot}03 \times 10^6$ Pa AT 300 °C.

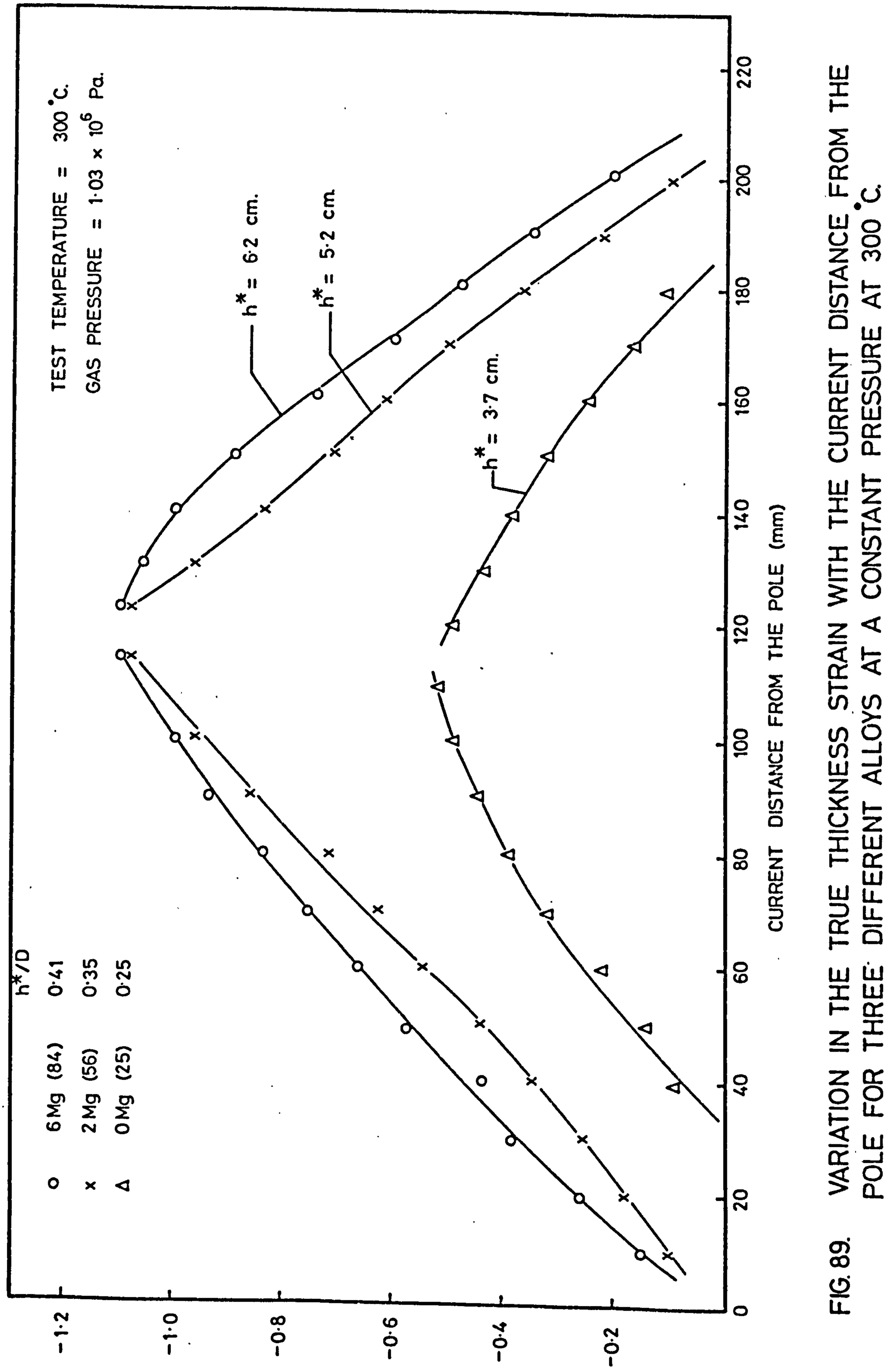


FIG. 89. VARIATION IN THE TRUE THICKNESS STRAIN WITH THE CURRENT DISTANCE FROM THE POLE FOR THREE DIFFERENT ALLOYS AT A CONSTANT PRESSURE AT 300 °C.

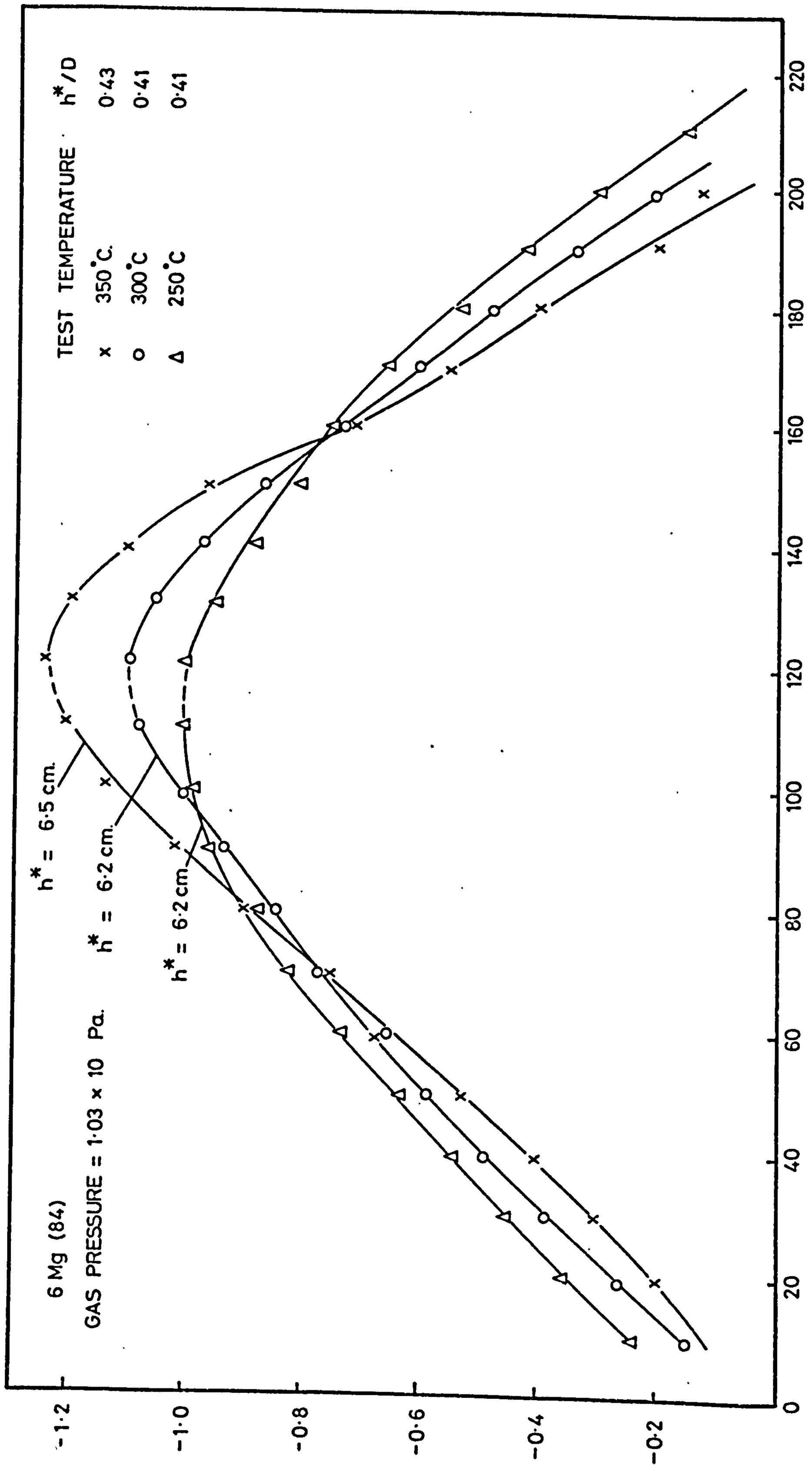


FIG.90. VARIATION IN THE TRUE THICKNESS STRAIN WITH THE CURRENT DISTANCE FROM THE POLE FOR 6Mg (84) AT VARIOUS TEMPERATURES AT A CONSTANT PRESSURE.

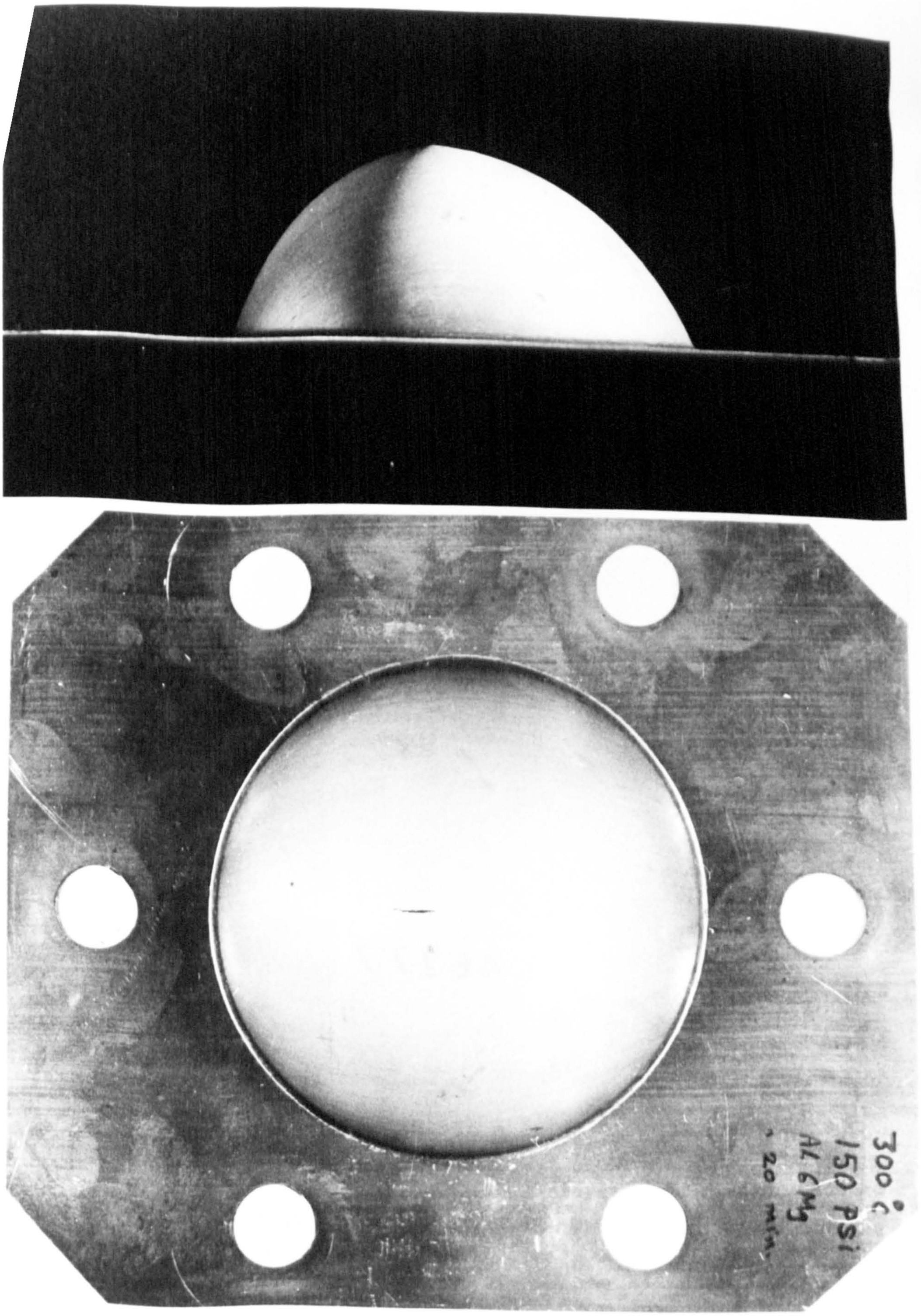
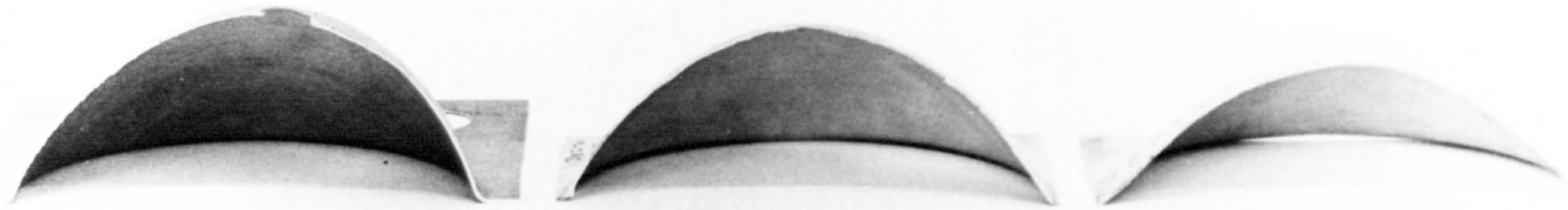


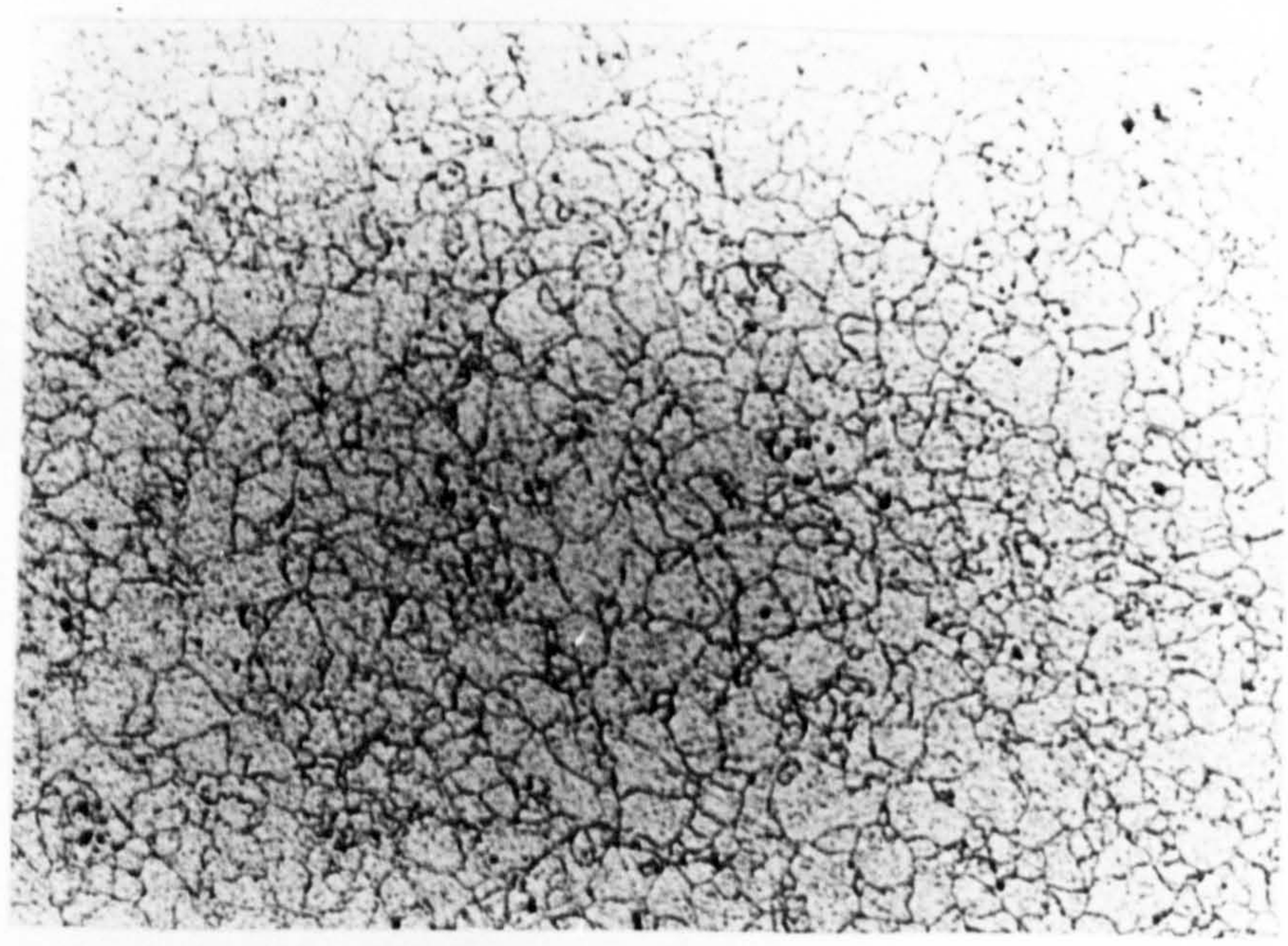
Fig. 91 Typical complete bulge before sectioning for 6 Mg(84), bulged at 300°C and ~1 M P_a.



(a) (b) (c)

Figure 92 Typical bulges after sectioning deformed at 300°C and ~1 MP_a
(a) 6 Mg(84) (b) 2 Mg(56) and (c) 0 Mg(25).

(a)



(b)

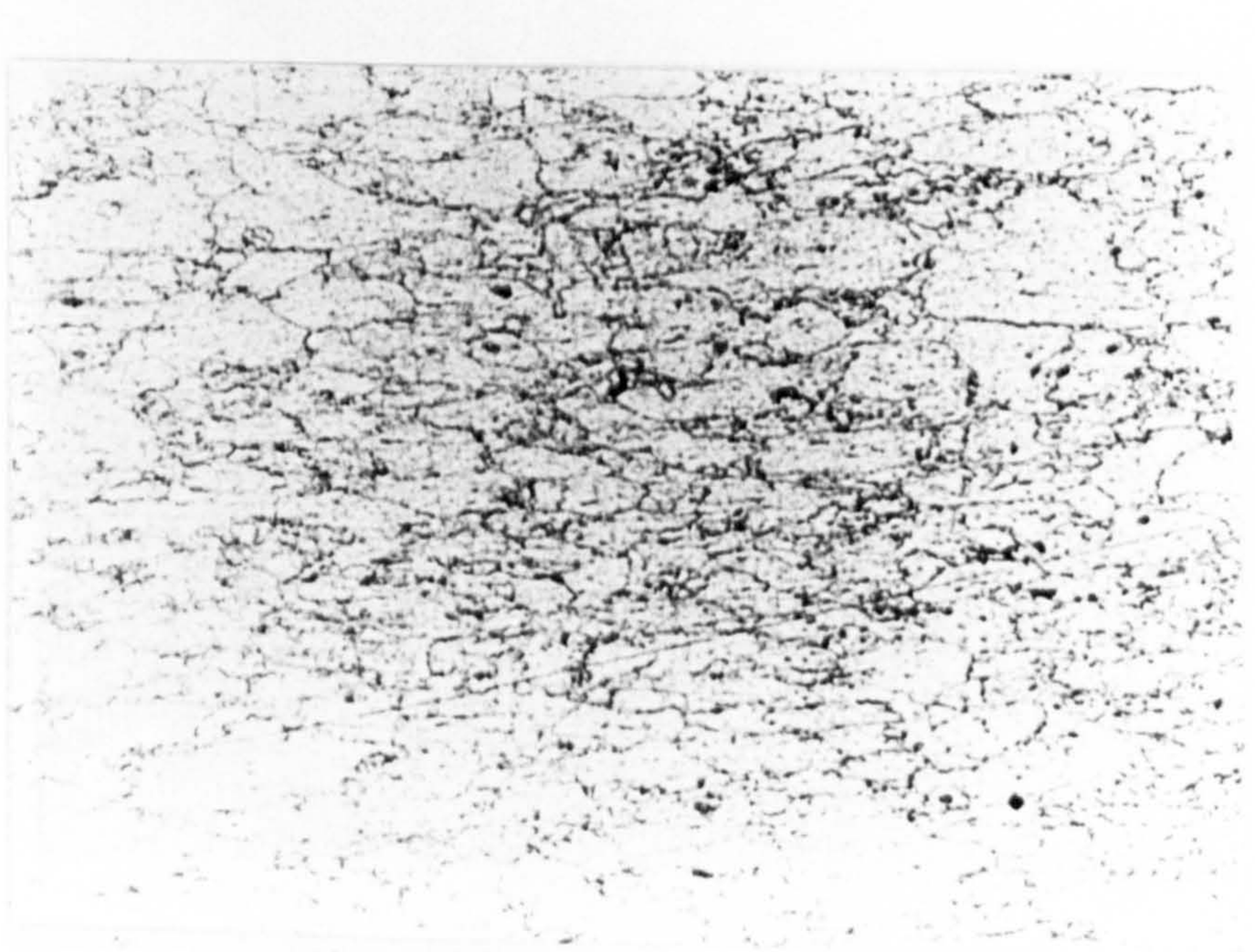
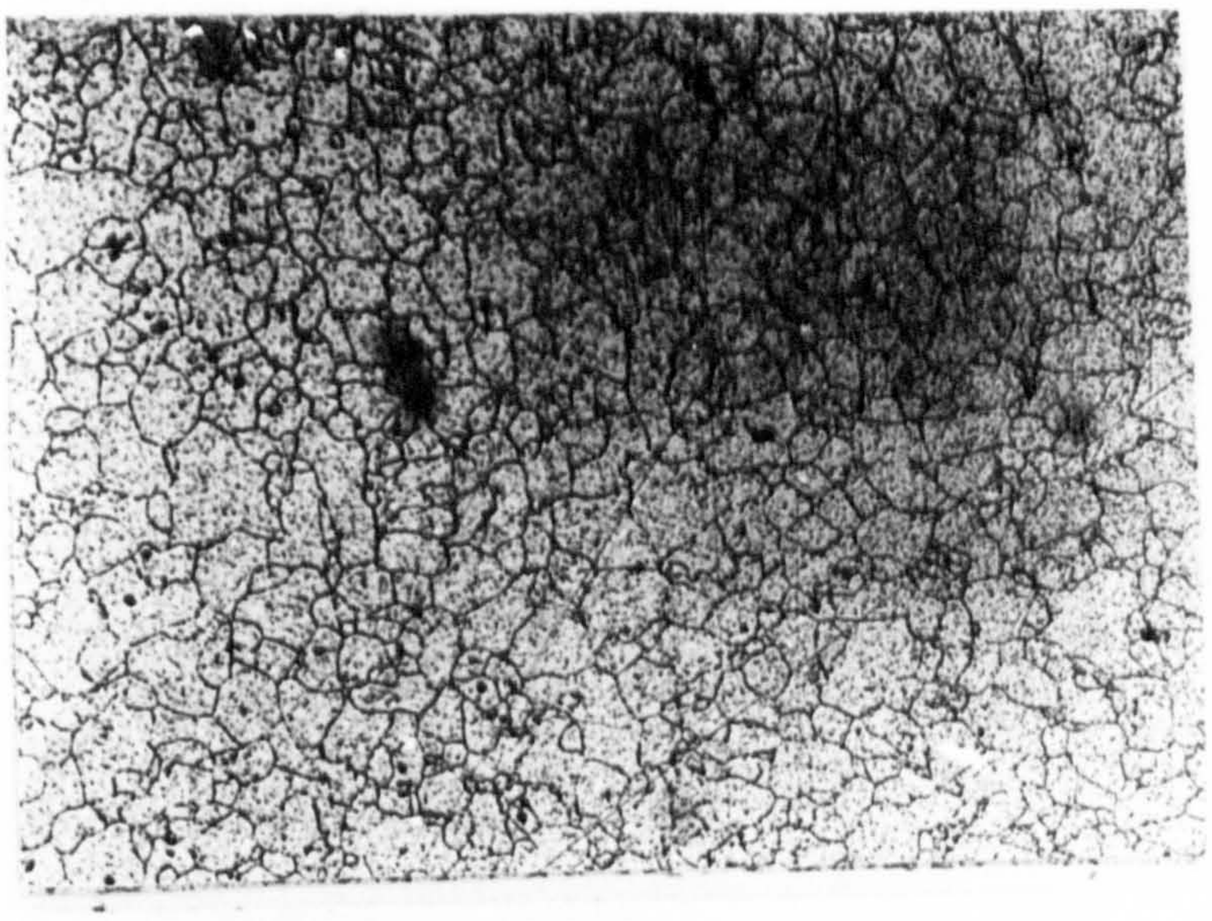


Fig.93 Microstructure of (a) 6 Mg(84), furnace cooled from 350°C and (b) 6 Mg(153), 40% cold rolled. (x 200).

(a)



(b)

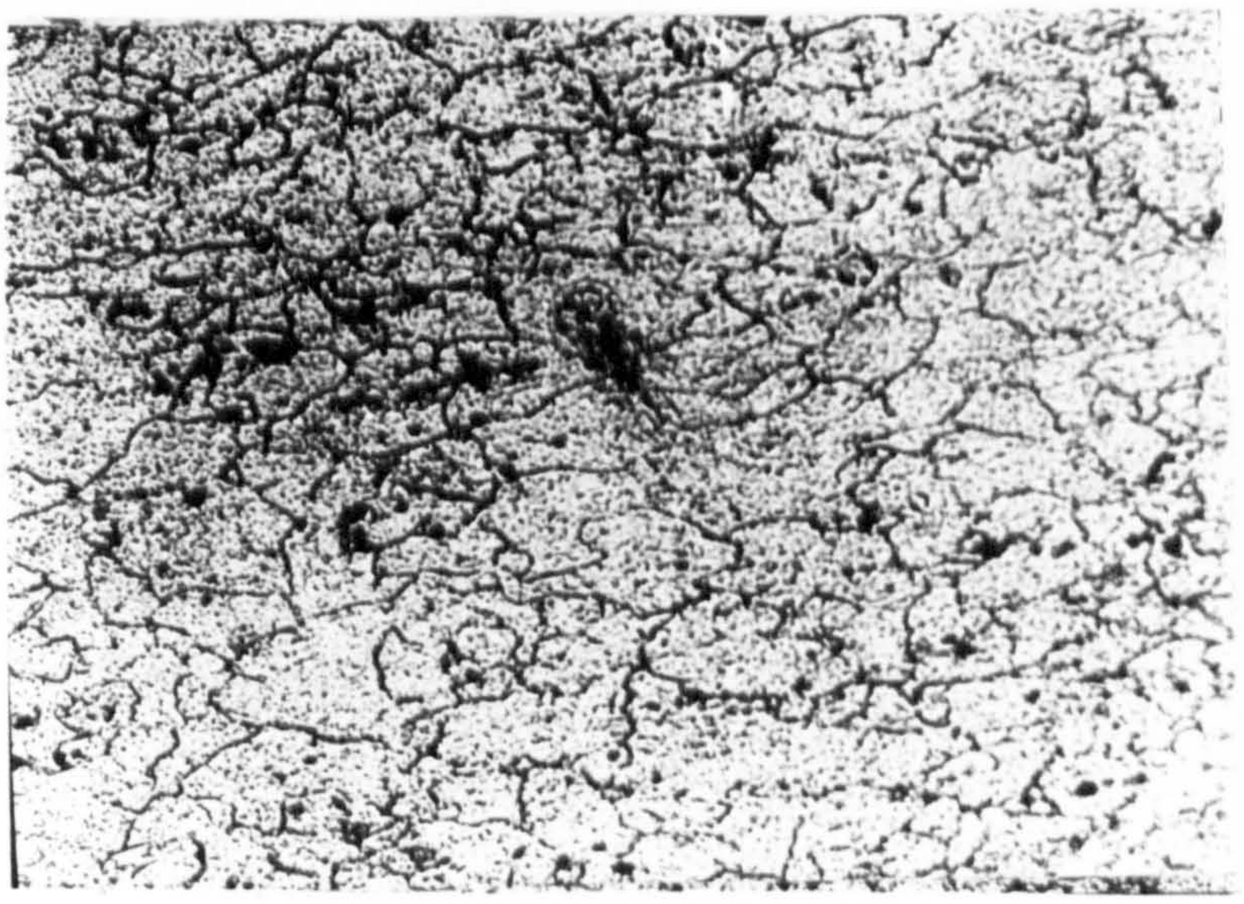
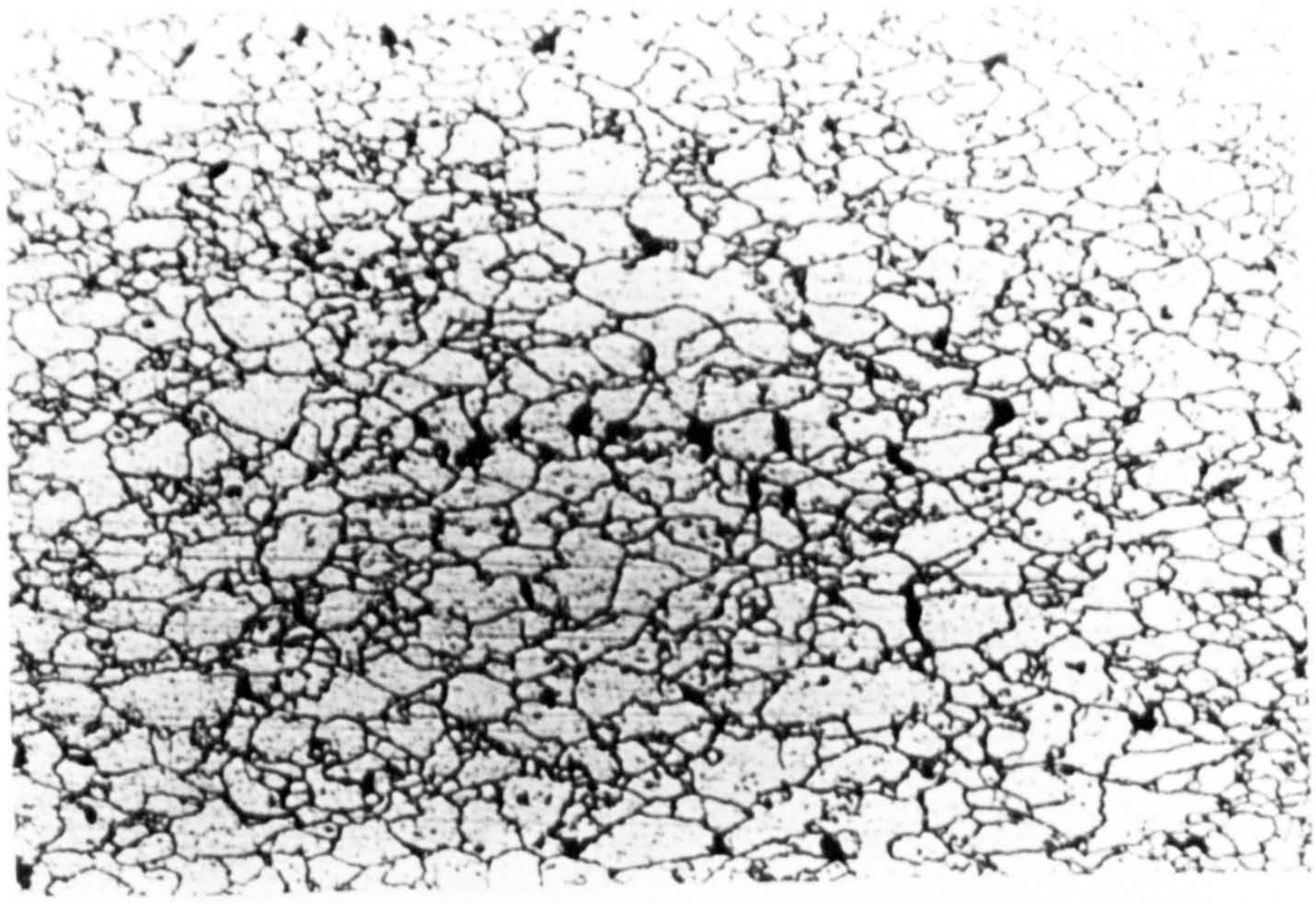


Fig. 94 The undeformed grip ends structure where deformation time is ~160 minutes at 300°C. (a) 6 Mg(84) (b) 6 Mg(153). (x 200).

(a)



(b)

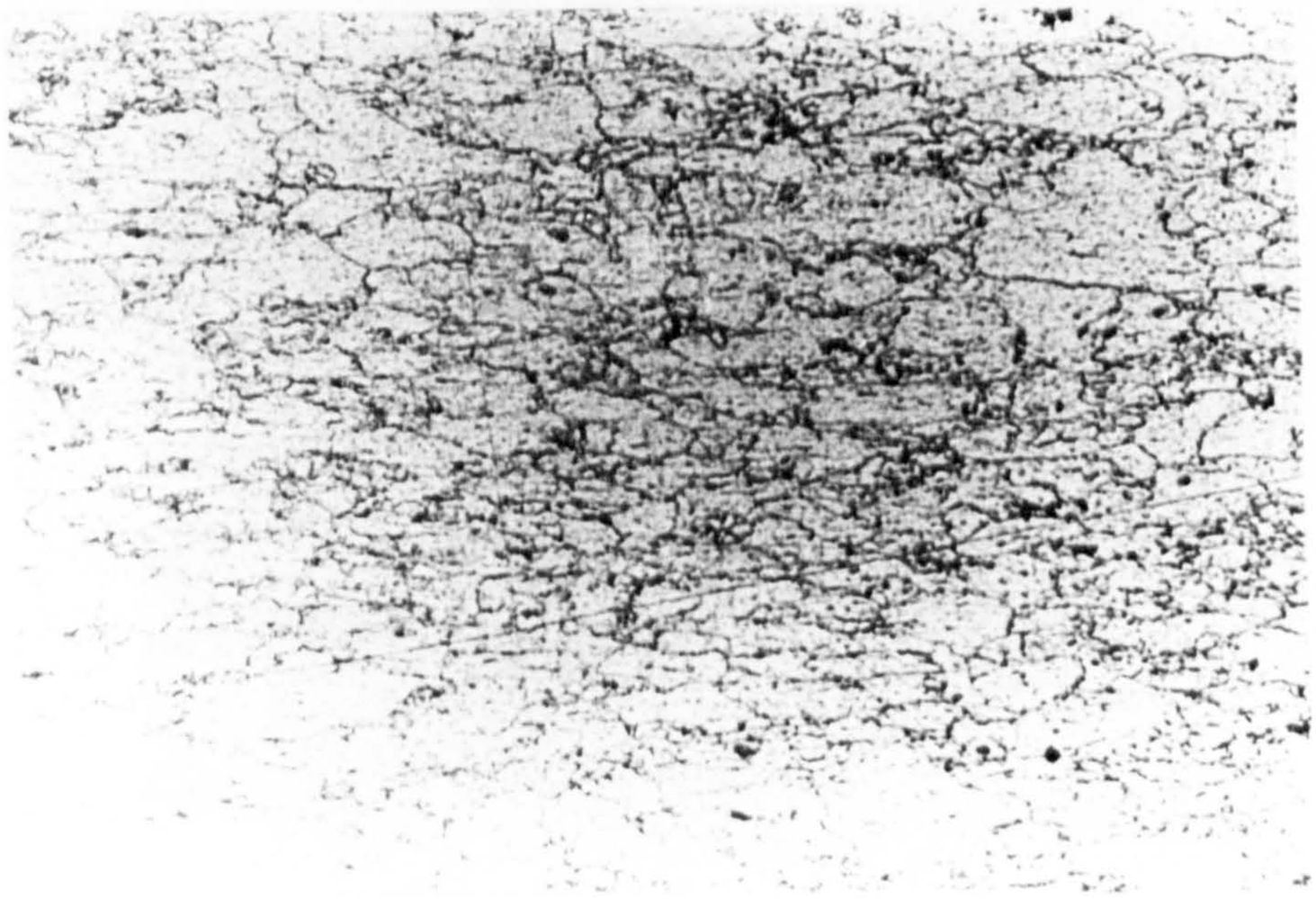
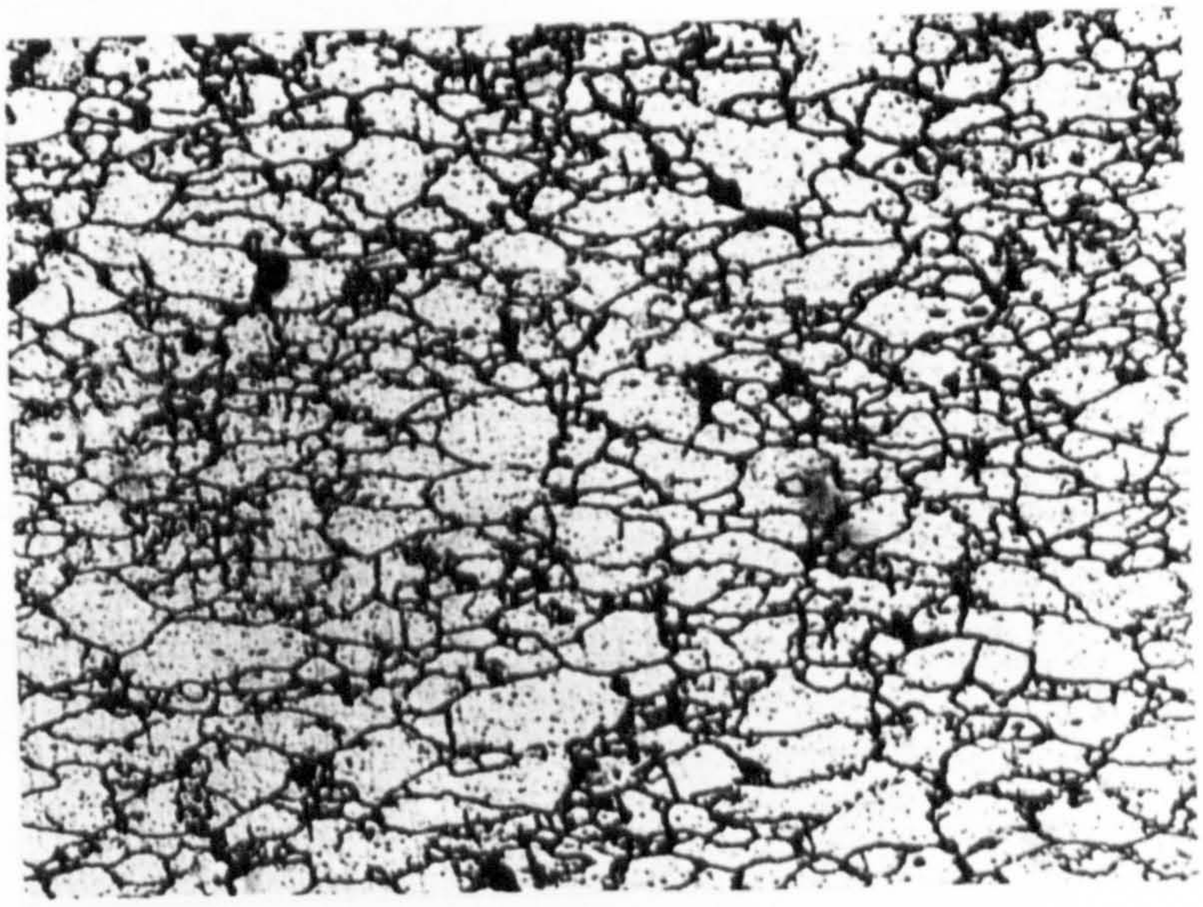


Fig. 95 Microstructure after 50% elongation at 300°C and $\dot{\varepsilon} = 1.67 \times 10^{-4}$ sec^{-1}.
(a) 6 Mg(84) (b) 6 Mg(153). (x 200).

(a)

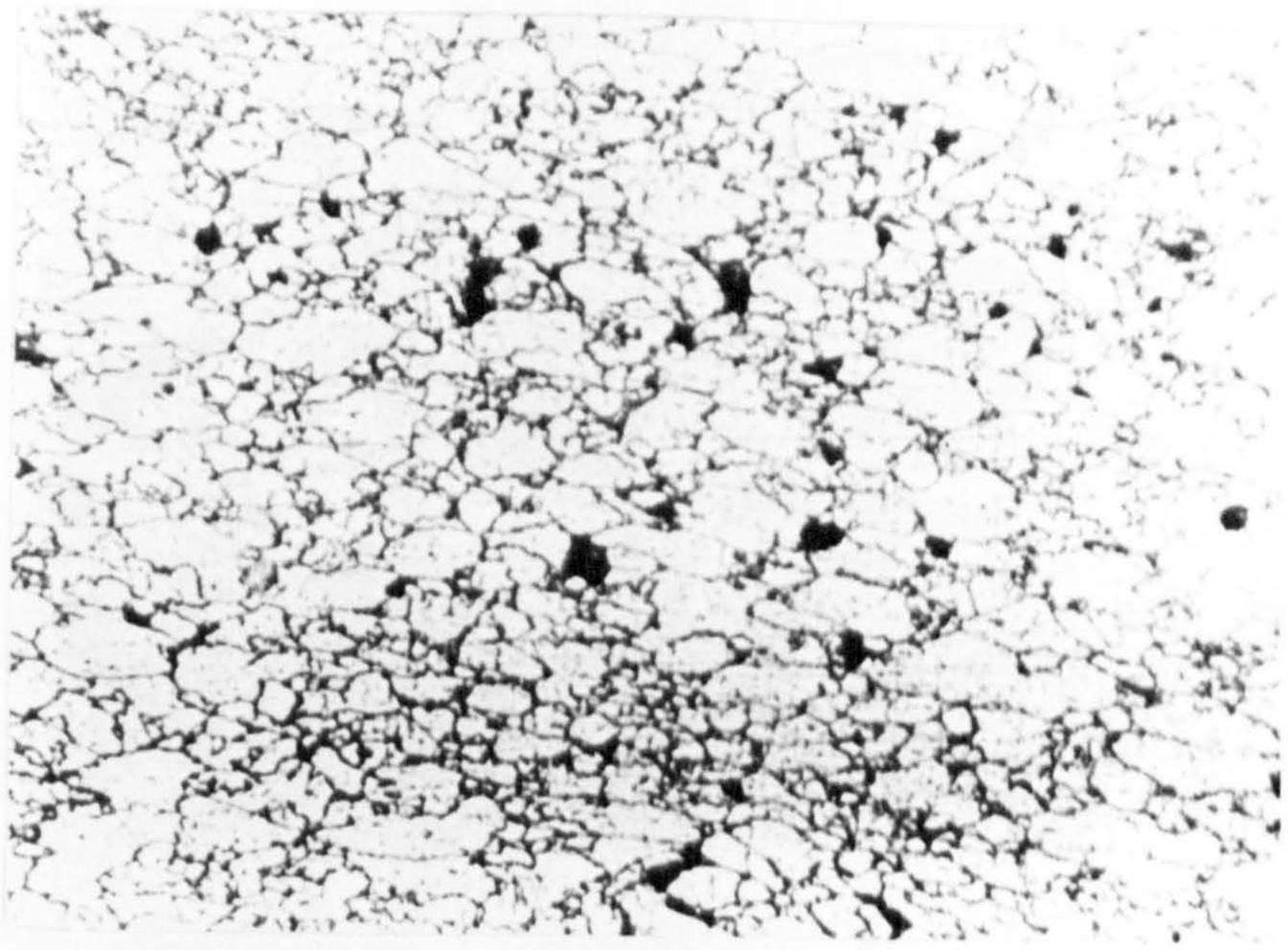


(b)



Fig. 96 Microstructure after 100% elongation at 300°C and $\dot{\varepsilon} = 1.67 \times 10^{-4}$ sec^{-1}.
(a) 6 Mg(84) (b) 6 Mg(153). (x 200).

(a)



(b)

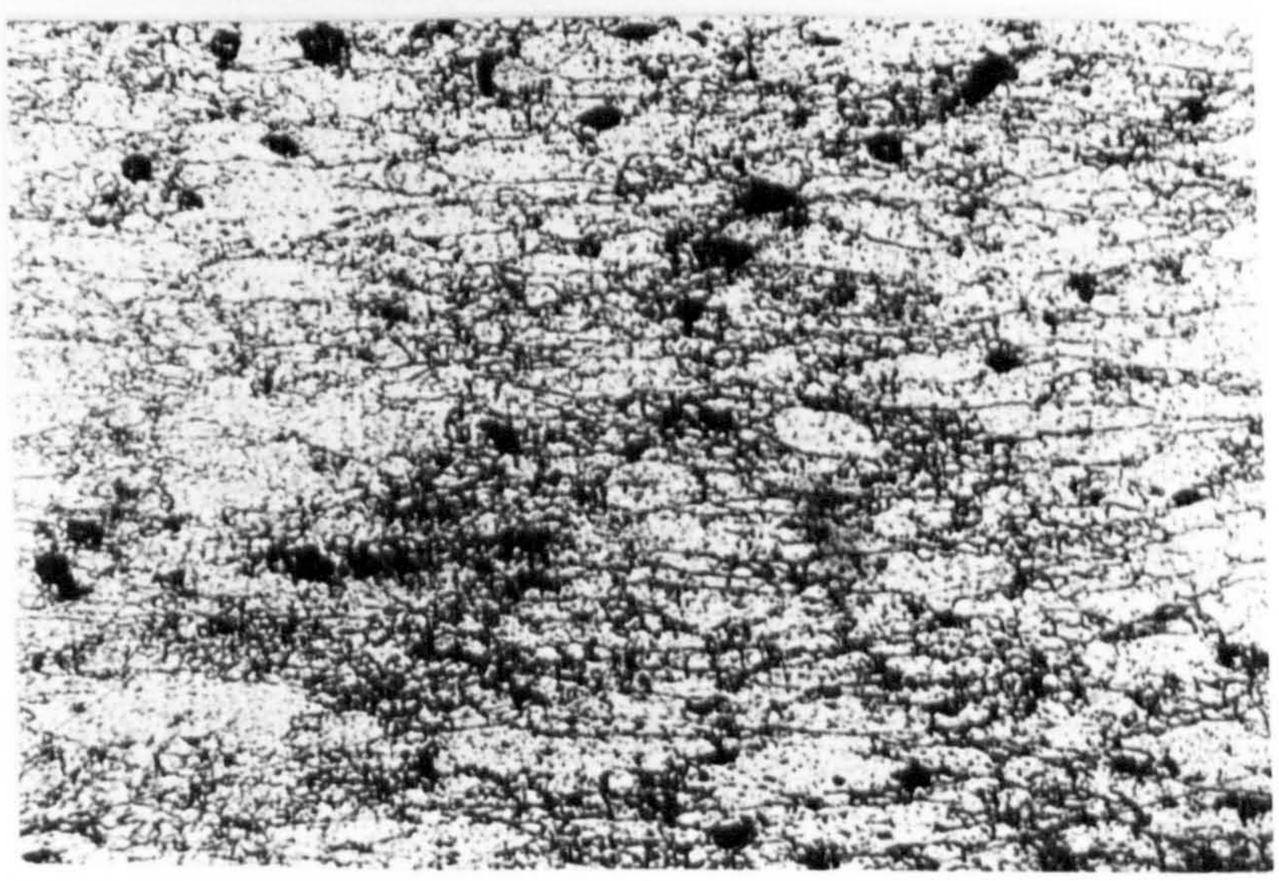
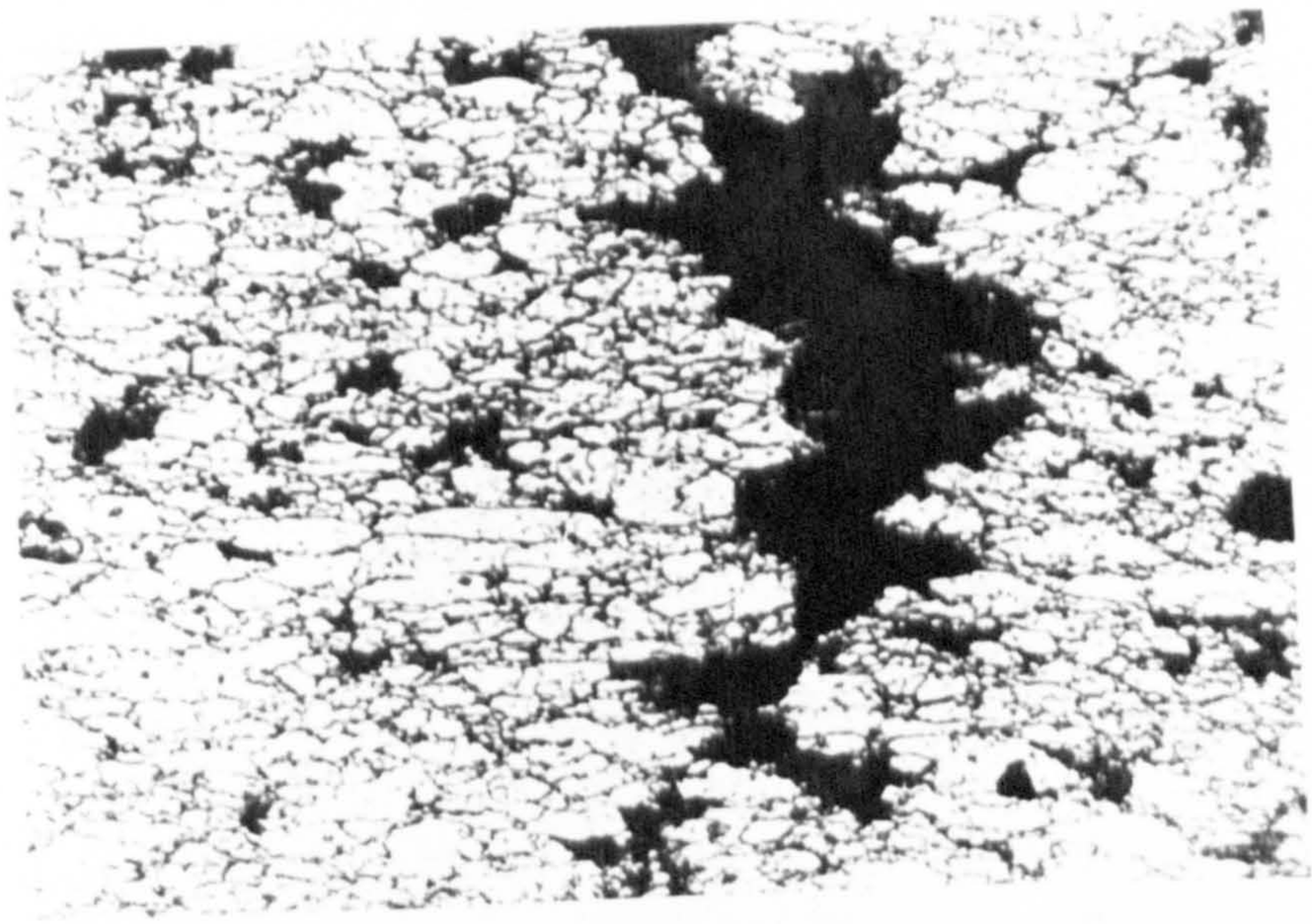


Fig. 97 Microstructure after 200% elongation at 300°C and $\dot{\epsilon} = 1.67 \times 10^{-4}$ sec^{-1}.
(a) 6 Mg(84) (b) 6 Mg(153). (x 200).

(a)



(b)

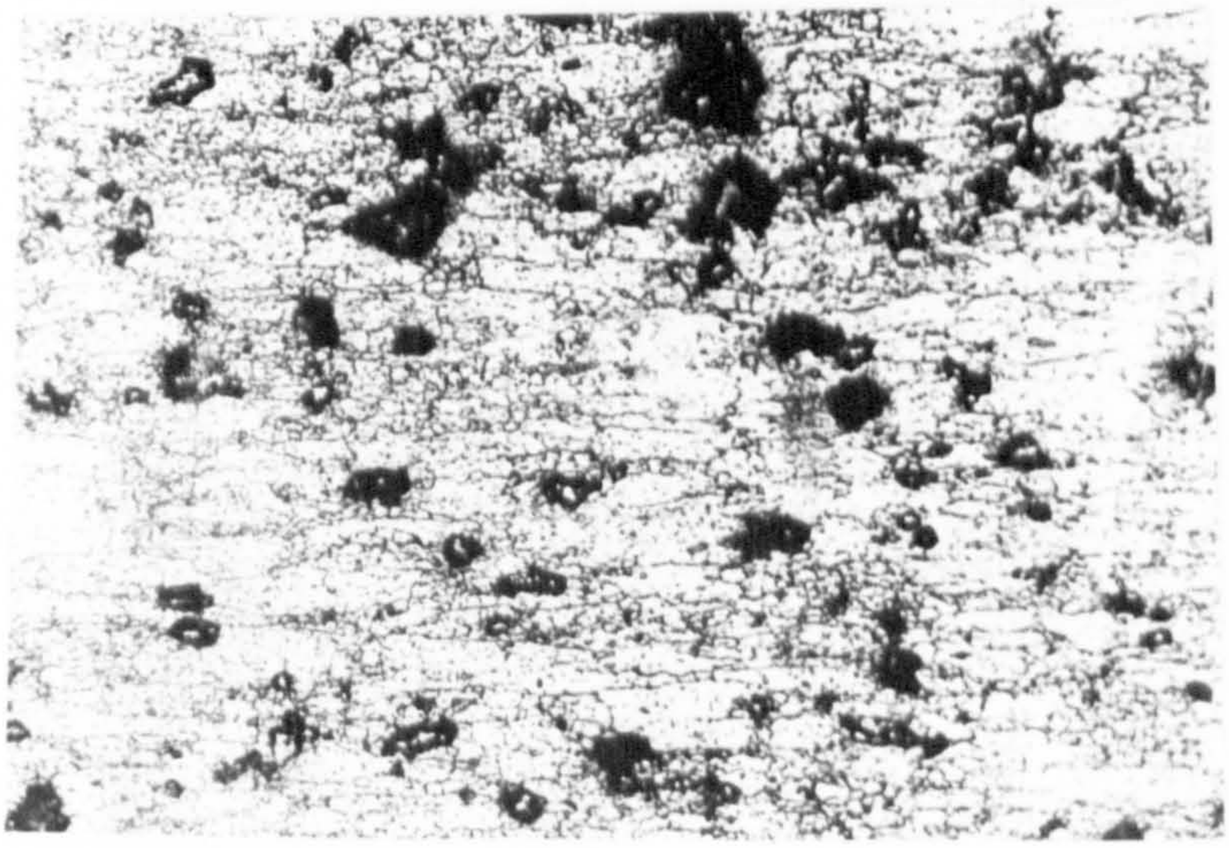
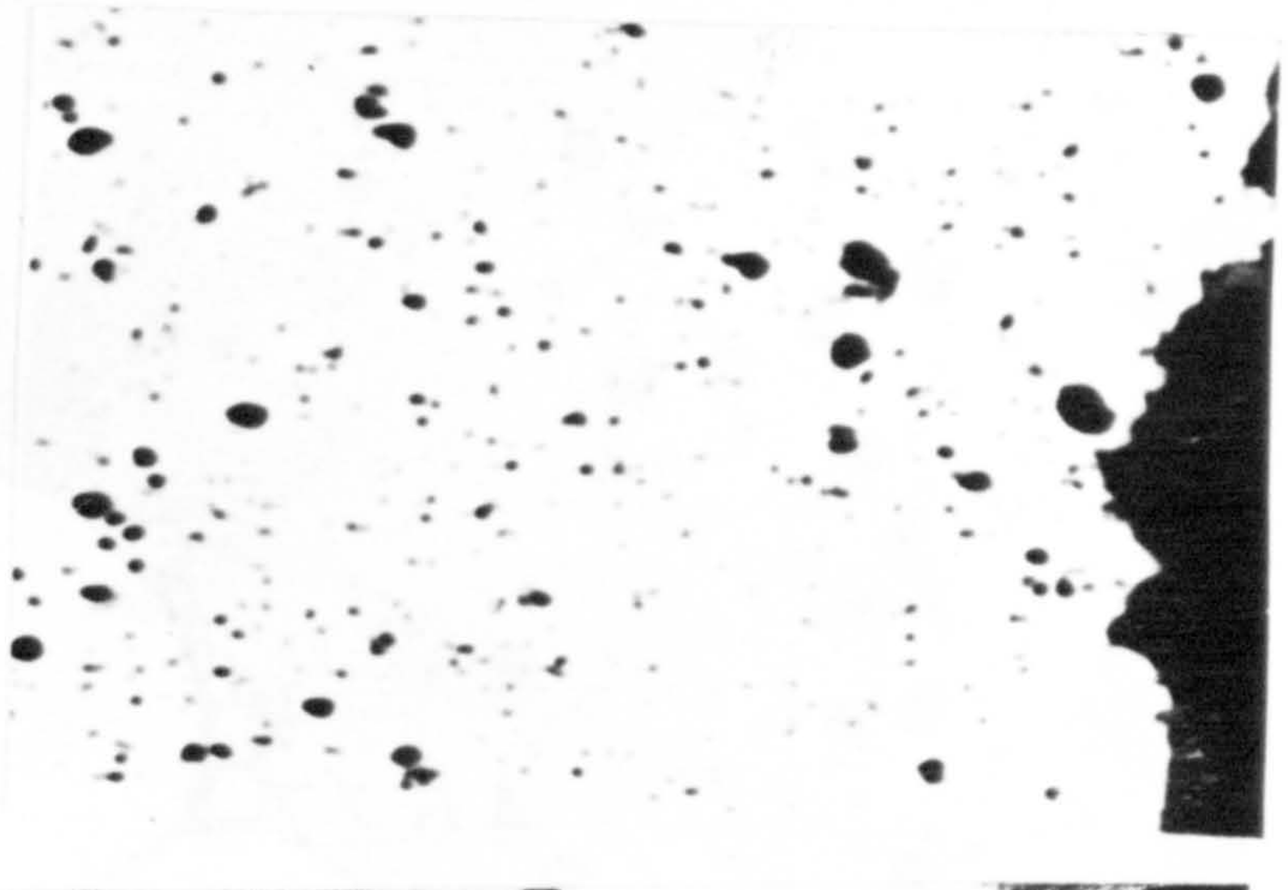


Fig. 98 Microstructure after 250% elongation at 300°C and $\dot{\varepsilon} = 1.67 \times 10^{-4}$ sec^{-1}.
(a) 6 Mg(84) (b) 6 Mg(153). (x 200).

(a)



(b)



(c)

(d)

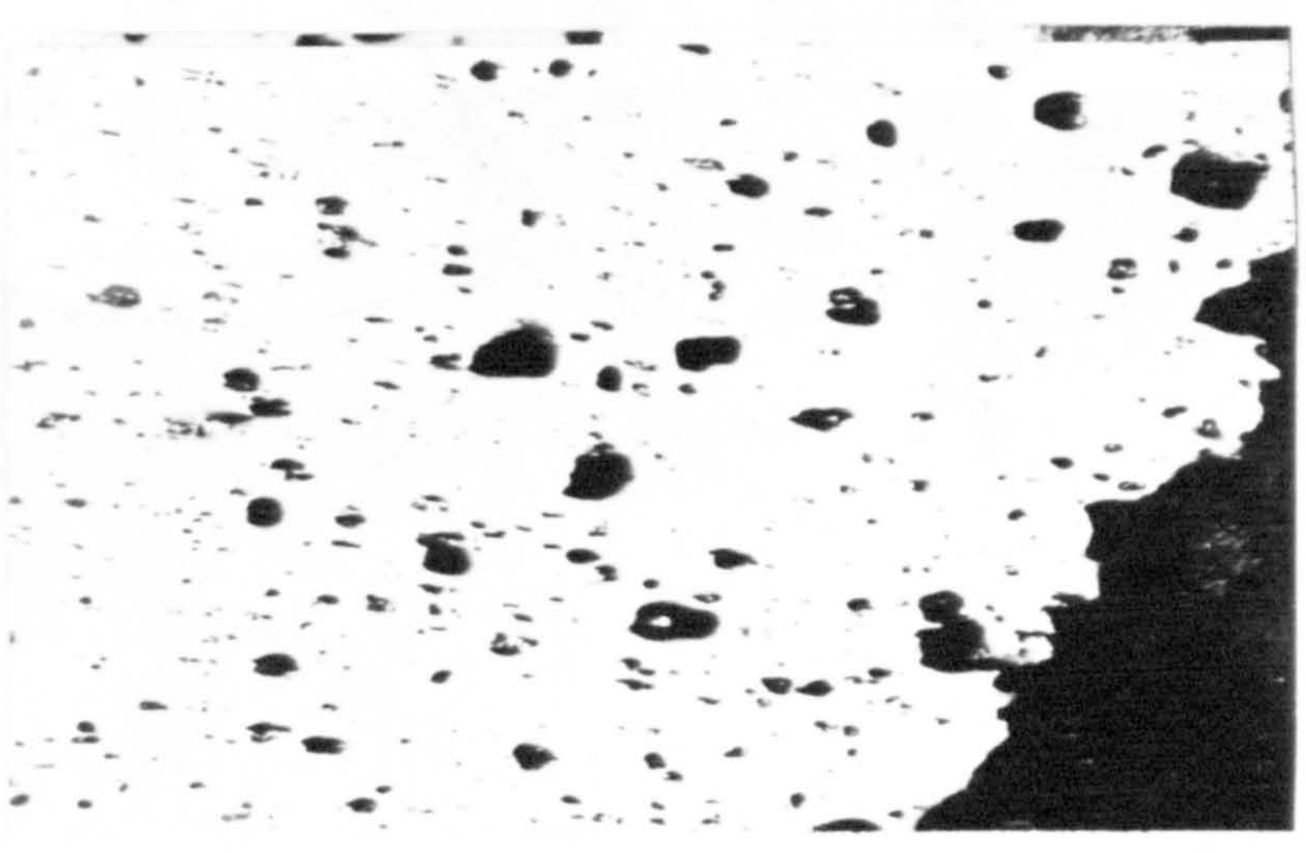


Fig. 99 Unetched specimen showing the cavitation after deformation at 250°C and $\dot{\epsilon} = 1.67 \times 10^{-4}$ sec^{-1} (a) 6 Mg(153), E_1 = 200% (b) 6 Mg(153) at fracture (c) 6 Mg(84), E_1 = 200% and (d) 6 Mg(84) at fracture. (x 75).

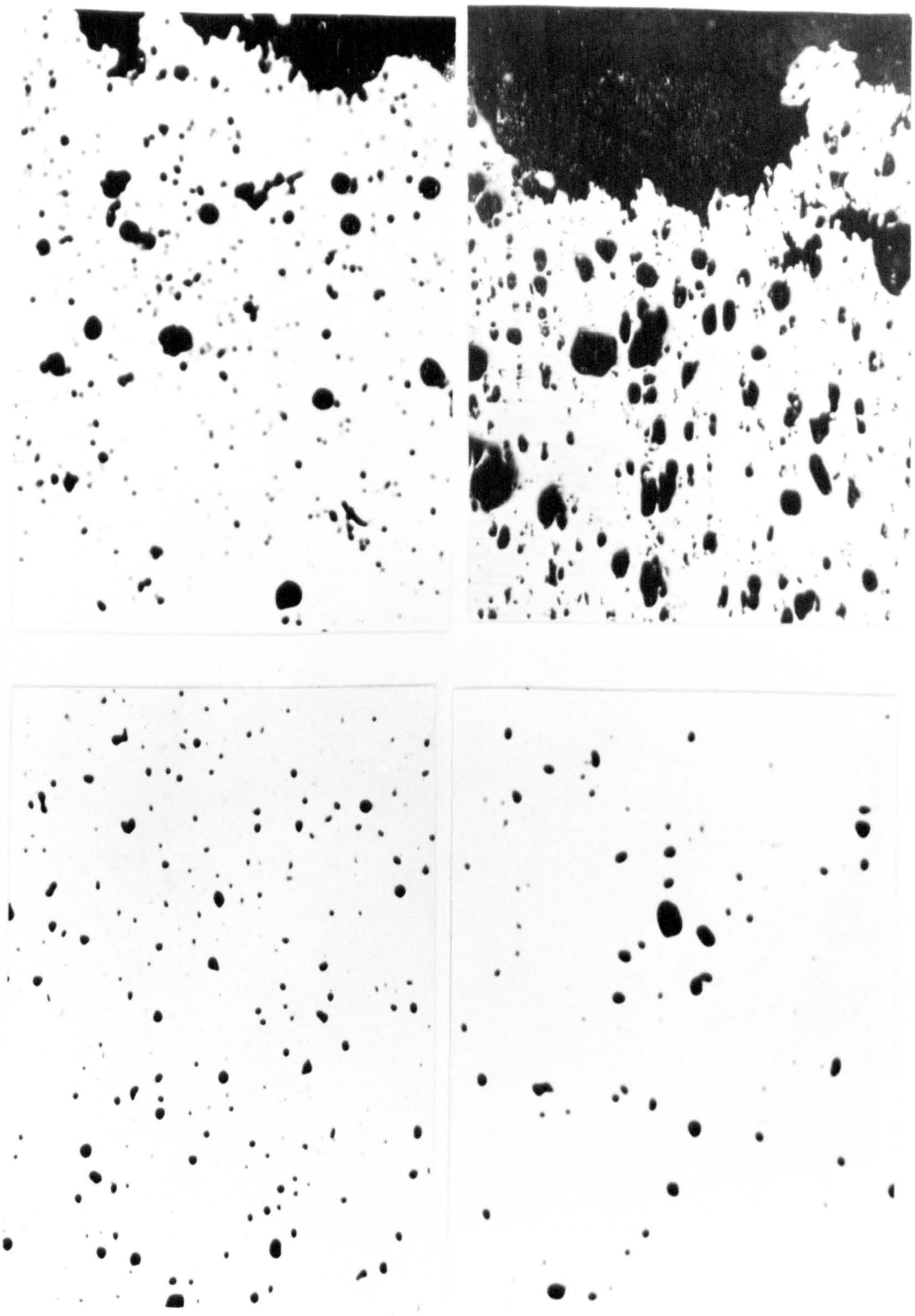


Fig. 100 Same as Fig. 99 at deformation temperature of 300°C.

(a)

(b)

(c)

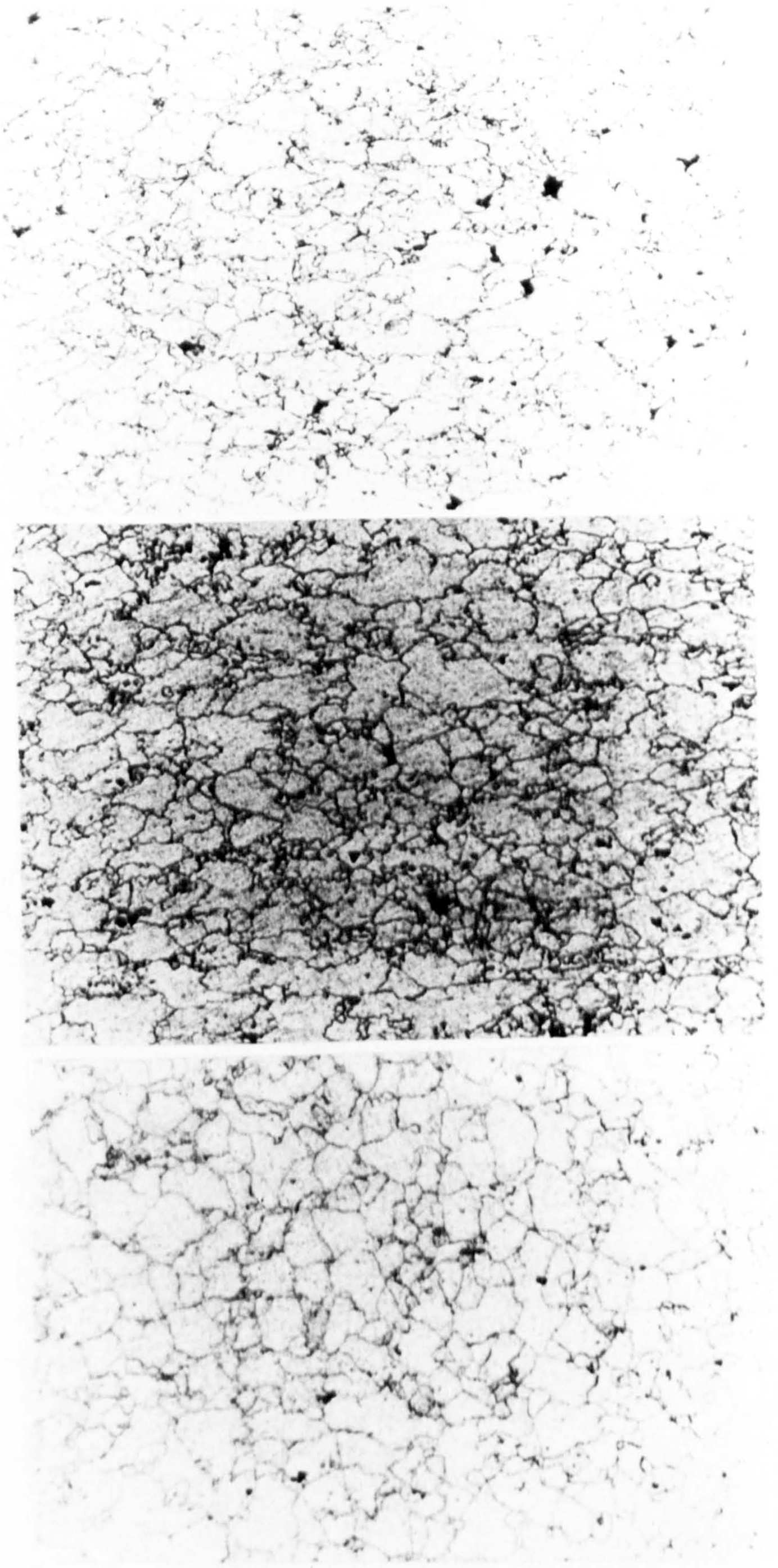


Fig. 102 Microstructure of 6 Mg(84) deformed at 300°C and $\dot{\varepsilon} = 1 \times 10^{-3}$ sec^{-1}.
(a) 200% elongation (b) 100% elongation and
(c) grip end. (x 200).

(a)

(b)

(c)

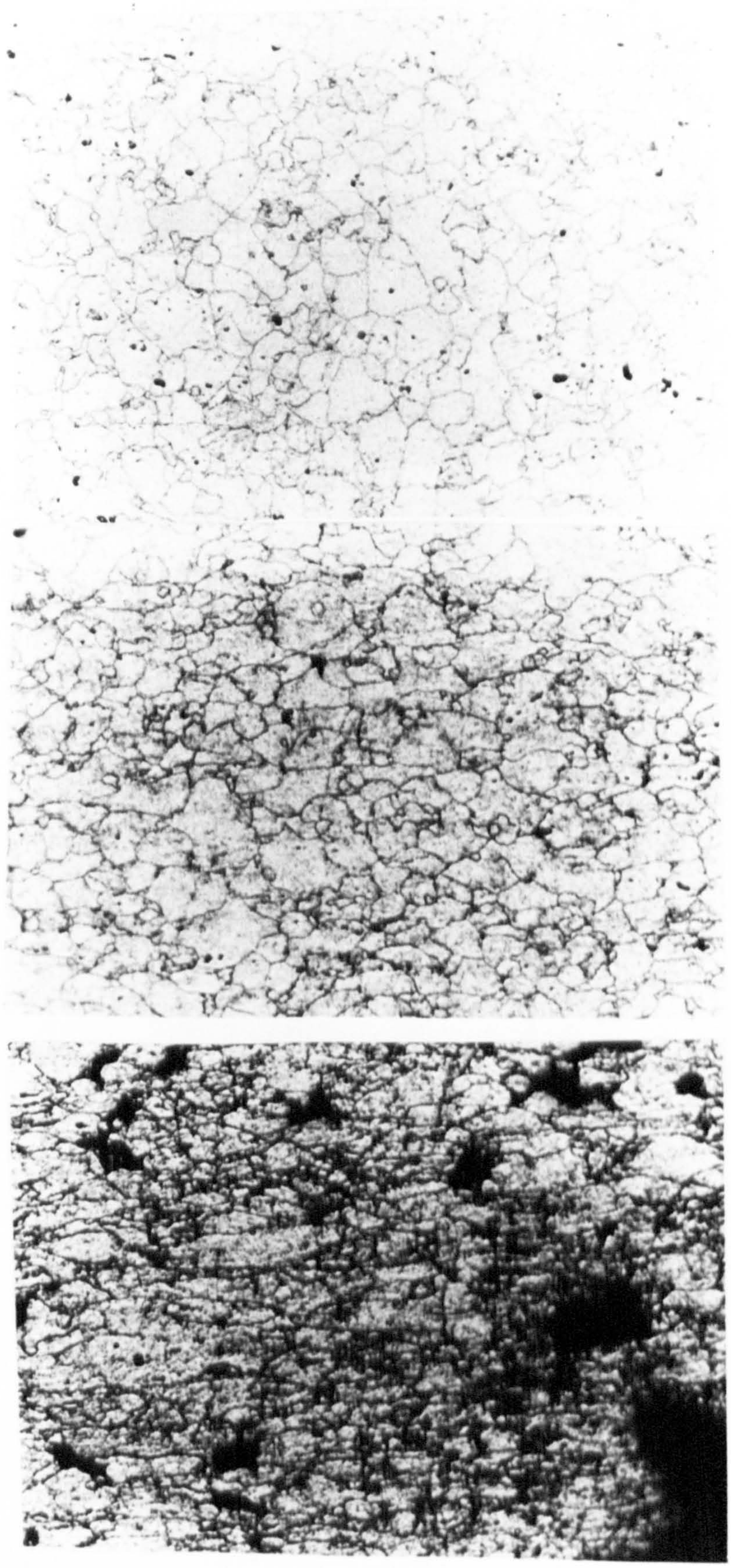
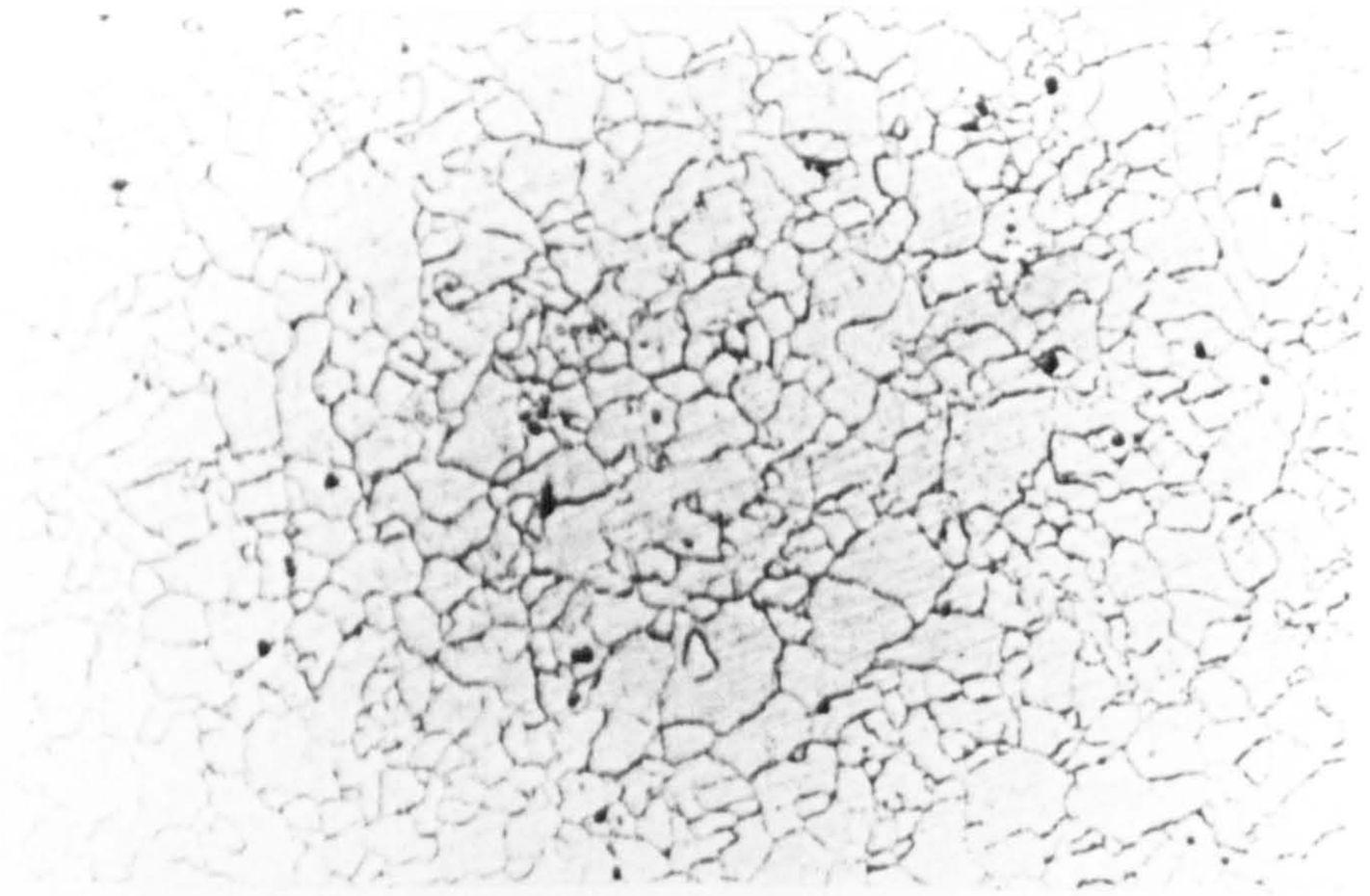
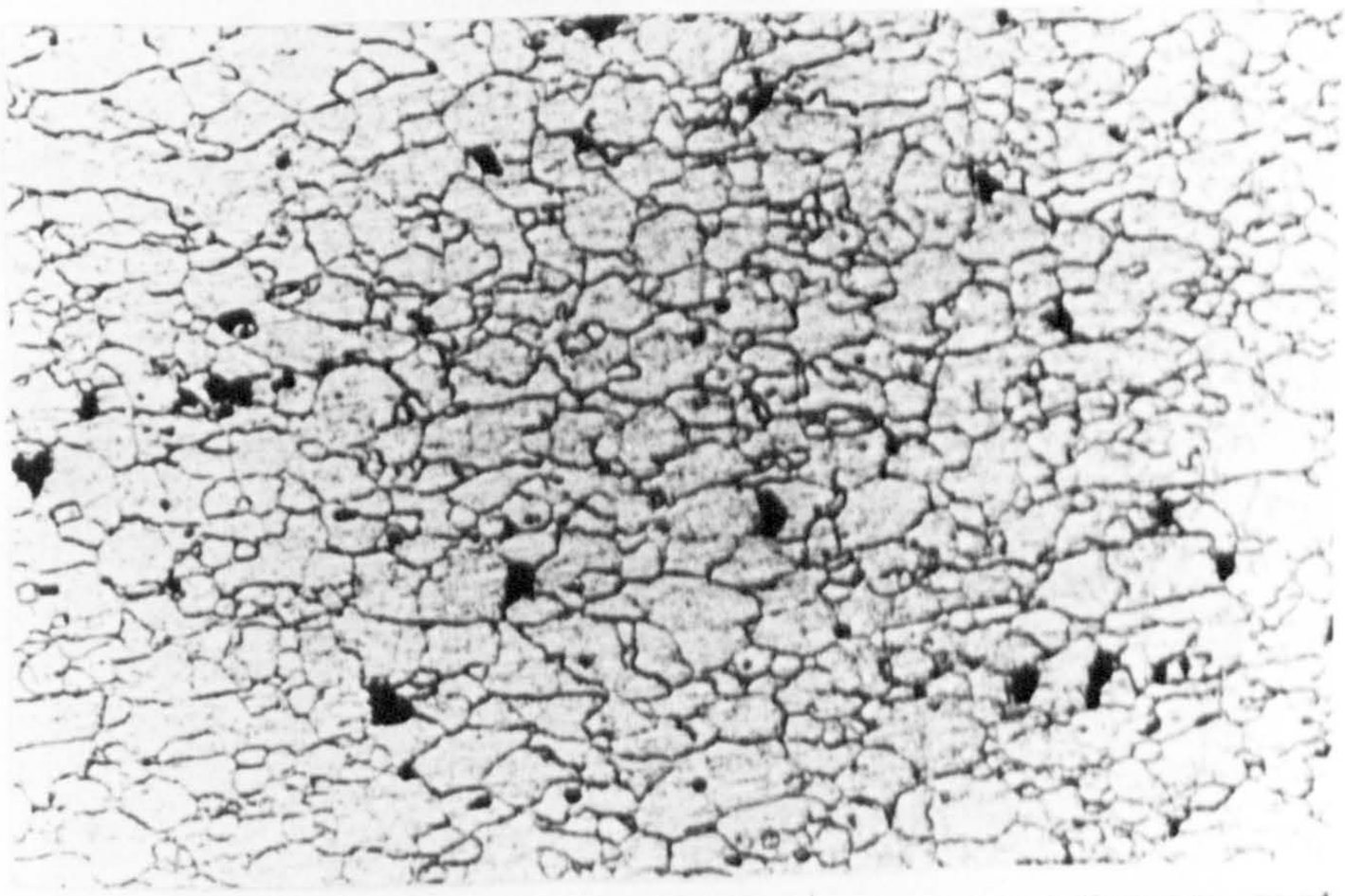


Fig. 103 Microstructure of 6 Mg(84) deformed at 400°C and $\dot{\epsilon} = 1 \times 10^{-3} sec^{-1}$. (a) grip end (b) 100% elongation and (c) 200% elongation. x 200.

(a)



(b)



(c)

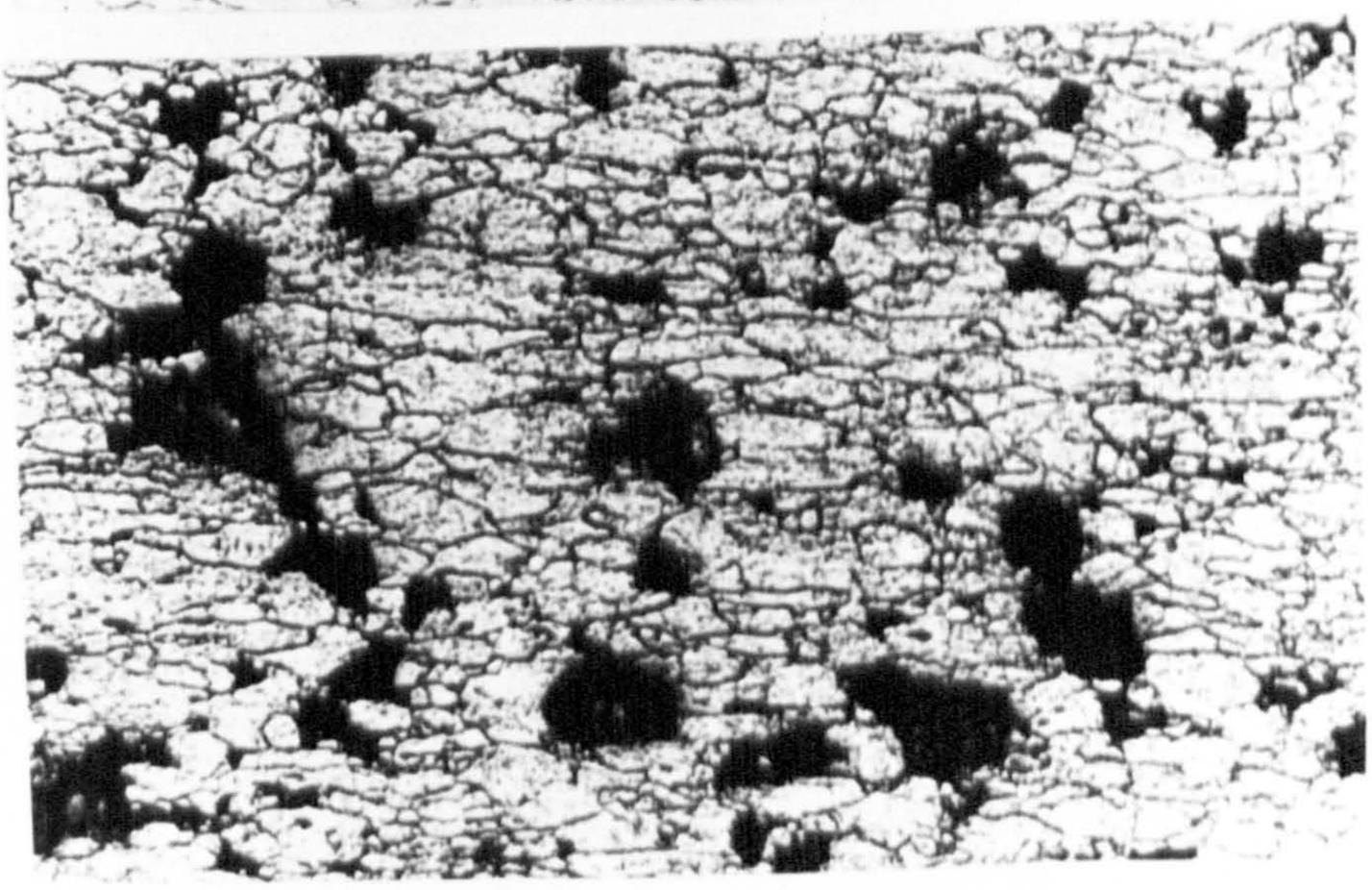


Fig 104 Microstructure of 6 Mg(84) deformed at 450°C and $\dot{\epsilon} = 1 \times 10^{-3}$ sec^{-1}. (a) grip end (b) 100% elongation (c) 200% elongation. x 200.

(a)

(b)

(c)

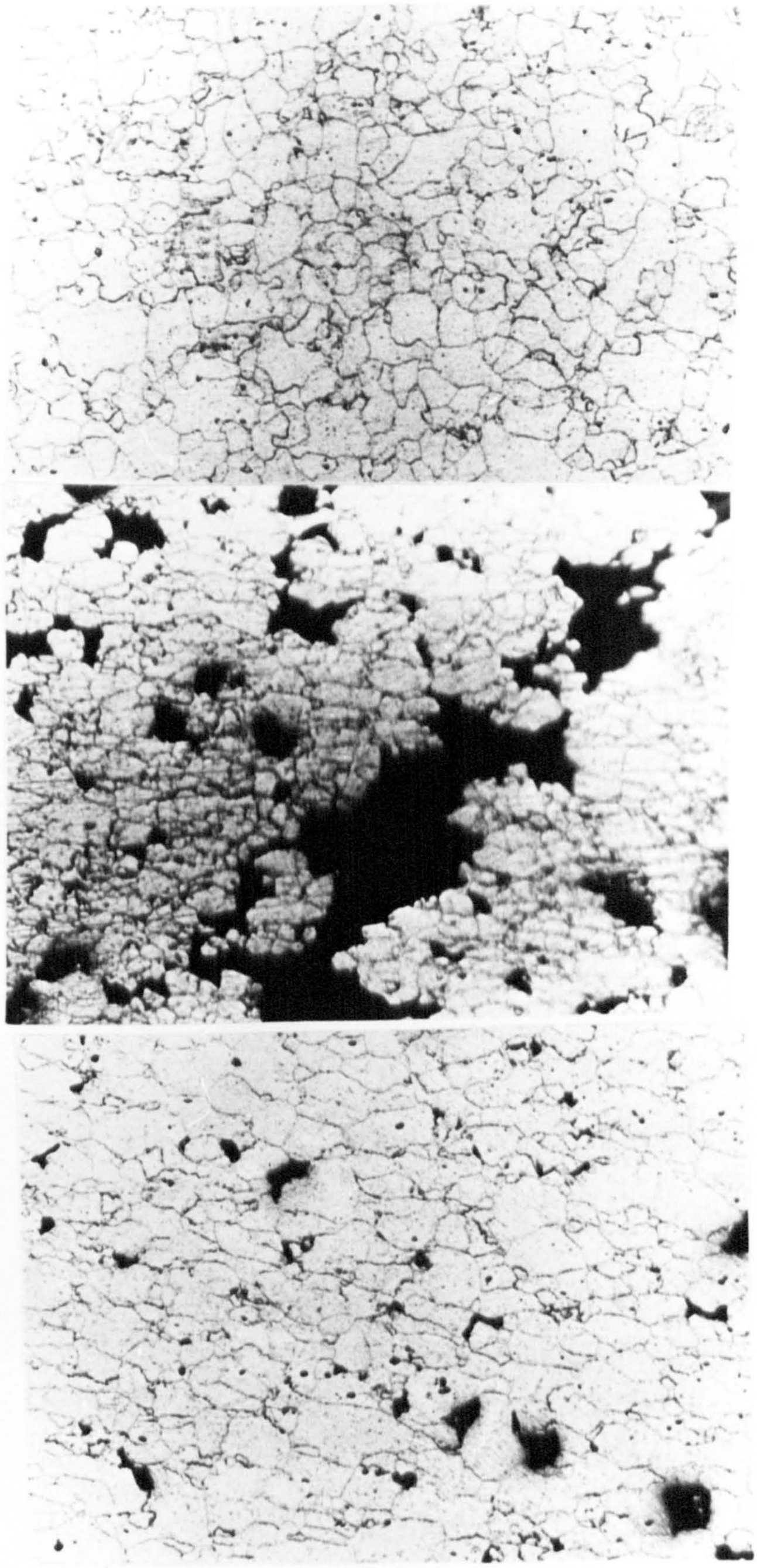
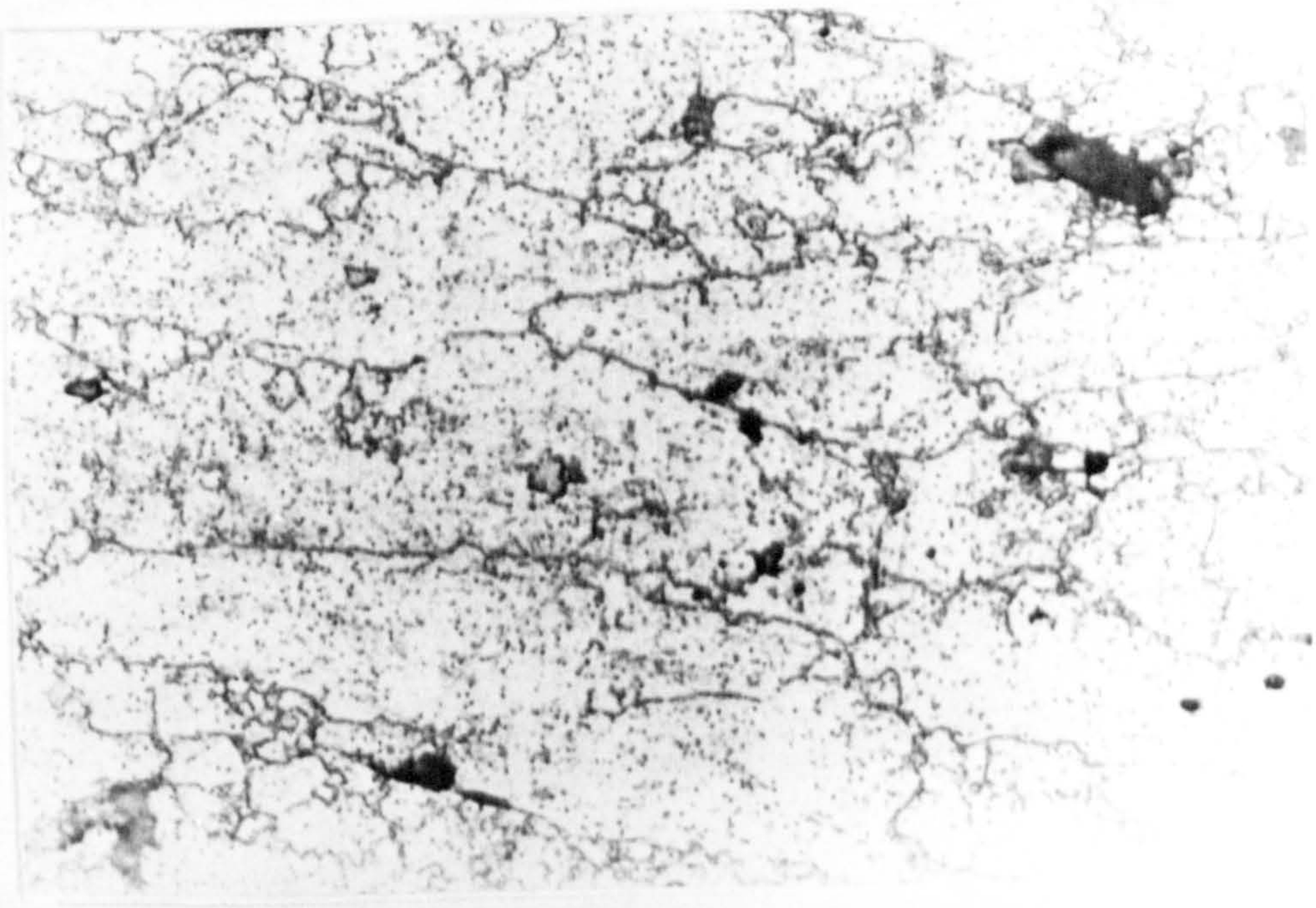


Fig. 105 Microstructure of 6 Mg(84) deformed at 500°C and $\dot{\epsilon} = 1 \times 10^{-3}$ sec^{-1}.
(a) grip end (b) 200% elongation and (c) 100% elongation. (x 200).

(a)



(b)

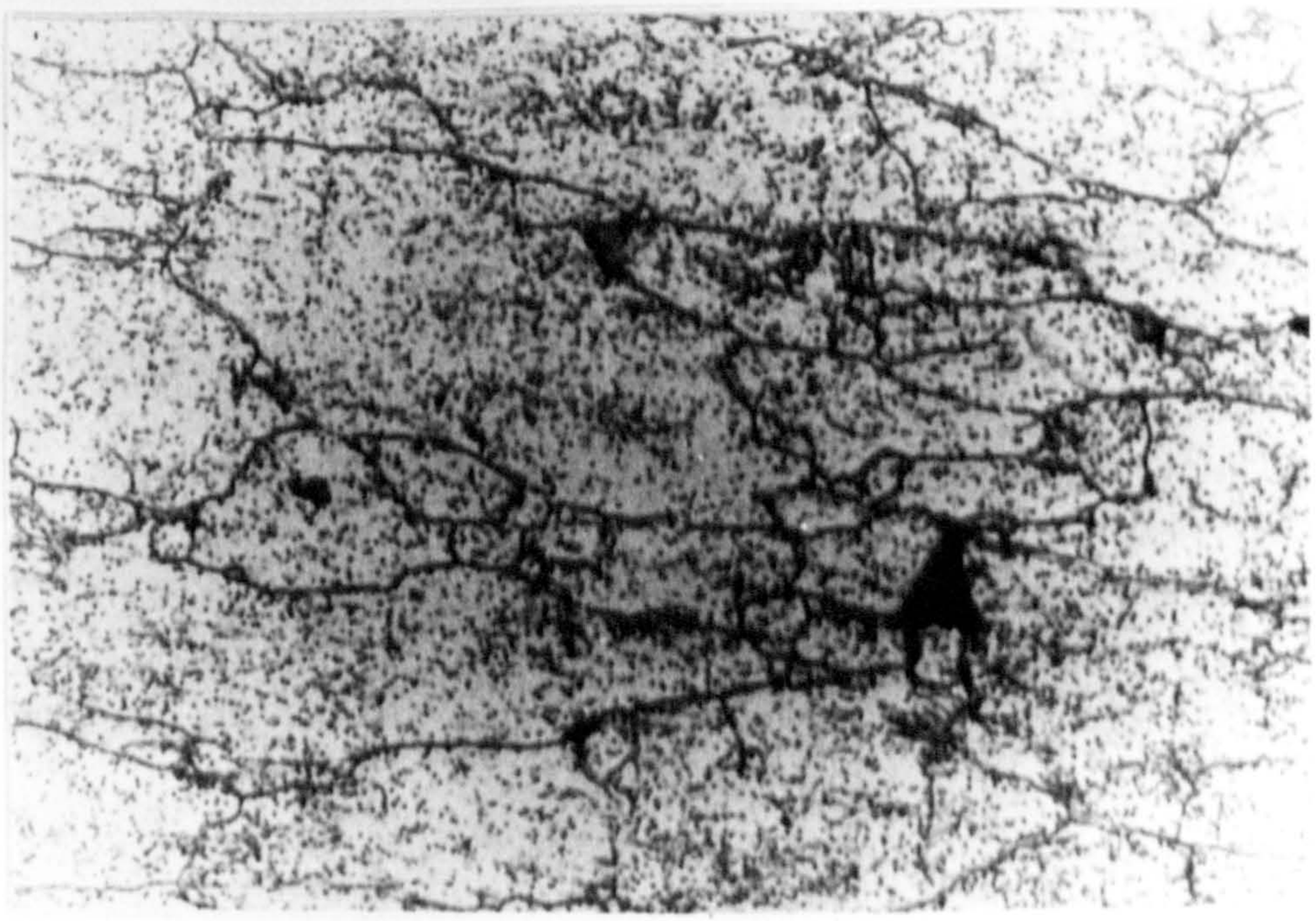
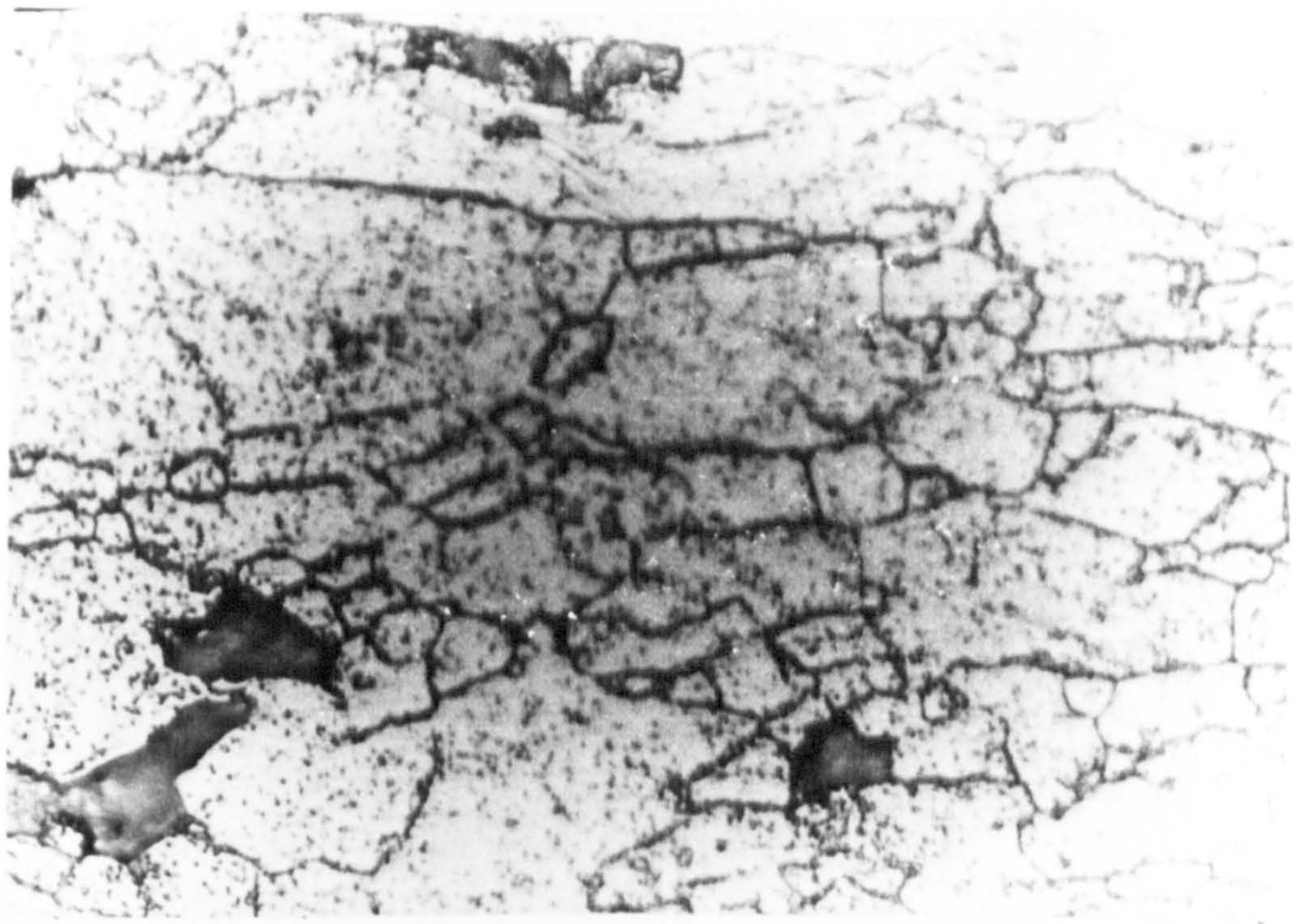


Fig. 106 Microstructure of 6 Mg(84) deformed to 200% elongation and $\dot{\epsilon} = 1 \times 10^{-3}$ sec^{-1}.
(a) 300°C, (b) 400°C, (c) 450°C and (d) 500°C.
(x 800).

(c)



(d)

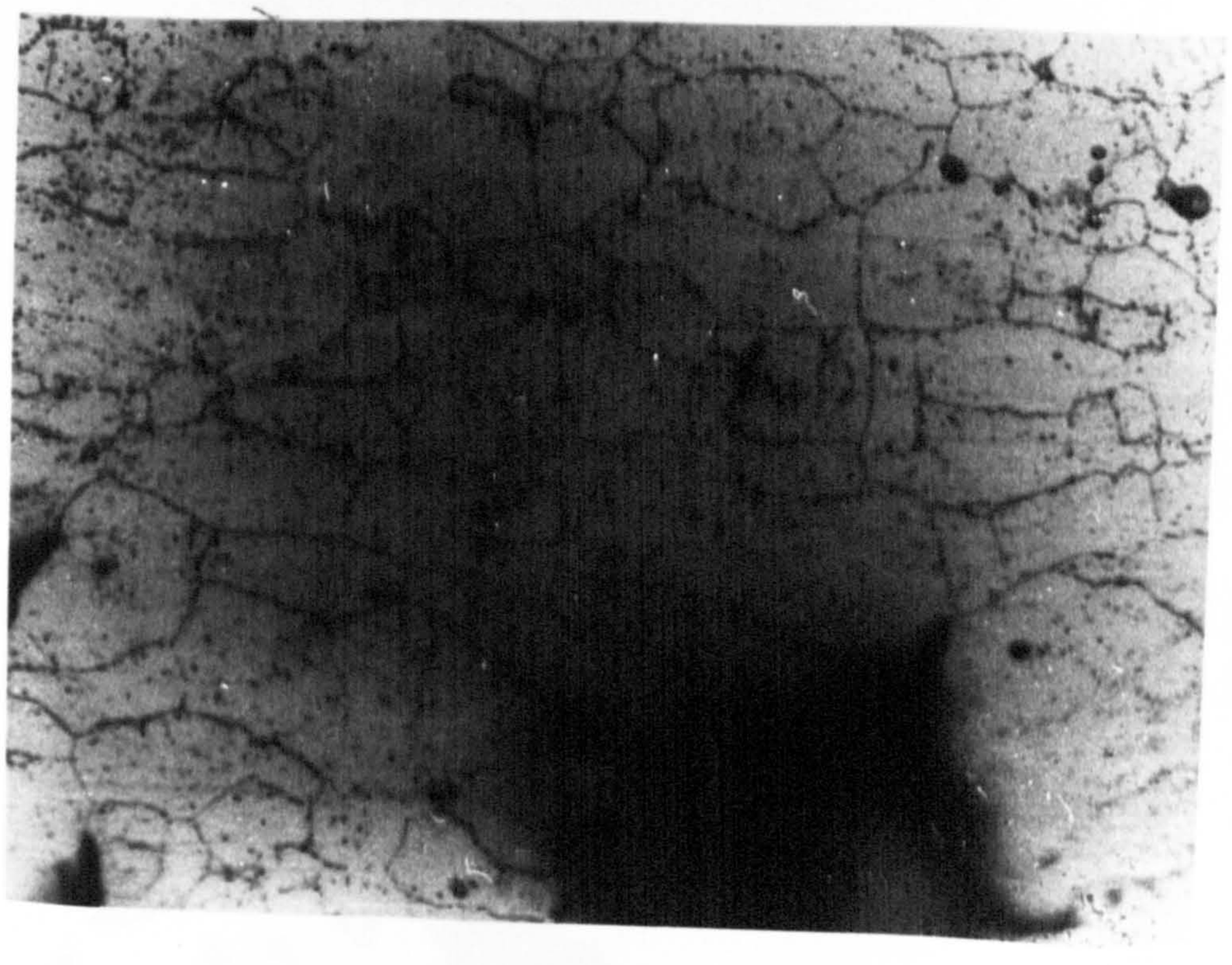


Fig. 106 continued

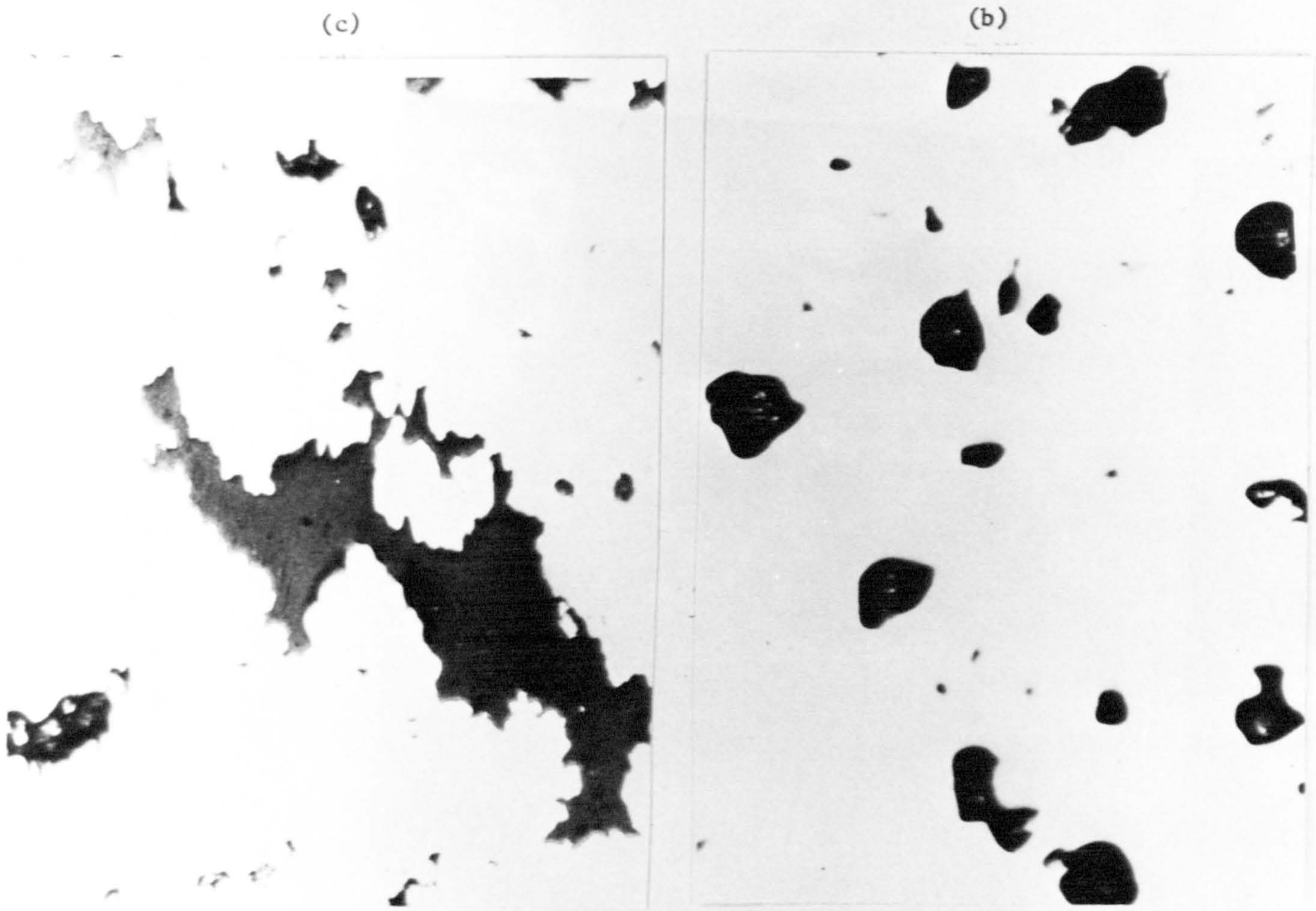
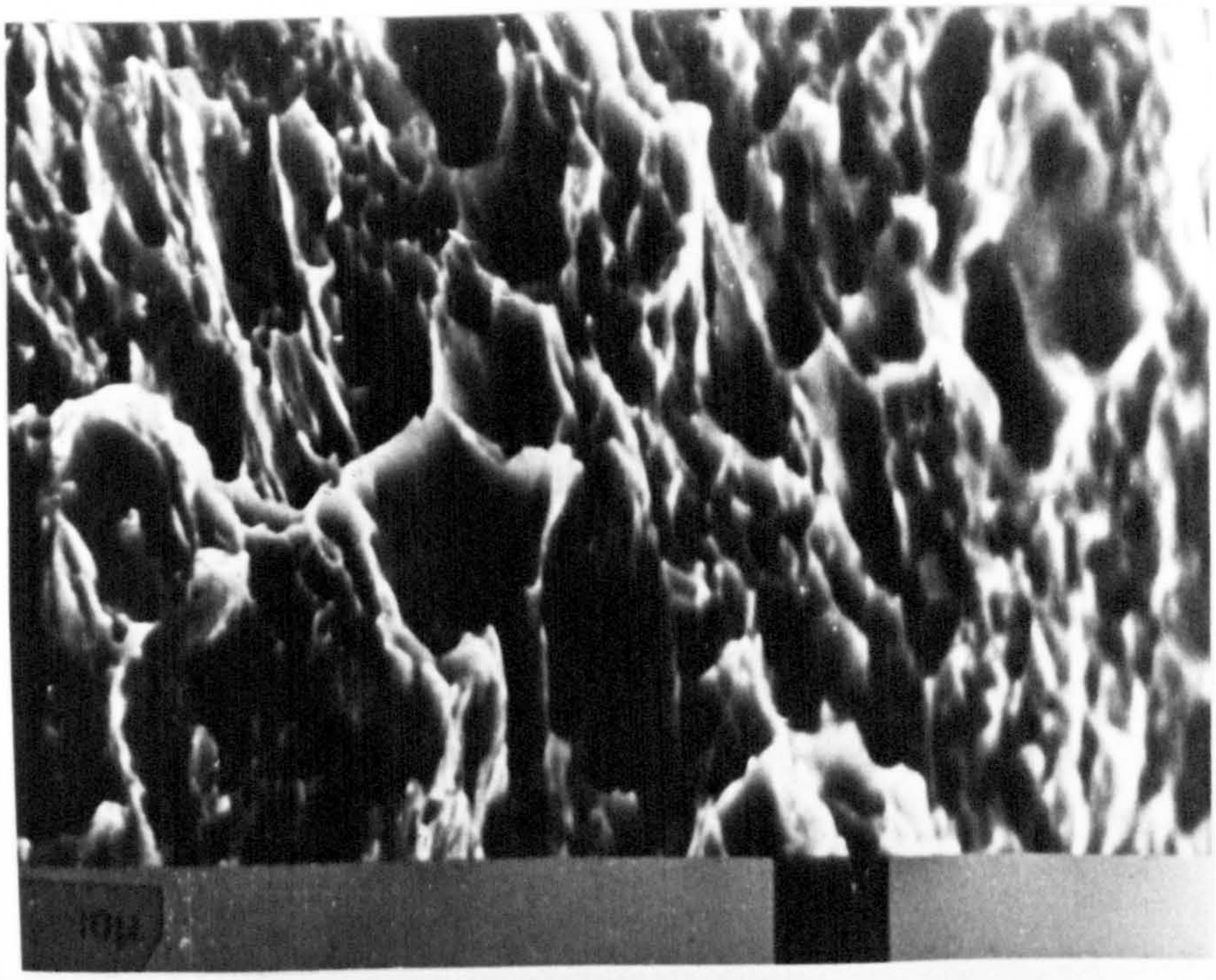


Fig. 107 Unetched specimens deformed at 500°C and $\dot{\epsilon} = 1 \times 10^{-3}$ sec^{-1}.
(a) grip end (b) 100% elongation (c) 200% elongation. (x 200).

(a)



(b)

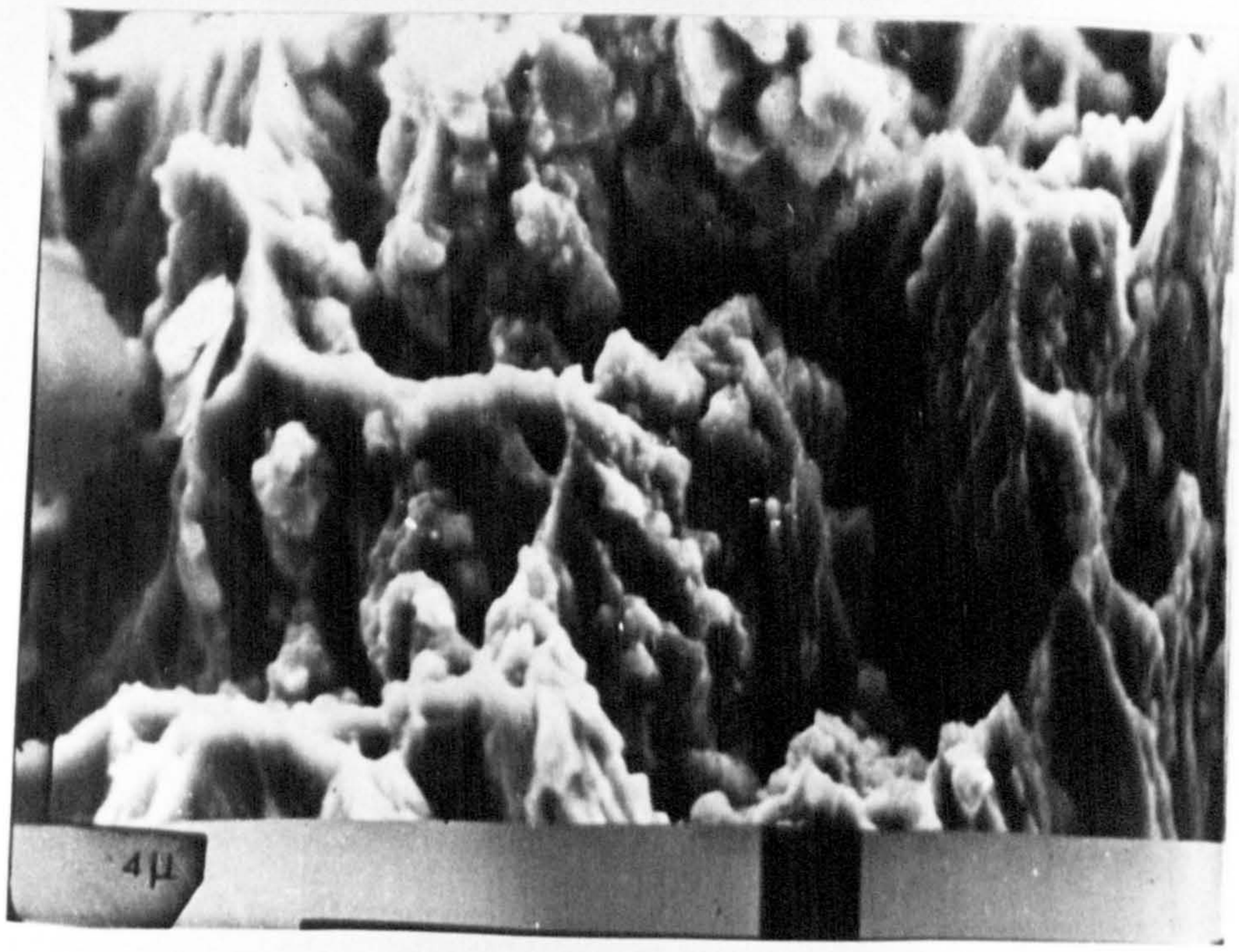
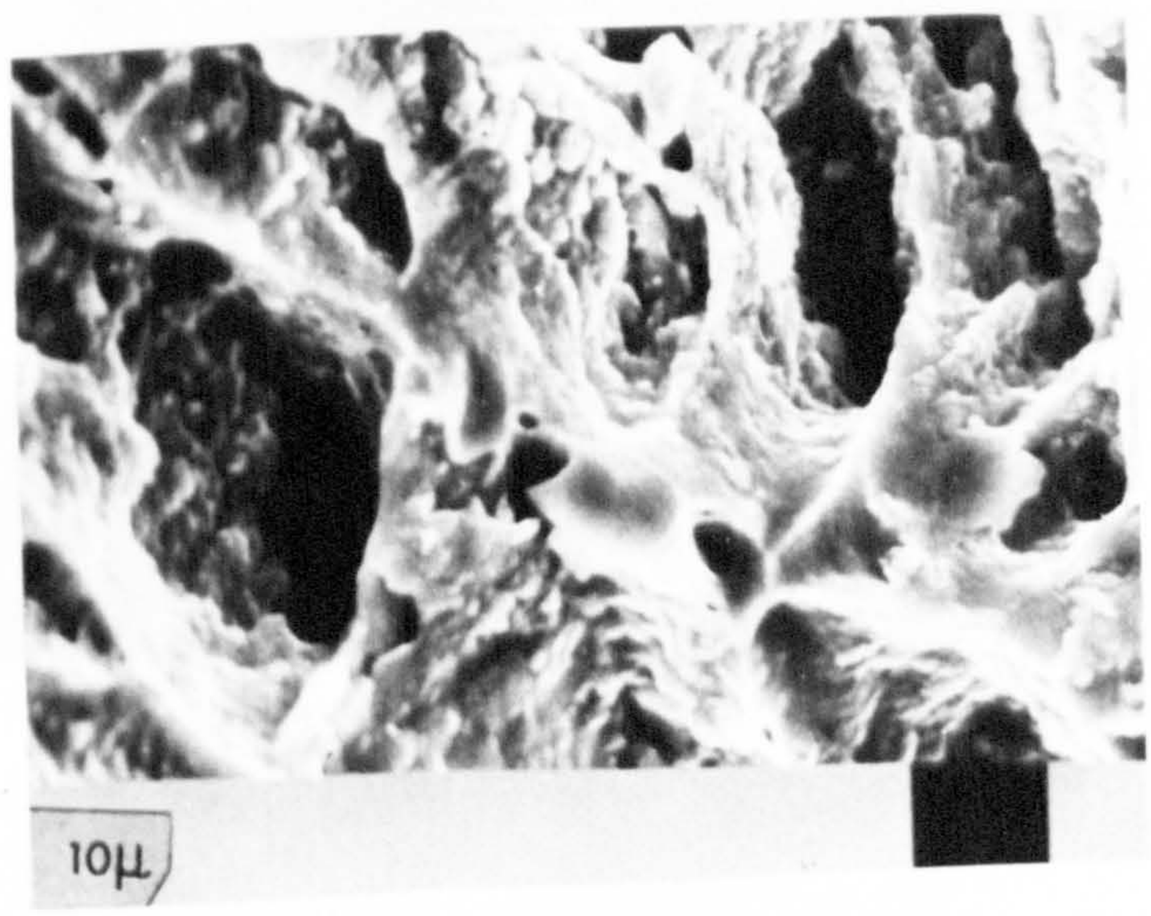


Fig. 108 Scanning fractographs for specimens deformed at $\dot{\varepsilon} = 1.67 \times 10^{-4}$ sec^{-1}.
(a) 6 Mg(153) at 300°C, (b) 6 Mg(84) at 300°C,
(c) 6 Mg(153) at 250°C and (d) 6 Mg(84) at 250°C

(c)



(d)

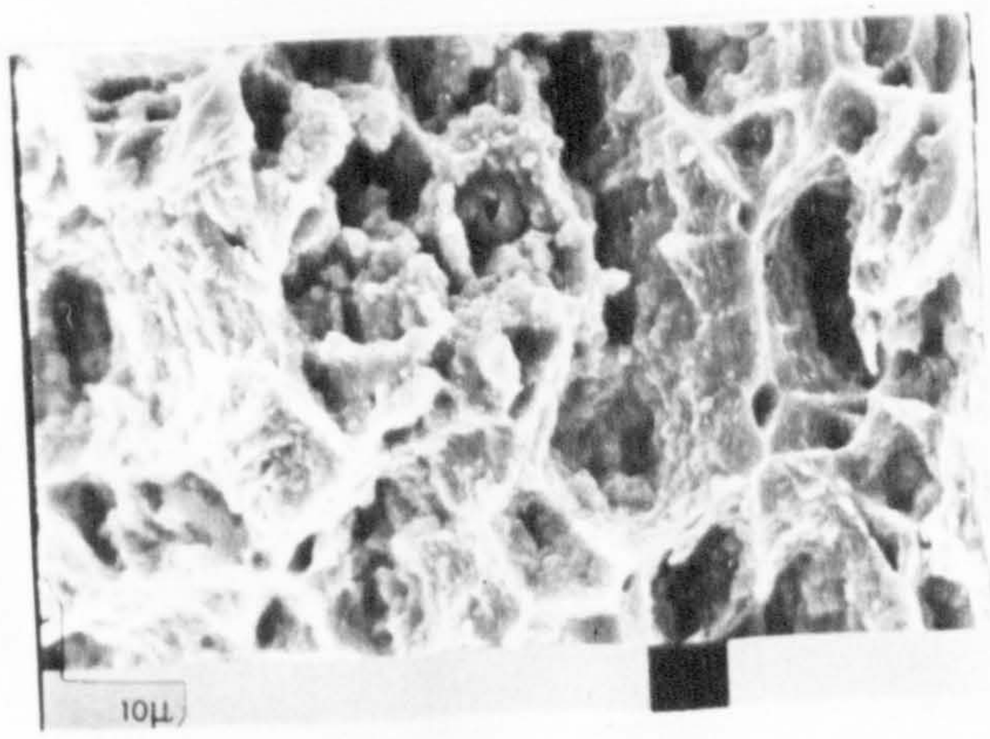
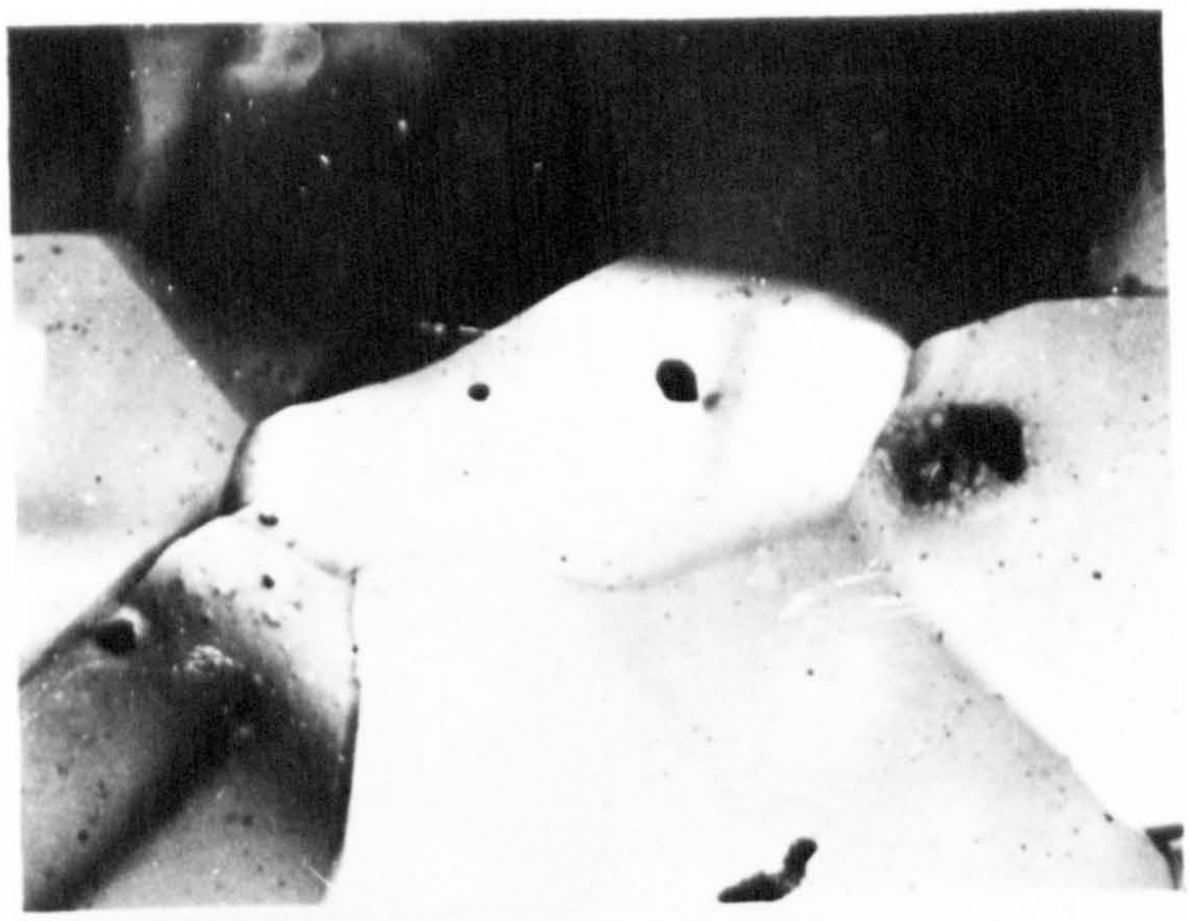


Fig. 108 continued



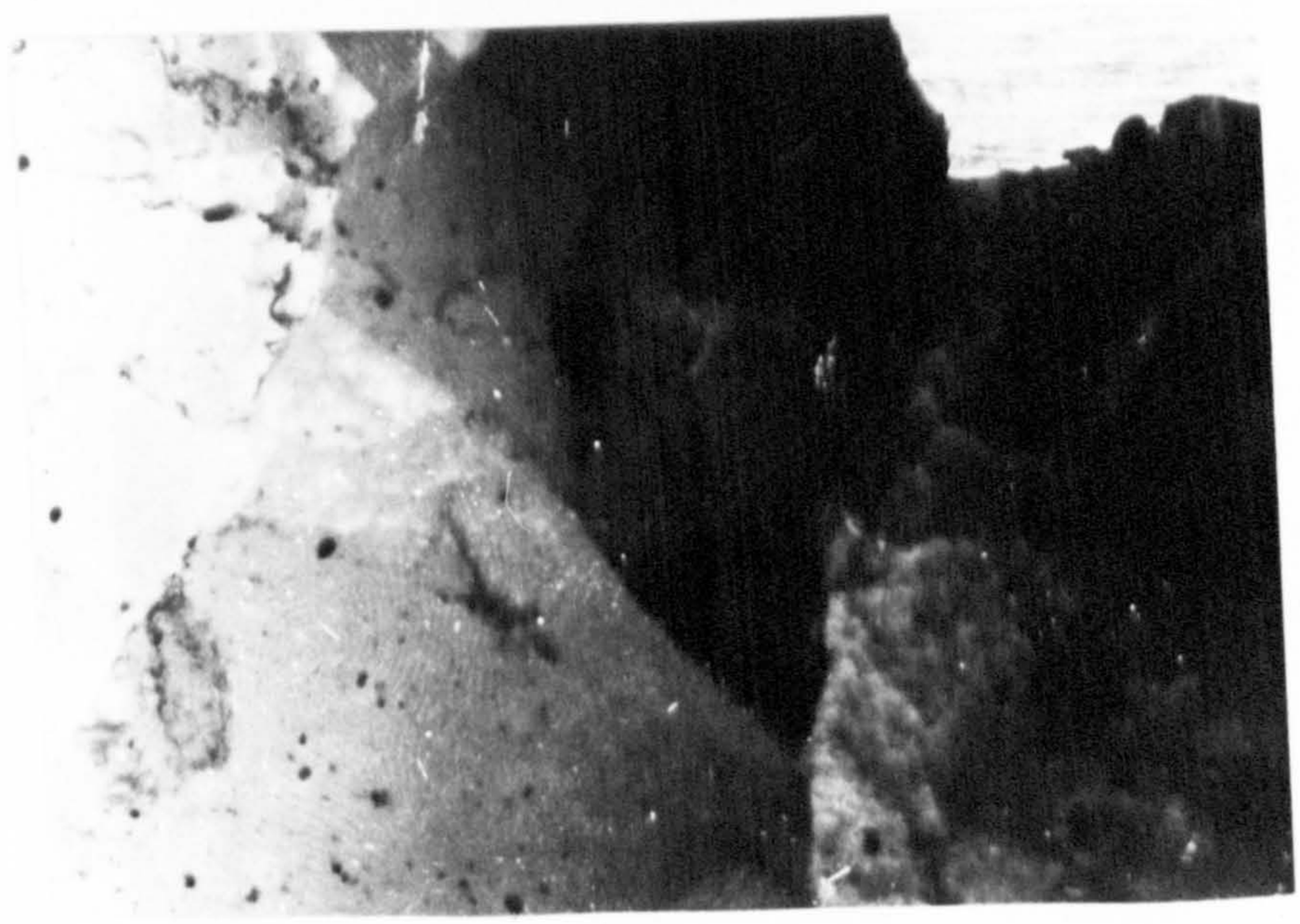
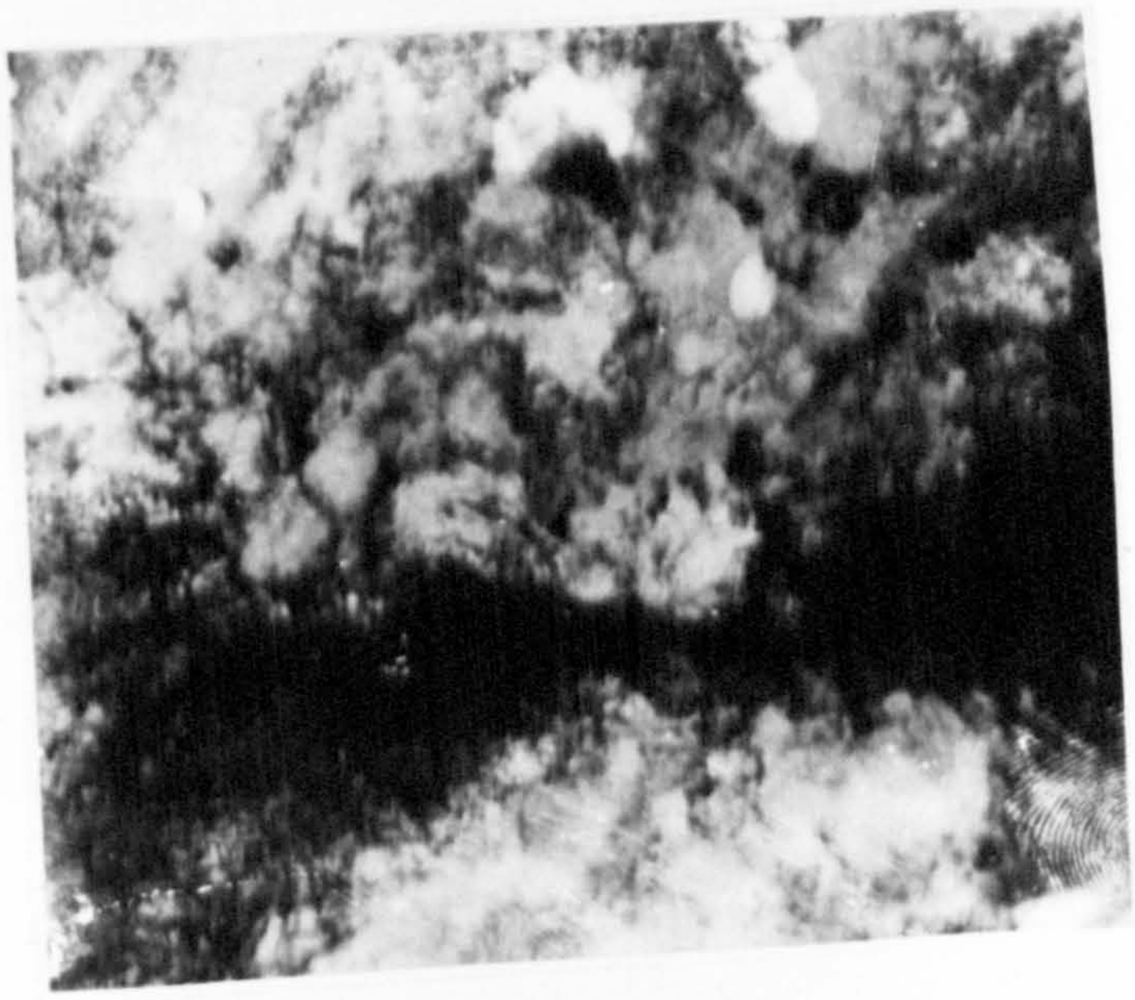


Fig. 109 Thin foil from grip end of 6 Mg(84) specimen deformed at strain rate of 1.67×10^{-4} sec^{-1}. (a) 250°C and (b) 300°C. (x 25 K).

(a)



(b)

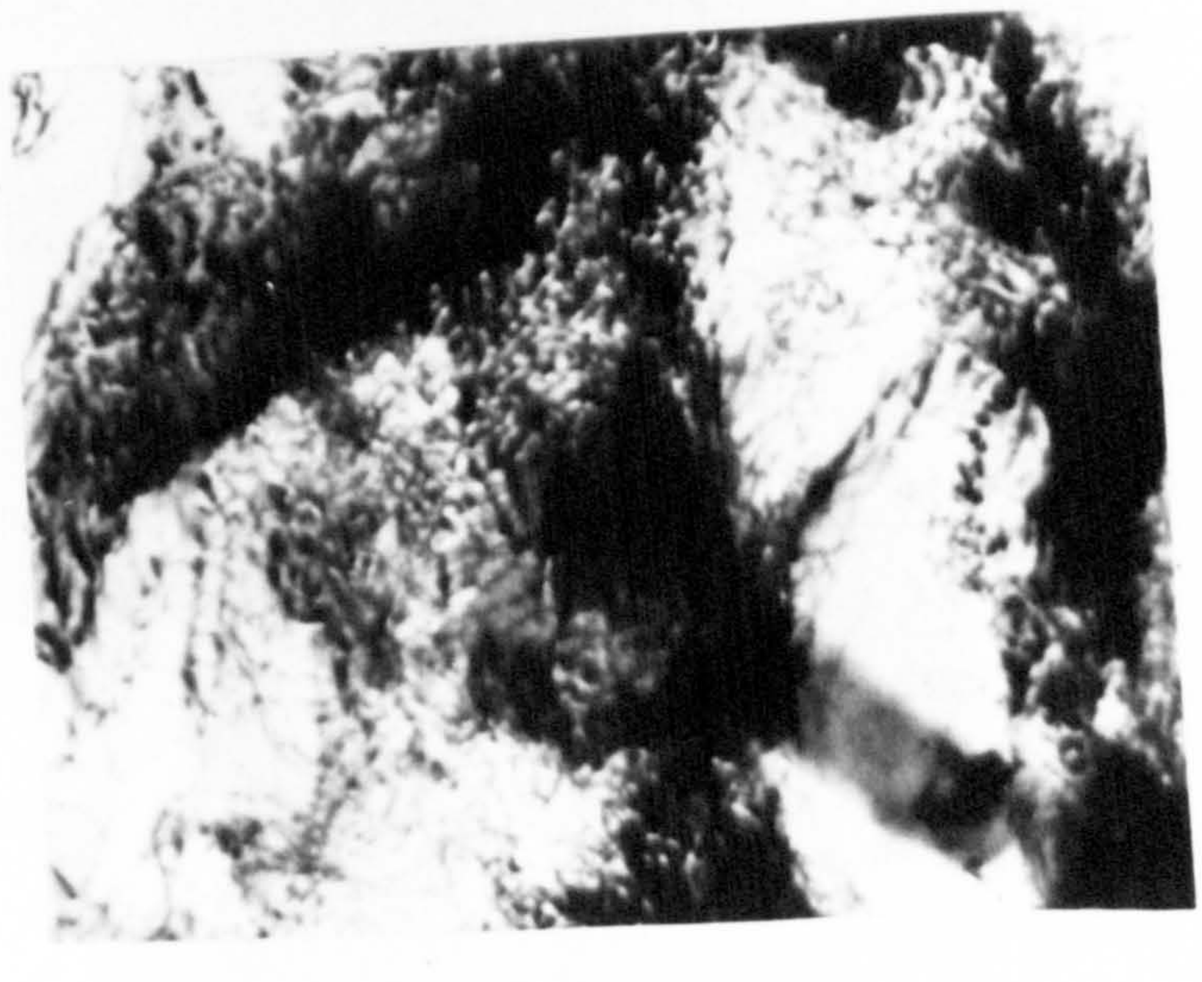
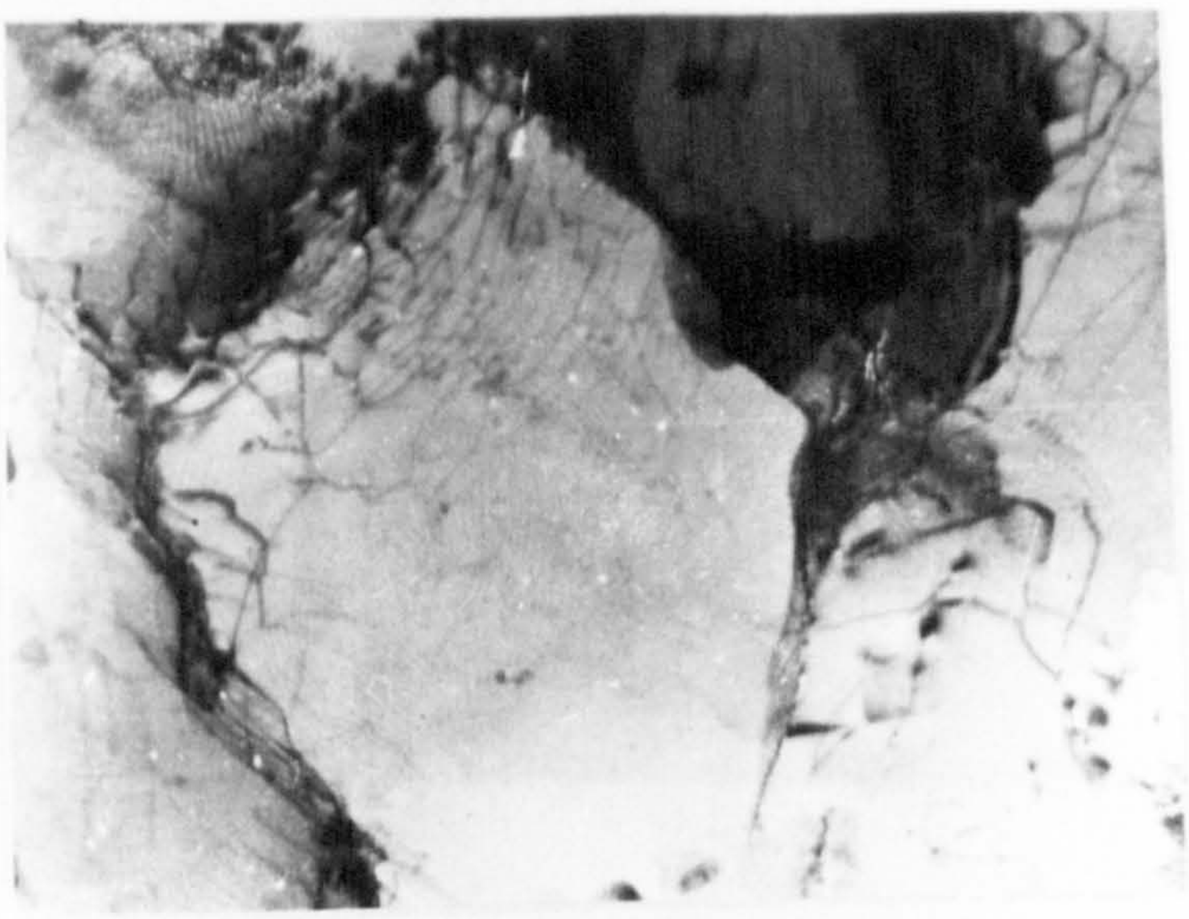


Fig. 110 Thin foil from grip end of 6 Mg(153) specimen deformed at strain rate of 1.67×10^{-4} sec^{-1}. (a) 250°C (b) 300°C. x 25 K.

(a)



(b)

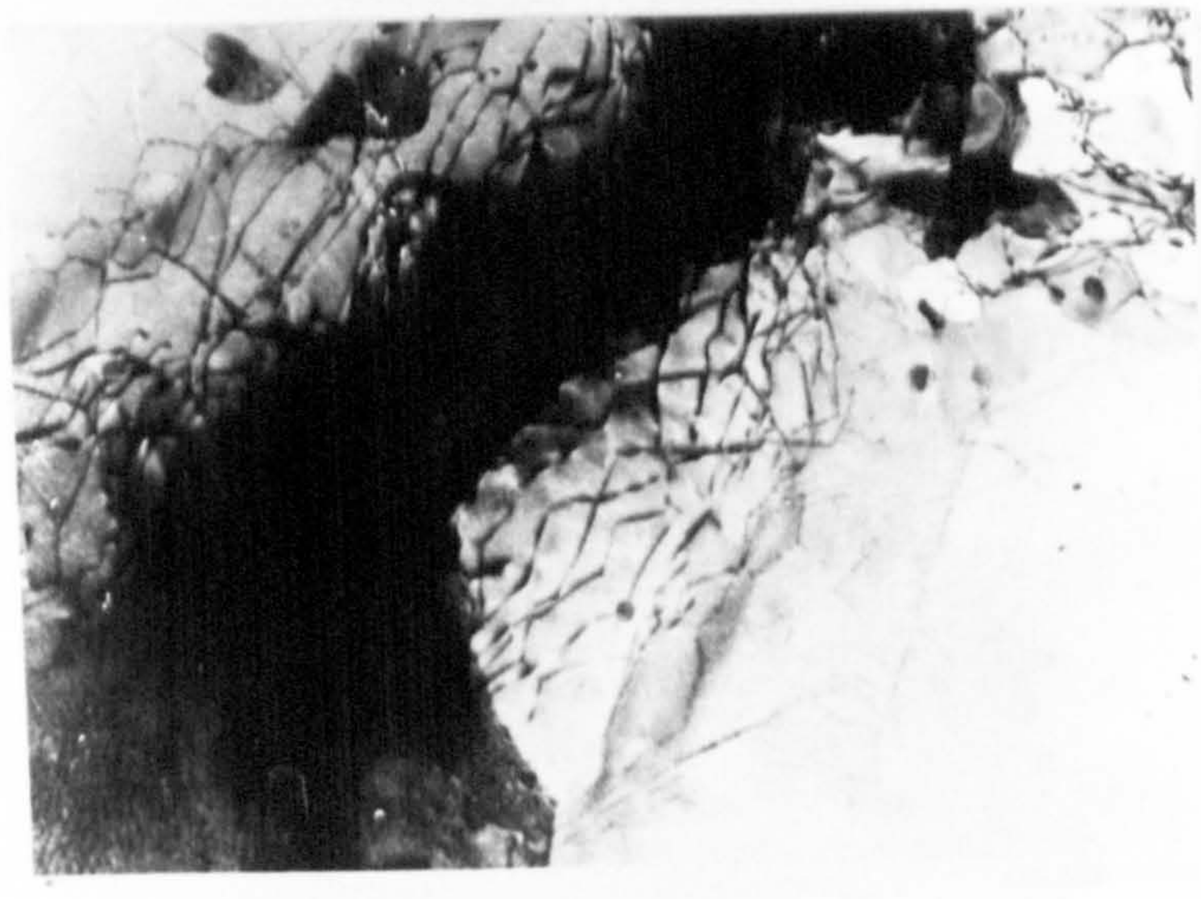
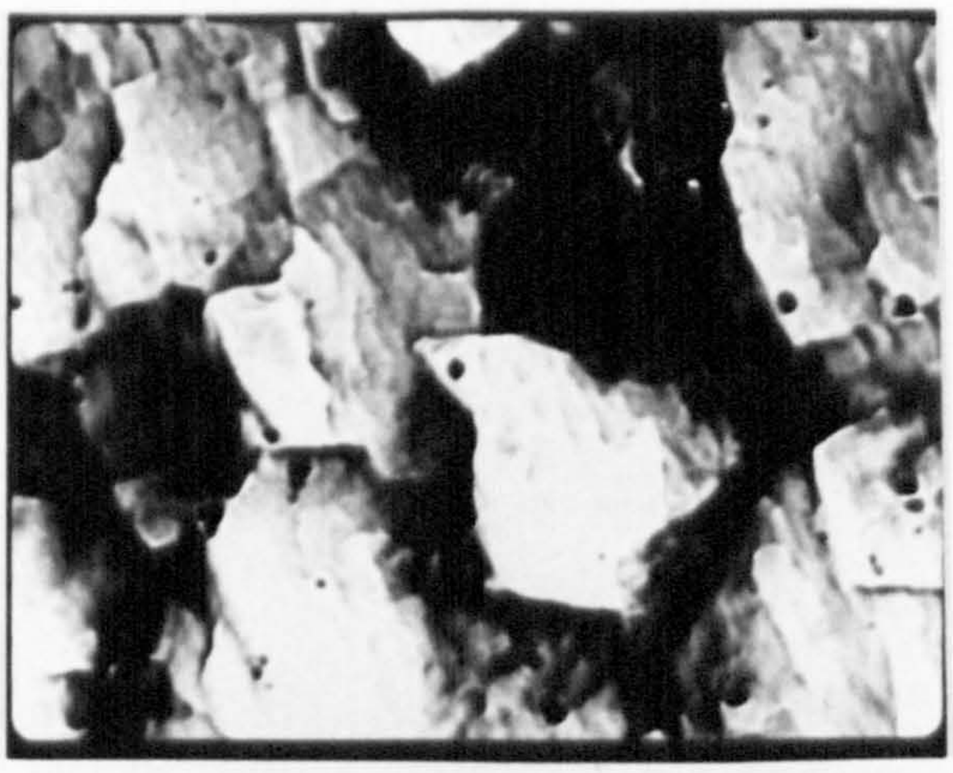


Fig. 114 Thin foil taken from deformed gauge length (100% elongation) of 6 Mg(84) at 250°C $\dot{\varepsilon} = 1.67 \times 10^{-4}$ sec^{-1}. x 25 K

(a)



(b)

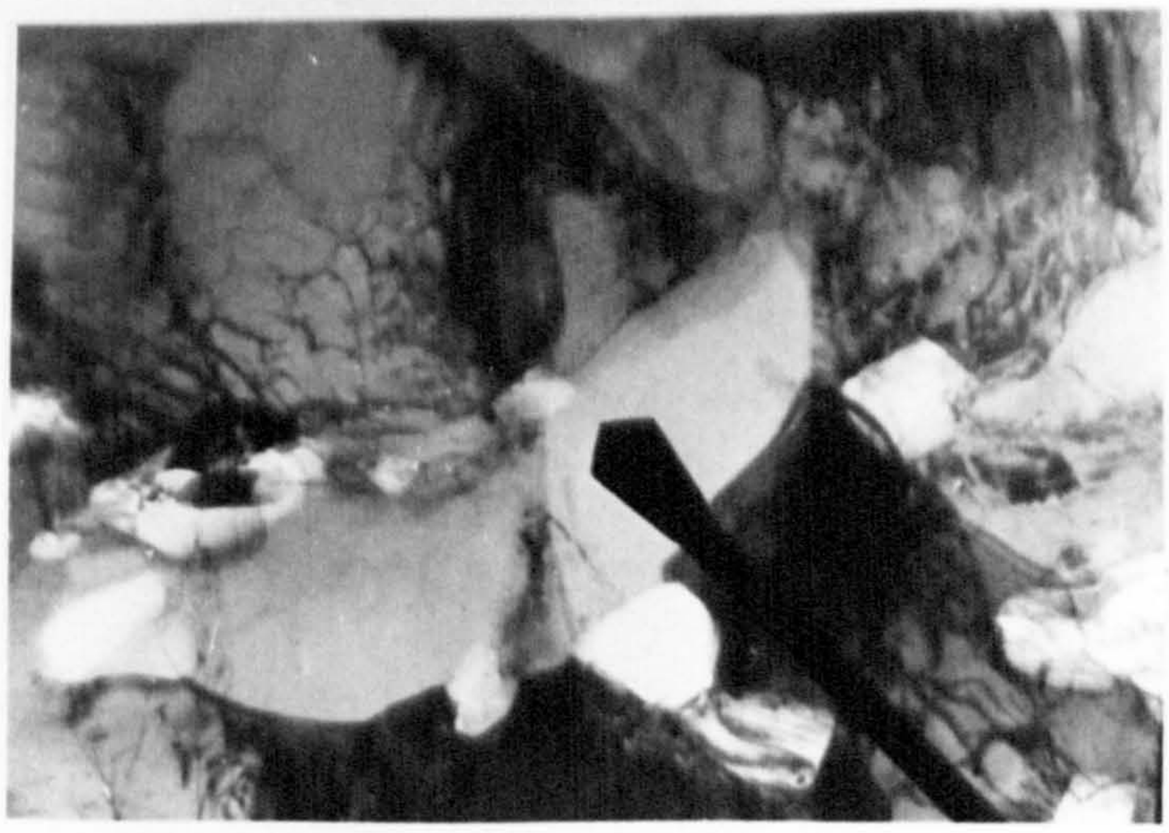
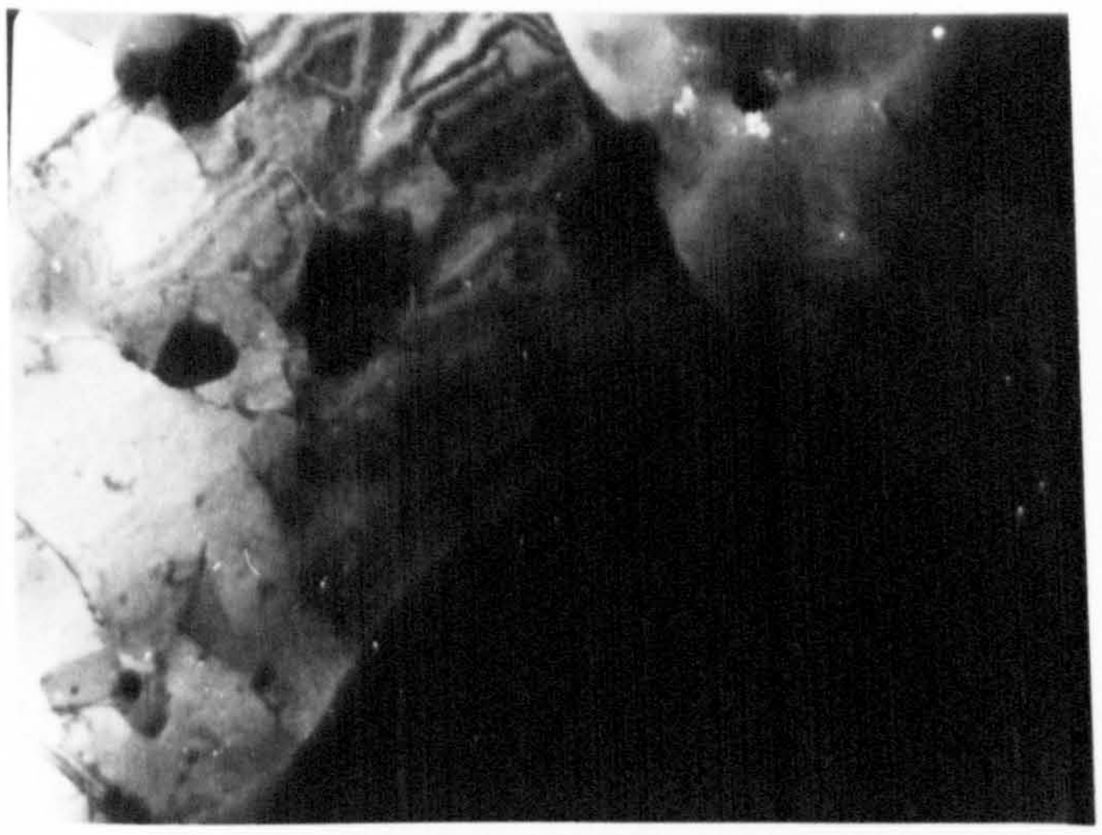


Fig. 112 Thin foil taken from deformed gauge length (200% elongation) of 6 Mg(153) at 250°C and $\dot{\epsilon} = 1.67 \times 10^{-4}$ sec^{-1}. x 25 K.

(a)



(b)

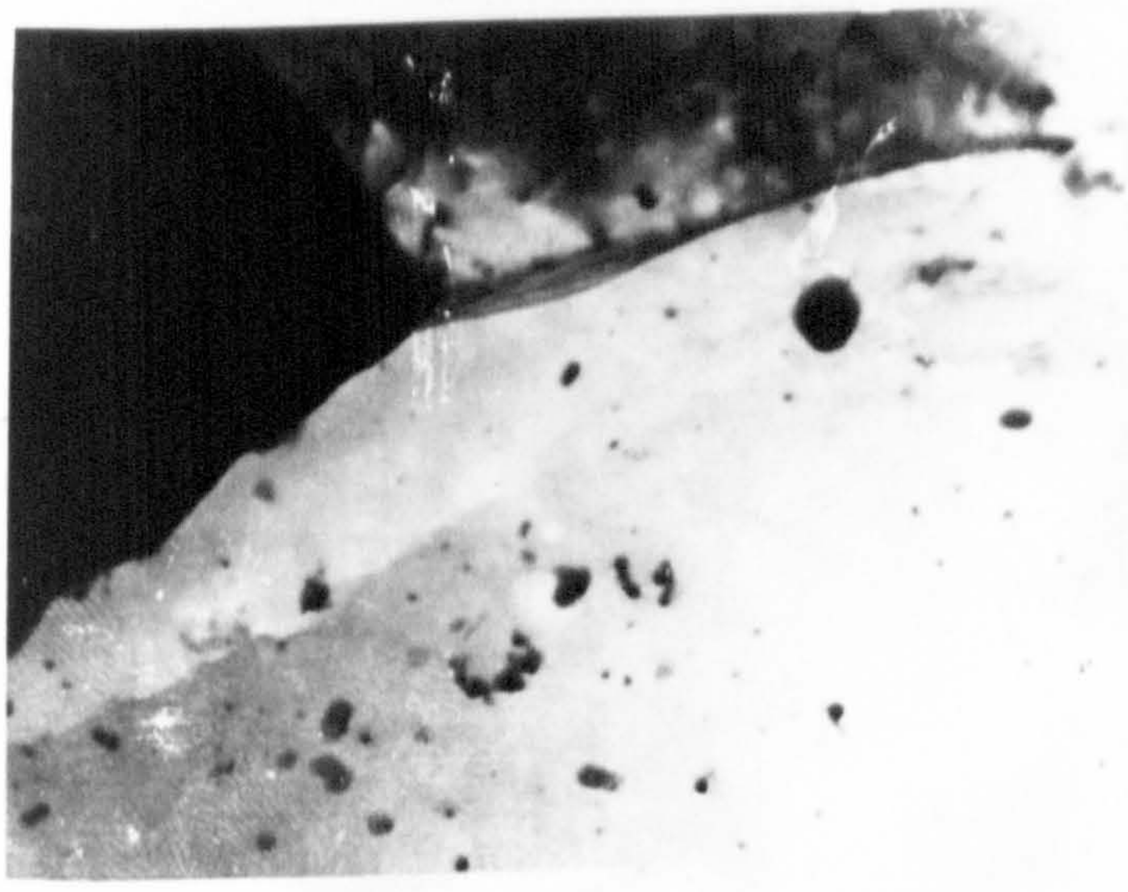
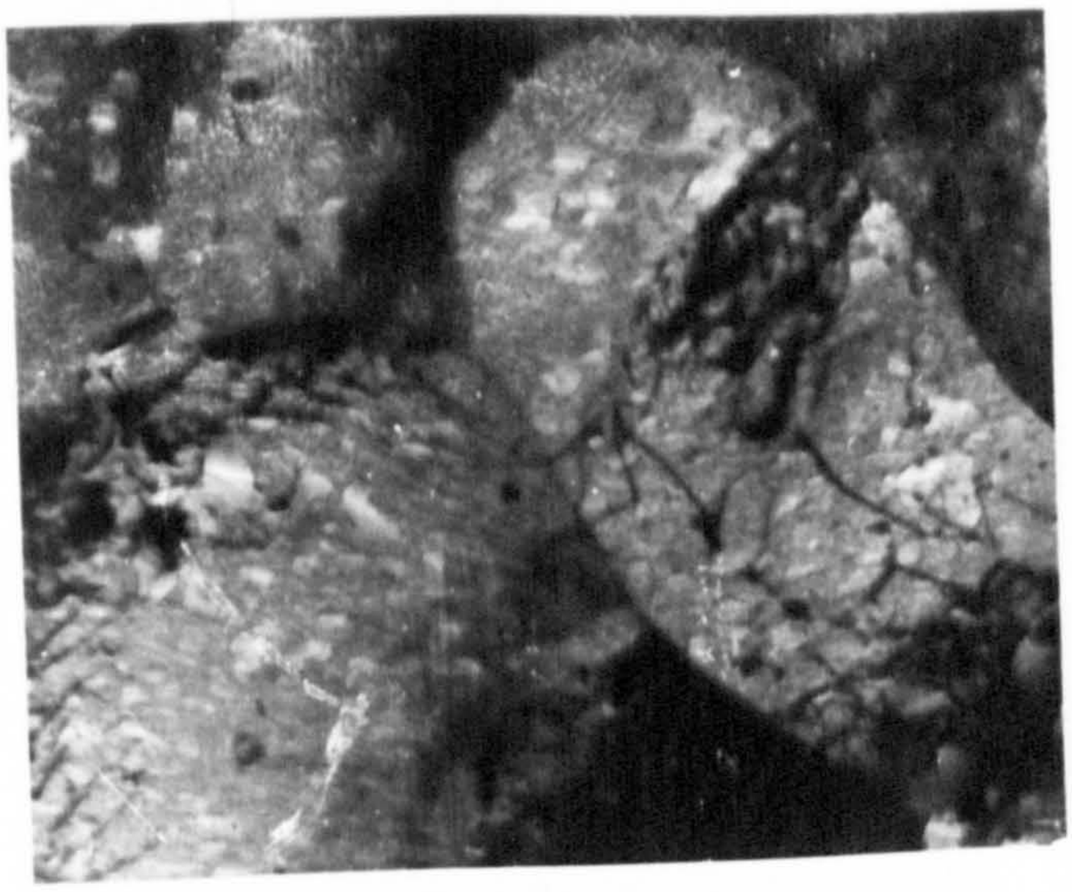


Fig. 113 Thin foil taken from deformed gauga length (200% elongation) of 6 Mg(84) at 300°C and $\dot{\epsilon} = 1.67 \times 10^{-4}$. x 25 K.

(a)



(b)

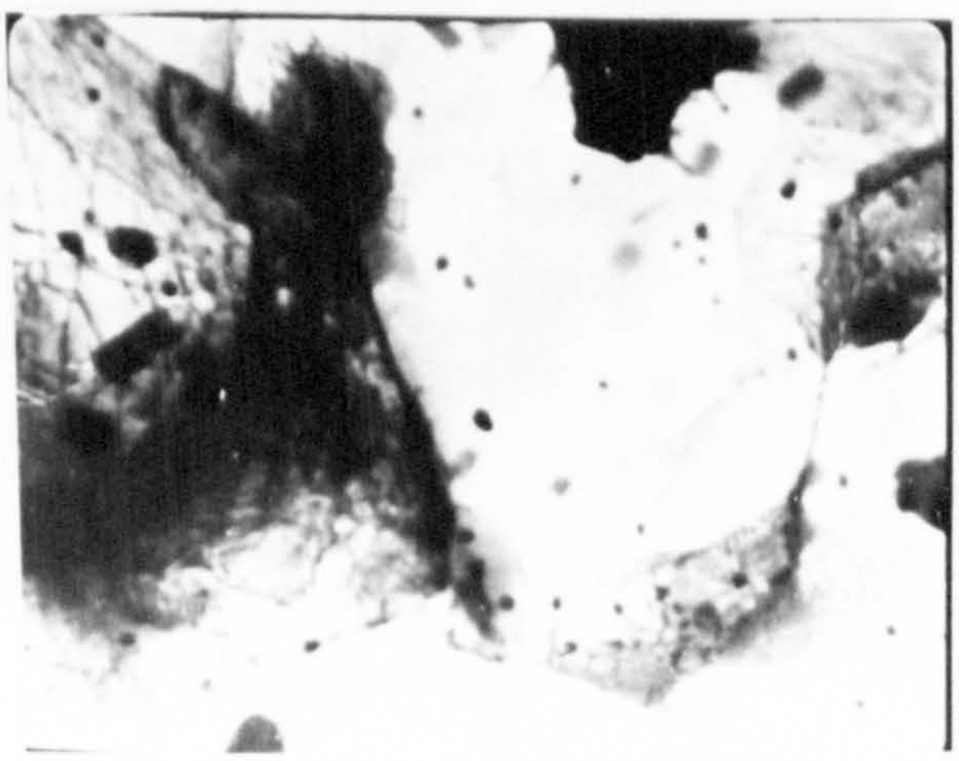
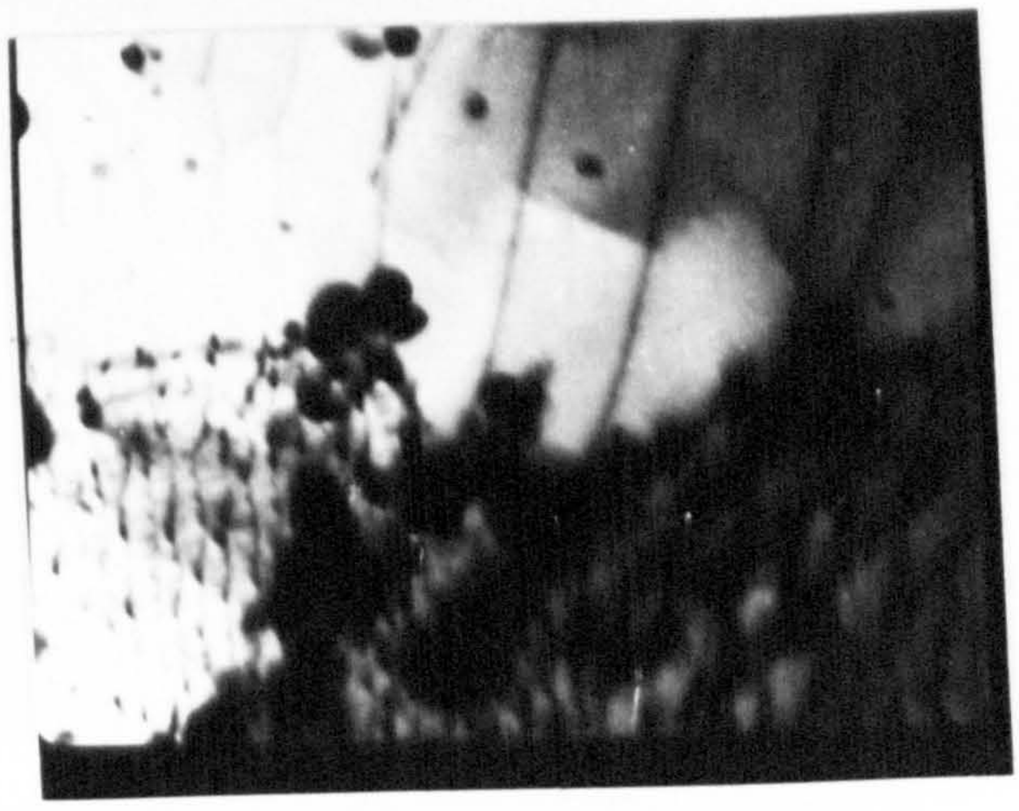


Fig. 114 Thin foil taken from deformed gauge length (200%) of 6 Mg(153) at 300°C and $\dot{\varepsilon} = 1.67 \times 10^{-4}$.

(a)



(b)

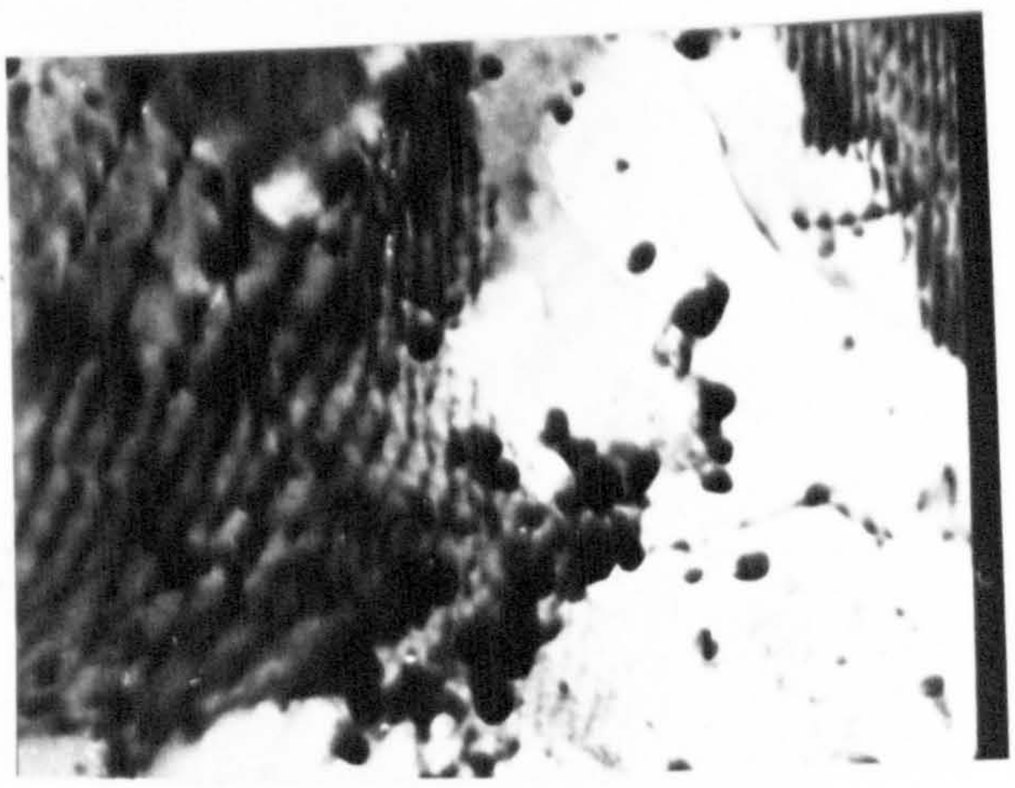
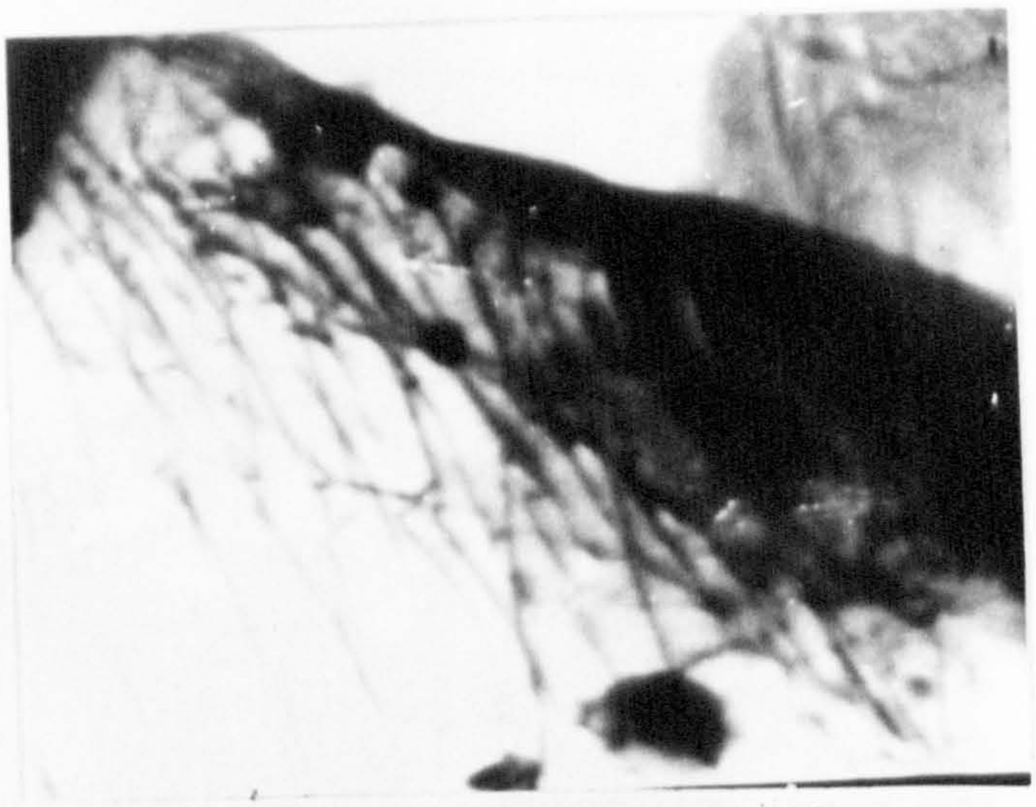


Fig. 115 Thin foil taken from deformed gauge length (200% elongation) of 6 Mg(84) at 300°C and $\dot{\varepsilon} = 1.67 \times 10^{-3}$ Sec^{-1}

(x 100 K).

(c)



(d)

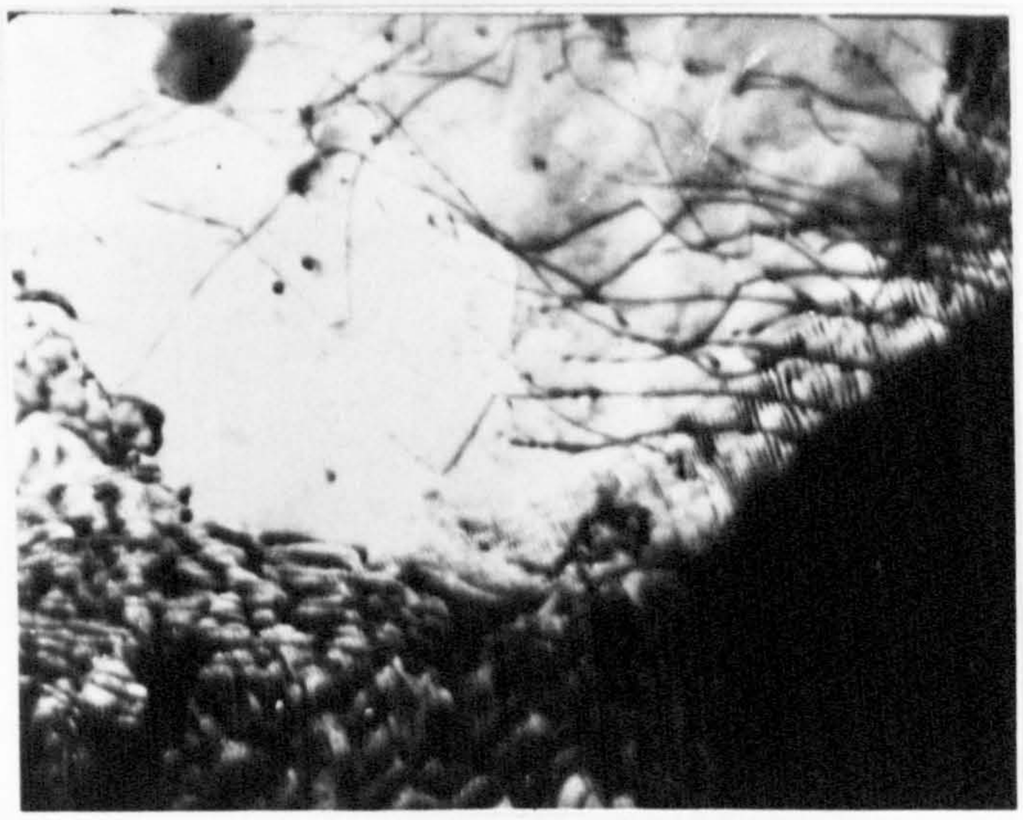
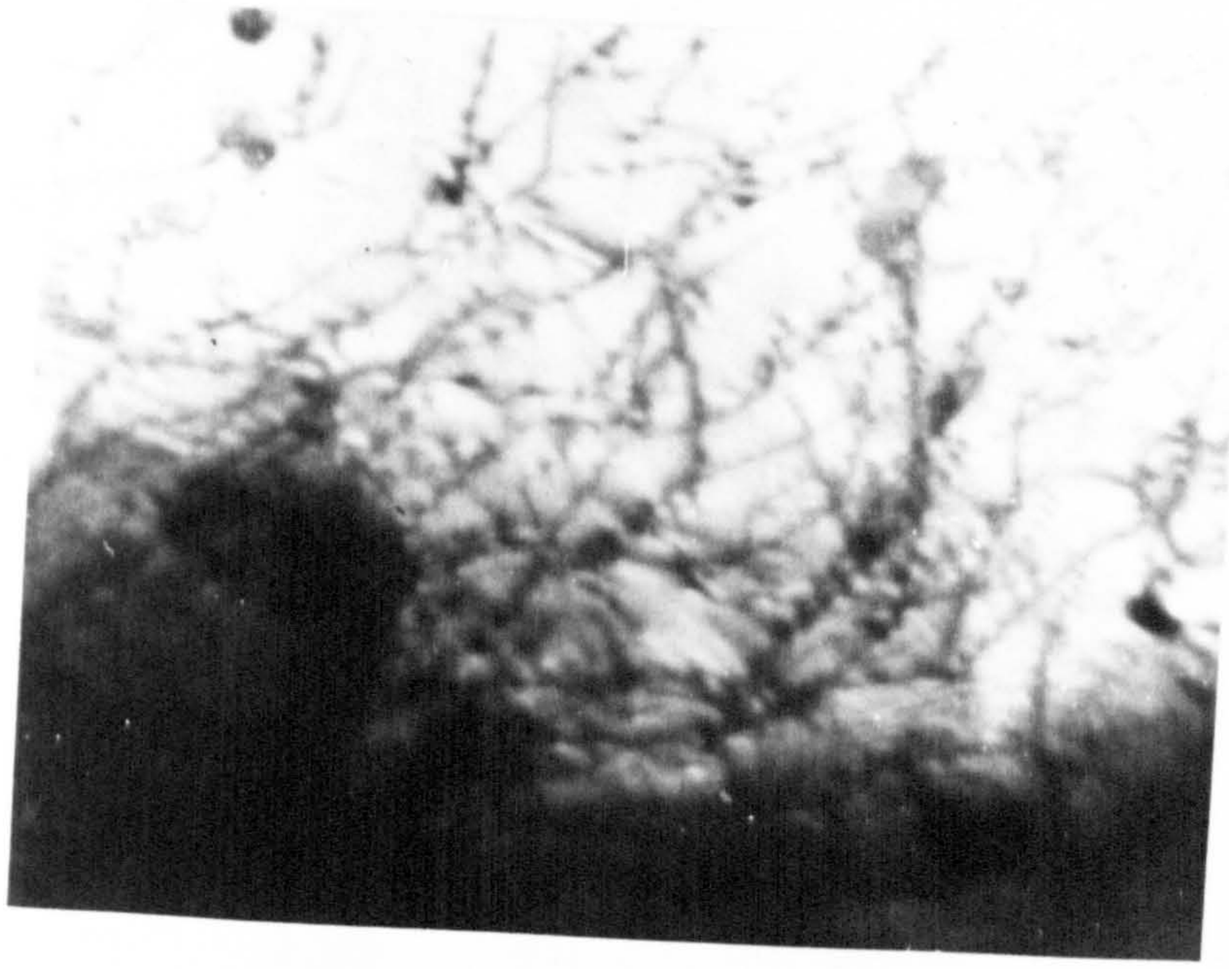


Fig. 115 continued

(a)



(b)

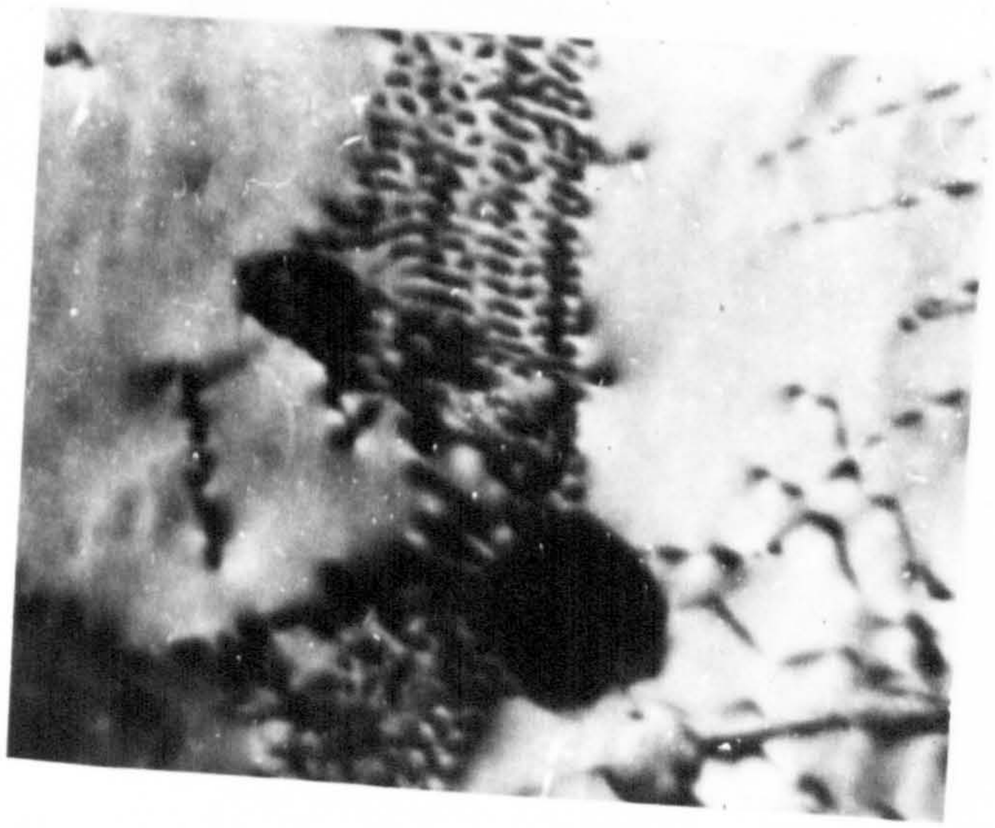
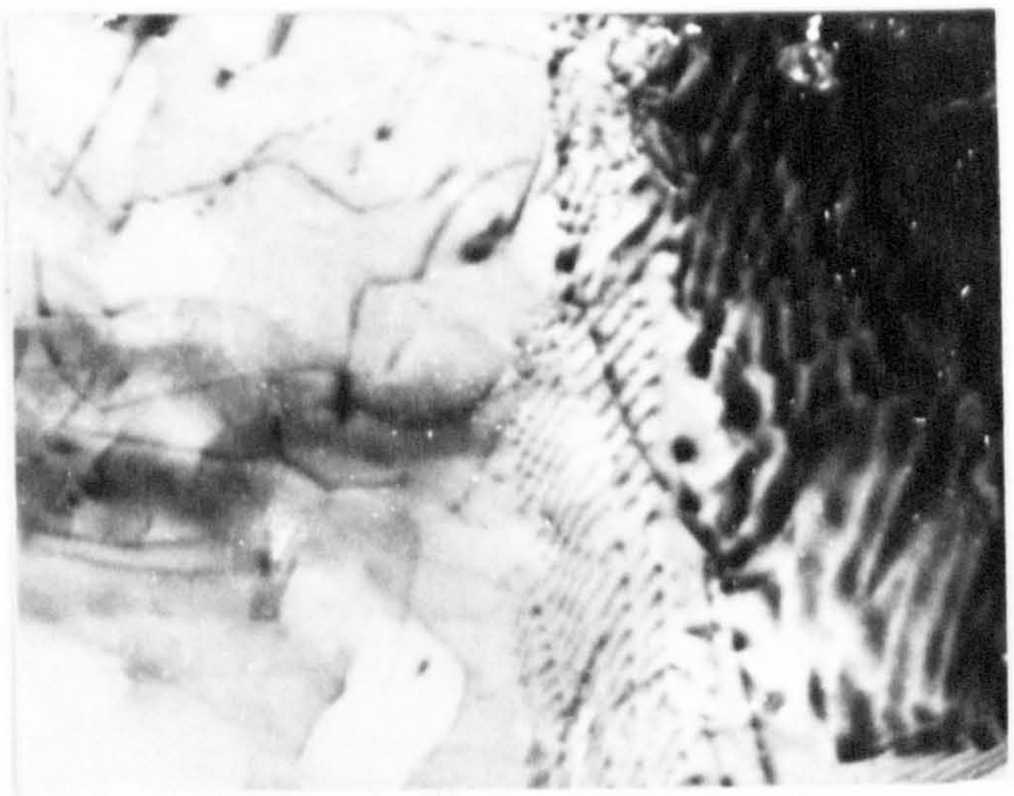


Fig. 116 Thin foil taken from deformed gauge length (200%) of 6 Mg(153) at 300°C and $\dot{\varepsilon} = 1.67 \times 10^{-4}$ (x 100 K).

(c)



(d)



Fig. 116 continued

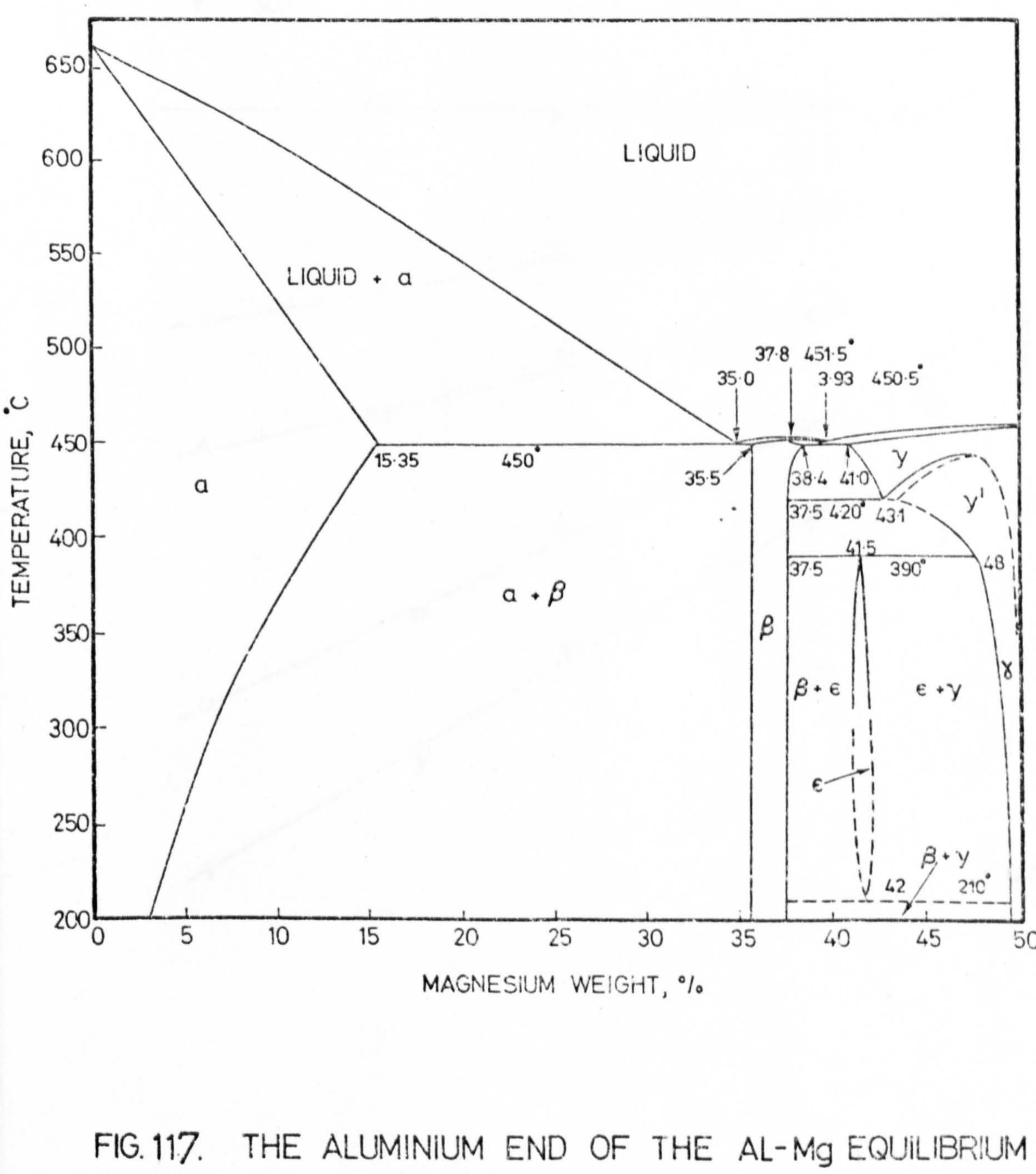


FIG. 117. THE ALUMINIUM END OF THE AL-Mg EQUILIBRIUM DIAGRAM.

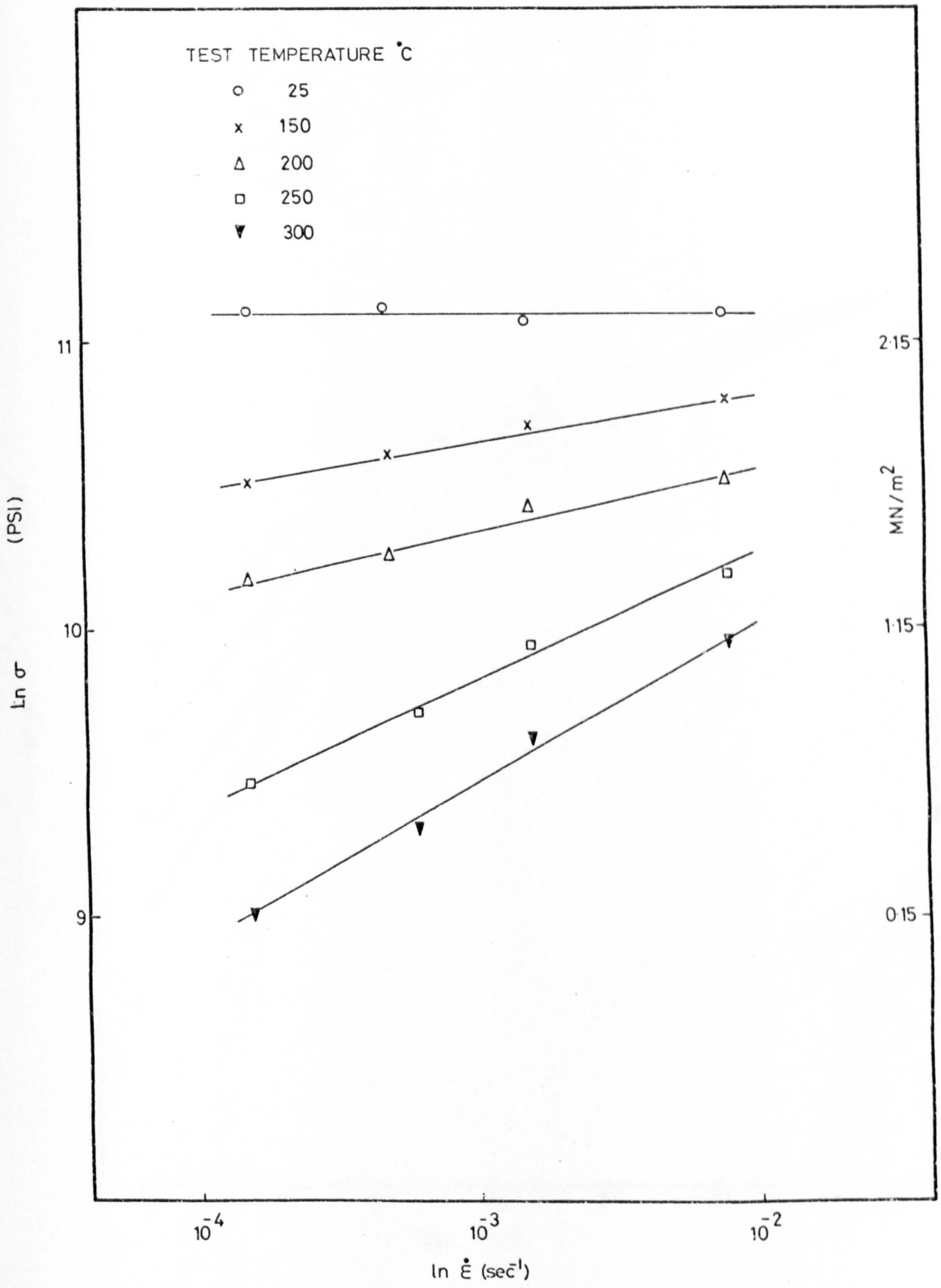


FIG.118 TRUE STRESS VS. STRAIN RATE FOR 6Mg(153) AT VARIOUS TEMPERATURES.

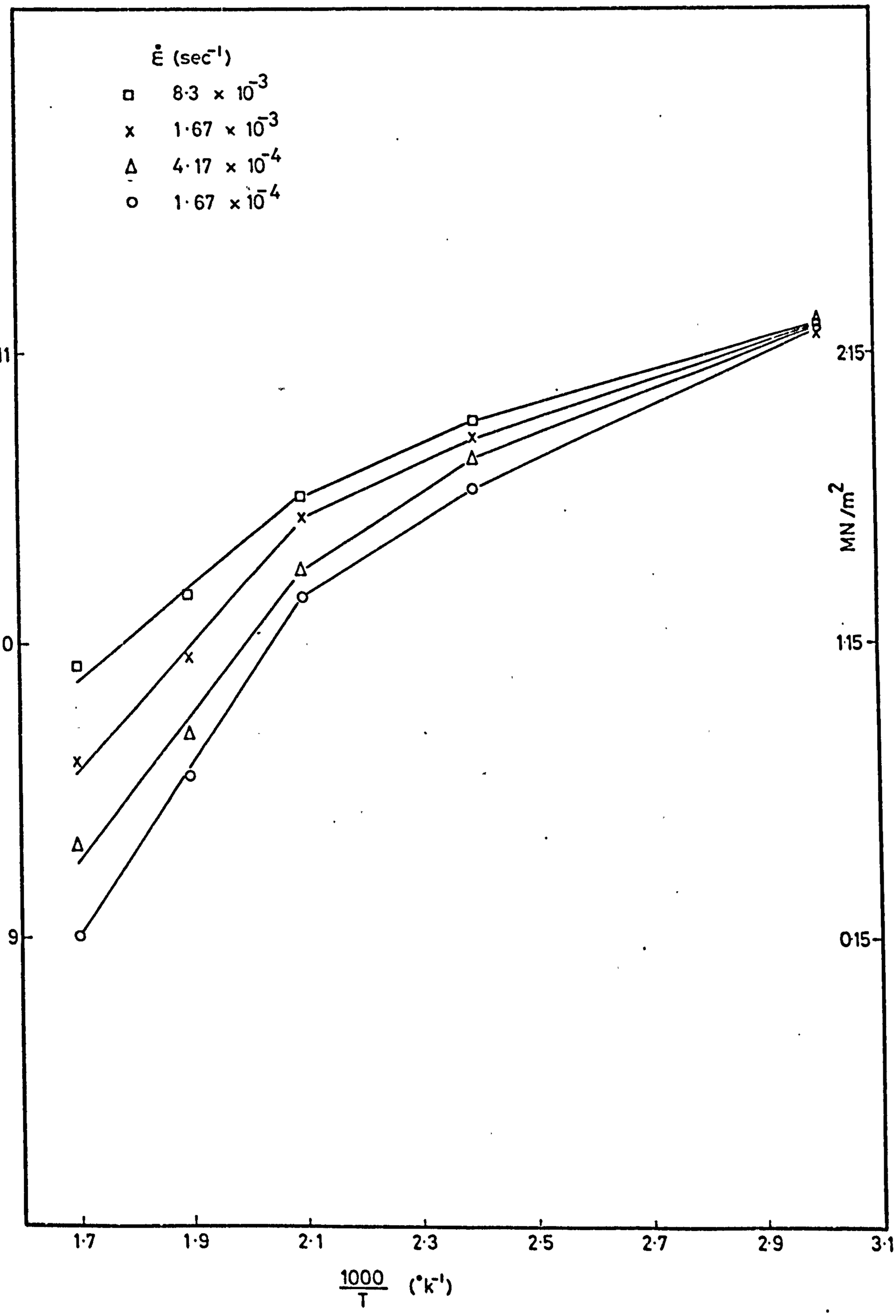


FIG.119. TRUE STRESS VS. RECIPROCAL TEMPERATURE FOR 6Mg (153) AT VARIOUS STRAIN RATES.

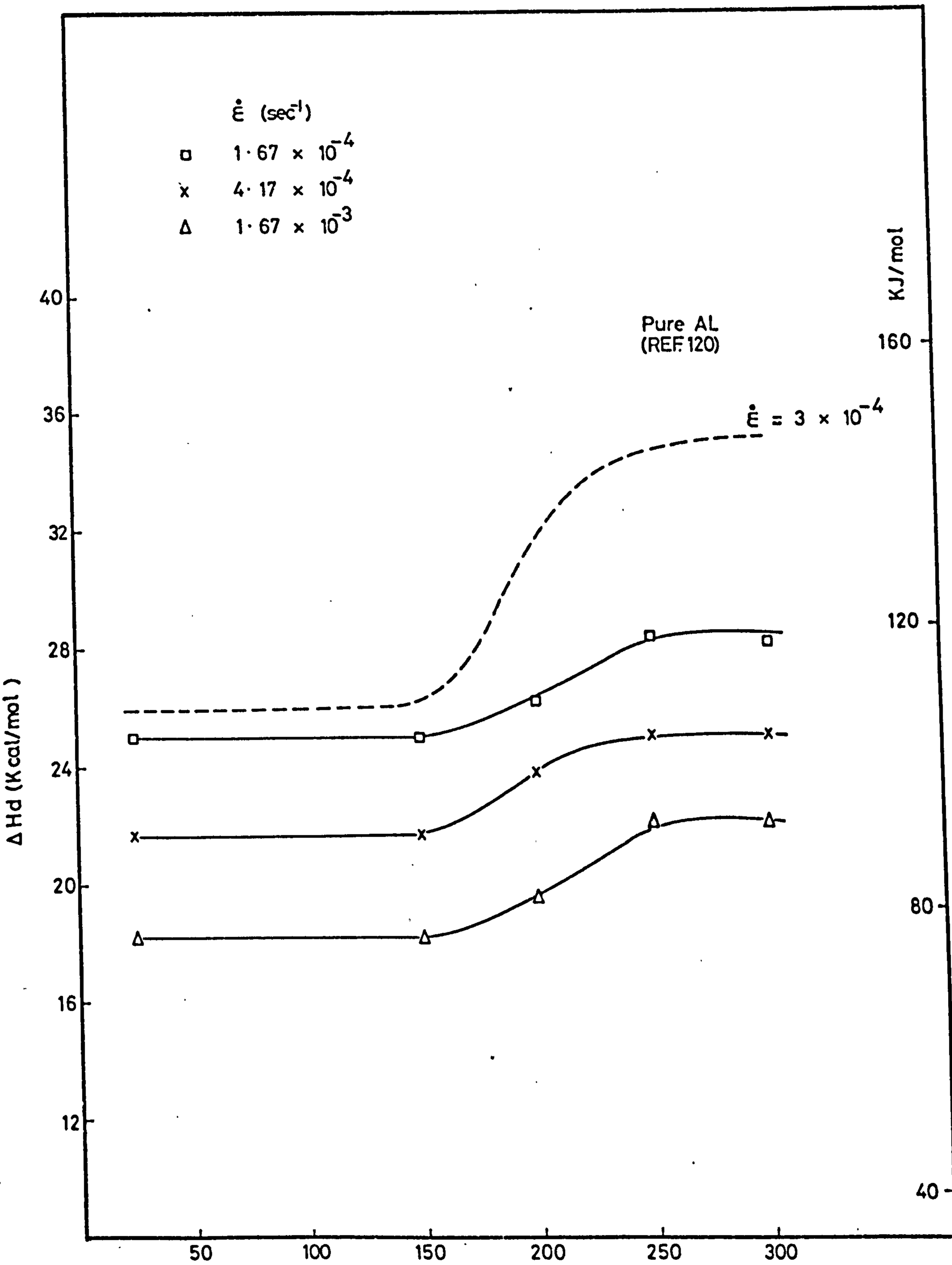


FIG.120. VARIATION OF ACTIVATION ENERGY FOR DEFORMATION OF 6Mg (153) WITH TEMPERATURE AT VARIOUS STRAIN RATES.

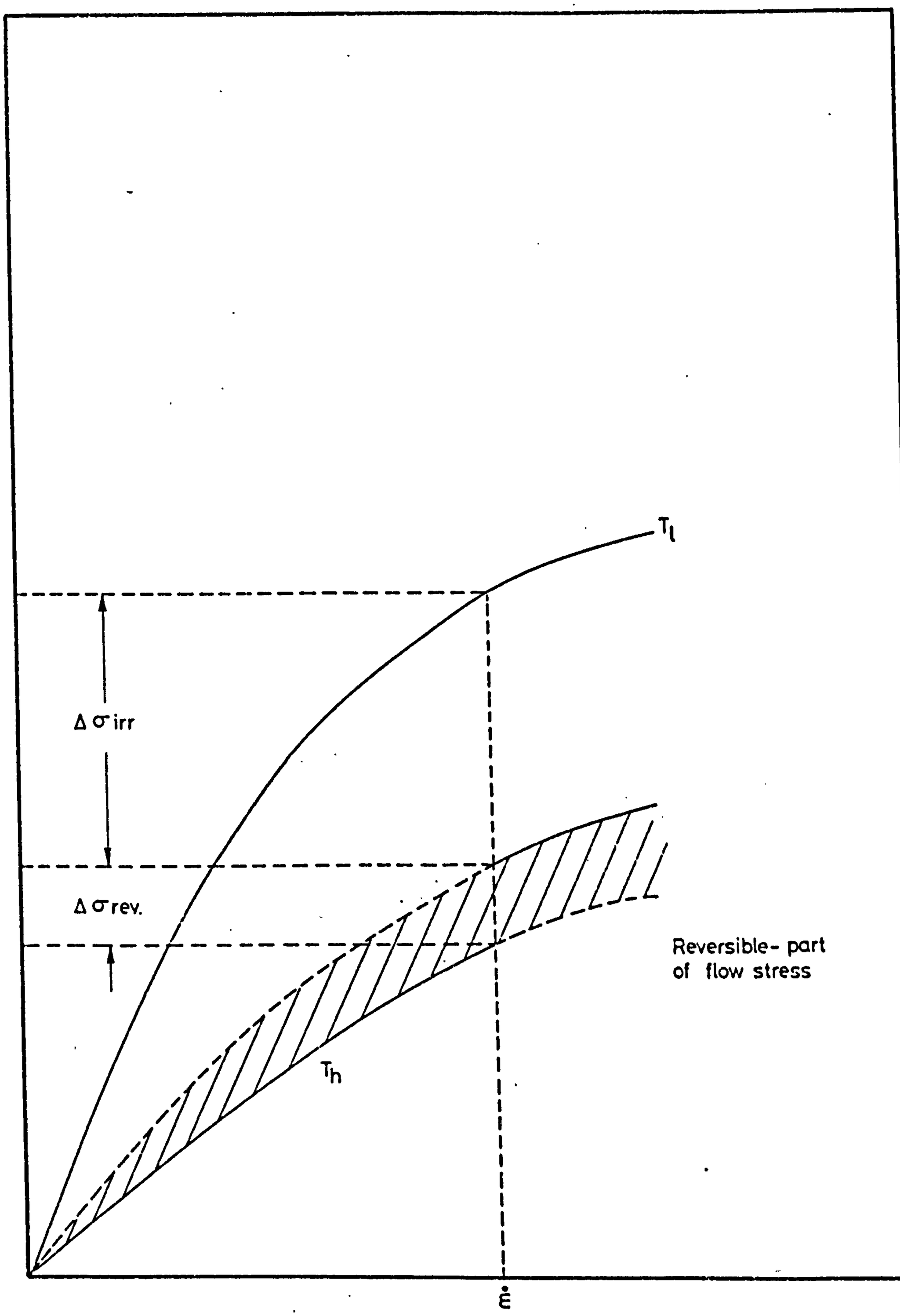


FIG. 121. SCHEMATIC STRESS-STRAIN CURVES AT TWO TEMPERATURES T_l AND T_h ($T_h > T_l$).

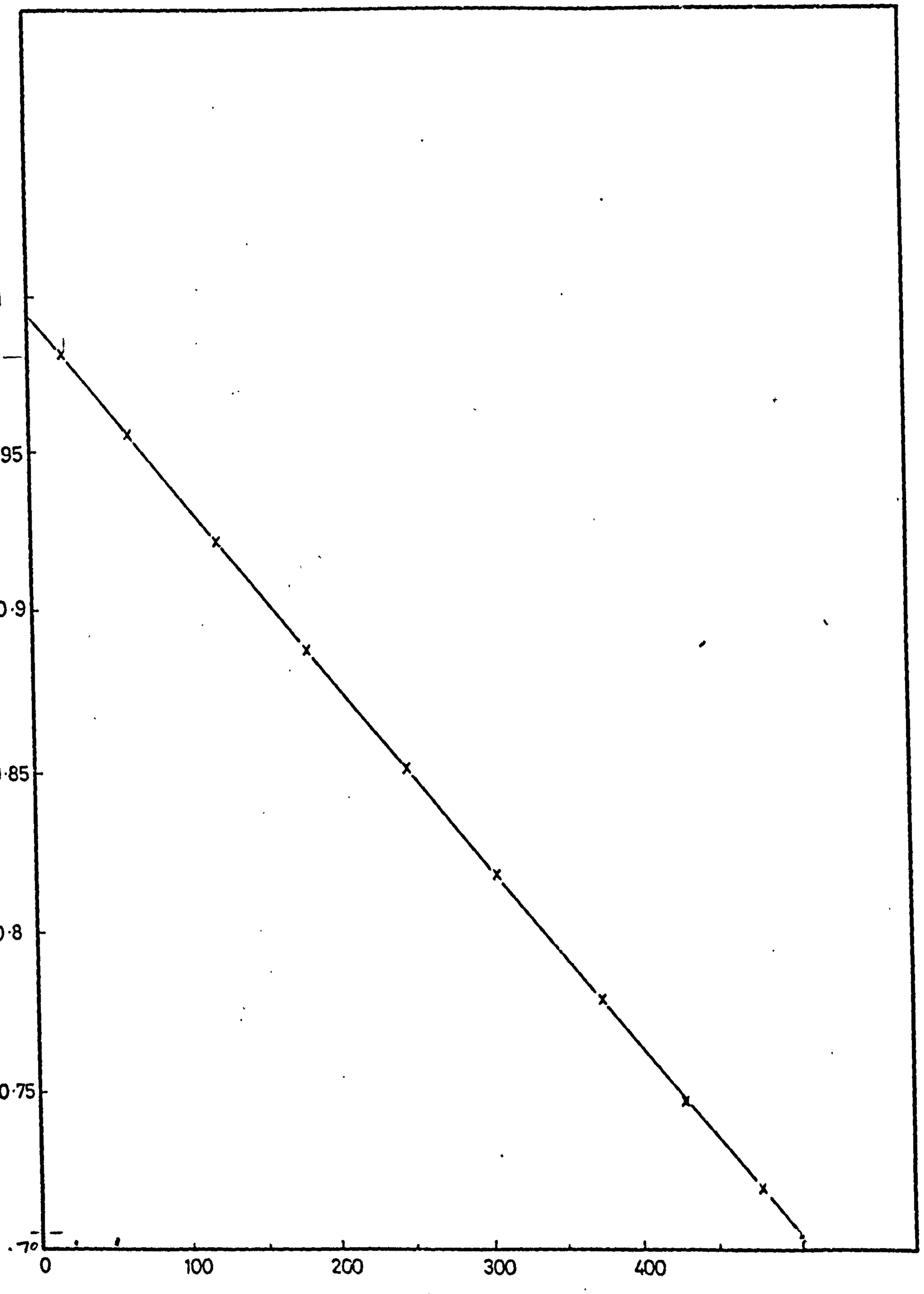


FIG.122. ELASTIC MODULUS (E) VS TEMPERATURE (REF.125)

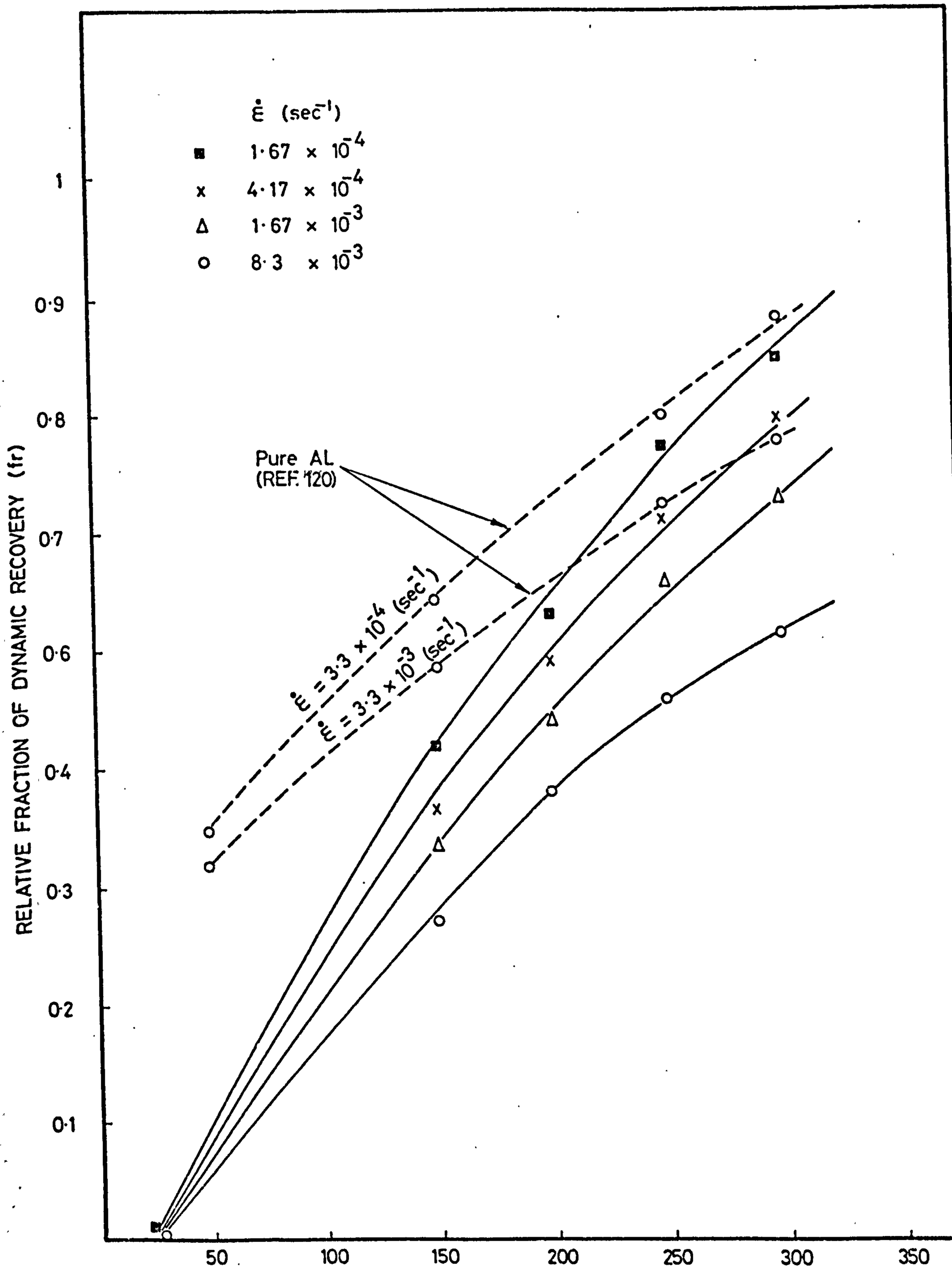


FIG.123. VARIATION OF RELATIVE FRACTION OF DYNAMIC RECOVERY WITH TEMPERATURE FOR 6Mg (153). AT VARIOUS STRAIN RATES.

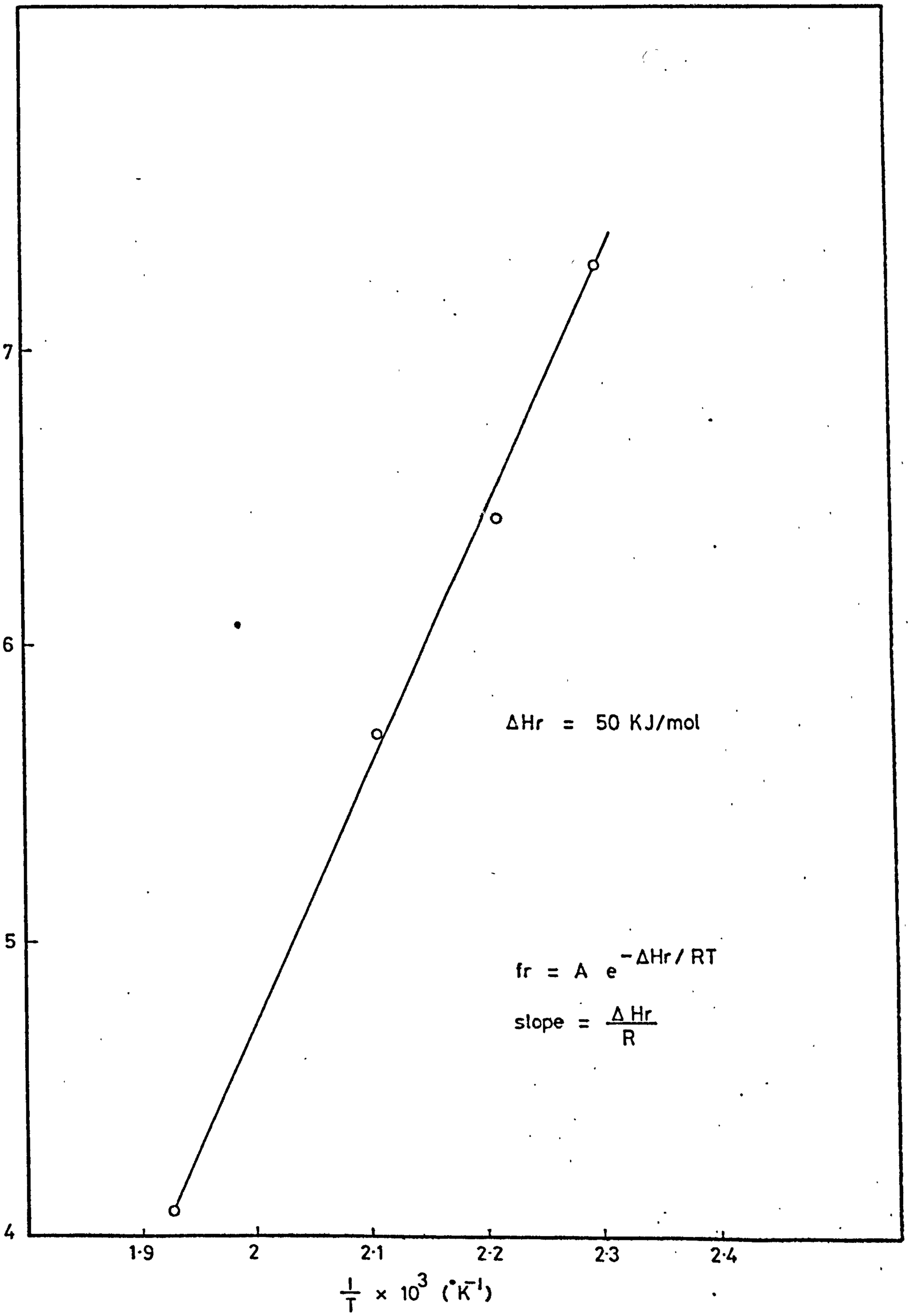


FIG. 124. VARIATION OF RATE OF DYNAMIC RECOVERY WITH RECIPROCAL TEMPERATURE AT STRAIN OF 0·1 AND RELATIVE FRACTION OF DYNAMIC RECOVERY OF 0·5 IN 6Mg (153).